COLLAPSED DIMENSION METHOD APPLIED TO PROBLEMS INVOLVING THERMAL RADIATION WITH PARTICIPATING MEDIA

A Thesis Submitted

for the Award of the Degree of

Doctor of Philosophy

by

Pinakeswar Mahanta

to the

DEPARTMENT OF MECHANICAL ENGINEERING

INDIAN INSTITUTE OF TECHNOLOGY, GUWAHATI

JUNE 2000

भारतीय प्रौद्योगिकी संस्थान गुवाहाटी
Indian Institute of Technology Guwahati

C E R T I F I C A T E

It is certified that the work contained in the thesis entitled **Collapsed Dimension Method Applied to Problems Involving Thermal Radiation with Participating Media,** by **Pinakeswar Mahanta**, a student in the department of Mechanical Engineering, Indian Institute of Technology, Guwahati for the award of the degree of Doctor of Philosophy has been carried out under my supervision and that this work has not been submitted elsewhere for a degree.

Dr. Subhash C. Mishra
Associate Professor
Department of Mechanical Engineering
Indian Institute of Technology, Guwahati

June 2000

भारतीय प्रौद्योगिकी संस्थान गुवाहाटी
Indian Institute of Technology Guwahati

Dedicated to -

Late Maheswar Mahanta

&

Smt. Nirada Mahanta

my parents for their constant guidance and blessings

भारतीय प्रौद्योगिकी संस्थान गुवाहाटी
Indian Institute of Technology Guwahati

Acknowledgements

It gives me great joy and profound pleasure to see that this piece of work has finally come into shape. During the period of my PhD programme, I have received help and support in various ways from many people, without which this thesis would not have taken the present shape. Each one played an indispensable role during my PhD programme, and my gratitude to all of them knows no bound. The limited words that I have, can only partially express my feelings towards them.

I am very much grateful to my thesis supervisor, Dr. Subhash C. Mishra, for his valuable, extensive and fatigueless guidance rendered to me during the course of the present research. It is because of him that I entered the exciting world of research in thermal radiation. I enjoyed each and every moment working under his supervision. I learned a lot many things from him, which will act as an asset for my future research. For me, he has been more than my thesis supervisor.

I gratefully acknowledge Dr. A. D. Sahashrabudhe, Head of the Department of Mechanical Engineering, IIT Guwahati, for his support and encouragement from the very beginning of this work.

I am very much thankful to Dr. A. K. Dass and Dr. A. Dewan for their advises at various stages of this work. They have been closely associated with my PhD programme.

I am greatly indebted to Dr. U. S. Dixit for making himself available for several

technical discussions. I used to get a great boost after having discussions with him.

I am thankful to Dr. S. Nandi of Computer Science and Engineering Department, for allowing me to use facilities in the Computer Center to the fullest extent.

All staff members of the Computer Center have been very much cooperative. I am thankful to Ashok, Pravakar, Saurabh, Ali, Rupa, Rahang and Naba for their help. I am also thankful to all the staff of the Mechanical Engineering Department for their cooperation.

In the newly formed academic environment of IIT Guwahati, I found it pleasant to work with a group of enthusiastic friends. I used to spend hours with my friends, Kalyan, Jiten and Prabal, discussing various topics in heat transfer and fluid mechanics. Discussion with them encouraged me for innovative ideas. I am thankful to them.

Last but not the least, the patience, forbearance, and understanding of my family members cannot be ignored. Mother's blessings have always been very effective. Her guidance and generous help in maintaining my family throughout the period of my research has been incomparable. Both my father and mother-in-laws have been very considerate to my situations. Their heartfelt moral support throughout my research period is greatly appreciated. I am indebted to my brothers, in encouraging me to undertake the programme. They rendered help to me in continuing this work from every possible way. I am thankful to both my elder brothers, Dr. Debendra Nath Mahanta and Dr. Hareswar Mahanta for their timely advice. They rendered help to me every possible way apart from attending my family as physician. Timely assistance of my younger sister Utpala helped me a lot. I am thankful to her. My brother in laws, Tamal, Pallab, Mithu and Babla assisted me in many ways. They extended help to my family as and when required. Moral support of my sister in law, Kutti has always been encouraging. Most importantly, I express my sincere thanks to my wife, Anita, for her matured understanding and unshak-

able faith in me. Without her austerity and sacrifice, I would not have even thought of doing even an M. Tech., leave alone Ph. D. In all respects, she has always been more than what I had expected from her. I lack words to express my debts towards her. Due to my hectic schedule I could not give the due attention to my sons, Saptarshi and Navarshi. In spite of that their timely maturity and tolerance, helped me to concentrate more on my research.

Pinakeswar Mahanta
IIT Guwahati
June 2000

Synopsis

Name of student: **Pinakeswar Mahanta** Roll No.: **974301**
Degree for which submitted: **PhD** Department: Mechanical Engineering

Thesis Title:

Collapsed Dimension Method Applied to Problems Involving Thermal Radiation with Participating Media

Name of thesis supervisor: **Dr. Subhash C. Mishra**

Month and year of thesis submission: **June 2000**

Thermal radiation is one of the fundamental modes of heat transfer. It plays a vital role in the design of high temperature engineering devices. While pure radiation addresses very high temperature phenomenon, radiation combined with conduction and/or convection represents high to medium temperature phenomenon. Radiative transfer in participating medium is very complex. This complexity is owing to the three-dimensional nature of radiation combined with complicated mechanisms of absorption, emission and scattering. Further complexity is encountered due to spatial, spectral and temperature dependent thermo-physical properties. Under these circumstances, radiative transfer equation governing the radiative transfer process is of integro-differential form. For very general situation, its solution becomes a formidable task.

In the past few decades, significant progress has been made in the development of numerical models for the analysis of radiative transfer problems. However,

till-date, there is hardly any method that is suitable for all applications. In general, an ideal radiation model should possess features such as: applicability to multi-dimensional and complex geometries, compatibility with conductive and/or convective heat transfer modes, adequate treatment of anisotropic scattering, treatment of entire range of optical thickness, ability to handle non-gray and inhomogeneous thermo-physical properties, low computational cost, etc. None of the existing radiation models possess all the aforementioned features.

Collapsed dimension method is one of the latest methods available for the analysis of radiative transfer problems with participating medium. This method has a very good prospect. In this method, three-dimensional radiative information is collapsed to a two-dimensional solution plane. Collapsing is done in terms of effective intensity and optical thickness coefficient. At any point in the solution domain, all the actual intensities contained in the discrete plane are represented by an effective intensity. Thus, the physical effect produced at a point under consideration is the same by an effective intensity and an infinite number of actual intensities, all focussed at the same point. In this way, in the collapsed dimension method, a circle of effective intensities contained in the solution plane represents a sphere of actual intensities.

Since effective intensities are contained only in the two-dimensional solution plane, unlike actual intensities which are identified with two angles, i.e,. polar and azimuthal angles, they are identified with only one angle, i.e, planar angle. Because of dependency of the effective intensity on one angle, mathematical expressions for radiative heat flux, incident radiation, divergence of radiative heat flux, boundary intensity, etc., are very much different than those being used in other methods. However, absence of one of the angular dimensions from the analysis brings a lot of positive features in the collapsed dimension method. For example, in a two-dimensional geometry in which solution domain is a two-dimensional plane, conduction and convection can be approximated as two-dimensional phenomena. But because of three-dimensional nature of radiation, at any point in the two-dimensional solution domain, intensities have to be traced in the three-dimensional space. In the collapsed dimension method, ray tracing is very simple. All effective intensities are confined to the

two-dimensional solution domain only. Thus, this method is computationally efficient. For the problems tested so far, the method has been found to work for the entire range of optical thickness situations, including very low optical thickness. This method has been successfully applied to anisotropic situations in one- and two-dimensional Cartesian enclosures. However, its applications to other test cases have not been reported.

Optical thickness coefficient plays a vital role in collapsing three-dimensional radiative information to the two-dimensional plane in terms of effective intensities. In earlier works on the collapsed dimension method, it has been felt that the optical thickness coefficient is geometry restrictive, i.e., optical thickness coefficients found for the Cartesian geometry can not be applied to other geometry. Further, it has also not been indicated how the optical thickness coefficients, which have been found for gray and homogeneous medium, would be applied for non-gray and inhomogeneous medium. Its application to conjugate problems has not been dealt with. Since in this method, effective intensities are defined only in the two-dimensional solution plane, its applicability to a three-dimensional enclosure, where the solution domain is a three-dimensional space, has not been studied. Hence, need was felt to explore the applicability of this method for all the aforementioned situations.

The research objective of the present work is to advance the development of the collapsed dimension method for more general situations. In the present work, mathematical foundation of the collapsed dimension method for general multi-dimensional enclosures is presented. By eliminating the constraints on the usage of the optical thickness coefficients found for gray and homogeneous medium for one- and two-dimensional Cartesian geometries, procedures are developed for using the same for all types of enclosures with inhomogeneous and non-gray situations. These developments have been tested by solving sample problems in various types of geometries with different types of medium conditions. Compatibility of the radiation module of the collapsed dimension method with other modes of heat transfer has been shown by solving combined radiation and conduction heat transfer problems in cylindrical geometry. For all the test problems considered in the present work, results have been validated

with those available in the literature. For all the test conditions, collapsed dimension method has been found to give very accurate results.

The thesis is organized in eight chapters. This thesis begins with the introduction chapter where, first the need for research in thermal radiation has been justified. Basics of thermal radiation with participating medium have been discussed. About 300 papers have been reviewed to present the developments in the existing radiation models. Based on the review, foundation for the present study has been laid out. Basics of the collapsed dimension methods are taken up in the second chapter. Chapter 3 deals with applications of the collapsed dimension method to radiative transfer problems in two-dimensional square, L-shaped, quadrilateral and three-dimensional Cartesian enclosures. For all the test cases, medium has been considered gray and homogeneous. Radiative transfer problems in one- and two-dimensional cylindrical enclosures are studied in Chapter 4. Both radiative and non-radiative equilibrium conditions are studied. Radiative transfer problems with temperature as well as flux boundary conditions are solved. A typical furnace problem is also taken up in this chapter. In Chapter 5, applications of the collapsed dimension method to combined radiation and conduction heat transfer problems are considered. Chapter 6 is devoted to the application of the collapsed dimension method to inhomogeneous and non-gray medium. In Chapter 7, a new angular discretization scheme is suggested and the same is tested for radiative transfer problems in one-dimensional Cartesian enclosures. Conclusions and recommendations are incorporated in Chapter 8.

• • •

Contents

List of Figures

List of Tables

भारतीय प्रौद्योगिकी संस्थान गुवाहाटी
Indian Institute of Technology Guwahati

Nomenclature

A	area, [m^2]
A	function of location, [-]
A	spatial coefficient, [-]
A_p	projected area, [m^2]
a_n	Mie scattering coefficient, [-]
a_1	anisotropy factor, [-]
B	spatial coefficient, [-]
b_m	integral angle factors, [-]
c_v	specific heat at constant volume, [kJ/kg K]
c_m	integral angle factors, [-]
D	diameter, [m]
$d\alpha$	angular thickness, [sr]
E	emissive power, [W/m^2]
E, W, N, S	compass directions
e, w, n, s	central points on faces of the control volume
E_b	blackbody emissive power, [W/m^2]

E_i total blackbody emitted flux, $[W/m^2]$

E_n exponential integral of order n, [-]

e east direction, [-]

G incident radiant energy, [W/m^2]

G$'$ effective incident radiant energy, [W/m^2]

$\overline{g_i g_j}$ direct exchange areas in zonal method, [m^2]

$\overline{g_i s_j}$ direct exchange areas in zonal method, [m^2]

$\overline{G_i G_j}$ total exchange areas in zonal method, [m^2]

$\overline{G_i S_j}$ total exchange areas in zonal method, [m^2]

I effective intensity, [W/m^2]

I_b Blackbody effective intensity, [W/m^2]

i real intensity, [W/m^2]

i indices, [-]

$\hat{i}$ unit vector in X-direction [-]

i_b blackbody real intensity (Planck function), [W/m^2]

J radiosity, [W/m^2]

j indices , [-]

$\hat{j}$ unit vector in Y-direction [-]

k thermal conductivity, [W/m K]

$\hat{k}$ unit vector in Z-direction [-]

L length, [m]

l geometric depth, [m]

M	direction index (M=N, S, E, W)
M	total number of discrete directions, [-]
N	conduction-radiation parameter,
	(Stark number) = $k\beta/4\sigma T_1^3$, [-]
N	order of S_N and P_N approximations, [-]
n	north direction, [-]
p	phase function, [-]
p	pressure, $[N/m^2]$
P_N	N-th order spherical harmonics approximation, [-]
P_n, P_n^m	(associated) Legendre polynomials, [-]
$\dot{Q}$	energy flow rate, [W]
$\dot{Q}'''$	heat production rate per unit volume, [W/m^3]
$q_{M,m}$	radiation heat flux in the direction specified (M) at the control volume surface center point specified (m), [W/m^2]
q	heat flux, [W/m^2]
q	heat flux vector, [W/m^2]
r	radial coordinate, [m]
$\vec{r}$	position vector, [m]
S	source function, [W/m^2]
S	path length, [m]
s	geometric path, [m]

s	south direction, [-]
$\hat{s}$	unit direction vector, [-]
$\overline{s_i g_j}$	direct exchange areas in zonal method, [m^2]
$\overline{s_i s_j}$	direct exchange areas in zonal method, [m^2]
$\overline{S_i G_j}$	direct exchange areas in zonal method, [m^2]
$\overline{S_i S_j}$	total exchange areas in zonal method, [m^2]
T	temperature, [K]
t	time, [s]
$\mathbf{v}$	velocity vector, [m/s]
V	volume, [m^3]
w	west direction, [-]
w	weight factor in Gaussian quadrature, [-]
Y	spherical harmonics, [-]
x, y, z	Cartesian coordinates, [m]
α	planar angle measured from a surface, [rad]
β	extinction coefficient, [m^{-1}]
δ	Kronecker's delta, [-]
$\delta\dot{Q}$	differential energy flow rate, [W]
ϵ	enclosure wall emissivity, [-]
η	optical thickness coefficient, [-]
η	direction cosine, [-]

λ wavelength, [μm]

θ zenith/polar/cone angle, [rad]

θ non-dimensional temperature

$\vec{\Theta}$ effective ray direction, [rad]

τ optical thickness/coordinate/depth, [-]

$\tilde{\tau}$ effective optical thickness, [-]

τ_L enclosure optical thickness, [-]

κ absorption coefficient, [m^{-1}]

μ direction cosine, [-]

μ dynamic viscosity, [kg/m s]

ζ direction cosine, [-]

σ_s scattering coefficient, [m^{-1}]

ϕ azimuthal angle, [rad]

Φ nondimensional medium emissive power

Φ dissipation function, [J/kg m^2]

Ψ nondimensional heat flux

ω single scattering albedo, [-]

Ω solid angle, [sr]

$\vec{\Omega}$ real ray direction, [sr]

ρ density, [g/m^3]

ρ radius ratio r_1/r, [-]

ρ reflectivity, [-]

σ	Stephan-Boltzmann constant $= 5.670 \times 10^{-8}$ W/m^2 K^4

Subscripts

a	absorption
arb	arbitrary
av	average
b	blackbody
CDM	collapsed dimension method
c	conductive
cart	Cartesian
concyl	concentric cylinder
exact	exact
e, w, n, s	central points on faces of the control volume
E, W, N, S	compass directions
g	gas
i, j, k	directions
in	input
L_x	direction
L_z	direction
M	direction index (M=N, S, E, W)
R	radiative, reference
S	south
s	scattering

T	total
w	wall
X	x-direction
Y	y-direction
x, y, z	in a given direction
λ	spectral

Superscripts

D	diffuse
R	radiative
S	specular
+	positive (north) direction
-	negative (south) direction
-	average value
'	dummy variables
*	non-dimensional

भारतीय प्रौद्योगिकी संस्थान गुवाहाटी
Indian Institute of Technology Guwahati

Abbreviations

AR	aspect ratio (radius/height)
BC	boundary condition
CDM	collapsed dimension method
CV	control volume
CVSCP	control volume surface central point
CPU	central processing unit
dev	deviation
DI	discretised intensity
DP	discrete plane
DOM	discrete ordinate method
DTM	discrete transfer method
FEM	finite element method
FVM	finite volume method
MCDM	modified collapsed dimension method
MCM	Monte Carlo method
OTC	optical thickness coefficient
REM^2	ray emission method

RTE	radiative transfer equation
SA	sucessesive approximation
SHM	spherical harmonics method
1-D	one-dimensional/dimension
2-D	two-dimensional/dimension
3-D	three-dimensional/dimension

Chapter 1

Introduction

Radiation plays a vital role in the functioning of many natural and artificial systems in the cosmos. The field of radiation is broad, but it is the thermal radiation in the spectral range $\lambda = 0.1\ \mu m$ to $100\ \mu m$ that governs the major engineering heat transfer processes. It is one of the fundamental modes of heat transfer. All bodies at temperatures greater than absolute zero take part in the radiative exchange. While pure radiation addresses the high temperature phenomena, radiation combined with conduction and/or convection represents medium to low temperature phenomena. It plays a dominant role in many engineering applications. Some typical examples are:

1. Design of energy conversion devices, such as boilers, internal combustion engines, combined cycle power plants, etc. It is reported in [1] that in conventional boilers, contribution from radiation to the total heat flux goes to the extent of 90%. In circulating fluidized bed boilers, this contribution is in the range of 15% to 60% [2–6]. In these boilers, radiative contribution to the total heat flux has been reported to be 15% to 35% by Han and Chow [4], 25% to 45% by Luan et al. [5] and 30% to 50% by Flamant et al. [6].

2. Industrial processes, such as heat transfer in furnaces and incinerators [7] etc.

3. Design and development of spacecraft and utilities: spacecraft with solid and liquid propellant, space vehicle reentry, space vehicle radiators, aerodynamic heating of high speed flight and reduction of payload cost for reusable launch vehicle [8]. Badrinarayan et al. [9] has reported requirement of reliable radiative transfer data for spacecraft thermal control system.

4. Processing of materials: fibrous and foam insulations [10–13], glass [14, 15] and metals [16, 17].

5. Precision heat transfer control in processing industries, such as optimization of diameter and quality of semiconductor crystals in Czochralski crystal growth furnace [18].

6. Design of energy conversion devices for the control of environmental pollution and green house effects [19, 20].

7. Nuclear reactors: Sun, fusion reactors, plasma generators [21].

8. Chemical process control, such as outside vapor deposition process [22] and optical fiber processing [23], etc., etc.

Thus the wide range of potential applications provide strong motivation for continued research in the field of radiative heat transfer.

Depending on whether or not radiation is influenced by the surrounding medium, thermal radiation is grouped as radiation with participating medium or radiation without participating medium. Radiation without participating medium is also termed as surface radiation signifying that radiation is basically a surface phenomenon. In this situation, radiation from opaque bodies emanates only from 0.1 μm or less of surface layers [24]. Radiation emanating from the surface hits another surface without any change in magnitude. Radiation in the outer space, where there is no medium at all, and even on the earth, in many engineering applications in which the medium is transparent to the wavelengths of all the thermal radiation concerned, fall under the scope of surface

radiation. In this, determination of unknown heat flux and/or temperature is relatively easy and various procedures are well documented in [25–30].

Radiation with participating medium, on the other hand, is a complex phenomenon. Medium emission is basically a volumetric phenomenon and as the enclosure boundaries are at finite temperatures, do take part in radiation, entire process is the result of surface and volumetric phenomena. In this, depending upon the medium, radiation traveling from one point to other undergoes complicated phenomena like absorption, emission and scattering. In this situation, appearance of two more variables, viz, polar and azimuthal angles to identify the intensity of radiation, complicates the analysis of radiative transfer. All types of problems involving combustion phenomena or high temperature radiating medium, fall under the purview of radiative transfer with participating medium. The practical importance of radiative transfer with participating medium on the one hand and complexity in its analysis on the other hand have attracted attention of researchers in the field of atmospheric science [25,31], nuclear physics [32–34], and thermal engineering [25–30], towards experimental as well as numerical modeling of radiative transfer problems.

Experimental works in the field of thermal radiation is limited. A survey conducted by Howell [35] indicates major emphasis of research on numerical modeling. It has been mentioned that only 2.95% of works contribute to experimental methods pertaining to evaluation of temperature and heat flux, whereas 22.14% of works cover the experimental works on property evaluation and correlations. Remaining ones being on the numerical methods. His survey is based on the publications made in the Journal of Heat Transfer for the period 1996 to 1999, Proceedings of International Heat Transfer Conference for the period 1982 to 1998 and Symposia of Radiative Transfer for the years 1995 and 1997.

Most of the experimental works in the field of thermal radiation are focussed on property evaluation [2,36–38]. Ramesh and Venkateshan [39] carried out experiments on the effects of surface radiation and partition resistance on natural convection heat transfer in partitioned enclosures with differential interferom-

eter. Rao and Venkateshan [40] calculated effects of free convection and radiation in horizontal fin arrays. In all the reported experiments [2,36,39,40], temperature level and its differentials are relatively low. Further, in these works, thermal radiation has only been used as the boundary condition. Medium has not been considered to be participating and the temperature level has also been not considered high.

Radiative transfer processes, however, at high temperature, are difficult to experiment. This is because, at high temperature, attaining a physical process for experimentation is unrealistic and cost prohibitive in most of the situations, like, nuclear explosion. Further, sophistication in instrumentation, availability of high temperature withstanding materials, etc., do not allow physical monitoring or experimentation of many processes. Such difficulties motivate researchers to adapt numerical experimentation to deal with the radiative transfer problems.

Unlike many other fields, in thermal radiation, there is no single numerical radiation method which can be applied to all types of problems. Research towards the development of numerical radiation methods started about five decades back. The failure of one method to the other, in terms of accurate results and unacceptably very high computational time in various conditions, has been the main motivation for the development of more than a dozen numerical radiation methods for the analysis of radiative transfer in participating medium. Reviewing the deficiencies of various numerical radiation methods, Howell [41] and Yang [42] have suggested following features for an ideal numerical radiation method.

1. Capability to handle multi-dimensional and complex geometry: Many methods work well for the simple geometry but fail to give correct prediction when applied to complex geometry.

2. Good accuracy: Method should give accurate results in all situations.

3. Ease of application: Method should be easy to formulate.

4. Compatibility with other modes of heat transfer: Some methods give accurate results when applied to pure radiation problems but find difficulty in its application to conjugate radiation, conduction and/or convection problems.

5. The method should work for different types of participating medium. All methods have been found to be working for absorbing-emitting media but not all have been reported giving accurate results for various types of scattering situations. Further, method should also work for entire range of optical thicknesses.

6. Economy: Method should operate with low computational cost. This is the prime concern, because in case of conjugate radiation, conduction and/or convection heat transfer problems, determination of divergence of radiative heat flux in the energy equation must be economical.

Besides aforementioned points, a good model should also be applicable to inhomogeneous and non gray medium.

Therefore, the objective of the research related to the development of numerical radiation methods for determination of radiative transfer rates should be aimed at achieving the above criteria.

In this introductory chapter, fundamentals of thermal radiation with participating medium will be presented briefly and difficulties in its analysis will be addressed. Literature review of the popular radiation methods will be highlighted and objectives and scope of the present work will be defined.

1.1 Fundamentals of Radiative Transfer in Participating Medium

Consider a general enclosure containing a participating medium with characteristics of absorption, emission and scattering. Assuming that all three modes

of heat transfer, i.e., radiation, conduction and convection are present in the enclosure, for full simulation of the processes, we need to consider one continuity equation, three momentum equations and one general equation for energy conservation. Further, if the medium is reactive and turbulent, species as well as turbulent equations are also required.

The general equation for energy conservation for a moving compressible fluid is given by [29]

$$\rho\, c_v(\frac{\partial T}{\partial t} + \mathbf{v}\cdot\nabla T) = -\nabla\cdot(-k\nabla T + q_R) - p\nabla\cdot\mathbf{v} + \mu\Phi + \dot{Q'''} \tag{1.1}$$

In Eq. (1.1), left hand side represents the contribution of energy transfer owing to advection, whereas terms on the right hand side respectively represent contribution due to diffusion or conduction, radiation, pressure work, viscous dissipation and internal generation.

Even though in Eq. (1.1), radiative flux q_R is a part of the total heat flux term, it itself is the most difficult part to evaluate, particularly in presence of participating medium. The radiative part in Eq. (1.1) is to be determined from the equation of conservation of radiative energy as given by

$$\nabla\cdot q_R = \kappa_\lambda[4\pi\, i_{b\lambda}(\tau_\lambda) - G(\tau_\lambda)] \tag{1.2}$$

where $i_{b\lambda}$ is the blackbody intensity function which depends explicitly on the local temperature T of the medium, κ_λ is the local linear spectral absorption coefficient and τ_λ is the spectral optical thickness defined as

$$\tau_\lambda = \int_0^S \beta_\lambda\, ds \tag{1.3}$$

where β_λ is the spectral extinction coefficient. Incident radiation G in Eq. (1.2) is given by

$$G(\tau_\lambda) = \int_{\phi=0}^{2\pi}\int_{\theta=0}^{\pi} i(\tau_\lambda,\theta,\phi)\, \sin\theta\, d\theta\, d\phi \tag{1.4}$$

where θ and ϕ are zenith/polar/cone angle and azimuthal angle respectively and $i(\tau_\lambda,\theta,\phi)$ is the intensity of radiation at any optical depth τ_λ in the direction (θ,ϕ). It is given by

$$i(\tau_\lambda,\theta,\phi) = i(0,\theta,\phi)\, \exp(-\tau_\lambda) + \int_{\tau_\lambda'=0}^{\tau_\lambda} S(\tau_\lambda',\theta',\phi')\exp(-(\tau_\lambda-\tau_\lambda'))\, d\tau_\lambda' \tag{1.5}$$

Equation (1.5) is the integral form of the radiative transfer equation (RTE). It describes the intensity of radiation at some optical depth τ_λ in the medium in terms of intensities reaching that position from all other locations $\tau_\lambda^{'}$ in medium and from the medium boundary at τ_λ=0. Equation (1.5) is obtained by integrating the differential form of RTE (Eq. (1.6)) from the point of origin of the ray $\tau_\lambda^{'}$=0 to the point $\tau_\lambda^{'} = \tau_\lambda$.

$$\frac{di(\tau_\lambda, \theta, \phi)}{d\tau} + i(\tau_\lambda, \theta, \phi) = S(\tau_\lambda, \theta, \phi) \tag{1.6}$$

where $S(\tau_\lambda, \theta, \phi)$ is the source function given by

$$\begin{aligned} S(\tau_\lambda, \theta, \phi) &= (1 - \omega_\lambda)\, i_{\lambda\, b}(\tau_\lambda) \\ &\quad + \frac{\omega_\lambda}{4\pi} \int_{\phi=0}^{2\pi} \int_{\theta=0}^{\pi} i(\tau_\lambda, \theta, \phi)\, p\left((\theta^{'}, \phi^{'}) \rightarrow (\theta, \phi)\right) \sin\theta^{'} d\theta^{'} d\phi^{'} \end{aligned} \tag{1.7}$$

where $\omega_\lambda = \frac{\sigma_{\lambda s}}{\kappa_\lambda + \sigma_{\lambda s}}$ is the spectral scattering albedo and $p\left((\theta^{'}, \phi^{'}) \rightarrow (\theta, \phi)\right)$ is the anisotropic phase function which represents the probability distribution of the energy scattered into the direction (θ, ϕ) from the ray traversing the elemental volume from all other directions $(\theta^{'}, \phi^{'})$. Equations (1.1)-(1.6) are well established in [25–30] and accepted for general engineering applications.

1.2 Complexities in the Analysis of Radiative Transfer

From the foregoing discussions, it is seen that RTE given by Eq. (1.5) is a third order integral equation in intensity $i(\tau_\lambda, \theta, \phi)$. For its evaluation, integral over the source function $S(\tau_\lambda, \theta, \phi)$ (Eq. (1.5)) must be carried out over the optical coordinate τ_λ. This optical coordinate τ_λ is a function of four independent variables (three spatial and one spectral). At a given spatial location, for a given wavelength λ, each intensity is identified with two angular dimensions (θ, ϕ). It is obvious from Eq. (1.7) that the source function itself is an unknown function of intensity which has to be integrated over two directions θ and ϕ. Moreover, temperature T which is related to the blackbody intensity term, $i_{\lambda,b}$, in the source function (Eq. (1.7)) is an unknown and it must be evaluated

in conjunction with the equation for conservation of total energy (Eq. (1.1)), further complicating the situation. Therefore, due to the presence of radiation, the general equation for conservation of total energy (Eq. (1.1)) turns out to be an integro-differential equation which brings enormous difficulties in its solution. Thus, there has always been a constant search for the development of an efficient and cost-effective method for predicting radiative transfer rates in energy conservation devices.

1.3 Review of the Existing Methods

During the past few decades, various numerical radiation methods have been developed for the solutions of radiative transfer problems. In majority of the methods, the integro-differential form of RTE is approximated either by simple partial differential equation or by integral equation. Angular discretization of intensity is common amongst most of the methods, except the zone method and the Monte Carlo method (MCM). In the zone method, discretization is done in the spatial domain. MCM views radiation differently. In the following sections, for understanding the development in the field of radiative transfer, up-to-date review of various methods for the analysis of radiative transfer problems with participating medium is presented. This review will also help in outlining the objective and scope of the present work.

1.3.1 Exact Analytical Method

It has been discussed in Section 1.2 that because of the large number of the associated variables and integro-differential form of the radiative transfer equation, its solution is a difficult task. The exact analytical solution of radiative transfer equation can only be obtained in highly idealized situations, like simple geometry, uniform radiative properties, homogeneous boundary conditions [43] and spectrally independent radiative properties [44], etc. Exact solution of 1-D planar medium has received much attention in the atmospheric science [25,45]

and neutron transport [32, 46]. Exact analytical solutions of radiative transfer problems in 1-D Cartesian enclosures are reported by many authors [47–50]. These are now the subject matters of text book on thermal radiation and are available in [26–30].

Formulations and solutions for radiative transfer problems in infinitely long cylindrical geometry were attempted during sixties by Heaslet and Warming [51] and Kesten [52]. However, not much literature are available on analytic solution of radiative transfer problems in cylindrical medium. Most of the available solutions pertaining to these geometries are devoted to absorbing-emitting medium [51–54]. Loyalka [53] has provided analytic solutions for radiative transfer problems in concentric cylindrical enclosure and his method is considered exact. However, his analysis was confined to absorbing-emitting medium only. Some results with isotropic scattering are reported by Crosbie and Farell [55]. Formulations and results with anisotropic scattering are reported by Azad and Modest [56], Crosbie and Dougherty [57] and Mahanta and Mishra [58].

For exact analytic solution of radiative transfer problems in multidimensional geometries, very few works are reported. One of the earliest attempts for 3-D space with anisotropic scattering is found in the work of Hunt [59]. He considered a phase function comprising of three terms in Legendre polynomials and reduced the integro-differential RTE to an integral equation. Cheng [60] used a rigorous approach to solve RTE in a two-dimensional rectangular enclosure with absorbing, emitting and isotropic scattering medium. Dua and Cheng [54] extended this method further to finite cylindrical enclosures. Crosbie and Koewing [61], Crosbie and Dougherty [57, 62], Crosbie and Schrenker [63, 64], Crosbie and Farrel [55], Crosbie and Davidson [65] have generated exact formulations for two-dimensional and three-dimensional rectangular and cylindrical geometries in absorbing, emitting and anisotropically scattering medium.

Most of the engineering systems, in reality, are associated with inhomogeneous medium with spectrally dependent radiative properties. A large class of problems involve radiation combined with conduction and/or convection. In such

circumstances, exact analytic solutions have no significant bearing [43]. However, exact analytic solutions for simple geometries are needed as they can serve as benchmarks to measure validity and accuracy of other approximate methods.

1.3.2 Monte Carlo Method

Monte Carlo method (MCM) is a class of numerical techniques, widely used to simulate almost all important physical processes. This method has been extensively used in the study of neutron transport [46] , atmospheric physics [66, 67], remote sensing and molecular biology [35, 68], etc. In radiation, its first ever use was reported during 1950's by Metropolis and Ulam [69]. They employed MCM for modeling of nuclear weapons.

The first ever engineering applications of the MCM to radiative transfer problems is reported by Howell and Perlmutter [70]. They used MCM for a simple case of radiative transfer analysis in a planar absorbing-emitting medium. More complex problems are reported in [71–86]. This method provides physical grasp of the radiative transfer process.

In simulation of radiation by the MCM, radiation is assumed to be composed of finite number of discrete energy bundles or photons. The photons are fired from the radiation source in the random directions and their subsequent histories are recorded until their final absorption in the system. The path of the photon is determined at each point of emission, absorption-emission, scattering or reflection by a random choice from a set of possible paths. Details on MCM are reported by Howell [68, 87], Haji-Sheikh [88], Modest [76] and Howell [89]. Numerical solution procedures are also presented by Yang et al. [90].

MCM has got abundant applications in the analysis of pure radiative heat transfer problems. In the absence of experimental data, this method has been considered a benchmark method for validating the results of any other meth-

ods [43, 68, 83, 84, 89]. However, for conjugate radiation, conduction and/or convection heat transfer problems, MCM is not preferred over other methods. This is because MCM has problem with matching the grid sizes with the conductive and/or convective heat transfer codes, and if sufficient number of photons are not fired, convergence is another problem. The convergence problem is caused by the statistical error inherent with this method. By firing large number of photons, statistical error can be minimized and convergence can be accelerated. However, this will only be at the cost of extra computational effort. In conjugate mode problems, iterative nature of the problems and the huge amount of computational time required by MCM, discourage usage of this method. To show its workability, Mishkin and Kowalski [74], Abed and Sacadura [75], Tiwari and Liu [78] and Liu and Tiwari [80] have applied this method to some sample problems involving conjugate mode heat transfer.

MCM is known for its appetite for computational time. The method becomes computationally prohibitive when scattering albedo and surface reflectivity become high [91]. However, keeping aside computational time, applications of MCM to the complicated situations with anisotropic scattering are reported by Taniguchi and Mochida [92], Farmer [82], Farmer and Howell [85] and Gupta et al. [73]. Spectral effects on radiative transfer have been studied by Modest and Sikka [93], Modest [76], Farmer and Howell [77, 94] and Taniguchi et al. [79].

To make MCM more attractive for conjugate problems, Kobiyama et al. [72] and Kobiyama [95] have studied ways of reducing the computational expenses. In certain test problems, they could reduce the computational time by up to 15%. Samsundar et al. [96] introduced energy partitioning as a measure to reduce computational time. Further, Sivathanu and Gore [97–99] evolved a discrete probability density function to reduce the computational time. Farmer and Howell [81] have taken a new step by using the hybrid method. In this method, P_N or diffusion approximation is hybridized with the MCM. Here, P_N or diffusion approximation is applied to high optical thickness range and MCM is applied to moderate to low optical thickness range. One important aspect

of continued research in recent years is in the field of parallel processing of the MCM. Taniguchi et al. [100] applied parallel processing technique to radiative transfer problems with non gray medium. They reported significant reduction of computational time. Farmer and Howell [85] and Farmer [82] described parallel processing architectures for computers and their relative advantages for MCM.

Another category of MCM, recently gaining importance is the application of inverse or reverse techniques to solve radiative transfer problems [35]. This technique is based on principle of reciprocity and appears very useful when conditions optically close to a surface or volume element with known conditions must be determined. Dunn [101], Subramaniam and Menğuç [102] and Walter and Buckius [103] have presented results for some problems using inverse MCM.

1.3.3 Zone Method

The zone method was developed by Hottel and Cohen [104] and Hottel and Sarofim [105] for calculating radiative exchange in enclosures. In this method, the bounding walls and volume of the enclosure are divided into a number of surface and volume elements respectively. They are known as zonal elements. Each element is assumed isothermal and of isotropic radiative properties. Direct and total exchange areas are defined for evaluating all possible radiant exchanges among zonal elements. Direct exchange areas are used for radiative exchanges among black zonal elements. To account for the single and multiple reflections, total exchange areas are defined. Each of the direct exchange areas (Fig. 1.1), $\overline{g_i g_j}$, $\overline{g_i s_j}$, $\overline{s_i g_j}$ or $\overline{s_i s_j}$ accounts for the geometric orientation of elements i and j with respect to each other and attenuation of radiation along the path joining the two elements. Here, s and g indicate the direct exchange area for surface and volume elements respectively. For total exchange areas, same notations are used with capital letters.

Radiative energy balance of each element is expressed in terms of the exchange

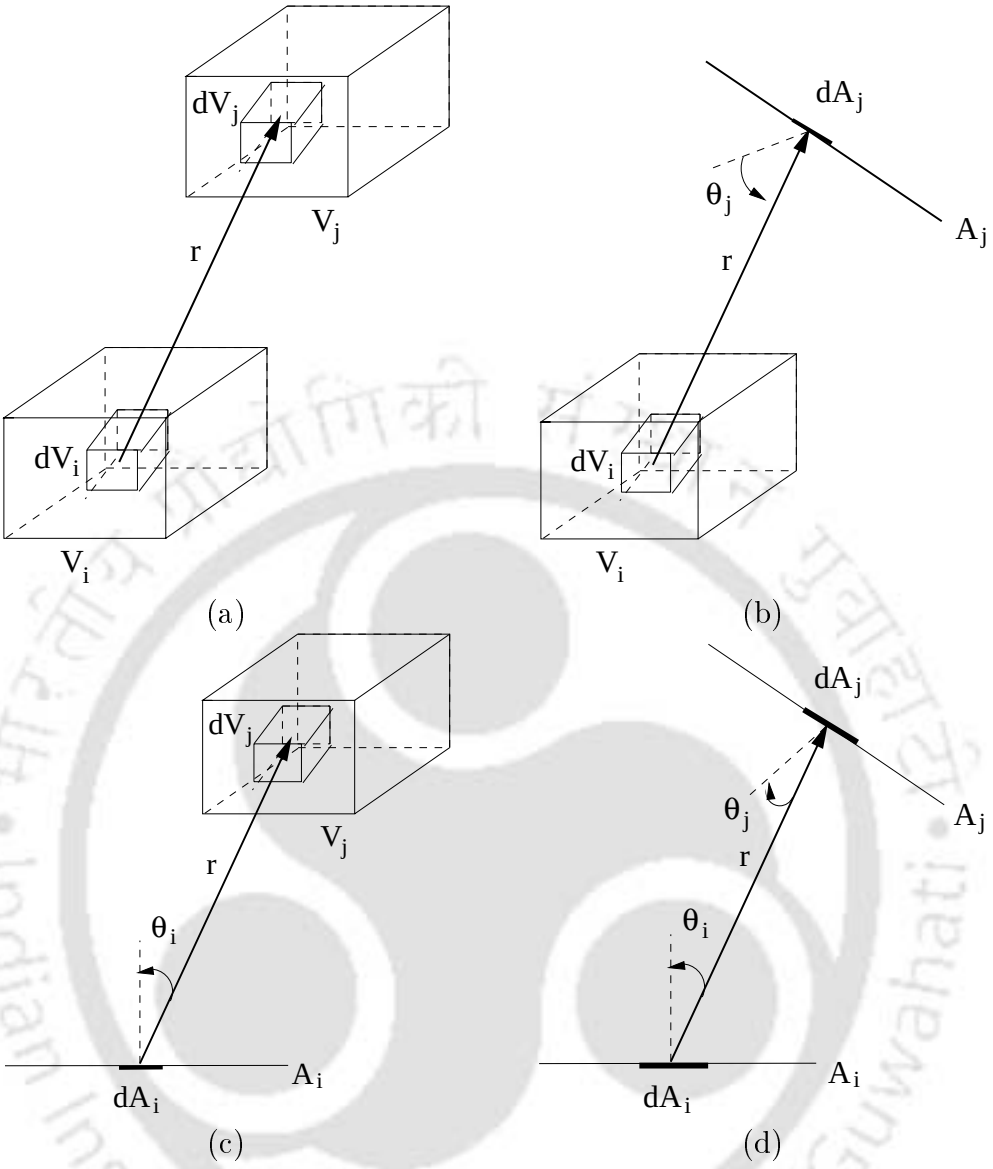

Figure 1.1: Radiative exchange between zonal elements.

areas. It is given by

$$Q_i = Q_{E,i} - \Sigma_j^M \overline{X_i Y_j}\, E_j \tag{1.8}$$

where $X, Y = S, G$.

In Eq. (1.8), left hand side represents the net radiant heat energy Q_i, whereas the right hand side represents the difference between the emitted radiation, $Q_{E,i}$ and total radiation received directly or indirectly through multiple reflection and scattering from all M directions in the domain. E_j is the total blackbody emitted flux ($\sigma\ T_j^4$) and $\overline{X_iY_j}$, the total exchange area from element i to j, is a function of the direct exchange areas $\overline{g_ig_j}$, $\overline{g_is_j}$, $\overline{s_ig_j}$ and $\overline{s_is_j}$ as well as the radiative properties of the medium. With specified temperature field, Eq. (1.8) can be used to evaluate radiant energy at each zonal element.

In Fig. 1.1, some possible radiative exchanges between zonal elements are shown. The total exchange areas are calculated from direct exchange areas $\overline{g_ig_j}$, $\overline{g_is_j}$, $\overline{s_ig_j}$ and $\overline{s_is_j}$. These represent the radiative exchange between any two elements when all the area elements in the system are assumed black. The direct exchange areas are defined as

$$q_{d,g_ig_j} = \overline{g_ig_j}E_{g_i} = \overline{g_ig_j}\sigma T_{g_i}^4 \tag{1.9}$$

$$q_{d,g_is_j} = \overline{g_is_j}E_{g_i} = \overline{g_is_j}\sigma T_{g_i}^4 \tag{1.10}$$

$$q_{d,s_ig_j} = \overline{s_ig_j}E_{g_i} = \overline{s_ig_j}\sigma T_{g_i}^4 \tag{1.11}$$

$$q_{d,s_is_j} = \overline{s_is_j}E_{g_i} = \overline{s_is_j}\sigma T_{g_i}^4 \tag{1.12}$$

where q_d represents the radiative energy emitted from element i and absorbed by element j. The values of direct exchange areas are calculated from the following equations

$$\overline{g_ig_j} = \int_{V_i}\int_{V_j} \frac{\kappa_i\ dV_i\kappa_j\ dV_j\tau(r)}{\pi\ r^2} \tag{1.13}$$

$$\overline{g_is_j} = \int_{V_i}\int_{A_j} \frac{\kappa_i\ dV_i\ dA_j\cos\theta_j\tau(r)}{\pi\ r^2} \tag{1.14}$$

$$\overline{s_ig_j} = \int_{A_i}\int_{V_j} \frac{\kappa_j\ dV_j\ dA_i\cos\theta_i\tau(r)}{\pi\ r^2} \tag{1.15}$$

$$\overline{s_is_j} = \int_{A_i}\int_{A_j} \frac{dA_i\cos\theta_i dA_j\cos\theta_j\tau(r)}{\pi\ r^2} \tag{1.16}$$

where $\tau(r)$ is the transmittance of the gas layer with a thickness r. It is obtained from Beer's law [28]

$$\tau(r) = \exp\left(-\int_0^r \kappa(r)\ dr\right) \tag{1.17}$$

Finally, the total exchange area is computed by considering the radiosity J.

$$\overline{G_iG_j} = \overline{g_ig_j} + \Sigma_M \overline{s_M g_j} J_{g_i,k} \tag{1.18}$$

where the first term on the right hand side of Eq. (1.18) represents the radiative energy emitted from the gas element i that reaches the gas element j directly. The second term represents the radiative energy originally emitted by the gas element i and reflected by wall element M that reaches the gas element j.

Similarly, for radiative exchange between gas and surface as well as between surface and surface elements, exchange areas are given by,

$$\overline{G_iS_j} = \frac{A_j\epsilon_j}{\rho_j} J_{g_i,j} \tag{1.19}$$

$$\overline{G_iS_j} = \overline{S_iG_j} \tag{1.20}$$

$$\overline{S_iS_j} = \frac{A_j\epsilon_j}{\rho_j} (J_{g_i,j} - \delta_{i,j}\epsilon_i) \tag{1.21}$$

where, $\delta_{i,j} = 1$ for $i = j$ and $\delta_{i,j} = 0$ for $i \neq j$.

Zone method has found extensive applications in the analysis of radiative exchange in the presence of participating medium [41, 91, 106–113]. For both radiative equilibrium and non-radiative equilibrium situations, it has been found to give exact results. However, for non-radiative equilibrium situations, the role of zone method has been primarily to validate the results of the benchmark problems obtained using other approximate methods. In such situations, it has been applied to problems with known temperature field. In non-radiative equilibrium problems involving radiation, conduction and/or convection, application of the zone method is not very encouraging. Further, difficulties are encountered if the medium is non gray, inhomogeneous and anisotropically scattering. For irregular geometries, the use of this method is not advocated [43, 89]. In the aforementioned situations, it is not that the method is incapable of giving the accurate results, rather if accuracy is demanded, compared to other methods, this method becomes computationally very expensive.

In non-radiative equilibrium problems involving radiation, conduction and/or convection, if the conduction and/or convection module(s) demands finer grid size, large computational time is required in finding the exchange areas [89]. It is impractical in zone method to use a grid as fine as those necessary for fluid flow calculations. This creates difficulty in matching the two grid systems. In addition, Eq (1.8), hypothetically not being a sparse matrix, is in an inconvenient form to be computed with the fluid flow and energy equation. The same is also true for non gray, inhomogeneous and anisotropically scattering medium [43]. In this situation, if the gradient in the source function is high, to get the accurate results, the entire system has to be divided into a large number of area and volume elements and radiative exchanges have to be found iteratively requiring very high computational time. In case of irregular geometries, even with homogeneous absorbing-emitting medium, large number of exchange areas are to be found out [89].

Further, assumption of isotropic nature of both the volume radiosity and surface radiosity, restricts application of zone method only to diffuse/isotropic enclosure/medium [90, 91]. Introduction of anisotropic scattering makes the method still more critical. So far not much work has been reported with anisotropic scattering [89].

Over the last few decades, efforts have been made towards the improvements in this method. Limited results have been reported to enhance the applicability of zone method by coupling the momentum and energy equations [107, 108, 113]. Steward and Tennakore [107] coupled this method with momentum and energy equations in modeling a combustor by considering two different grid schemes, one for radiation part and the other for fluid flow and temperature field. Smith et al. [113] and Sistino [108] coupled the zone method with the momentum and energy equations for combined radiation-convection problem in a cylindrical duct with absorbing, emitting and isotropically scattering medium. Yuen and Takara [91] modified the zone method with introduction of scattering and reflecting exchange factors. They tested the improved scheme in the presence of absorbing, emitting and anisotropically scattering medium in a 3-D Cartesian enclosure.

1.3.4 Flux Method

Compared to the zone method and the MCM, flux method has been widely employed in solving radiative transfer problems associated with combustion. This is due to its simplicity and ease in application. In this method, RTE is converted to a set of partial differential equations which are amenable to simultaneous solution of the equations governing the transport of mass, momentum, species and energy.

In this method, angular distribution of the intensity field is approximated by a set of uniform intensity angular regions [114, 115]. The integro-differential form of the equation of transfer is averaged over each of the finite angular regions to result in a set of flux equations.

Different multi-flux methods are obtained depending on the number of discrete directions considered. If the entire solid angle is divided uniformly into 2, 4 and 6 divisions, the result is two-flux, four-flux and six-flux methods. The two-flux method (Fig. 1.2) is the simplest of all the multi-flux meth-

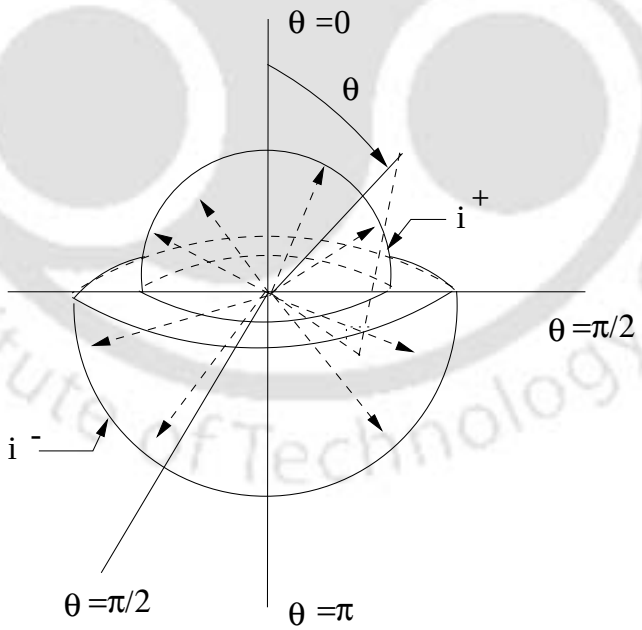

Figure 1.2: Approximation of intensities in two-flux method.

ods. This method has independently been described by Schuster [116] and Schwarzchild [117]. They applied two-flux approximation to the radiative exchange in planar absorbing-emitting medium. Subsequently, Richer and Quack [118], Lowes et al. [119] and Verma [120] developed more accurate four-flux method (Fig. 1.3). Siddal and Selçuk [121] and Patankar and Spalding [122] have reported even more accurate six-flux method. For higher accuracy, Sasse et al. [123] combined the features of zone method with six-flux method. They reported the resulting hybrid method to be highly accurate and computationally efficient. Abramzon and Lisin [124] have presented a general analysis for the flux method in 3-D Cartesian enclosure. They have shown that many other flux methods described in literature can be obtained from this general formulation. Selçuk [125, 126] describes evaluation of multi-dimensional flux methods for combustion chambers. Further, its application has been extended to non gray as well as inhomogeneous medium by Spuckler

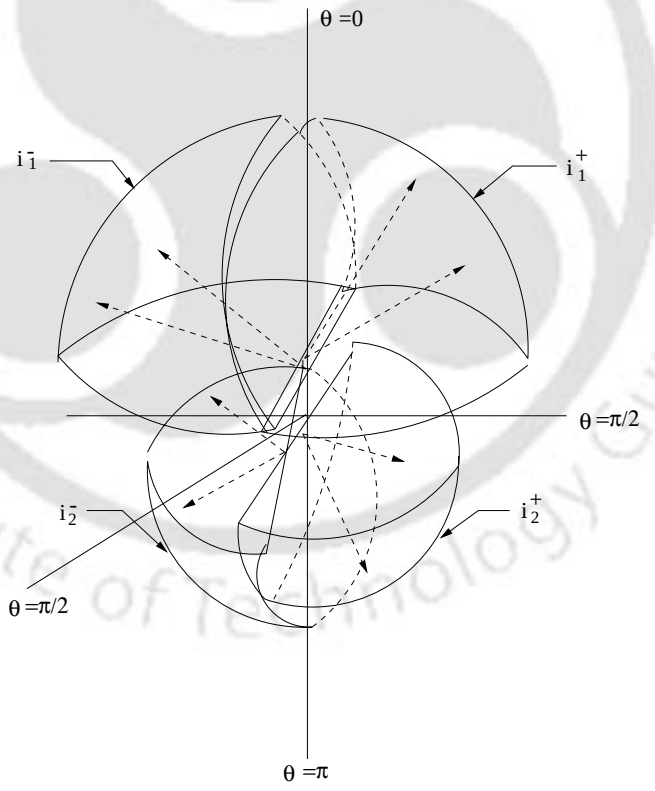

Figure 1.3: Approximation of intensities in four-flux method.

and Siegel [127].

In flux method, Demarco and Lockwood [128] and Lockwood and Shah [114, 129] approximated the radiant intensity distribution by

$$i = A_1\eta + A_2\zeta + A_3\beta + B_1\eta^2 + B_2\zeta^2 + B_3\beta^2 \tag{1.22}$$

where A's and B's are spatial coefficients and η, ζ and β are direction cosines with respect to the three principal axes. Khalil et al. [115] and Lockwood and Shah [129] presented the validation studies of this method. Applicability of multi-flux methods in practical engineering problems are limited by three major drawbacks as outlined by Viskanta and Menğuç [43].

- There is no coupling between radial and axial fluxes. This makes the RTE unrealistic.
- Approximation of the intensity distribution, from which the flux equations are obtained, is arbitrary.
- Model equations can not correctly approximate highly forward scattering situation, even though theoretically it is feasible.

Properties of multi-flux method have been inherited by methods like discrete transfer method, finite volume method, discrete ordinate method etc. The disadvantages of the multi-flux method cited above are absent in these methods.

1.3.5 P_N Approximations

The P_N approximations or spherical harmonics method (SHM) provides approximate solutions of arbitrarily high order. This is achieved by transforming the RTE into a set of simple partial differential equations. In this method, angularly dependent intensity field is expressed in a series approximation.

This method was first proposed by Jeans [31] in his work on radiative transfer in stars. Earlier, SHM was mostly used in atmospheric science [31] and neutron

transport [32]. In case of pure radiative transfer studies, SHM was applied to 1-D Cartesian enclosure by Chandrasekhar [25] and Kourganoff [130]. Details on this method are available in [27–29].

In P_N approximations, intensity is expressed by a series of spherical harmonics [29, 43].

$$i_\lambda(x,y,z,\theta,\phi) = \Sigma_{n=0}^{N}\ \Sigma_{m=-n}^{n} A_{n,\lambda}^{m}(x,y,z) Y_n^m(\theta,\phi) \tag{1.23}$$

with

$$\begin{aligned} Y_n^m(\theta,\phi) &= (-1)^{\left(\frac{m+|m|}{2}\right)} \times \\ &\left[\frac{2n+1}{4\pi}\frac{(n-|m|!)}{(n+|m|!)}\right]^{\frac{1}{2}} P_n^{|m|}(\cos\theta)\exp(im\phi) \end{aligned} \tag{1.24}$$

where Y_n^m are the spherical harmonics and P_n^m are associated Legendre polynomials. Depending upon the order of approximation, it is termed (i.e., N=1, 2, 3) as P_1, P_2 and P_3 approximations respectively. The applications of this method to various class of problems are reported in [131–146].

One positive aspect of P_N approximations is the conversion of the governing integro-differential RTE to a set of simple partial differential equations. The differential form of the RTE makes P_N approximations compatible with the grid requirements of the momentum and energy equations associated with real life problems. The weakness of P_N approximations is that the lower order approximations are accurate only for optically thick medium [43]. Accuracy in P_N approximations slowly improve for higher order approximations while mathematical complexity of the problem increases extremely rapidly [43]. Even order approximations produce inaccurate results and usually they cancel out in formulations. As P_N approximations are tedious and cumbersome [43], errors can easily result during long derivations [134, 140, 141]. For ease of derivation, hence, most of the works reported so far are based on P_1 and P_3 approximations.

Higenyi and Bayazitoglu [131, 132] applied P_1 approximation to Cartesian as well as cylindrical enclosures containing gray medium. Ratzell lll and How-

ell [136] produced results for absorbing, emitting and scattering medium confined in 2-D rectangular enclosures. Their analysis involved P_1 approximation. Menğuç and Viskanta [140, 141] have given the general formulations of P_1 and P_3 approximations for absorbing, emitting and anisotropically scattering medium in 2-D Cartesian, finite cylindrical as well as 3-D Cartesian enclosures. Ou and Nan [134] formulated a generalized P_N approximation for multi-dimensional enclosures. Cotta et al. [137] introduced reflecting boundary conditions in P_N approximations. Liu et al. [147] have analyzed the effect of anisotropy on radiative transfer in 2-D rectangular enclosure using P_1 approximation. Their results compare well with higher order DOM used by Kim and Lee [143]. Karp and Petrack [138] have given a comparative study of SHM and DOM for azimuthally dependent intensity calculations. Kamiuto et al. [145] further applied P_1 approximation for solution of inverse scattering problems.

In conjugate problems, P_1 approximation has been used by Ratzell lll and Howell [135], Ratzel lll et al. [148], Ahluwalia and Im [133] and Hariss [144]. Hartung and Hassan [146] applied modified diffusion approximation to practical problems such as radiative transport around axisymmetric blunt body vehicles. P_1 approximation does not yield accurate results in low optical thickness situations (optical thickness below 1) [43]. To make it work for low optical thickness range, Modest [76] has developed modified differential approximation and improved differential approximation.

The treatment of anisotropic scattering by P_N approximations has made it useful in modeling combustion systems using coal, where anisotropic scattering is an important factor. The anisotropic scattering has been modeled using various types of phase functions. To solve radiative transport problems in 3-D Cartesian enclosure with anisotropically scattering medium, Menğuç and Viskanta [140] have used the delta-Eddington phase function in P_3 approximation.

1.3.6 Discrete Ordinate Method

The discrete ordinate method (DOM) is considered a standard solution technique in the field of astrophysics [25] and neutron transport [33, 46, 149]. Most recent fundamental developments in this method is in nuclear science and radiative transfer studies [150, 151].

In this method, angular distribution of intensity, at any point in the enclosure, is represented by a discrete set of intensities spanned over the entire solid angle of 4π. Any quantity that involves the integral of intensity is estimated by an angular quadrature scheme. For example, irradiation $G(\vec{r})$ is expressed as

$$G(\vec{r}) = \int_{\Omega=4\pi} i(\vec{r}, \hat{s})\, d\Omega = \Sigma_{i=1}^{M}\, w_i\, i_i(\vec{r}) \tag{1.25}$$

where in Eq. (1.25), w_i are the quadrature weights and M is the total number of discrete directions and $\vec{r}$ is the position vector at which RTE is calculated.

The accuracy of DOM strongly depends on the choice of angular quadrature scheme. The most popular quadrature scheme in use is S_N method [149]. In this method, the factor N is always even and number of discrete directions are specified to be $M = N(N+2)$.

DOM has been implemented in Cartesian enclosures by Fiveland [151] and Kim [152]. It has been successfully used for 2-D and 3-D Cartesian enclosures with anisotropically scattering medium by Fiveland [151, 153–155], Fiveland and Jessee [156], Jamaluddin and Smith [157], Jamaluddin and Fiveland [158] and Truelove [159, 160]. The method has been extended to cylindrical enclosures by Vaillon et al. [161, 162], Jamaluddin and Smith [163, 164], Jendoubi and Kim [165] and Wu and Liou [166]. Wang and Bayazitoglu [167] have reported application of DOM for 1-D non gray planar medium. In multi-dimensional enclosures, Fiveland and Jamaluddin [168] have applied DOM for non gray medium.

Lewis and Miller [46] presented S_4 approximation to be slightly more accurate than P_3 approximation. But, major drawback of the S_N method is the presence of ray effects and false scattering [46, 169, 170]. Pessoa-Filho and Thynell [170],

Chai et al. [171] and Pasini and Casteliano [172] claim that ray effects arise due to the approximation of the angular distribution of radiation by a set of discrete ordinates. Under this circumstances, radiation can be lost if it does not fall into one of the discrete ordinate directions. Unless an infinite number of directions are used, ray effects can not be totally eliminated. Also, as the single scattering albedo increases, the radiation field becomes more isotropic and the ray effects become less noticeable. However, with increasing single scattering albedo and/or enclosure optical thickness of the medium, the convergence rate may become very slow [43]. The false scattering effect arises due to the spatial discretization. The false scattering occurs once the spatial discretization is performed over domains where the intensity or its slope is discontinuous [170]. Fraction of radiant intensity at a spatial location and at a particular direction propagate falsely to another spatial location in the same direction. To arrest this false propagation, various investigators employed Fredholm integral form of RTE [55, 173, 174].

DOM has been modified by various researchers. Liu et al. [175] introduced a spatial discretization scheme for prediction of primitive variables (radiation intensity) while Cheong and Song [176] developed a second order DOM to achieve better accuracy and less computational time.

The DOM has been applied for limited number of combined radiation and conduction problems as reported by Sakami et al. [177] and Kim and Baek [178]. Kim [152] applied S_N method for combined radiation-convection problems in Cartesian enclosures and justified his results with Mie-anisotropic scattering. Applicability of DOM for problems involving collimated radiation is reported in [152]. Computer time and memory requirements of this method are relatively high as compared to P_N approximation and zone method [179]. Theory of parallel processing has been attempted by Goncalves and Coelho [180] to reduce computational time in DOM.

1.3.7 Finite Volume Method

The finite volume method (FVM) was conceived by G. D. Raithby and reported by Raithby and Chui [181]. This method shares same philosophy as the finite volume technique currently used in predicting fluid flow and convective heat transfer. This method inherits some features of flux method and DOM.

In FVM, the inflow and outflow of radiant energy across the control volume faces are balanced with attenuation and augmentation of radiant energy within the control volume and the control angle. Total solid angle 4π steradians, is discretized into a finite number of discrete control angles in any convenient manner, depending on the problem being dealt with.

Numerous applications to FVM are reported in the literature [22,171,181–192]. Chui and Raithby [184] and Chai et al. [171] have provided results for 2-D Cartesian enclosures. Further, Kim and Baek [185] have used FVM to produce results for 3-D Cartesian enclosures. Chui et al. [183], Moder et al. [186] and Kim and Baek [187] have extended FVM to cylindrical geometries. All the test results have shown very good agreement with benchmark results. For the body fitted coordinates and for reducing computational time required in mesh generation, FVM has been used with non-orthogonal meshes [188–190]. Reported results by Baek et al. [188], Murthy and Mathur [189, 190] are in good agreement with the other methods. Using a Cartesian coordinate FVM, Chai et al. [171] have suggested a block-off-region procedure to model radiative transfer in irregular geometries. Further, this method has been successfully applied to translationally and rotationally periodic domains [191]. Lee et al. [22] applied this method for more complicated problems with coupled radiation-convection heat transfer around a circular cylinder in a cross flow. However, further study of this method is required to study the spectral effects, specular, partially specular as well as mix boundary conditions and variable thermo-physical properties of the medium.

Because of similarity in methodology, FVM can be called as a second generation DOM. Both methods converge increasingly slowly as the optical thickness

is increased due to the sequential nature of the solution algorithm [192]. Another similarity between these methods is that the spatial discretization scheme is same for both. However, angular discretization procedure for both of them differs. As discussed in the previous section, in DOM, a quadrature scheme is used to evaluate the integral, in contrast with the profile assumption and analytical integration being used in the FVM. Raithby [193] has discussed the major differences between FVM and DOM in the following lines:

1. The FVM is fully conservative (in medium as well as at enclosure walls). In case of non-Cartesian coordinate system, for loss of symmetry in ordinates, DOM often fails to predict correct information in on the boundaries.

2. The DOM does not ensure conservation in scattering. Conservation requires that none of the radiant energy scattered from solid angle Ω^j be lost. The DOM approximation of the scattered radiation from Ω^j into all directions is given by

$$\sigma_s \int_{4\pi} \int_{\omega_j} i(s^{'}, s) \frac{\phi(s^{'}, s)}{4\pi} d\Omega^{'} \, d\Omega = \sigma_s \, i_j w_j \left[\frac{1}{4\pi} \Sigma_k \phi(j,k) w_k \right] \tag{1.26}$$

   In case of isotropic scattering, $\phi = 1$, and Eq. (1.26) is satisfied by integral given by

$$\int_{4\pi} d\Omega = \Sigma_{j=1}^{J} w_j = 4\pi \tag{1.27}$$

   But it seems that in DOM, weights can not be found, in general, that satisfy the required conditions for anisotropic scattering. Special requirements to obtain discrete ordinate quadrature sets are discussed by Fiveland [155]. In case of FVM, such problem does not arise as the method employs the conservation of energy principle.

3. FVM is flexible in directional discretization making it compatible to CFD code. However, DOM is rigid in angular distribution.

1.3.8 Finite Element Method

Finite element method (FEM) is one of the promising methods for analyzing radiative transfer problems. This method has been described by Shih [194], Gallaghar [195] and Huebner [196]. FEM is widely used for structural, thermal, fluids, electro magnetics and other applications. In radiative heat transfer, application of FEM for radiative exchange between gray surfaces in absence of participating medium, dates back to the early sixties [8]. Presently, this method gained popularity for analyzing conjugate radiation, conduction and/or convection problems. This is owing to the fact that the FEM can provide a match between the computational grids of the radiation module and that of the conduction and/or convection modes of heat transfer. The most appealing feature of FEM is in handling the complex geometries [28, 194].

In [197–202], FEM has been applied to combined radiation, conduction and/or convection heat transfer problems. There boundary conditions with specified temperature as well as heat flux have been considered. Most of the reported FEM results are based on Galerkin finite element method, which requires evaluation of integral form of the RTE. This method can be considered as a sequence of three tasks. First, for a 2-D problem in Cartesian coordinates, the source function, say, $S(x, y)$, is approximated by a linear combination of piecewise local basis functions. Then a weak equation that requires less restrictive inter elemental continuity is derived. Finally, the physical coordinates are transformed into isoparametric coordinates so that algebraic functions are greatly simplified [194, 203]. FEM based on variational calculus has been proposed by Ritz [204].

Combined conduction and radiation heat transfer in 1-D Cartesian and cylindrical geometries have been analyzed by Fernandes et al. [199], Wu et al. [200] and Fernandes and Francis [201]. Pure radiation in a gray non-scattering medium confined in 2-D rectangular geometries were analyzed by Razzaque et al. [202]. They have reported high computational time and because of this, FEM is generally restricted to coarse elements [89].

To reduce the computational time, Tan [205] proposed a new scheme. However, derivation of the same is very complicated. Razzaque et al. [206] extended their earlier works [202] to combined problems with inclusion of conduction and obtained highly accurate results with finer elements. Sokman and Razzaque [207] included isotropic scattering to combined conduction-radiation problems with boundary heat flux conditions. Applicability of FEM to conjugate problems with boundary layer flow is reported by Utreja and Chung [208]. Chung and Kim [209] have reported solutions for 2-D flow of a radiatively scattering medium in a diverging/converging channels.

1.3.9 Ray Emission Method

The ray emission method (REM^2) is one of the latest developments in the field of radiative transfer [21, 210, 211]. It is the generalized numerical method for analyzing radiative transfer problems in participating medium. This method is an extension of the zone method. The method got versatility in application in finding view factors for specular and diffuse surfaces in absorbing, emitting and isotropically scattering medium with complex geometries [212].

In this method, angular discretization is done using numerous polyhedrons. Specular and diffuse surfaces are discretized with various polygons. To facilitate calculations, surface and volumetric radiation are expressed in terms of effective radiation areas A_i^R.

Intensity of radiation at any location $\vec{r}$ in the direction $\hat{s}$ can be expressed from radiative energy balance as [21, 210, 211] (Fig. 1.4).

$$\begin{aligned}\frac{di_\lambda(\vec{r},\hat{s})}{dS} &= -(\kappa_\lambda+\sigma_{s,\lambda})\, i_\lambda(\vec{r},\hat{s}) + \kappa_\lambda\, i_{b,\lambda}(T) \\ &\quad + \frac{\sigma_{s,\lambda}}{4\pi}\int_{4\pi} i_\lambda(\hat{r},\hat{s}')p_\lambda(\hat{s}'\rightarrow\hat{s})d\Omega \qquad (1.28)\end{aligned}$$

where κ_λ and $\sigma_{s,\lambda}$ are spectral absorption and scattering coefficients, respectively. $p_\lambda(\hat{s}'\rightarrow\hat{s})$ is a phase function from the direction $\hat{s}'$ to $\hat{s}$.

With reference to Fig. 1.4, the ray passing through the radiation element at-

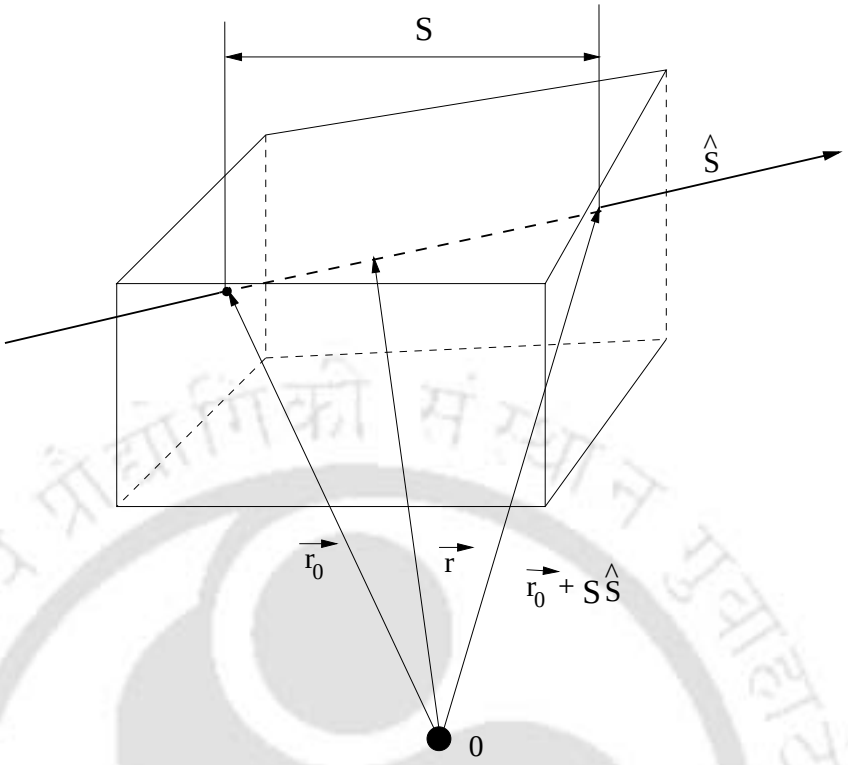

Figure 1.4: Attenuation of radiation ray along the direction $\hat{s}$.

tenuates and a part of it is scattered. The ray is separated into absorbed, scattered, and transmitted fractions. Further, scattered ray is assumed isotropic. As a result, third term in Eq. (1.28) is approximated as

$$\frac{\sigma_{s,\lambda}}{4\pi}\int_{4\pi} i_\lambda(\vec{r},\hat{s}')p_\lambda(\hat{s}'\rightarrow\hat{s})d\Omega \;=\; \frac{\sigma_{s,\lambda}}{4\pi}\int_{4\pi} i_\lambda(\vec{r},\hat{s}')d\Omega = \sigma_{s,\lambda}i_\lambda^D \quad (1.29)$$

where, i_λ^D is the average diffuse radiant intensity and it takes care of both emitted and scattered radiant intensities. Introducing the extinction coefficient $\beta_\lambda = (\kappa_\lambda + \sigma_{s,\lambda})$, Eq. (1.28) is rewritten as

$$\frac{di_\lambda(\vec{r},\hat{s})}{dS} = \beta_\lambda[-i_\lambda(\vec{r},\hat{s}) + (1-\omega)i_{b,\lambda}(T) + \omega i_\lambda^D] \quad (1.30)$$

Solution of Eq. (1.30) along $\hat{s}$ direction is

$$\begin{aligned} i_\lambda(\vec{r}_0 + S\hat{s},\hat{s}) \;&=\; i_\lambda(\vec{r}_0,\hat{s})\exp(-\beta_\lambda\,\bar{S}) \\ &\quad +[(1-\omega)i_{b,\lambda}(T) + \omega i_\lambda^D][1-\exp(-\beta_\lambda\bar{S})] \end{aligned} \quad (1.31)$$

where $\bar{S}$ is the average thickness of radiation element in direction $\hat{s}$. It is defined as

$$\bar{S} = \frac{V}{A(\hat{s})} \tag{1.32}$$

where V and $A(\hat{s})$ are volume and projected surface area normal to $\hat{s}$, respectively.

Radiant energy emitted from the element i, either volume or surface, in participating medium can be approximated as

$$dQ_{j,i,\lambda}(\hat{s}) = A(\hat{s})[(1-\omega^D-\omega^S)i_{b,\lambda}+\omega^D i_\lambda^D][1-\exp(-\beta_\lambda \bar{S}_i)]d\Omega \tag{1.33}$$

Considering a volume or surface element i, the general form of Eq. (1.33) is

$$dQ_{j,i,\lambda}(\hat{s}) = A_i(\hat{s})[(1-\omega^D-\omega^S)i_{b,\lambda}+\omega^D i_\lambda^D] \times [1-\exp(-\beta_\lambda \bar{S}_i)]d\Omega \tag{1.34}$$

where, $\beta_\lambda \bar{S}_i >> 1$ for a surface element and $\omega^S = 0$ for a volume element. Integrating Eq. (1.34) over all solid angles, the spectral radiative energy from radiation element i is given by

$$Q_{j,i,\lambda}(s) = [(1-\omega^D-\omega^S)i_{b,\lambda}+\omega^D i_\lambda^D] \times \int_{4\pi} A_i(\hat{s})[1-\exp(-\beta_\lambda \bar{S}_i)]d\Omega \tag{1.35}$$

In the literature [21, 210, 211], for verification of the present model, the case of a participating medium with $\beta_\lambda \bar{S}_i >> 1$ has been considered. In absence of the concave surfaces, the average projection area becomes one-quarter of the total surface area. The value of $[1-\exp(-\beta_\lambda \bar{S}_i)]$ becomes unity for $\beta_\lambda \bar{S}_i >> 1$. Then the integral in Eq. (1.35) simplifies to

$$\int_{4\pi} A(\hat{s})[1-\exp\left(-\beta_\lambda \bar{S}\right)]d\Omega \rightarrow \int_{4\pi} \frac{A_T}{4} d\Omega = \pi A_T \tag{1.36}$$

where A_T is the total surface area. Now, an effective radiation area A^R is introduced as

$$A^R = \frac{1}{\pi}\int_{4\pi} A(\hat{s})[1-\exp(-\beta_\lambda \bar{S}_i)]d\Omega \tag{1.37}$$

A^R is identical to the surface area for a surface element in which the reversed side is not considered. For the case of $\beta_\lambda \bar{S}_i >> 1$, A^R is expressed as

$$A^R \rightarrow \frac{1}{\pi}\int_{4\pi} A(\hat{s})\beta_\lambda \bar{S}_i d\Omega = 4\beta_\lambda V \tag{1.38}$$

Finally, the rate of radiation energy emitted and isotropically scattered by the radiation element can be expressed in generalized form as

$$Q_{J,i,\lambda} = \pi[(1 - \omega_i^D - \omega_i^S)\, i_{b,\lambda} + \omega_i^D\, i_\lambda^D]\, A_i^R \tag{1.39}$$

In the present method, both the surface and volume elements are taken care by introducing the generalized form of the Eqs. (1.34) and (1.35). Numerical integration of Eq. (1.31) is simplified by introducing the effective radiation area A^R and average thickness $\bar{S}$.

Some of the advantages of this method are:

1. Both surface and volumetric radiations can be tackled by REM^2.
2. Unlike zone method, no distinction is needed for volume and/or surface elements.
3. This method can be used with the finite element method for the solution of combined radiation, conduction and/or convection problems [211].
4. REM^2 is easy to apply for complicated geometries.
5. This method is suitable for both supercomputers with vector processor and for computers with parallel processors [212].
6. It can be applied to real life problems. Maruyama and Aihara [18] applied REM^2 in Czochralski crystal growth furnace for precision heat transfer calculation of silicon growth and fusion generators [21].
7. In this method, there is substantial savings in computational time in comparison to MCM [213].

Although REM^2 is having lots of advantages, it also has some drawbacks. One of the drawbacks is the assumption of isotropic scattering. With this isotropic assumption, Maruyama and Guo [214] applied REM^2 in case of non gray and anisotropic medium in arbitrary configurations. They have reported 10-30% deviations in the values of heat flux and divergence of heat flux.

1.3.10 Discrete Transfer Method

Discrete transfer method (DTM) proposed by Shah [215] and Lockwood and Shah [216] is a ray tracing method, and is a combination of several methods. This method exhibits features of the zone method [105], flux method [125] and the MCM [71]. This method is numerically exact and geometrically flexible. Further, it can be used for solving conjugate radiation, conduction and/or convection heat transfer problems [217–219]. One of the important features of the DTM is that it is ideal for implementing on parallel computer architectures [220, 221].

In DTM, at any point in a given direction, angular distribution of intensity over the entire spherical space is done by solving directly the integral form of RTE. This is achieved by discretizing the entire spherical solid angle into finite number of sub-solid angles, all of equal sizes [215, 216, 218, 222, 223]. In each sub-solid angle, intensity is assumed isotropic but has different values in different sub-solid angles. In Fig. 1.5, a typical angular discretization of a hemispherical solid angle is shown.

In DTM, to get the heat flux information at any point in the solution domain, at the point of interest, intensities coming from the entire spherical space (4π steradians) are found and are integrated over the angular directions. For example, at any optical depth τ, heat flux due to a hemisphere of intensities is obtained by integrating the intensity i over the hemisphere.

$$\begin{aligned} q(\tau) &= \int_{\phi=0}^{2\pi} \int_{\theta=0}^{\frac{\pi}{2}} i(\tau,\theta,\phi)\cos\theta\sin\theta\, d\theta\, d\phi \\ &= \Sigma_{j=1}^{M}\Sigma_{i=1}^{N}\, i(\tau,\theta_i,\phi_j)\cos\theta_i\sin\theta_i\sin(\Delta\theta)\Delta\phi \end{aligned} \tag{1.40}$$

where θ and ϕ are zenith and azimuthal angles (Fig. 1.5) respectively, and for numerical integration, θ and ϕ are equally divided into M and N sub-divisions respectively. For evaluation of net heat flux, heat flux due to other hemisphere of intensities have to be found according to the above equation and vector sum of the two be taken.

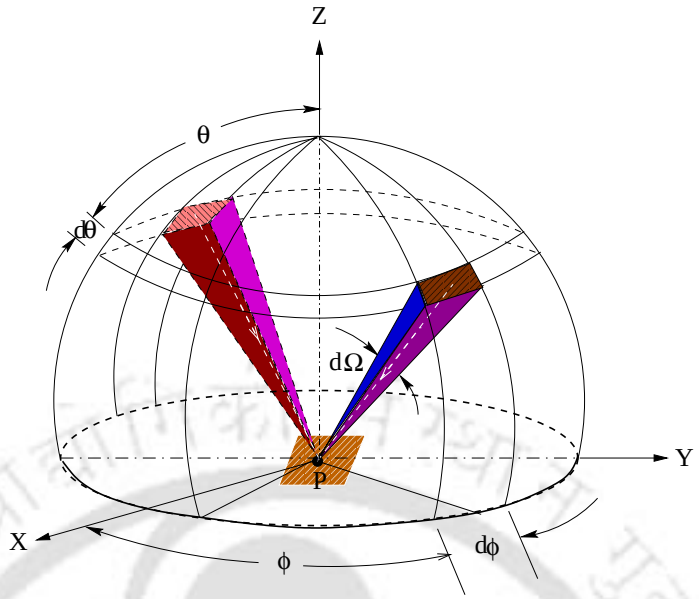

Figure 1.5: A hemisphere with representative rays.

In DTM, the incident radiation G is given by

$$\begin{aligned} G &= \int_{\phi=0}^{2\pi}\int_{\theta=0}^{\pi} i(\theta_i,\phi_j,\tau)\sin\theta d\theta\ d\phi \\ &= \Sigma_{j=1}^{M}\Sigma_{i=1}^{N}\ i(\tau,\theta_i,\phi_j)\sin\theta_i\sin(\Delta\theta)\Delta\phi \end{aligned} \tag{1.41}$$

In Eqs. (1.40) and (1.41), intensity is given by

$$i_{n+1}(\tau,\theta,\phi) = i_n\exp(-\tau) + S(\tau,\theta,\phi)\Big[1-\exp(-\tau)\Big] \tag{1.42}$$

Above definition of intensity is based on the fact that the distance between points n and $n+1$ along the ray direction is small enough and the source function S given by the following equation can be assumed constant over the path-leg.

$$S(\tau,\theta,\phi) = (1-\omega)i_b + \frac{\omega}{4\pi}\int_{\phi=0}^{2\pi}\int_{\theta=0}^{\pi} i(\tau,\theta^{'},\phi^{'})\ p((\theta^{'},\phi^{'})\rightarrow(\theta,\phi))\sin\theta^{'}\ d\theta^{'}\ d\phi^{'} \tag{1.43}$$

where $p\left((\theta^{'},\phi^{'})\rightarrow(\theta,\phi)\right)$ is the phase function. In case of linear anisotropic scattering, phase function takes the form

$$p(\theta^{'},\phi^{'})\rightarrow(\theta,\phi) = 1 + a_1\cos\theta\cos\theta^{'} \tag{1.44}$$

where a_1 is the anisotropy factor. Source function in terms of non-dimensional heat flux and non-dimensional incident radiation can be written as

$$S(\tau,\theta,\phi) = (1-\omega)i_b + \frac{\omega}{4\pi}\left(G(\tau) + \pi\ a_1 \cos\theta q(\tau)\right) \tag{1.45}$$

To find intensity at any point in the enclosure, intensity is traced from the boundary of the enclosure. Thus in Eq. (1.42), when $n+1$ is next to the boundary and $n\ (=0)$ is on the boundary, the boundary intensity $i(0)$ is found from

$$i(0) = \frac{\epsilon_w \sigma T_w^4}{\pi} + \frac{(1-\epsilon_w)}{\pi}\int_{\phi=0}^{2\pi}\int_{\theta=0}^{\frac{\pi}{2}} i(\theta)\sin\theta\cos\theta d\theta d\phi \tag{1.46}$$

where ϵ_w and T_w are the emissivity and temperature of the bounding wall respectively.

DTM has been successfully applied to a large class of problems [217–224]. Further, this method has also been incorporated in commercial computational fluid dynamics solvers such as FLUENT, FLOW3D, CFX, etc. For simple problems in 1-D and 2-D Cartesian enclosures, DTM has been reported to give accurate results [215]. However, with increase in complexity in problem (geometry, scattering etc), results are obtained at the expense of large number of rays. Under radiative equilibrium situation, DTM has been found to be non conservative [222]. Coelho and Carvalho [222] and Cumber [224] have suggested some improvements to the DTM.

1.3.11 YIX Method

The YIX method has been developed by Tan and Howell [225]. This method is used to solve the exact integral equations with the help of distance-angular integration form of the RTE. By constructing and prestoring the numerical integral formulae for distance integral for appropriate kernel functions, this method eliminates the time consuming evaluations of space integral kernels in formal computation. Further, when the number of elements in the system is large, the resulting coefficient matrix is sparse. Thus considerable time or storage can be saved. Compared to zone and MCM, this method takes less computational time and memory storage [226].

Tan and Howell [225] used YIX method for calculation of radiative transfer in multi-dimensional geometries with inhomogeneous participating medium. Hsu and Tan [227] demonstrated workability of YIX method for combined mode problems with L-shaped enclosures with inhomogeneous and non gray participating medium. Hensen and Malalasekera [228] compared MCM results with YIX method for similar kind of problems. Further, Hsu et al. [226], Hsu and Tan [227] and Hsu and Farmer [229] demonstrated results for non gray, inhomogeneous participating medium with isotropic and anisotropic scattering.

In YIX method, accuracy of integration is strongly affected by distribution of the integration points in the distance quadrature and the order of the discrete ordinate set or number of angular quadrature points. Due to limited number of angular quadrature points, ray effect is predominant in YIX method. In high optical thickness region, radiation behaves like a isotropic diffusion process, hence less number of angular quadrature sets are sufficient to accurately predict radiation in optically thick region. In low optical thickness limits, medium behaves like transparent one, imposing requirement of large number of angular quadrature sets to capture radiation accurately. With the same number of quadrature sets, both for optically thick and thin regions, ray effect becomes severe in this method [226, 230]. Hsu et al. [230] proposed an adaptive angular quadrature sets to mitigate the ray effects. They reported that the modified method can handle collimated incident radiation as well. This promising method, however, requires further study to establish its generality to tackle radiative transfer problems.

1.3.12 Other Methods

In literature, there are a few other methods available for the solution of radiative transfer problems. As not much work has been reported on these methods, before some definitive evaluations can be made, they require further investigations. However, for the sake of completeness, they are included herein.

Taniguchi et al. [231] proposed the heat ray method and they applied the same to multi-dimensional enclosure with absorbing-emitting medium. This method

is based on Bouguer's law and yields radiant energy absorption distribution in non-isothermal enclosures containing combustion gases. Compared to zone and MCM, this method is found to be more accurate and less time consuming when the radiative properties of the system are constant [231]. However, its application to conjugate problems and arbitrary geometries are not yet reported.

Shih and Chen [232] have proposed discretized intensity method. They applied this method for the solution of combined radiation-conduction problem in 2-D enclosures with absorbing-emitting medium. Further, Shih and Ren [233] applied this method to 2-D recirculating radiative flows. Further application of this method has not been reported.

1.3.13 Limitations of the Existing Methods

From the aforementioned discussions, it is evident that no single radiation method can be regarded most suitable for all types of problems. Some methods have been used frequently, while others that appeared promising at one time, are no longer being used on a regular basis. In the earlier section, the existing methods have been discussed at length. Some of the limitations of the existing methods are discussed herein.

MCM is the most flexible method, but it has been well known for statistical errors and its appetite for computational time. Both MCM and zone method have been found to have limited applications in combined radiation, conduction and/or convection problems. DOM, DTM, FVM, REM^2 and YIX method have been reported to be prone to ray effects. Except MCM and perhaps the zone method, none of the methods work accurately in low optical thickness range. The SHM and S_N methods are popular for accuracy. However, P_3 approximation does not always provide adequate accuracy and S_N method can not easily be extended to irregular domain. Further, higher order SHM is very complicated to formulate. The REM^2 method can not correctly handle anisotropic scattering. In summary, most of the methods discussed, suffer from

one or more of the following limitations:

1. Difficulty in applications with multi-dimensional and complex geometries.
2. Incompatibility in solution philosophy and grid requirement with fluid flow, conductive and/or convective heat transfer analysis.
3. Inaccurate results in low optical thickness range.
4. Complexity in formulations.
5. Inability to handle non uniform radiative properties.
6. Difficulty in treating spectrally dependent radiative properties.
7. Inadequate treatment of anisotropic scattering.
8. Insufficient accuracy.
9. Unacceptably high computational cost.

Because of the aforementioned points, constant research have been undergoing either to bring improvements to the existing methods or to develop new numerical methods. This very fact has been one of the motivating factors for the present research.

1.4 A Promising New Method

Literature survey conducted from the available sources shows the need for a promising method for the analysis of problems involving thermal radiation with participating medium. The collapsed dimension method (CDM) has been found to be one such method. It is one of the ray tracing methods. The development of this method has got some ideas from the works of Shih and co-workers [232,234] on discretized intensity method. Some light on CDM was

thrown by Blank [235]. Detailed developments on CDM have been made by Mishra [236] and have been reported in [237–239]. In [236], CDM has been termed as effective intensity approach.

CDM seems to be promising in terms of problem formulation, computational efforts and accuracy of results. In this, 3-D radiative information is mapped into 2-D plane in terms of effective intensity and optical thickness coefficient (OTC). At any point in the solution domain, all the actual intensities contained in the discrete plane are represented by an effective intensity. Thus, the physical effect produced at a point under consideration is the same by an effective intensity and an infinite number of actual intensities, all focussed at the same point. In this way, in CDM, a circle of effective intensities contained in the solution plane represents a sphere of actual intensities.

Since effective intensities are contained only in the 2-D plane, unlike actual intensities which are identified with two angles, i.e,. polar and azimuthal angles, they are identified with only one angle, i.e, planar angle. Because of dependency of the effective intensity on one angle, mathematical expressions for radiative heat flux, incident radiation, divergence of radiative heat flux, boundary intensity, etc., are very much different than those being used in other methods. However, absence of one of the angular dimensions from the analysis brings a lot of positive features in CDM. For example, in a 2-D geometry in which solution domain is a 2-D plane, conduction and convection can be approximated as 2-D phenomena. But because of 3-D nature of radiation, at any point in the 2-D solution domain, intensities have to be traced in the 3-D space. In CDM, ray tracing is very simple. All effective intensities are confined to the 2-D solution domain only. Thus, this method is computationally efficient. For the problems tested so far, the method has been found to work for the entire range of optical thickness situations, including very low optical thickness. This method has been successfully applied to anisotropic situations in 1-D and 2-D Cartesian enclosures. However, its applications to other test cases have not been reported.

OTC plays a vital role in collapsing 3-D radiative information to the 2-D plane

in terms of effective intensities. In earlier works on CDM, it has been felt that the OTC is geometry restrictive, i.e., OTCs found for the Cartesian geometry can not be applied to other geometry. Further, it has also not been indicated how the OTCs, which have been found for gray and homogeneous medium, would be applied for non-gray and inhomogeneous medium. Its application to conjugate problems has not been dealt with. Since in this method, effective intensities are defined only in the 2-D solution plane, its applicability to a 3-D enclosure, where the solution domain is a 3-D space, has not been studied. Hence, need was felt to explore the applicability of this method for all the aforementioned situations.

1.5 Objective and Scope of the Present Work

The present work aims at further development of CDM for more general situations. The objective and scope of the present work are the following:

- Providing mathematical foundation of the CDM for general multidimensional enclosures.

- Elimination of the constraints on the usage of the OTCs found for 1-D and 2-D Cartesian geometries and development of procedures for using the same for all types of enclosures.

- Extension of OTCs found for gray and homogeneous medium to non gray and inhomogeneous medium.

- Validating the above developments by solving sample problems (pure radiative as well as conjugate problems) in various types of geometries with different types of medium and boundary conditions.

1.6 Thesis Outline

This thesis is organized in eight chapters. Detailed description of CDM is incorporated in Chapter 2. This chapter contains basic assumptions, general formulations and solution procedure for solving radiative transfer problems in general enclosures containing participating medium.

Chapter 3 deals with the application of CDM to finite (2-D) arbitrary enclosures, such as, square, L-shaped and quadrilateral enclosures. Application of CDM to 3-D Cartesian enclosures has also been taken up in this chapter.

In Chapter 4, applicability of CDM to cylindrical and concentric cylindrical enclosures is discussed. Both infinite (1-D) and finite (2-D) cylindrical enclosures are considered. Radiative transfer problems with both temperature and flux boundary conditions are taken up. A typical cylindrical furnace problem has also been discussed in this chapter. For all the the test cases, results are verified with that available in the literature.

Applicability of CDM to combined radiation-conduction mode problems is considered in Chapter 5. Here the problem of combined radiation-conduction in 1-D concentric cylindrical enclosure has been solved and validated with the results available in the literature.

Chapter 6 deals with the application of CDM to non gray and inhomogeneous medium. Test cases for 1-D planar medium are validated with DTM and other existing methods.

In Chapter 7, a new angular discretization scheme has been suggested. The new scheme is used to enhance the accuracy and reduce the computational effort of CDM. The suggested discretization scheme has been tested over 1-D Cartesian enclosures.

Finally, Chapter 8 summarizes the conclusions and future scope of the present work.

Chapter 2

Collapsed Dimension Method

2.1 Introduction

It has been discussed in Chapter 1 that the analysis of thermal radiation is very difficult in the presence of participating medium. This difficulty is because of 3-D nature of radiation and a large number of associated independent variables, viz., three spatial, two angular and one spectral variables. In the presence of other modes of heat transfer, such as conduction and/or convection, formulations and solutions further become complicated. In such situations, even if conduction and/or convection can be modeled as 1-D or 2-D phenomena, radiation has to be still considered a 3-D phenomenon.

In any thermal problem involving radiation, there is no way to get rid of spatial and spectral variables. For example, if geometry under consideration is a 2-D one, heat flux and temperature variations have to be found in the 2-D solution domain. Further, if radiation is wavelength dependent, for correct analysis, spectral effect has to be considered. However, the angular dimensions appearing in the analysis are only because of the nature of radiation. As far as the end results, such as heat flux and temperature, are concerned, the angular dimensions have nothing to do. Heat flux is a vector quantity, and its direction is always fixed and temperature is a scalar quantity. Keeping above

points in mind, to obviate the difficulties due to the angular dimensions, the basic objective of majority of the methods has been to make radiation less and less dependent on angular dimensions. This very fact is clear from the literature review made in Chapter 1.

Except MCM and the zone method, all other existing methods handle 3-D nature of radiation by different forms of angular discretization schemes [43, 125,153,184,187]. MCM is a statistical method in which history of the bundles of photons is traced as they travel through the enclosure. Zone method, on the other hand, approximates spatial rather than directional behavior by breaking up an enclosure into finite, isothermal sub volumes.

With angular discretization of radiative intensity, numerical procedure becomes easy and subsequently its solutions are found with less effort. However, because of such approximations, most of the numerical methods exhibit their limitations in terms of computational effort and accuracy. Further, all methods can not be applied to all type of problems. Hence, the need for new methods still exists.

In the present work, CDM [235–240] is considered for the solution of problems involving thermal radiation with participating medium. This particular method has been chosen because of its attractive features such as applicability over entire range of optical thickness, ease in formulations and accurate prediction of heat flux and temperature, etc. In this method radiative information from 3-D space is mapped into a 2-D plane. Hence, formulations in this method are entirely different from rest of the methods.

Effective intensity and OTC are two important parameters involved in CDM. Effective intensity is defined in the 2-D plane and is a quantity analogous to the 3-D intensity. OTC is a parameter which enables translation of 3-D radiative quantities to a 2-D plane. To differentiate between the two types intensities, hence onwards, the intensities in conventional approach will be referred as real intensities. Further, radiation rays in conventional approach and CDM will be referred as real rays and effective rays respectively.

In the present chapter, CDM is revisited. Its methodology is explained and formulations are presented for the solution of radiative transfer problems in general enclosures.

2.2 The Method

As shown in Fig. 2.1, consider an elemental area dA contained in the $X-Y$ plane. The point P of this elemental area will be receiving radiation from all the directions. To find out the radiative energy falling on the elemental area from the top, we need to consider a hemisphere of real rays centered at point P. One such real ray QP is shown with a thick arrow. Let an elemental solid angle $d\Omega$ be constructed around the ray QP. If θ and ϕ are zenith (polar/cone) and azimuthal angles, respectively, then the elemental solid angle dΩ is equal to $\sin\theta d\theta d\phi$. The real intensity $i(\theta,\phi)$, is defined as the radiative energy

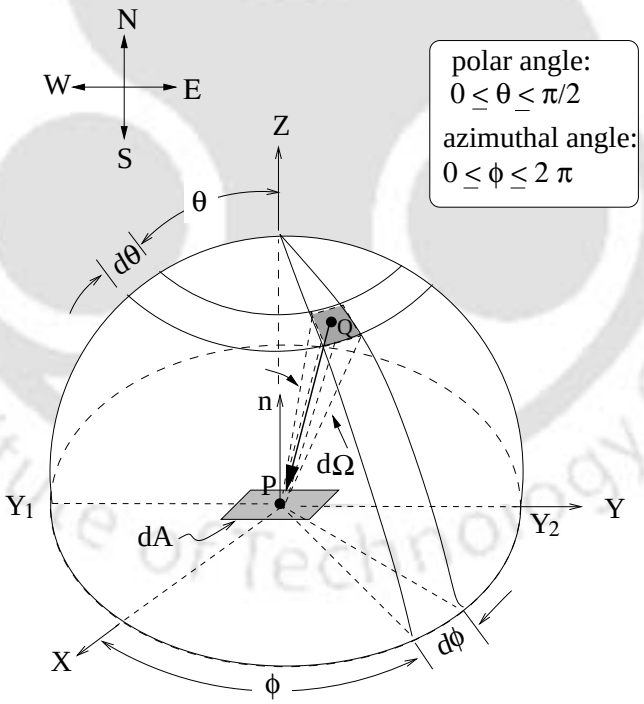

Figure 2.1: A hemisphere of south bound real rays with real intensity $i(\theta,\phi)$ focussed at the center P of the elemental area dA.

flow rate per unit area normal to the ray direction per unit differential solid angle [25–30].

$$i(\theta,\phi) = \frac{\delta\dot{Q}}{dA_P\, d\Omega} = \frac{\delta\dot{Q}}{(dA\cos\theta)\sin\theta d\theta d\phi} \tag{2.1}$$

where $\delta\dot{Q}$ is the differential energy flow rate through the elemental area dA and dA_P is the projection of this area on a plane normal to the ray direction (θ,ϕ).

In the present work, for the sake of convenience, we will associate terms like south bound, north bound, east bound and west bound with radiation rays, hemisphere and heat flux, etc. For example, in Fig. 2.1, the elemental area over the $X-Y$ plane is facing the north direction. This face of the elemental area is receiving radiation from the entire hemisphere above it. Then all the rays within the hemisphere converge to a point on the elemental area and such rays are identified as south bound rays. Similarly, heat flux due to all south bound rays will be termed as south bound heat flux. Likewise, depending upon the orientation of the elemental area, the rays can be east bound, west bound or north bound.

In order to find the heat flux due to a hemisphere of intensities, we have to integrate a hemisphere real intensities $i(\theta,\phi)$ over the solid angle $\Omega = 2\pi$. For example, to find the heat flux at point P of the elemental area dA in Fig. 2.1, we have to integrate the south bound hemisphere of real intensities $i(\theta,\phi)$ over the solid angle $\Omega = 2\pi$, as per the following equation.

$$q_{s,p} = \int_{\phi=0}^{2\pi}\int_{\theta=0}^{\pi/2} i(\theta,\phi)\sin\theta\cos\theta\; d\theta\; d\phi \tag{2.2}$$

To understand the concept of effective intensity, let us consider Fig. 2.2. As shown in the figure, south bound hemisphere is centered at point P of the elemental area dA. The base of the hemisphere coincide with the elemental area dA and lies on the $X-Y$ plane. The diameter Y_1Y_2 of the hemisphere coincide with the Y axis. The Z axis is normal to the elemental area dA. The hemisphere is now divided into a number of longitudinal planes. Each plane has an infinitesimal angular thickness depicted by the shaded regions

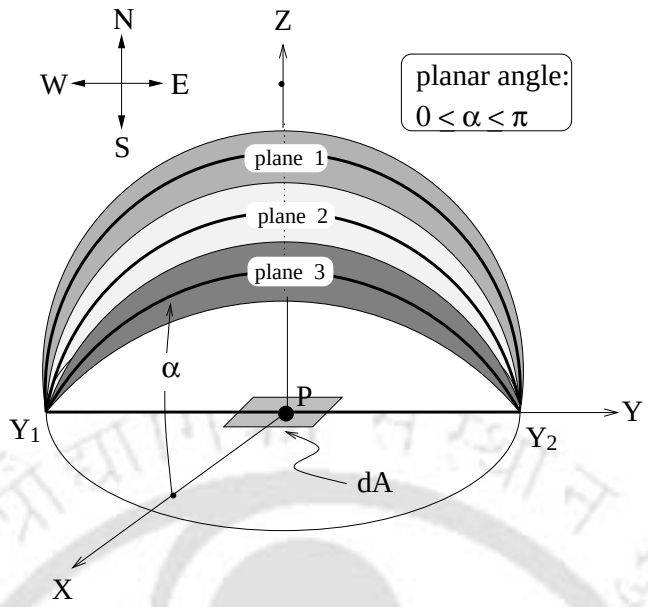

Figure 2.2: Discretization of hemisphere into longitudinal planes.

around the plane and contains an infinite number of real intensities $i(\theta, \phi)$. The bases of all such planes are coincident with Y_1Y_2. These longitudinal planes are termed as **discrete planes**. In this figure, three such discrete planes are shown. Orientation of discrete plane is measured from the surface of the elemental area. The angle representing the position of the discrete plane from the elemental area is called the **planar angle** α.

In Fig. 2.2, south bound hemisphere has been discretized in such a way that the discrete planes are along Y_1Y_2. The way in which the hemisphere has to be discretized is problem specific - it is mainly governed by the orientation of the **solution plane**. To make this point clear, let us consider a rectangular (2-D) control volume ABCD in Fig. 2.3. This control volume is infinite in the Y-direction. Let us consider n, s, f and b as the central points on the north, south, front and the back faces of the control volume. These points are designated as **control volume surface central points** (CVSCPs). Radiative information are desired at these points. A plane which passes through these points is termed as the **solution plane**.

For determination of south bound heat flux through the north face of the con-

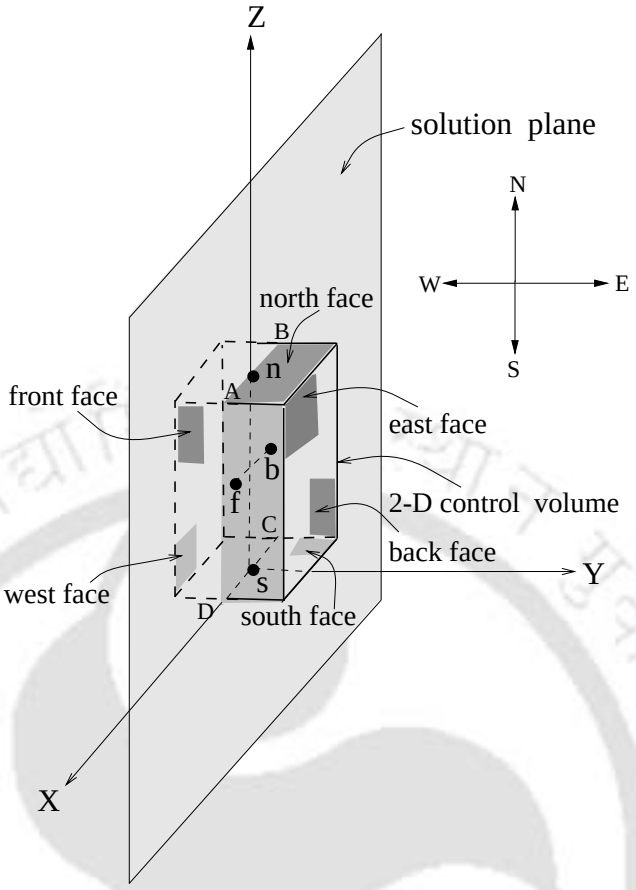

Figure 2.3: Solution plane and the 2-D control volume.

trol volume at the CVSCP n, we need to consider a hemisphere of south bound rays centered at CVSCP n (Fig. 2.4). In this figure, north face corresponds to elemental area dA and CVSCP n corresponds to point P. The hemisphere is discretized in such a way that each discrete plane is normal to the solution plane. Thus, for point n, we have to discretize the hemisphere in such a way that the base of the discrete planes will coincide with the Y axis, in other words, will be normal to the solution plane.

Figure 2.4a presents a representative plane of the discretized hemisphere. This discrete plane makes an angle α as measured from surface of the elemental dA. The plane has an angular thickness $d\alpha$. This is more clearly seen from Fig. 2.4b. It gives a view of the discrete plane when it is seen from the Y axis

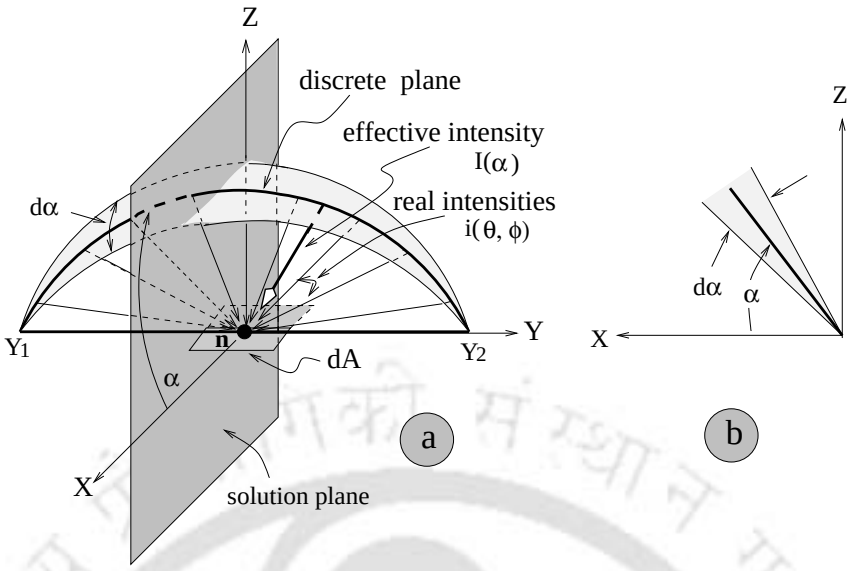

Figure 2.4: (a) Real intensities $i(\theta, \phi)$ and an effective intensities $I(\alpha)$ in a representative discrete plane, (b) Discrete plane when viewed from Y axis towards $X - Z$ plane.

towards the $X - Z$ plane.

In actuality, a discrete plane contains infinite number of real intensities $i(\theta, \phi)$, each focussed at point n, as shown in Fig. 2.4a. At this stage, in CDM [236], it is assumed that in each discrete plane, it is possible to define an effective intensity $I(\alpha)$ which stores the information of all the real intensities $i(\theta, \phi)$, lying in this discrete plane and focussed at the point of interest n and it produces the same effect as that by a conglomeration of real intensities of that plane. This effective intensity is shown with bold arrow in Fig. 2.4a. The physical significance of this assumption is that it should be possible to translate the effect of a plane of real intensities in terms of a single effective intensity. Since we are finally interested in reducing 3-D radiative problem to a 2-D problem in the 2-D solution plane, this kind of translation from a plane of real intensities to a single effective intensity will be useful only if this effective intensity lies on the solution plane. This essentially mean that effective intensity must lie along the intersection of the discrete plane and solution plane. This vital point is illustrated in Fig. 2.5.

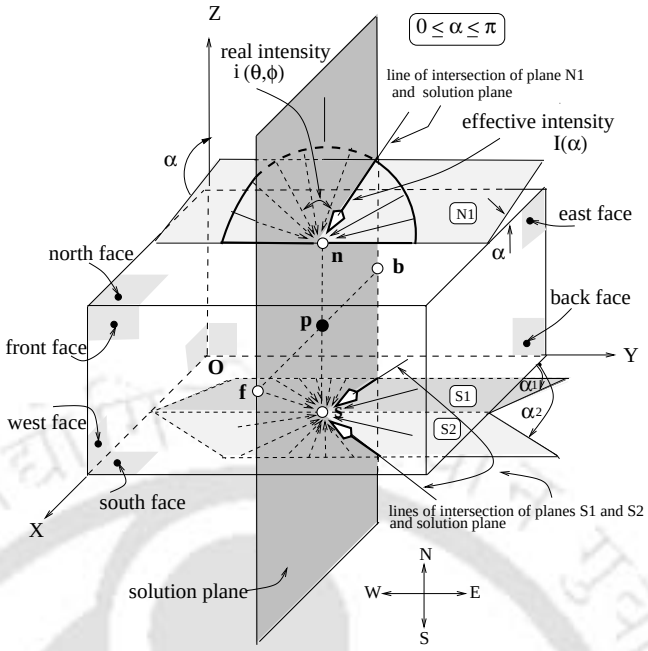

Figure 2.5: Angular location of the effective intensities in the solution plane.

In Fig. 2.5, a 2-D control volume about point P is shown. Here X and Z dimensions are finite and Y dimension is infinite. CVSCPs at north, south, front and back faces are represented by n, s, f and b respectively. The solution plane normal to the north, south, front and back faces of the control volume has been shown passing through four CVSCPs. If we are to find south bound heat flux at CVSCP n, we will have to consider a hemisphere of south bound rays and discretize it into longitudinal planes perpendicular to the solution plane as described earlier. One such discrete plane N_1, making an angle α with $X-Y$ plane, is depicted in the figure. For the sake of convenience, angular thickness of the discrete plane has not been shown. Some token real intensities $i(\theta,\phi)$ lying in this plane N_1 are also shown. As per CDM, the equivalent of all these real intensities is to be a single effective intensity $I(\alpha)$ lying in both the discrete and solution plane. This criterion is satisfied only if the effective intensity $I(\alpha)$ lies along the line of intersection of the discrete plane and the solution plane. Thus angular location of effective intensity $I(\alpha)$ in a discrete plane is given by the angular orientation of line of intersection of the discrete plane and the solution plane.

The effective intensity $I(\alpha)$ (shown with bold arrow) will have the same effect at point n as all the real intensities $i(\theta, \phi)$ in this discrete plane focussed at the point n. Similarly, at CVSCP s, calculation of north bound heat flux can be done by considering a hemisphere of north bound real intensities $i(\theta, \phi)$ centered at s and discretizing the hemisphere in a similar manner into discrete planes. Fig. 2.5 shows two such discrete planes S_1 and S_2 at angle α_1 and α_2 respectively with south surface of the control volume. These discrete planes contain north bound real intensities focussed at CVSCPs. Corresponding effective intensities at the intersections of these discrete planes and solution plane are shown with bold arrows.

From the foregoing discussions, it is clear that at any CVSCP, say n, corresponding to the south bound hemisphere of real intensities focussed at n, there will only be a south bound semi circle of effective intensities $I(\alpha)$ focussed at n and contained in the solution plane. Similarly, corresponding to the north bound hemisphere of real intensities focussed at point n, there will only be a north bound semi circle of effective intensities $I(\alpha)$ focussed at n and contained in the solution plane. This way, in CDM, 3-D radiative information are translated to a 2-D solution plane in terms of effective intensities.

As in CDM, effective intensities are defined only in the 2-D solution plane, unlike real intensities, only one angle, viz., planar angle α is sufficient to identify the effective intensity. Corresponding to a hemisphere of real intensities $i(\theta, \phi)$ ($0 \leq \theta \leq \pi/2$ and $0 \leq \phi \leq 2\pi$), in CDM, there will be a semi circle of effective intensities with planar angle α in the range $0 \leq \alpha \leq \pi$.

In actuality, in a semi circle, there will be an infinite number of effective intensities corresponding to an infinite number of discrete planes of the hemisphere. But in actual analysis, we will be dealing with a finite number of effective intensities. Thus each effective intensity is assumed to have its uniform influence over some angular span corresponding to the angular thickness of the discrete plane. For example, in Fig. 2.6, over a semi circle, seven representative effective intensities have been shown, and each intensity is shown acting over some angular span. Here, each effective intensity corresponds to a discrete plane and

the shaded angular sections represents the thickness of the respective discrete plane.

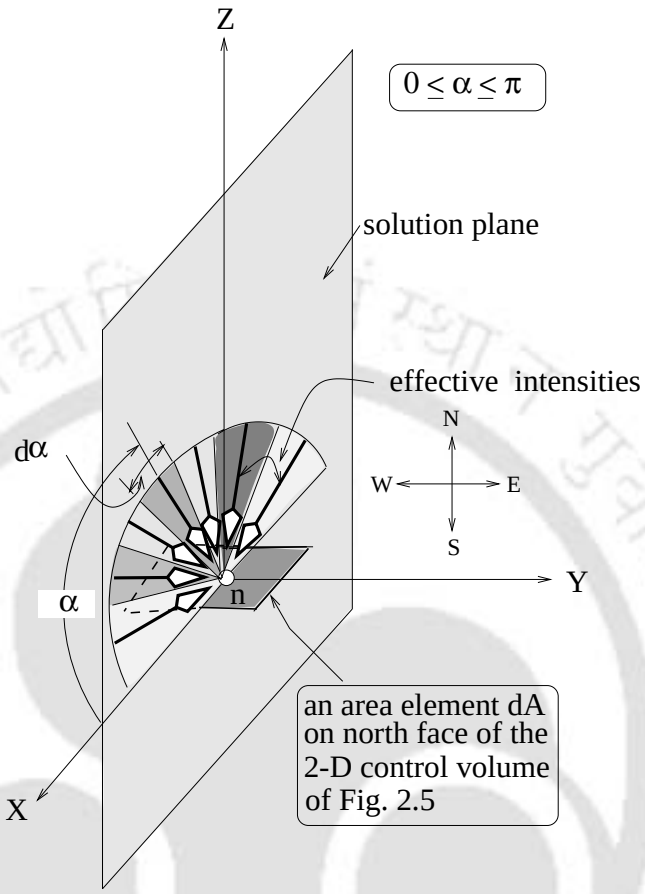

Figure 2.6: Some representative south bound effective intensities spanned over $0 \leq \alpha \leq \pi$.

It has been mentioned before that the radiative information (radiative heat flux herein) at any point in CDM and that in the conventional approach will be the same. Noting well the confinement of all the effective intensities in the 2-D solution plane, we can define effective intensity as energy flow rate per unit area normal to the ray direction α per unit differential planar angle. Mathematically,

$$I(\alpha) = \frac{\delta \dot{Q}}{dA_P \, d\alpha} = \frac{\delta \dot{Q}}{dA \, \sin\alpha \, d\alpha} \tag{2.3}$$

where, $\delta \dot{Q}$ is the differential energy flow rate and dA_P is the projected area on

a plane normal to the effective intensity.

Following above definition of the effective intensity, the expression for south bound heat flux, in CDM is given by

$$q_{S,P} = \int_{\alpha=0}^{\pi} I(\alpha) \sin\alpha \, d\alpha \tag{2.4}$$

The effective incident radiation $G^{'}$ is given by

$$G^{'} = \int_{\alpha=0}^{2\pi} I(\alpha) \, d\alpha \tag{2.5}$$

2.3 Optical Thickness Coefficient

In CDM, apart from the effective intensity, the other most important parameter controlling the method is the OTC. In fact, OTC scales the radiative properties from a 3-D domain into a 2-D solution plane. In this section importance of OTC, its method of calculation and evaluation for different geometries have been discussed.

Determination of heat flux and temperature at any location strongly depends on the optical depth τ that the intensities encounter. These quantities are the integrated effects of intensities (real intensities in conventional approach and effective intensities in CDM). To arrive at a specific location, intensities travel different geometric lengths. As a result, optical depth encountered by each intensity will be different. In CDM, all the real intensities $i(\theta, \phi)$ in a discrete plane are replaced by an equivalent effective intensity $I(\alpha)$ which is contained in the discrete plane as well as in the solution plane. Hence, information about the optical depths of all the real intensities are to be taken care by an equivalent optical depth to be encountered by the effective intensity. This is achieved by OTC.

As discussed in [236], OTCs for a given set of radiative parameters are found by comparing heat flux by CDM with that of a reference method for 1-D planar medium. The reference method can be experimental or exact numerical

method. Mishra [236] has taken exact method to be the reference method. Further, in the derivation of OTCs, he has assumed that radiative properties such as extinction coefficient β and scattering coefficient σ_s are constant and uniform and are wavelength independent.

Analytic expression of heat flux in CDM contains OTC η as an unknown variable (right hand side of Eq. (2.7)). Thus by equating the expressions of heat flux in CDM and the reference method, for a given set of radiative parameters, OTCs can be evaluated. For instance, for 1-D planar medium, the general expression of heat flux from both exact [29] and CDM [236] at a location would provide the same result. Keeping this very fact in mind, heat flux expressions for absorbing, emitting and anisotropically scattering media in radiative equilibrium are equated.

$$\Psi_{exact} = \Psi_{CDM} \tag{2.6}$$

or,

$$1 - 2\int_0^{\tau_L} \Phi(\tau^{'})E_2(\tau^{'})d\tau^{'} + (\frac{a_1\omega}{2})\Psi\int_0^{\tau_L} E_3(\tau^{'})d\tau^{'} = 1 - \Sigma_{m=1}^{N} b_m \int_0^{\frac{\tau_L\eta}{\sin\alpha}} \left(\phi(\tau^{'}) - \left(\frac{a_1\omega}{\pi}\sin\alpha\right)\Psi\right)\exp\left(\frac{-\tau^{'}\eta}{\sin\alpha}\right) d\left(\frac{\tau^{'}\eta}{\sin\alpha}\right) \tag{2.7}$$

where Φ is the non-dimensional emissive power, Ψ is the non-dimensional heat flux and E_2 and E_3 are the exponential integrals of order 2 and 3 respectively. In Eq. (2.7), b_m is the integral angle factor, which is given by

$$\Sigma_{m=1}^{N} b_m = \int_{\alpha=0}^{\frac{\pi}{2}} \sin\alpha \; d\alpha \tag{2.8}$$

where

$$b_m = \left|\sin\left(\frac{(2m-1)\pi}{2(2N-1)}\right) - \sin\left(\frac{(2m-3)\pi}{2(2N-1)}\right)\right| \quad m = 2, 3, \cdots N \tag{2.9}$$

In the above equations, N is the number of effective intensities over a quadrant of circle ($0 \leq \alpha \leq \frac{\pi}{2}$).

It can be mentioned here that the non-dimensional emissive power $\Phi(\tau)$ and the non-dimensional heat flux Ψ are the known quantities. These are known from

the reference method. For a given set of radiative parameters, for example, τ_L and $a_1\omega$, with the known values of Φ and Ψ, the only unknown in Eq. (2.7) is the OTC η. Therefore, Eq. (2.7) can be written as a function of OTC η.

$$f(\eta) = 0 \tag{2.10}$$

Equation (2.10) can be solved by any root finding technique. Mishra [236] has used Newton-Raphson method.

Following the above procedure, for both radiative and non-radiative equilibrium situations, OTCs for 1-D planar absorbing, emitting and anisotropically scattering gray and homogeneous medium are found. In earlier works on CDM [235–239], it has been argued that OTCs found for 1-D planar medium will be equally applicable to similar class of problems in multi-dimensional enclosures. This fact has been proved for some sample cases of pure radiative transfer problems in 2-D square enclosure [235, 238] containing gray and homogeneous medium.

Although it has been argued that OTCs found for 1-D planar medium would be applicable for multi-dimensional enclosures, in earlier works on CDM [235–239], no information was provided how OTCs would be applied to (a) finite and infinite cylindrical enclosures, (b) enclosures other than 2-D square enclosures like L-shaped, quadrilateral, etc, (c) 3-D enclosures. Further, OTC had been found and applied only for gray and homogeneous medium. Whether OTCs would have to be found afresh or how they would be applied for non gray and inhomogeneous medium, no thought had been given in any of the earlier works on CDM. Further, application of OTCs for combined mode problems were also not known.

In the present work, it has been found that the OTC found by Mishra [236] for 1-D planar gray and homogeneous medium, with some modifications can be applied to all class of problems - gray/non gray, homogeneous/inhomogeneous, pure radiative/conjugate modes, 1-D/multi-dimensional geometries. As OTCs found in [236] is the basis of all the developments presented in this work, the same are presented in Appendices A & B.

In Appendix A, OTC expressions are presented for radiative equilibrium situation. OTCs for non-radiative equilibrium situation have been presented in Appendix B.

2.3.1 Optical Thickness Coefficients for Arbitrary Enclosures

The expressions for OTCs presented in Appendices A & B are applicable to radiative transfer problems in 1-D planar and 2-D square enclosures containing gray and homogeneous medium. As discussed above, no criterion existed before for the evaluation of OTCs for cylindrical enclosures and other types of 2-D enclosures like L-shaped, quadrilateral, etc. and 3-D enclosures.

It has been mentioned in [236] that the task for generating OTC data and developing the expressions as presented in Appendices A & B, have been rigorous. It had been envisaged that OTCs for cylindrical and other non-regular geometries would have to be found through the procedures similar to that for the Cartesian enclosures. However, because of the complicated geometry, medium conditions and lack of reference data, the task of generating OTC for such situations seemed very difficult.

Seeing the complexities involved in the conventional approach, a free thought was given to use the already found OTCs for all types of situations - various types of enclosures and medium conditions. This has been done in steps. First OTCs were generalized for gray and homogeneous medium in multi-dimensional enclosures and then for gray and inhomogeneous medium and finally for non gray and homogeneous medium.

In the following paragraphs, generalization of OTCs for multi-dimensional enclosures with gray and homogeneous medium is described. For other cases, descriptions have been given in the respective places in the validation studies.

In case of gray and homogeneous medium, for a given radiative situation, the functional relationship of different radiative parameters, such as extinction co-

efficient β, scattering albedo ω, etc., with OTCs are compared. Effect of these radiative parameters on OTCs are then found out. This ultimately results in a suitable geometric factor. This geometric factor multiplied with the optical thickness (in a given co-ordinate direction) of the reference enclosure, yields the new value of optical thickness for the arbitrary enclosure. Corresponding to this new value of optical thickness τ_{arb}, OTC is calculated from the expressions of OTCs given for 1-D planar medium (1-D Cartesian enclosure) (Appendices A & B).

For example, under radiative equilibrium situation, consider radiative transfer in 1-D planar absorbing, emitting, linearly anisotropically scattering gray and homogeneous medium. The expressions of OTCs for this situation are given in Appendix A. A close look on these expressions reveal that OTCs under radiative equilibrium situation depend on the scattering albedo ω, anisotropy $a_1\omega$, extinction coefficient β or enclosure optical thickness τ_L. The enclosure optical thickness τ_L contains information about the geometry of the enclosure as well as the extinction coefficient β. A functional relation of different parameters with OTC is given in Eq. (2.11).

$$\eta = f(\omega, a_1\omega, \tau_L) \tag{2.11}$$

Suppose, two different enclosures having same boundary conditions contain gray and homogeneous participating medium. Say one of the enclosures is a 1-D Cartesian enclosure. It is considered as the reference enclosure. The other enclosure is of arbitrary shape, and is referred as the test enclosure. If participating medium is same for both the enclosures, the sole difference between the two systems is only in the geometry of the systems. The characteristic geometric length of the test enclosure is compared with that of the reference enclosure (1-D Cartesian enclosure). This gives a geometric factor. Multiplying this geometric factor with the optical thickness for the reference Cartesian enclosure in a given coordinate direction, a new value of optical thickness is found in the given co-ordinate direction. Corresponding to this new value of optical thickness and other radiative parameters like ω and $a_1\omega$, OTCs are calculated from the expressions given in Appendices A & and B.

For a general arbitrary enclosure, in a given coordinate direction at any geometric length l_{arb}, optical depth τ_{arb} in that co-ordinate direction is

$$\tau_{arb} = \beta \, l_{arb} \tag{2.12}$$

The same for a Cartesian enclosure at any geometric length l_{cart} is

$$\tau_{cart} = \beta \, l_{cart} \tag{2.13}$$

By comparing Eqs. (2.12) and (2.13) for extinction coefficient β, arbitrary optical depth τ_{arb} is written in terms of τ_{cart}, l_{cart} and l_{arb} as

$$\tau_{arb} = \left(\frac{l_{arb}}{l_{cart}} \right) \tau_{cart} \tag{2.14}$$

To find out OTC η_{arb} for an arbitrary geometry at any optical depth, OTC corresponding to τ_{arb} is found from the expressions for OTCs given in Appendices A & B. In Eq. (2.14), l_{arb}/l_{cart} is the geometric factor.

For example, for an infinite (1-D) concentric cylindrical enclosure with inner and outer radii r_1 and r_2 respectively, in the radial plane, geometric depth l_{concyl} is given by

$$l_{concyl} = r(1 - \rho) \tag{2.15}$$

From Eq. (2.14), the geometric factor for this enclosure is found to be

$$\text{geometric factor} = \frac{r(1-\rho)}{l_{cart}} \tag{2.16}$$

where $\rho = \frac{r_1}{r_2}$ is the radius ratio.

2.4 Radiative Transfer Equation

The RTE forms the basis for the quantitative study of radiative transfer in a participating medium. Physically, RTE is a mathematical statement of conservation of radiant energy along a pencil of ray. In the conventional approach, various authors have developed RTE utilizing concepts of geometric

optics [241], quantum mechanics [242] and Boltzmann equation of molecular theory of gases [243, 244] on microscopic level. In engineering applications, thermal radiation is best represented at macroscopic level. In the following sections, RTE as used in CDM [236] are presented.

2.4.1 Basic Assumptions

In deriving RTE in CDM, certain assumptions are made. They are the following:

1. Participating medium has been assumed to be in local thermodynamic equilibrium. Under such condition, emission of radiant energy is independent of the characteristics of incident radiation. Hence, in the absence of the local thermodynamic equilibrium, the emission term becomes much more complex [245]. But cases in which this condition does not prevail, are rarely encountered in thermal radiation [28, 30, 43] and such cases will not be considered in the present work.

2. Another major assumption in this analysis is the diffuse-gray assumption which eliminates all spectral effects and directional characteristics of emission, absorption and reflection of radiation. The adoption of this assumption neither implies that these effects are insignificant, nor that the CDM is conceptually incapable of accounting for them. Instead, this assumption simplifies the formulation and allows the results of the method to be validated against 'exact' solutions of benchmark cases which often ignore frequency dependence and directional emission, absorption or reflection.

3. State of polarization is neglected and participating medium is assumed to have constant refractive index.

4. Scattering is considered to be single, independent and inelastic throughout the analysis [30, 36, 246].

5. Radiative properties like absorption coefficient, scattering coefficient and scattering phase function are assumed to be known.

2.4.2 Radiative Transfer Equation in Collapsed Dimension Method

Figure 2.7 presents a general 3-D enclosure containing a participating medium with characteristics of absorption, emission and scattering. It has been discussed in Section 2.2 that 3-D nature of radiation is mapped into a 2-D solution plane. Let us consider an effective intensity $I(s_w, \alpha)$ emitted from enclosure boundary and traveling along a line of sight from s to $s+ds$ at an angle α on a solution plane $X-Z$. Here s_w corresponds to the value of the coordinate s at the wall. Different terms that contribute to the radiation as effective intensity travels from s to $s+ds$ can be written in terms of effective intensity as,

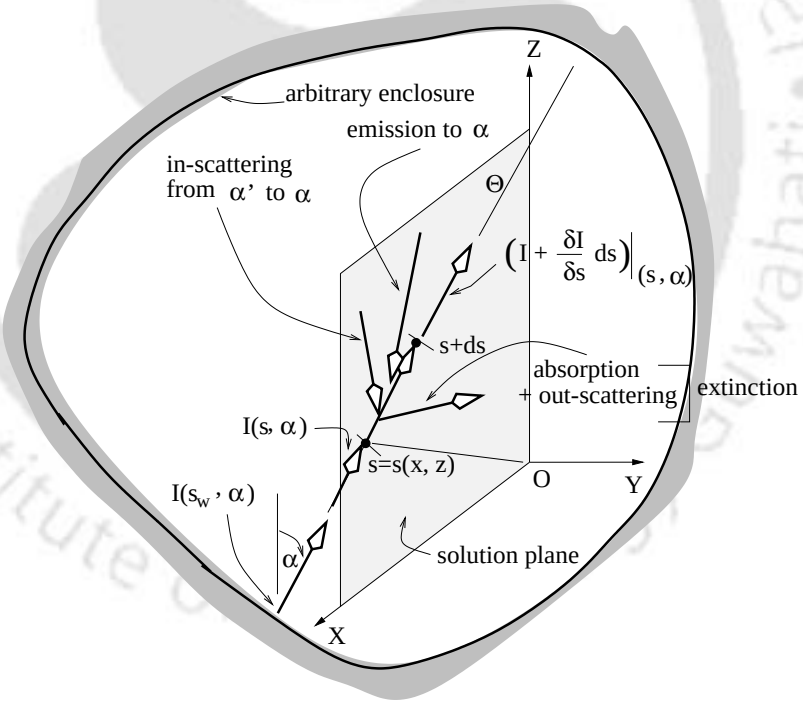

Figure 2.7: Radiative phenomena undergone by effective intensities on a 2-D solution plane in a general enclosure.

1. Differential change in effective intensity through ds is

$$= \frac{\partial I(s,\alpha)}{\partial s}\, ds\, dA \tag{2.17}$$

2. Loss of radiant energy by absorption

$$= -(\kappa\eta)\, I(s,\alpha)\, ds\, dA \tag{2.18}$$

3. Loss of radiant energy by out scattering

$$= -(\sigma_s\eta)\, I(s,\alpha)\, ds\, dA \tag{2.19}$$

4. Emission from medium in α direction

$$= -(\kappa\eta)\, I_b(s)\, ds\, dA \tag{2.20}$$

5. In-scattering from all directions $\alpha^{'}$ to α is

$$= \frac{1}{2\pi} \int_{\alpha'} p(\alpha^{'} \rightarrow \alpha)\, I(s,\alpha^{'})\, d\alpha^{'}\, ds\, dA \tag{2.21}$$

In Eq. (2.20), I_b is the blackbody effective intensity function. It is related to temperature by the following relation [236]

$$I_b = \frac{\sigma\, T^4}{2} \tag{2.22}$$

In Eq.(2.21), $p(\alpha^{'} \rightarrow \alpha)$ represents the scattering phase function and it gives the probability distribution of the energy scattered in direction α from effective intensity traversing in the elemental control volume from all other directions $\alpha^{'}$. Alternatively, $\frac{p(\alpha^{'} \rightarrow \alpha)\, d\alpha^{'}}{2\pi}$ represents the probability that an effective intensity traversing the elemental control volume at an angle $\alpha^{'}$ confined in the differential planar angle $d\alpha^{'}$ will get scattered in the direction α, confined by the differential planar angle $d\alpha$. This phase function must satisfy conservation of scattered energy leading to the following equation.

$$\frac{1}{2\pi} \int_{\alpha'} p(\alpha^{'} \rightarrow \alpha)\, d\alpha^{'} = 1.0 \tag{2.23}$$

In case of isotropic scattering, energy is equally distributed. In this situation, phase function takes the form:

$$p(\alpha^{'} \rightarrow \alpha) = 1.0. \tag{2.24}$$

Considering the energy balance (Eqs. (2.17-2.21)), the following relationship is obtained

$$\begin{aligned} \frac{dI(s,\alpha)}{ds} &= (\kappa\ \eta)\ I_b(s) - (\beta\ \eta)\ I(s,\alpha) \\ &\quad + \frac{\sigma_s \eta}{2\pi} \int_{\alpha'=2\pi} I(s,\alpha^{'})\ p(\alpha^{'} \rightarrow \alpha)\ d\alpha \end{aligned} \tag{2.25}$$

Equation (2.25) is generally expressed in terms of optical thickness τ. Optical thickness takes into account the radiative properties of the participating medium and geometric length or characteristic length (L) of the enclosure. Mathematically, optical thickness is given by,

$$\tau = \int_0^L (\kappa + \sigma_s) ds = \int_0^L \beta\ ds \tag{2.26}$$

where β is the extinction coefficient of participating medium and is given by

$$\beta = \kappa + \sigma_s \tag{2.27}$$

Here, κ and σ_s are absorption and scattering coefficients of the participating medium respectively. Physically, β gives the measure of radiant energy lost or extinct in a control volume due to absorption and scattering. The extinction coefficient takes care of both absorption and scattering coefficients. Further, both β and σ_s are easily measurable properties of the medium and they can be measured independently [2]. With known values of β and σ_s, absorption coefficient κ can be calculated from Eq. (2.27).

Further, as per assumption, scattering is considered single, inelastic and independent. Scattering albedo gives the relative measure of scattering to extinction of a participating medium. It is given by,

$$\omega = \frac{\sigma_s}{(\kappa + \sigma_s)} \tag{2.28}$$

Incorporating scattering albedo ω, Eq. (2.25) is written in terms of effective optical thickness $\tilde{\tau}$ as

$$\frac{dI(\tilde{\tau},\alpha)}{d\tilde{\tau}} = -I(\tilde{\tau},\alpha) - (1-\omega)I_b(\tau) + \frac{\omega}{2\pi}\int_{\alpha'=2\pi} I(\tilde{\tau},\alpha')p(\alpha' \rightarrow \alpha)\, d\alpha' \tag{2.29}$$

where $\tilde{\tau} = \tau\eta$.

It should be noted in Eq. (2.29) that the argument for I_b has been taken to be τ rather than $\tilde{\tau}$. This is for the reason that this argument is essentially indicative of the point in the solution plane at which I_b has to be computed. This argument has no other implication here. Similarly, for certain other quantities, like heat flux and emissive power, only τ will be used as argument.

The Eq. (2.29) is written in compact form as

$$\frac{dI(\tilde{\tau},\alpha)}{d\tilde{\tau}} + I(\tilde{\tau},\alpha) = S(\tilde{\tau},\alpha) \tag{2.30}$$

where, $S(\tilde{\tau},\alpha)$ is the source function and it gives a measure of emission and in-scattering in a control volume. It is expressed as

$$S(\tilde{\tau},\alpha) = (1-\omega)I_b(\tau) + \frac{\omega}{2\pi}\int_{\alpha'=2\pi} I(\tilde{\tau},\alpha')\, p(\alpha' \rightarrow \alpha)d\alpha' \tag{2.31}$$

Equation (2.30) is the differential form of RTE. In integral form, RTE can be expressed as

$$I(\tilde{\tau},\alpha) = I(0,\alpha)\exp(-\tilde{\tau}) + \int_0^{\tilde{\tau}} S(\tilde{\tau},\alpha)\exp\left(-(\tilde{\tau}-\tilde{\tau}')\right) d\tilde{\tau}' \tag{2.32}$$

If anisotropy is approximated by linear anisotropic phase function (Eq. (2.33)) [236]

$$p(\alpha' \rightarrow \alpha) = 1 + a_1 \sin\alpha\ \sin\alpha' \tag{2.33}$$

from Eqs. (2.4) and Eq.(2.5), the source function in terms of heat flux and effective incident radiation is given as

$$S = (1-\omega)I_b + \frac{\omega}{2\pi}\left[G' + a_1 \sin\alpha\ q_R(\tau)\right] \tag{2.34}$$

In the above equations, a_1 is the anisotropy factor. It represents the degree of anisotropy and it lies between -1 and +1. For $a_1 > 0$, the scattering is forward and for $a_1 < 0$ scattering it is backward. For isotropic scattering, a_1=0.

In non-dimensional form, Eq. (2.34) for the source function is expressed as

$$S^* = (1-\omega)I_b^* + \frac{\omega}{2\pi}\left[G'^* + 2a_1 \sin\alpha \Psi_R(\tau)\right] \tag{2.35}$$

If in a given direction α, optical path-leg between two points, say n and $n+1$ in the solution plane is small, effective intensity given in Eq. (2.32) can be written in non-dimensional form as

$$I_{n+1}^* = I_n^* \exp(-\tau\eta) + S^*(1-\exp(-\tau\eta)) \tag{2.36}$$

In arriving at Eq. (2.36) from Eq. (2.32), it is assumed that the source function given by Eq. (2.34) (or Eq. (2.35) in non-dimensional form) is constant over the optical path-leg between the points n and $n+1$.

In the above equations, effective intensity and source function have been non-dimensionalized as

$$I^* = \frac{I}{\frac{\sigma T_R^4}{2}} \tag{2.37}$$

$$S^* = \frac{S}{\frac{\sigma T_R^4}{2}} \tag{2.38}$$

Here T_R is the reference temperature. Depending upon the type of problem, T_R could be one of the bounding wall temperature or the medium temperature, if it is constant. For example, radiative equilibrium situation is considered as the boundary emission phenomena. In this case, medium temperature is unknown whereas bounding walls temperatures are known. Thus in case of radiative equilibrium, T_R is taken as one of the bounding walls temperature [215, 239, 247]. On the other hand, non-radiative equilibrium situation is associated with medium emission phenomena. In this situation, when we are solving only for the radiative part of the problem, medium is assumed at constant and uniform temperature [54, 151, 215, 239]. Thus in this case T_R is the medium temperature T_g. It should be further noted that in non-radiative equilibrium problems, conduction and/or convection modes have to be taken into account. When the problem is solved for the conjugate mode, medium temperature is not at all constant; it is unknown. In this situation, T_R has to be taken as one of the bounding walls temperatures [248–250]. In case of variable temperature

in gas, the highest temperature in gas is taken the reference temperature. Details of radiative and non-radiative equilibrium situations in the light of CDM is discussed in next section.

2.4.3 Boundary Intensity

In CDM, the ray tracing is always done from enclosure boundary. To start the ray tracing, information about boundary intensity is required. For a diffuse gray boundary (wall) with emissivity ϵ_w and temperature T_w, in CDM boundary intensity is given by [236]

$$I(0,\alpha) = \epsilon_w \frac{\sigma T_w^4}{2} + \frac{1-\epsilon_w}{2} \int_{\alpha=0}^{\pi} I(\alpha) \sin\alpha \, d\alpha \tag{2.39}$$

where first term on the right hand side represents emitted component of effective intensity and the second term is the reflected component of the effective intensity. It should be noted that because of the confinement of all effective intensities in the 2-D plane, the form of Eq. (2.39), is different than that found in other methods.

In non-dimensional form, Eq. (2.39) is written as

$$I^*(0,\alpha) = \epsilon_w \frac{T^{*4}_w}{2} + \frac{1-\epsilon_w}{2} \int_{\alpha=0}^{\pi} I^*(\alpha) \sin\alpha \, d\alpha \tag{2.40}$$

where T_R is the reference temperature.

For the boundary with imposed heat flux, the equation of the boundary intensity has been given in Chapter 4.

2.5 Divergence of Radiative Heat Flux

In a given control volume, RTE gives the conservation of radiative energy along a given ray direction. However, the equation for conservation of total energy (Eq. (1.1)) is based on net energy balance in a control volume. Radiation,

being 3-D phenomena, RTE can not fully describe radiative component in energy equation. To accommodate conservation of radiative energy in a control volume, it is necessary to integrate RTE over the control volume. This results in divergence of radiative heat flux. How the divergence of radiative heat flux enters in calculation in overall energy equation is already mentioned in Section 1.1. Divergence of radiative flux gives a measure of net radiative energy absorbed or emitted in a control volume. Important phenomena such as radiative and non-radiative equilibrium situations are perfectly described by divergence of radiative heat flux.

In CDM, divergence of radiative heat flux is given by [236]

$$\nabla \cdot \ q_R = (\kappa\eta) \left(2\pi \ I_b - G^{'}\right) \tag{2.41}$$

In Eq. (2.41), the first and the second terms on right hand side represent emitted and absorbed components of radiative energy respectively.

So long as the absorbed and emitted components of radiation are unbalanced, the quantity $\nabla \cdot q_R$ remains non-zero. As a result there is accumulation of radiative energy inside a control volume. This situation is termed as non-radiative equilibrium situation. Such a situation is generally encountered in most of the real life problems where radiation always accompany conductive and/or convective mode of heat transfer. Further, temperature of the participating medium, under this situation is medium to low. However, at relatively very high temperature, effect of radiation becomes significant. Under such situation, energy absorbed in a control volume is immediately released, without storing any radiative energy inside the control volume. This leads to a situation with $\nabla \cdot q_R$=0. Such a phenomenon is termed as radiative equilibrium. Hence under radiative equilibrium situation, temperature of the medium is determined using the divergence of the radiative heat flux.

$$I_b = \frac{G^{'}}{2\pi} = \frac{\sigma T_g^4}{2} \tag{2.42}$$

From the above equation, T_g is obtained as

$$T_g = \left(\frac{G^{'}}{\sigma\pi}\right)^4 \tag{2.43}$$

In non-dimensional form, Eq. (2.41) can be written as

$$\nabla \cdot \Psi_R = \eta(1-\omega)\left[\pi\, I_b^* - \frac{G'^*}{2}\right] \tag{2.44}$$

Here, non-dimensionalization is done by taking the reference temperature T_R as either the temperature of medium T_g (in case of isothermal medium) or as bounding wall temperature (for radiative equilibrium situation). $I_b{}^*$ is the non-dimensional blackbody intensity. It is given as

$$I_b^* = \left(\frac{T_g}{T_R}\right)^4 = \theta^4 \tag{2.45}$$

2.6 Solution Procedure

In this section, solution procedure for the radiative transfer problems in CDM has been described. The methodology has been described with reference to a 2-D Cartesian enclosure. The participating medium has been assumed absorbing, emitting and anisotropically scattering. The solution procedure described herein for 2-D Cartesian enclosure will very well be equally applicable to any other geometry.

Earlier, it has been described in Section 2.2 with reference to Fig. 2.5, that in CDM, at a given specific point, each effective intensity represents an infinite number of real intensities, $i(\theta, \phi)$, all acting in the same plane and all focussed on the same point. Thus the effect of all the real intensities in the discrete plane is, in effect, collapsed in terms of a single intensity, $I(\alpha)$. Theoretically, the infinite number of real intensities in a sphere should be transformed into a circle of an infinite number effective intensities in the 2-D solution plane. However, since we are dealing with the numerical simulations, only a finite number of effective intensities can be considered on the 2-D solution plane. Consequently, each effective intensity will be considered to act over an angle $\Delta\alpha$, as has been discussed in Section 2.2 with reference to Fig. 2.6.

Shown in Fig. 2.8 is a general 2-D gray Cartesian enclosure. Coordinate system considered has been shown in this figure. The enclosure has finite

dimensions L_x and L_z in X and Z directions, respectively, and it is infinite in Y direction. The solution domain is divided into an array of $N_x \times N_z$ control volumes. Thus, the surfaces of the enclosure are divided into N_x and N_z area elements in X and Z directions, respectively. For a typical control volume (i, j), nomenclature of CVSCPs is shown in this figure.

For a control volume (i, j), as shown in Fig. 2.8, the north, south, east and west CVSCPs are designated as $n(i, j), s(i, j), e(i, j)$, and $w(i, j)$, respectively. From the figure under consideration, it is clear that a CVSCP is common to two adjacent control volumes. For example, CVSCP n is common to the control volume (i,j) and $(i, j+1)$. Hence we can use the nomenclature, $n(i, j) = s(i, j + 1)$.

The non-dimensional heat flux $\Psi_{M,m}$ at the CVSCP m $(m = n, s, e, w)$ can be

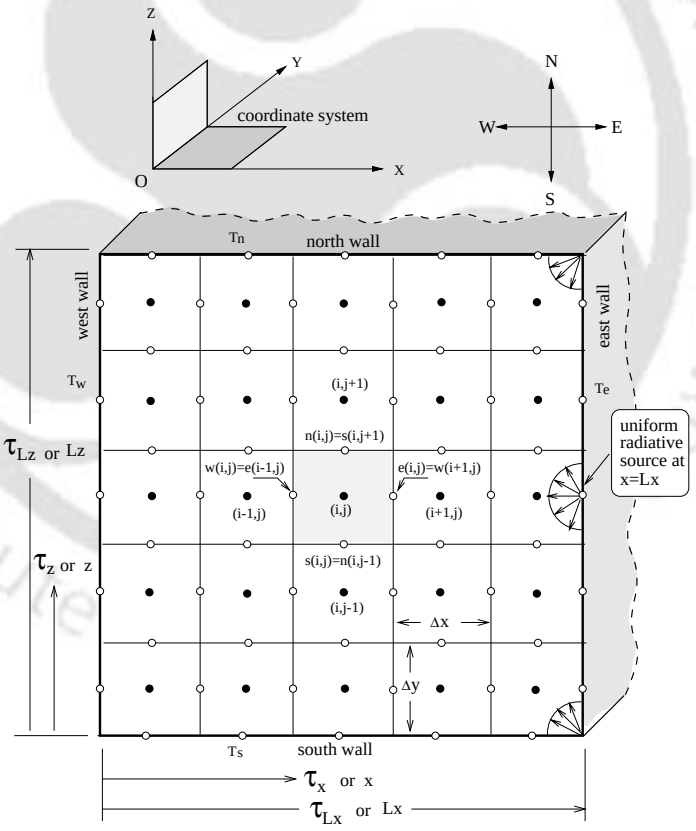

Figure 2.8: A 2-D Cartesian enclosure.

calculated by the numerical integration of Eq. (2.4) by considering the finite number of non-dimensional effective intensities $I^*(\alpha)$ incident on the CVSCP and contained within the semi circle corresponding to the general direction M ($M = N, S, E, W$). Thus Eq. (2.4), in non-dimensional form can be written as

$$\Psi_{M,m} = \frac{1}{2}\Big[\int_{\alpha=0}^{\pi} I^*(\alpha)\ \sin\alpha d\alpha\Big] = \frac{1}{2}\Big[\Sigma_{n=1}^{N} c_n I^*(\alpha_n)\Big]_{M,m} \tag{2.46}$$

where in general

$$c_n = \Big|\cos(\alpha_n + \frac{\Delta\alpha_n}{2}) - \cos(\alpha_n - \frac{\Delta\alpha_n}{2})\Big| \tag{2.47}$$

Here, $|.|$ indicates the absolute value, and the term $\Delta\alpha_n$ is the angle over which the n th effective ray, $I^*(\alpha_n)$ is acting.

The non-dimensional effective incident radiation, $G^{'*}$, at any CVSCP m is found from Eq. (2.5) as

$$G^{'*} = \Big[\int_{\alpha=0}^{2\pi} I^*(\alpha)d\alpha\Big]_m = \Big[\Sigma_{n=1}^{2N} I^*(\alpha_n)\Delta\alpha_n\Big]_m \tag{2.48}$$

where in the above equation, N is the number of effective rays over angle π.

Equations (2.46) and (2.48) have been obtained by non-dimensionalization of Eqs. (2.4) and (2.5) respectively. Here q and $G^{'}$ have been nondimensionalized as

$$\Psi = \frac{q}{\sigma T_R^4}$$

$$G^{'*} = \frac{G^{'}}{\sigma T_R^4/2}$$

At each CVSCP shown in Fig. 2.8, as per our nomenclature, there are two heat fluxes. For example, at the CVSCP $n(i,j)$, we have south bound heat flux due to south bound effective intensities coming to the CVSCP $n(i,j)$, $q_{S,n}$, and the north bound heat flux due to north bound effective intensities coming to the same CVSCP $n(i,j)$. Similarly at the CVSCP $s(i,j)$, we will have $q_{N,s}$ and $q_{S,s}$, and at CVSCPs $e(i,j)$ and $w(i,j)$, we will have $q_{E,e}$, $q_{W,e}$, $q_{E,w}$, $q_{W,w}$,

respectively. Each of these eight heat fluxes is obtained through appropriate integration of a semi circle of effective intensities, as per Eq. (2.32).

At any CVSCP, m, for determination of heat flux, $\Psi_{M,m}$ and effective incident radiation $G^{'*}$, as per Eqs. (2.46) and (2.48) respectively, we first need to know the magnitude of effective intensities reaching that point from various directions as per Eq. (2.32). In the finite difference control volume formulations, the magnitude of these effective intensities incident on each CVSCP from various directions can be found through the recursive use of Eq. (2.32) over the path traveled by a ray. This path is divided into a number of short legs and Eq. (2.32) is recursively integrated over each of these legs. If the path legs are kept small, it is reasonable to specify the source function $S(\tau(\alpha))$, given Eq. (2.31) as a constant equal to $S(\tau(\frac{\alpha}{2}))$- which is the value of the source function at the exact middle of the integration path leg $\tau(\alpha)$. Under this circumstances, Eqs. (2.35) and (2.36) are being used, in non-dimensional form, instead of Eqs. (2.31) and (2.32) respectively.

Further, source function at the mid-path location is found using the bilinear interpolation of the previously computed source values at four CVSCPs n, s, e, and w. In case of 1-D enclosure, source function at the desired mid-point location is found by taking the average of the source values at the two CVSCPs.

The integration of Eq. (2.36) is started at the boundary and is carried out over a short path leg of the ray originating at the enclosure boundary. In this case $I^*(0, \alpha)$ is the value of $I^*(\tau(\alpha))$ at the boundary and is known from the boundary conditions given by Eq. (2.40). By the integration of the first leg, the $I^*(\tau(\alpha))$ value at the end of this leg is obtained. This in turn, serves as the $I^*(0, \alpha)$ for the integration over the next path leg of the same ray. Thus by recursive use of Eq. (2.36), the $I^*(\tau(\alpha))$ values at all the concerned points along the path of the ray can be obtained. Here, $\tau(\alpha)$ is the optical thickness of the current path leg increment.

In calculation of effective intensity I^* in Eq. (2.36), value of OTC on the solution plane, along the ray direction under consideration is essential. These

OTC values are calculated depending on the nature of enclosure and radiative situation. The prestored OTC values are used to find optical path length $\tilde{\tau}$.

2.7 Summary

In this chapter, physics of the CDM has been described. All pertinent equations used in CDM have been provided. The generalization of OTC for general enclosures has been discussed. Solution procedure in CDM has been discussed with reference to a general 2-D gray Cartesian enclosure containing absorbing, emitting and anisotropically scattering medium. The formulations and solution procedures presented in this chapter are the basis of all the validation studies presented in subsequent chapters.

Chapter 3

Validation Studies: Cartesian Enclosures

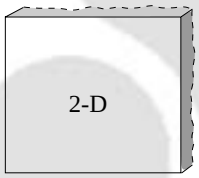

Square enclosure

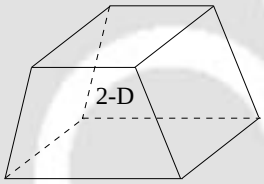

Quadrilateral enclosure

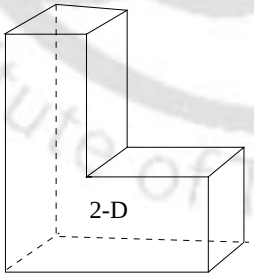

L-shaped enclosure

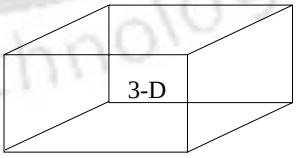

Cubical enclosure

3.1 Introduction

In the literature, considerable efforts have been directed towards the correct analysis of radiative transfer problems in multi-dimensional enclosures. This is because of its importance in many engineering applications, such as combustors, furnaces, heat exchangers, nuclear reactors, etc. Various numerical methods pertaining to the analysis of thermal radiation problems with participating medium in multi-dimensional enclosures are available. Crosbie and co-workers have developed exact solutions for 2-D and 3-D Cartesian enclosures with scattering medium [61–65]. Raithby and Chui [181], Chui and Raithby [184], Baek et al. [188], Murthy and Mathur [189] and Chui [184] have applied FVM for 2-D Cartesian enclosures with absorbing, emitting and scattering medium. Fiveland [151], Truelove [159], Jamaluddin and Smith [157] and Kim [152] have used DOM to treat radiative transfer problems in 2-D Cartesian enclosures. MCM has also been used extensively for radiative transfer problems in 2-D and 3-D Cartesian enclosures with participating medium [83, 90]. Sasse et al. [123] have proposed a hybrid six-flux/zone method to solve radiative transfer problem in rectangular enclosures. Ou and Kuo-Nun [134] have provided a generalized solution to multi-dimensional radiative transfer problems with participating medium. They employed SHM in their analysis. Ratzel lll and Howell [135, 136] have used P_N approximations for 2-D rectangular enclosures containing absorbing, emitting and scattering medium, while Menğuç and Viskanta [140] have used the same for 3-D Cartesian enclosures.

In this chapter, CDM is applied to radiative transfer problems in multidimensional enclosures. To test its applicability, this method has been applied to different types of enclosures, such as 2-D square, L-shaped and quadrilateral enclosures. Further, its applicability to 3-D Cartesian enclosure is also discussed.

For all the geometries considered in this chapter, participating medium has been assumed gray and homogeneous. Depending upon the availability of results in the literature, CDM results have been compared with the DTM,

FVM and MCM.

3.2 2-D Arbitrary Enclosures

In this section, radiative transfer problems in different types of 2-D enclosures, such as square, L-shaped and quadrilateral enclosures are considered. The gray and homogeneous participating medium is considered absorbing-emitting. Enclosure boundaries are assumed black and are at specified temperatures.

For the analysis of problems considered in this chapter, medium temperature T_g has been used as the reference temperature T_R. Thus the effective intensity I, source function S, heat flux q and incident radiation $G^{'}$ used in the solution have been non-dimensionalized respectively as

$$\begin{aligned} I^* &= \frac{I}{\frac{\sigma T_g^4}{2}} \\ S^* &= \frac{S}{\frac{\sigma T_g^4}{2}} \\ \Psi &= \frac{q}{\sigma T_g^4} \\ G^{'*} &= \frac{G}{\frac{\sigma T_g^4}{2}} \end{aligned}$$

Accordingly, non-dimensional form of the equations for effective intensity I (Eq.(2.32)), source function S (Eq. (2.34)), heat flux q (Eq. (2.4)) and incident radiation $G^{'}$ (Eq. (2.5)) are

$$I^*_{n+1} = I^*_n \exp(-\tau\eta) + S^*(1 - \exp(-\tau\eta)) \tag{3.1}$$

$$S^* = (1-\omega)I^*_b + \frac{\omega}{2\pi}\left[G^{'*} + 2a_1 \sin\alpha \Psi_R(\tau)\right] \tag{3.2}$$

$$\Psi = \frac{1}{2}\int_{\alpha=0}^{2\pi} I^*(\alpha)\sin\alpha d\alpha \tag{3.3}$$

$$G^{'*} = \int_{\alpha=0}^{2\pi} I^*(\alpha) d\alpha \tag{3.4}$$

The boundary effective intensity (Eq. (2.39)), in non-dimensional form is given by

$$I^*(0,\alpha) = \epsilon_w \frac{T_w^4}{T_g^4} + \frac{1-\epsilon_w}{2} \int_{\alpha=0}^{\pi} I^*(\alpha) \sin\alpha \; d\alpha \tag{3.5}$$

3.2.1 2-D Rectangular Enclosure

In Fig. 3.1, a 2-D rectangular enclosure is shown. The enclosure is finite in X and Z directions and is infinite along the Y direction. Its lengths in X and Z directions are L_x=L_z=L respectively. Extinction coefficient β of the medium is constant. The enclosure optical thickness corresponding to the finite lengths are $\tau_{L_x} = \beta L_x$ and $\tau_{L_z} = \beta L_z$. The boundary walls of the enclosure are at zero temperature, while the absorbing-emitting medium is isothermal with temperature T_g.

This benchmark problem has been studied by Fiveland [151], Truelove [159] Raithby and Chui [181] and Chui [184].

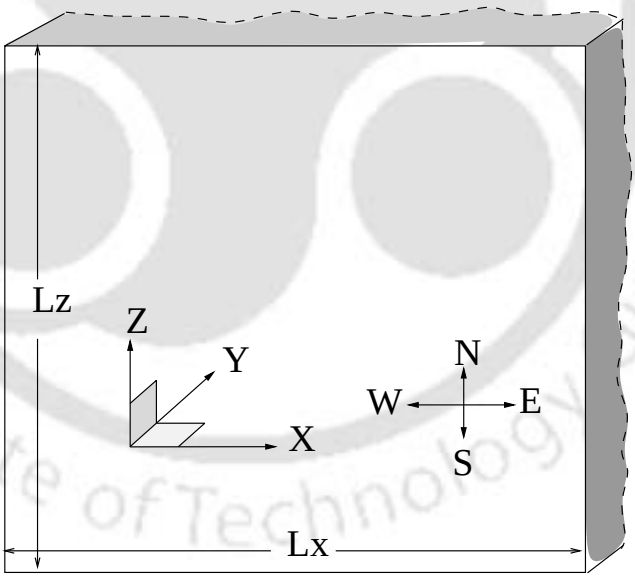

Figure 3.1: 2-D Cartesian enclosure under consideration.

For solving this test problem, methodology given in Chapter 2 has been followed. As per the procedure described in Section 2.6, all calculations are

confined in the solution plane.

Figures 3.2 and 3.3 present the variations of non-dimensional heat flux Ψ along the north wall of the square enclosure. In Fig. 3.2, results have been presented for extinction coefficient β=1.0, 2.0, 3.0 and 5.0. In this figure, 32 effective intensities/rays in CDM have been compared with 64 rays in DTM [215].

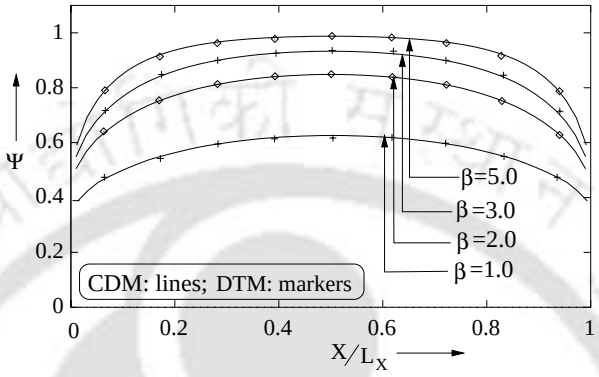

Figure 3.2: Variation of wall heat flux Ψ along north wall in a square enclosure for extinction coefficient β=1.0, 2.0, 3.0 and 5.0.

Results from both the methods agree well. In Fig. 3.3, results on variation of non-dimensional wall heat flux Ψ have been presented for extinction coefficient β=0.1, 1.0 and 5.0. Here, CDM results have been compared with DTM [215] and FVM [181]. Comparison of CDM results with 32 rays with 64 rays from DTM [215] and FVM with (20$\times$ 20) angular discretization and (12$\times$1) volume discretization [181] are excellent.

It should be noted that for the absorbing-emitting medium considered in this chapter, source function given by Eq. (2.34) (and Eq. (3.2)) is constant and this constant value is unity in Eq. (3.2) ($\omega = 0$ and $I_b^* = 1$). Here, to arrive at Eq. (2.36) from Eq. (2.32), no approximation is required. Therefore, to find out heat flux, etc. at any point, intensity information is found in a single step. In other words, there is no restriction on the length of geometric/optical path-leg between any two upstream (point n in Eq. (2.36)) and downstream points (point $n+1$ in Eq. (2.36)) in a given ray direction. Thus, if one is interested in intensity distribution, and hence the heat flux information only

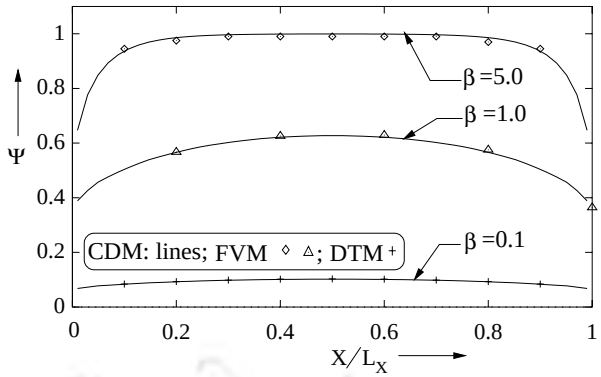

Figure 3.3: Variation of wall heat flux Ψ along north wall in a square enclosure for extinction coefficient β=0.1, 1.0 and 5.0.

along the bounding walls, there is no need for discretizing the entire volume under consideration. However, as we are interested in finding variations of heat flux along the bounding wall, the number of control volumes required will depend on the number of locations where heat flux data are desired. To find out the intensity at any point in the enclosure (including those at walls), the integration along the ray direction has been performed in a single step. As far as the number of control volumes and integration step along the ray direction are concerned, above points hold true for all the problems considered in the present chapter.

For results presented in Figs. 3.2 and 3.3, (10 $\times$ 1) control volumes have been used.

Effect of number of rays on the variations of non-dimensional wall heat flux Ψ along the north wall of the square enclosure (Fig. 3.1) has been presented in Figs. 3.4 and 3.5. In Fig. 3.4, results are presented for 8, 16, 24, 32 and 64 number of rays, whereas in Fig. 3.5, the same are given for 24 and 32 rays. For results presented in Figs. 3.4 and 3.5, extinction coefficient β has been taken 1.0 and 5.0 respectively. From these figures, it is evident that 32 rays in CDM are sufficient for correct prediction of wall heat flux.

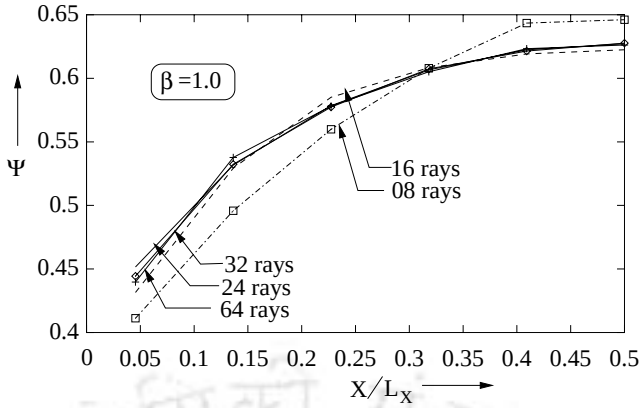

Figure 3.4: Variation of wall heat flux Ψ along north wall in a square enclosure for extinction coefficient β=1.0.

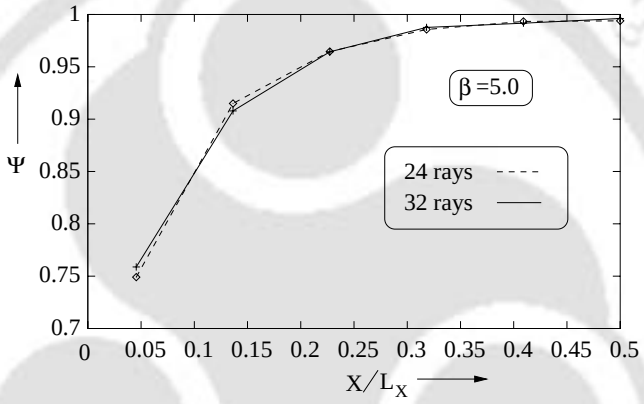

Figure 3.5: Variation of wall heat flux Ψ along north wall in a square enclosure for extinction coefficient β=5.0.

3.2.2 L-Shaped Enclosure

In this section, CDM is applied to radiative transfer problem in a L-shaped enclosure (Fig. 3.6). The enclosed gray and homogeneous medium is absorbing-emitting and is at uniform temperature T_g. The bounding walls are black and are at zero temperature. The enclosure is finite in X and Z directions and is infinite in the Y direction. The extinction coefficient β of the medium is constant.

The enclosure under consideration being a 2-D one, the solution in any $X-Z$

plane will be same at all Y values. Therefore, for our analysis, we restrict our attention to the $X - Z$ plane as our solution plane which is formed by points A, B, C, D, E and F. In this solution plane, the south boundary AB is of length L_S. Lengths of other boundaries are expressed in terms of L_S. For this particular problem, lengths of BC, CD, DE and EF are each $0.5L_S$ and that of FA is L_S.

Radiative transfer problem in this type of enclosure has been studied by Malalasekara and James [251], Hsu and Tan [227] and Henson and Malalasekara [228].

Corresponding to length L_S, the enclosure optical thickness along the south boundary is $\tau_L = \beta L_S$. The optical thickness along all other boundaries have been expressed in terms of the optical thickness τ_L along the south wall.

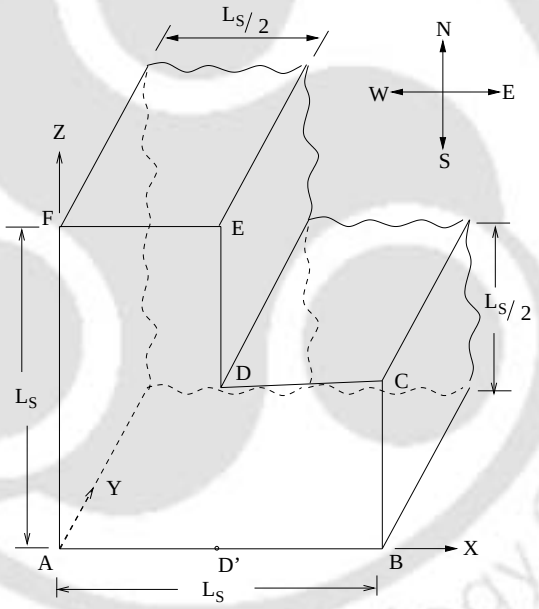

Figure 3.6: L-shaped enclosure under consideration.

In this problem as well, with OTCs known, the solution procedure outlined in Section 2.6 has been followed. The entire calculations are confined in $X - Z$ plane which is the solution plane. In this particular situation, OTCs given in Appendix B can not be used directly. OTCs in this case are found following the procedures given in Section 2.3.1. With south wall as the reference wall,

geometric factor along the south wall is calculated to be L_S/L_{cart}. This geometric factor is multiplied with the optical thickness of the 1-D planar medium and the resulting value is substituted in the expressions of OTCs given in Appendix B. This yields OTCs for this enclosure along the south wall. In our calculations, we have considered the geometric factor for the south wall to be unity. Similarly, to find OTCs along the east, north and west walls of the L-shaped enclosure, geometric factors for these walls have been calculated and used in the same manner. In this particular test enclosure, geometric factors for each of the east faces, i.e., faces BC and DE have been calculated as 0.5. Similarly, for each of the north faces, i.e., faces CD and EF is 0.5. Finally, along the west face (FA), the geometric factor is found to be 1.0.

In Figs. 3.7 and 3.8, variations of non-dimensional heat flux Ψ along the south face have been presented. For both these figures, results have been obtained with (40×1) control volumes.

In Fig. 3.7, results have been presented for extinction coefficient β=0.1, 1.0 and 5.0. Here, CDM results with 32 rays have been compared with DTM [227] results with 84 rays. It is observed from this figure that the heat flux at the midpoint of the south wall suddenly jumps to the high value. This trend is observed for all values of β. In this enclosure, the first half from left $AD^{'}$ receives more radiation than the other half $D^{'}B$. At the midpoint $D^{'}$, there

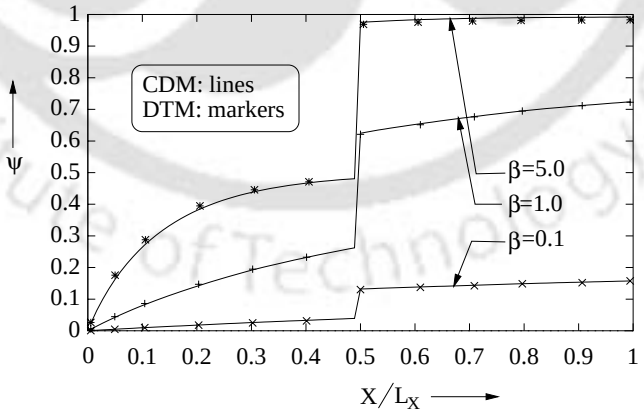

Figure 3.7: Variation of wall heat flux Ψ along south wall in a L-shaped enclosure.

is a sharp change in slope of the heat flux. This is due to the complex nature of geometry involved. However, if large number of control volumes are not considered, a different trend in the variation of heat flux near the mid point is observed. This very fact is obvious from Fig. 3.8. In this figure, heat flux along the south wall has been calculated for three different numbers of control volumes, i.e. (10 ×1), (50 × 1), (200 × 1). Result has been presented for extinction coefficient β=1.0. Like Figs. 3.6 and 3.7, 32 rays have been considered in this case also. From this figure, it is seen that with (10 × 1) control volumes, the sudden jump in the heat flux at the mid point is not observed. The observed trend is due to the shading effect of the sharp corners of the enclosures. If the control volume is coarse, radiation is not captured correctly.

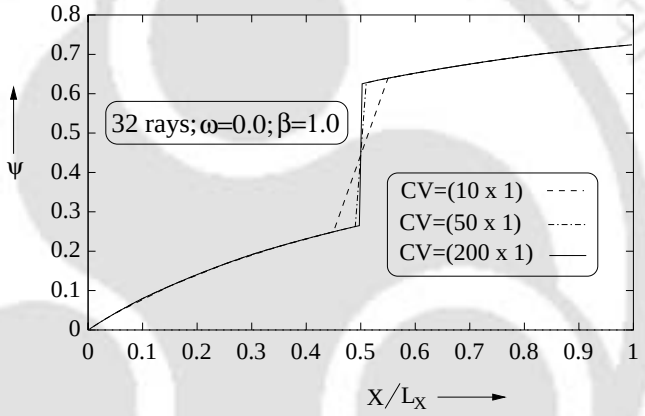

Figure 3.8: Variation of wall heat flux Ψ along the south wall.

Figure 3.9, presents the variation of non-dimensional heat flux Ψ, for the north wall CD. Here, CDM results with 32 rays are comparable to the DTM [228] results with 84 rays.

Figures 3.10 and 3.11 present the variations of heat flux Ψ along the east wall of the L-shaped enclosure. For both these figures, results are given for β=0.1, 1.0 and 5.0. Here CDM results are obtained with 32 rays and (40 × 1) control volumes. In Fig. 3.10, wall heat fluxes are found for the lower half of east face (BC in Fig. 3.6) of the enclosure, whereas in Fig. 3.11, results on heat flux have been given for upper half of the east face DE. From both these figures,

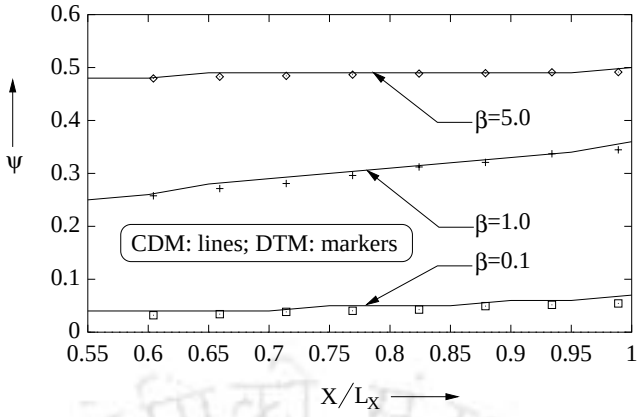

Figure 3.9: Variation of wall heat flux Ψ along north wall (along CD in Fig. 3.6) in a L-shaped enclosure.

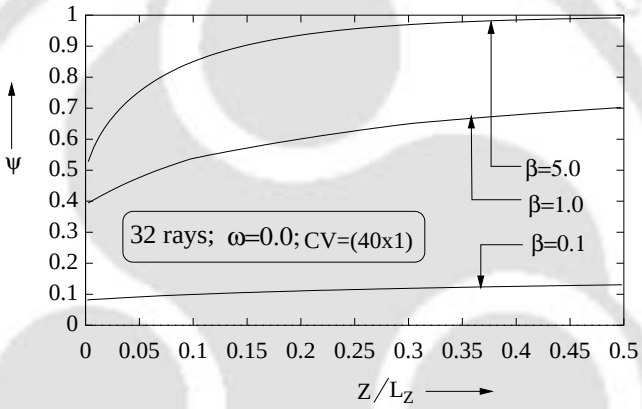

Figure 3.10: Variation of wall heat flux Ψ along east wall (along BC in Fig. 3.6) in a L-shaped enclosure.

it is seen that with increase in β, wall heat flux increases.

For a given β (=5.0), to have the idea of variations in the magnitudes of non-dimensional heat flux Ψ along the periphery of the enclosure, results have been presented in Fig. 3.12. In this figure, peripheral length is measured from the point A in the counter clockwise direction. These results have been obtained with 32 rays in CDM. It is seen from this figure that at all the corner points, there is a jump in the heat flux values. This is attributed to the geometry of the enclosure.

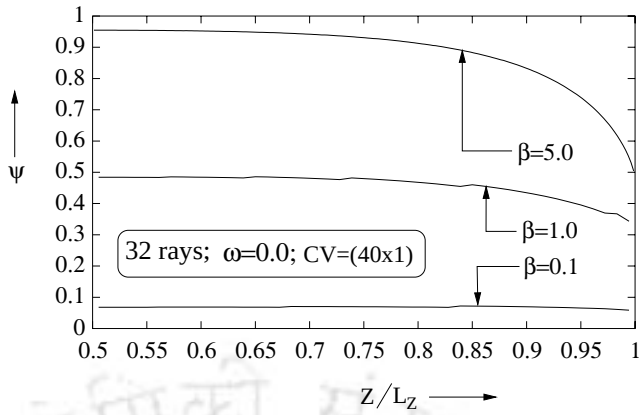

Figure 3.11: Variation of non-dimensional wall heat flux Ψ along east wall.

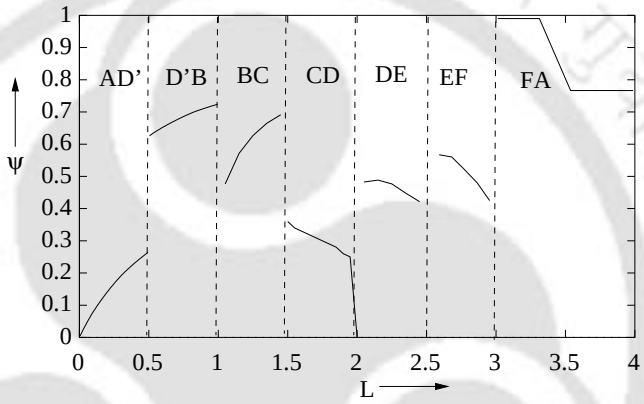

Figure 3.12: Variation of wall heat flux Ψ along the periphery of the L-shaped enclosure.

3.2.3 2-D Quadrilateral Enclosure

Shown in Fig. 3.13 is a 2-D quadrilateral enclosure containing absorbing-emitting, gray and homogeneous medium. The black bounding walls are at zero temperature and enclosed medium is isothermal with temperature T_g. The enclosure is finite in X and Z directions and is infinite in Y direction. The vertices of the face $ABCD$, in counterclockwise order, are (0,0), (2.2,0), (1.5,1.2) and (2.2,0). Thus length of the south wall is $L_S = 2.2$ units.

As in the previous two cases described in this chapter, non-dimensionalization of radiative quantities in this case also has been done with medium temperature

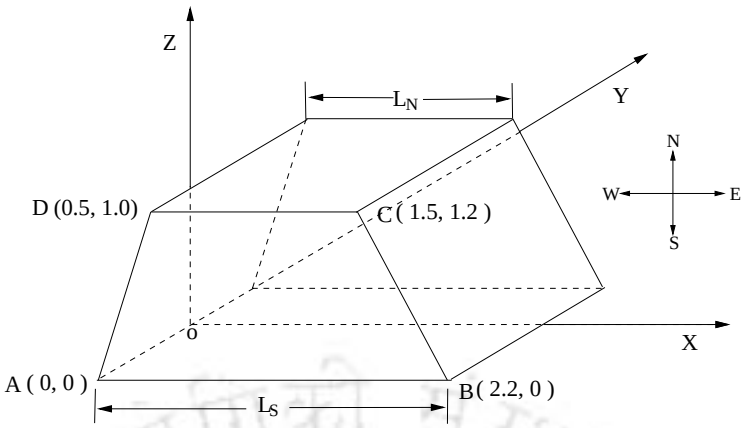

Figure 3.13: Quadrilateral enclosure under consideration.

T_g as the reference temperature.

This benchmark problem has been studied by Raithby and Chui [181], Chui and Raithby [184], Baek et al. [188], Chai et al. [252] and Murthy and Mathur [190]. The geometric complexity of this type of problem is obvious as all faces of the enclosure are non-orthogonal.

To find the radiative information at any point in the enclosure, the entire domain has to be discretized into finite number of control volumes. In order to find the desired results (such as heat flux) at any CVSCP, it is necessary to trace the rays emitted from all the bounding walls which are seen from the CVSCP under consideration. Hence, it is essential to calculate the optical path lengths τ corresponding to all the intensities which are focussed at the concerned CVSCP. Thus lot of geometric relations are involved in calculation of the optical path lengths of each intensity.

To validate the CDM results with those available in the literature, the distribution of heat flux is found along the north face of the enclosure. For finding the OTCs along any wall, characteristic length L_S of the south wall has been taken as reference. Corresponding to this length, the enclosure optical thickness $\tau_L = \beta L_S$. Following the procedure of calculation of OTCs as described in Section 2.3.1, the geometric factor with reference to a 1-D planar medium is $\frac{L_S}{L_{cart}}$. Hence, by knowing the geometric factor, OTCs along the south wall

are calculated by multiplying the geometric factor with the enclosure optical thickness for 1-D planar medium, and this quantity is substituted in the expressions of OTCs in Appendix B. As normalization is done with respect to the south wall, this geometric factor becomes unity for the south wall. For other walls, length of each wall has been calculated with reference to the south wall. The ratio of the length of a wall to that of the south wall gives rise to a geometric factor. Following the similar procedure as mentioned above, the OTCs corresponding to other walls have been calculated. In our study, as we are concerned about the variation of heat flux only along the north wall, only the geometric factor of the north wall is calculated. For the geometry under consideration, this value is 0.4635.

Figures 3.14 and 3.15 present variations of non-dimensional heat flux Ψ along the north wall of the quadrilateral enclosure. In Fig. 3.14, this variation is shown for first of half of the north wall. In this figure, CDM results with 16 and 32 rays have been compared with 32 rays in DTM [215]. Extinction coefficient of the medium has been taken as 5.0. These results are presented for (40×1) quadrilateral control volumes. From this figure, it is seen that CDM results with 32 rays compare well with 32 rays in DTM.

In Fig. 3.15, variations of Ψ along the north wall of the quadrilateral enclosure have been presented for β=0.1, 1.0, 5.0 and 10.0. Here, CDM results have been

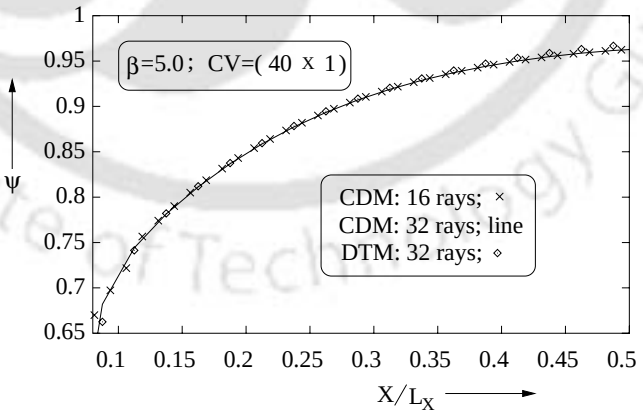

Figure 3.14: Variation of wall heat flux Ψ along north wall in a quadrilateral enclosure.

generated by considering 32 rays and (40 × 1) control volumes. These results have been compared with the FVM. FVM results [184] are for (16 × 16) angular discretization with (4 × 16) control volumes. From this figure, it is seen that for β=10.0, the radiative heat flux along the wall is nearly equal to unity. This is because the intensity impinging on the north wall is influenced only by the neighboring hot medium. Near the corner, a rapid decrease in heat flux is observed. This is due to the influence of the neighboring cold walls. With low value of the extinction coefficient β=0.1, the radiative heat flux to the wall is significantly reduced. This is because of the far-reaching effect of the other cold walls and negligible self-extinction coefficient of the optically thin medium. It is seen from the figure that the CDM results compare very well with that of FVM.

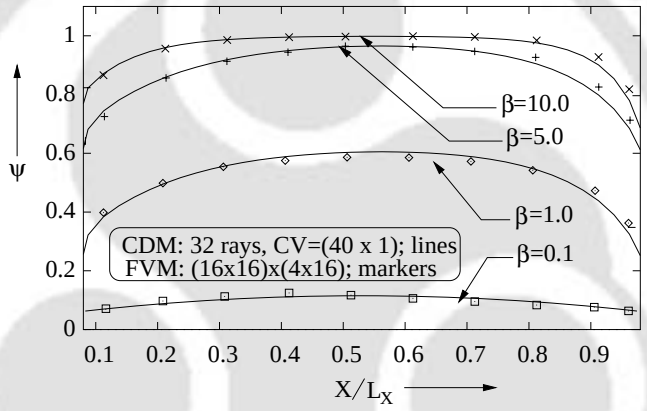

Figure 3.15: Variation of wall heat flux Ψ along north wall in a quadrilateral enclosure.

3.2.4 3-D Cartesian Enclosure

So far applicability of CDM has been tested for radiative transfer problems in 2-D Cartesian enclosures. It has been mentioned in Chapter 2 that in CDM, all the radiative information are mapped to a 2-D solution plane. Thus all calculations are restricted to the 2-D solution plane only. As far as 2-D Cartesian enclosures are concerned, finding solutions in 2-D solution plane is fully

justified. However, in case of 3-D geometries, heat flux and temperature information are to be found out in 3-D space. In other words, in such enclosures, solution domain is the 3-D space instead of a 2-D plane. Under these circumstances, earlier it had been thought that application of CDM to 3-D Cartesian enclosures would be a difficult task.

In the present work, it has been found that by selecting a number of solution planes, instead of a single solution plane as in the case of 2-D Cartesian enclosures, CDM can easily be applied to radiative transfer problems in 3-D Cartesian enclosures. In the following paragraphs, a sample test problem is chosen to authenticate the above assertion.

Shown in Fig. 3.16 is a 3-D cuboid. The enclosure walls are black and are at zero temperature. The enclosed medium is absorbing-emitting and isothermal with temperature T_g. As in earlier cases considered in this chapter, in this case also the medium temperature T_g has been taken as the reference temperature T_R.

The optical thickness of the enclosure along X-direction is $\tau_L = \beta L_X$. Optical thicknesses along other sides have been expressed in terms of τ_L. For the

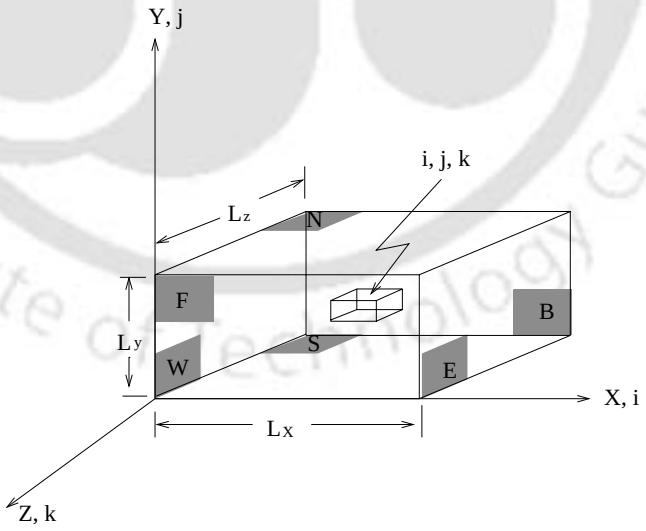

Figure 3.16: A General 3-D Cartesian enclosure.

enclosure under consideration, aspect ratio AR is defined as the ratio of the length of the wall under consideration to that of the length of the south wall. If for a given enclosure, both the ARs are taken unity, geometric factors along each wall will be unity. In this situation, OTCs given in Appendix B are directly applicable. In case of aspect ratio AR other than unity, geometric factor for calculation of OTCs along a given wall is nothing but the AR.

To find out heat flux and temperature information along any plane, the solution plane in CDM is made to coincide with the plane under consideration (plane in which the solution is desired). In 3-D Cartesian enclosure, solutions are desired in 3-D space. The 3-D solution space can thus be represented by a finite number of 2-D solution planes. In CDM, all such planes have to be considered for the analysis. Above points can be made clear from the following.

To find out radiative information, e.g. heat flux, temperature, etc., at six CVSCPs of the control volume, say, (i, j, k) of the enclosure (Fig. 3.13), we have to consider six different solution planes and have to find out the radiative information on all six such planes. In fact, all six control faces are the part of six different solution planes.

Since in the problem under consideration, all walls are black and are at zero temperature and medium is isothermal with temperature T_g; distribution of heat flux along bounding walls facing each other will be the same. For a cubical enclosure, it will be same on all the walls. For cubical enclosure (both ARs as unity), in Fig. 3.17, variation of non-dimensional heat flux Ψ with $\frac{Y}{L_Y}$ at the location $(L_x/2, L_y, Z = 0)$ has been presented. Results are given for six different values of extinction coefficient β (0.1, 0.5, 1.0, 2.0, 3.0 and 5.0). For all the cases, in CDM, 32 rays have been used. Number of control volumes considered is $(20 \times 1 \times 1)$. Here, CDM results have been compared with MCM [86]. Both the results compare well.

As mentioned in earlier sections, for absorbing, emitting gray and homogeneous isothermal medium considered here, number of control volumes has no effect on the magnitude of heat flux.

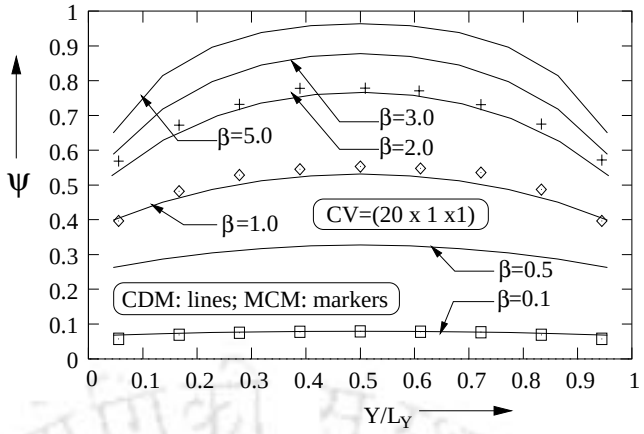

Figure 3.17: Variation of wall heat flux Ψ in 3-D Cartesian enclosure.

Figure 3.18 present the variation of non-dimensional heat flux Ψ at location $(L_x/2, L_y, Z = 0)$ for a 3-D Cartesian enclosure. Here, results are produced for $L_y/L_x = 0.5$ and $L_y/L_x = 1.0$. Variation of heat flux for four different values of extinction coefficient β (1.0, 2.0, 3.0 and 5.0) have been presented. These results are obtained with 32 rays and $(20 \times 1 \times 1)$ control volumes. Comparison of Figs. 3.17 and 3.18 shows that with decrease in aspect ratio $AR = L_y/L_x$, wall heat flux decrease. This is because of the fact that with decrease in aspect ratio, the gas volume decreases and thus contribution from gas to the radiative heat flux also decreases. Wall being at zero temperature, its contribution remains same in both the cases.

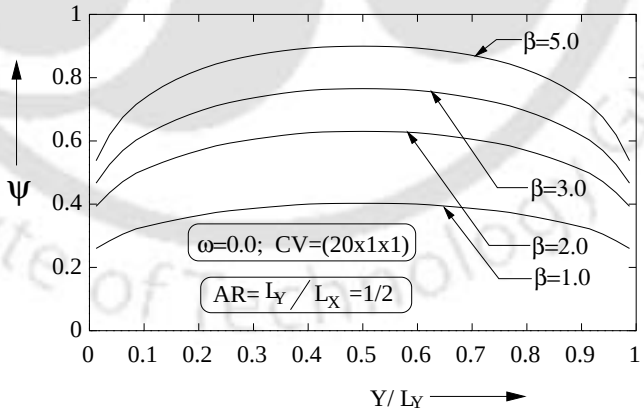

Figure 3.18: Effect of extinction coefficient β on variation of heat flux Ψ in 3-D Cartesian enclosure containing absorbing-emitting medium.

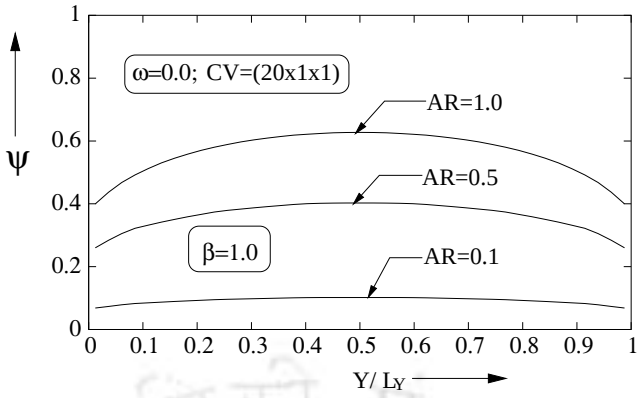

Figure 3.19: Effect of aspect ratio (AR) on variation of wall heat flux Ψ in 3-D Cartesian enclosure.

In Fig. 3.19, with $L_z/L_x = 1$, the effect of aspect ratios $AR = L_y/L_x$ on variations of non-dimensional heat flux at location $(L_x/2, L_y, Z = 0)$ has been presented. In this figure, CDM results have been generated with 32 rays and $(20 \times 1 \times 1)$ control volumes. Aspect ratios AR=0.1, 0.5 and 1.0 are considered with extinction coefficient β=1.0. From this figure, it is clear that for a fixed extinction coefficient β, heat transfer decreases with decrease in the aspect ratio. Reason for the observed trend is the same as that given for results in Fig. 3.18.

3.3 Summary

In this Chapter, CDM has been validated for radiative transfer problems in different types of Cartesian enclosures with participating medium. Here applicability of CDM has been tested for different types of 2-D Cartesian enclosures such as square, L-shaped and quadrilateral enclosures. Applicability of CDM has also been demonstrated for radiative transfer problem in 3-D Cartesian enclosure. In all the test problems considered in this chapter, gray and homogeneous participating medium has been assumed absorbing-emitting. Tests have been done with enclosure bounding walls as black and medium with uniform and constant temperature. Procedures for the evaluation of OTCs for

different enclosures considered in this chapter are also discussed. The validation studies presented in this chapter have shown that for the benchmark problems in 2-D Cartesian enclosures, CDM is able to correctly predict the radiative information.

Applicability of CDM to radiative transfer problems in various types of cylindrical enclosures has been discussed in the next chapter.

Chapter 4

Validation Studies: Cylindrical Enclosures

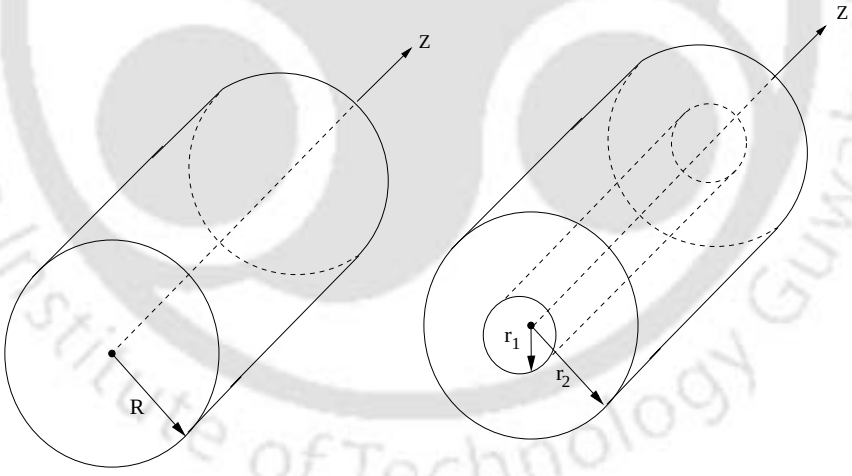

Single cylindrical enclosure

Concentric cylindrical enclosure

4.1 Introduction

Analysis of radiative transfer in cylindrical enclosures with participating medium has got wide applications in high temperature devices, such as boilers, heat exchangers, space radiators, nuclear reactors, etc. Solutions of radiative transfer problems in cylindrical enclosures have been reported by various investigators. Heaslet and Warming [51], Loyalka [53], Dua and Cheng [54] and Kesten [52] have provided exact solutions for infinitely long cylindrical enclosure with absorbing-emitting medium. The same with isotropic scattering has been reported by Crosbie and Farell [55]. Exact formulations and results for radiative transfer in infinite cylindrical enclosure for anisotropic scattering situation are available in [56–58]. Because of the limited applications of the exact methods towards the solution of real life conjugate radiation, conduction and/or convection problems, various numerical methods pertaining to radiative transfer in cylindrical enclosures have been developed [141, 151, 162, 166, 184, 215, 247, 253, 254].

In this Chapter, CDM is applied to solve radiative transfer problems in gray cylindrical enclosures with participating medium. Both infinite (1-D) and finite (2-D) single as well as concentric cylindrical enclosures are considered. The absorbing-emitting and/or anisotropically scattering medium considered is gray and homogeneous. For the above geometries, sample problems have been considered in radiative as well as non-radiative equilibrium situations.

In the validation studies on CDM, for both radiative and non-radiative equilibrium situations, full/wide range of parameters have been considered. The ranges of parameters considered are summarized in Table 4.1.

The formulations developed for general enclosures, given in Chapter 2, are also applicable to the problems considered in this chapter. For the cylindrical enclosures under consideration, OTCs under different situations are obtained by calculating the geometric factor and multiplying the same with enclosure optical thickness τ_L. Corresponding to this new value of τ_L, for given values of r_1/r_2, $a_1\omega$ and/or ω, OTC for the cylindrical geometry under consideration

Parameters	Range
Scattering albedo	$0 \leq \omega \leq +1.0$
Anisotropy factor	$-1.0 \leq a_1 \leq +1.0$
Radius ratio	$0 \leq r_1/r_2 \leq 1.0$
Enclosure optical thickness	$0.001 \leq \tau_L \leq 5.0$

Table 4.1: Range of parameters used for validation studies with cylindrical enclosures.

is found from the expressions of OTCs given in Appendices A & B for 1-D planar geometry.

For infinitely long (1-D) cylindrical enclosure, the geometric factor along the radial direction is D/L_{cart}. L_{cart} for 1-D cylindrical geometry is the diameter D, and hence for this case, the geometric factor comes to be unity. In case of 1-D concentric cylindrical enclosure, the geometric factor is $(1-\rho)$, where ρ is the radius ratio r_1/r_2. Since properties considered are isotropic, OTCs for 1-D cylindrical enclosure equally hold good for 2-D cylindrical enclosures.

To check the accuracy of the results obtained from the CDM, depending upon the availability of results, comparisons have been made with exact methods, DTM, P_3 approximation, MCM and FVM. The convergence limit for all set of iterative problems has been taken as 10^{-6}.

4.2 Non-Radiative Equilibrium

In this section, radiative transfer problems in gray cylindrical enclosures containing absorbing, emitting and anisotropically scattering medium have been considered. The cylindrical enclosures considered are infinite (1-D) and finite (2-D) single as well as concentric enclosures. The contained medium is gray and homogeneous. The cases with constant medium temperature T_g with boundaries at zero temperature as well as medium with varying temperature and boundaries at finite temperatures are considered. A sample case of radiative transfer problem in a finite cylindrical enclosure with flux boundary

condition is also considered. All the problems considered under this section belong to the class of non-radiative equilibrium.

For non-dimensionalization of effective intensity, source function, incident radiation, heat flux, etc., depending upon the problem, the reference temperature has been chosen differently. This point will be mentioned in the respective places.

4.2.1 Infinite (1-D) Single Cylindrical Enclosures

Let us consider a single gray cylindrical enclosure as shown in Fig. 4.1. The enclosed gray and homogeneous medium is absorbing, emitting and anisotropically scattering. For infinite (1-D) single cylindrical enclosures, the axial dimension Z is infinite and radial dimension r is finite. The radiative properties, for example, wall emissivity ϵ_w and imposed condition such as temperature do not vary in the circumferential direction ϕ. As in Z and ϕ dimensions, there is no variation of properties, one has to find radiative information only in one dimension, i.e. r-dimension.

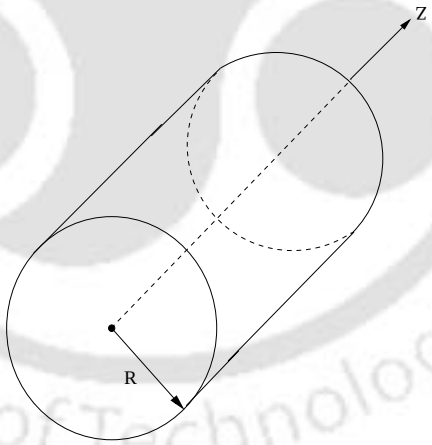

Figure 4.1: Cylindrical enclosure under consideration.

For the chosen geometry, the medium temperature is constant and uniform throughout and boundary is at zero temperature. The anisotropy has been approximated by linear anisotropic phase function (Eq. 2.33). This benchmark

problem for absorbing-emitting with/without scattering has been considered by Dua and Cheng [54] and Azad and Modest [56].

In this problem, as medium temperature T_g is the only known temperature, for non-dimensionalization purpose, it has been taken as the reference temperature T_R and for this section, non-dimensionalization procedure given in Chapter 3, Section 3.2 holds valid.

In the following paragraphs, CDM results for heat flux are discussed for various radiative parameters, like optical thickness τ_L, scattering albedo ω, the factor $a_1\omega$ and wall emissivity ϵ_w. Depending upon the availability of results in the literature, CDM results are compared with results from various methods.

Variations of non-dimensional wall heat flux Ψ with enclosure optical thickness τ_L for absorbing-emitting medium ($\omega = 0$) for 1-D black ($\epsilon_w = 1$) cylindrical enclosure is given in Figs. 4.2. In this figure, CDM results with 6, 10, 24 and 32 effective intensities/rays are compared with DTM results [215]. It is seen from this figure that CDM results with 32 rays compare exactly with the DTM results with 128 rays. Further, it is observed from this figure that except medium optical thickness range ($0.5 \leq \tau_L \leq 2.5$), in CDM even less number of rays are sufficient to correctly predict the wall heat flux.

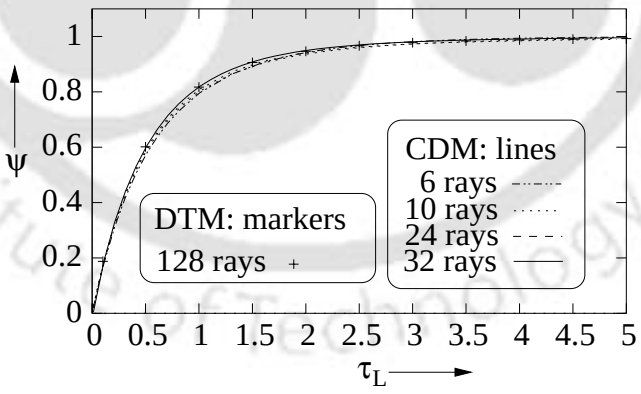

Figure 4.2: Variation of wall heat flux Ψ with enclosure optical depth τ_L.

Effect of wall emissivity ϵ_w on variations of wall heat flux Ψ with enclosure

optical depth τ_L is shown in Fig. 4.3. In this figure, for $\epsilon_w = 1$, CDM results with 32 rays are compared with DTM results with 128 rays [215] and exact results [58]. For $\epsilon_w \neq 1$, CDM results with 32 rays have been compared with exact results [58]. For a given τ_L, as ϵ_w decreases, wall heat flux Ψ also decreases. This is because, with decrease in ϵ_w, reflectivity $(1 - \epsilon_w)$ increases and thus bounding wall reflects more and more radiation to the medium. From this figure it is seen that over the the wide range of τ_L, for all values of ϵ_w, CDM results compare very well with the DTM and exact results.

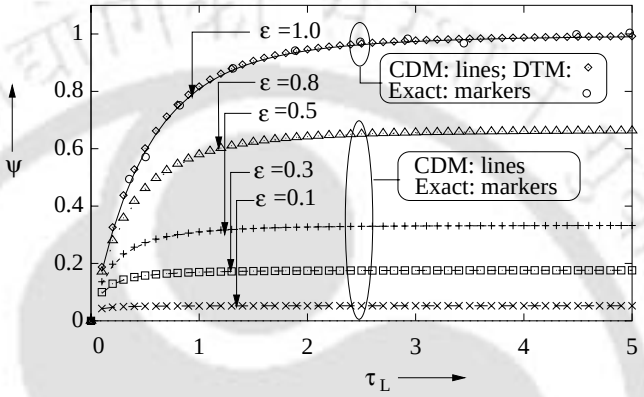

Figure 4.3: Effect of wall emissivity ϵ_w on variation of wall heat flux Ψ with enclosure optical depth τ_L.

As regards to the number of control volumes required in CDM for absorbing-emitting medium ($\omega = 0$) for non-radiative equilibrium problem with constant and uniform medium temperature is concerned, the explanation given in Chapter 3, Section 3.1 holds true. However, in the presence of scattering, source function S^* (Eq. 2.35) is an unknown. Both the incident radiation G'^* and heat flux Ψ_R are unknown quantities in the expression for the source function S^* (Eq. 2.35). In this situation, to arrive at the Eq. (2.36) from Eq. (2.32), in CDM, approximations are involved. Equation (2.36) holds true only over small optical path-leg. This means, requirements for a large number of control volumes. To get the correct results from CDM, the number of control volumes required are mentioned at the appropriate places. This justification also holds true for all types of medium (even absorbing-emitting) considered for problems under radiative equilibrium. For radiative equilibrium situation, source function is always unknown.

Further, when source function is an unknown, solution starts with an initial guess for incident radiation $G^{'*}$ and heat flux Ψ_R. With this, the solution procedure becomes iterative one and calculation continues till solution converges. In the present study, all the result are from converged solutions with convergence criterion of 10^{-6}.

In Fig. 4.4, effect of scattering albedo ω on wall heat flux Ψ for 1-D black (ϵ_w=1) cylindrical enclosure has been presented for isotropic scattering situation ($a_1 = 0$). Here CDM results have been provided for three different values of ω. For ω=0.1, 0.5 and 0.9, in the present work, 50, 100 and 150 control volumes respectively have been found sufficient with 32 rays. Results presented in this figure have been compared with the results from the exact method [58]. It is seen from the figure that over the wide range of optical thickness considered here ($0.001 \leq \tau_L \leq 5$), CDM results are found to compare very well with that of the exact results. From Fig. 4.4, it is clear that with increase in ω, wall heat

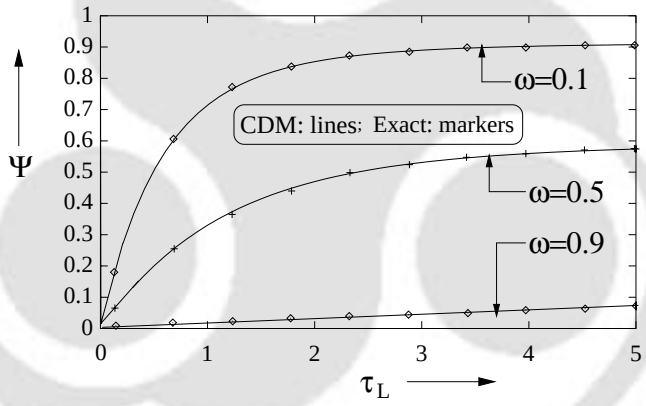

Figure 4.4: Effect of scattering albedo ω on variation of wall heat flux Ψ with enclosure optical depth τ_L.

flux significantly reduces. This can be explained in the following manner. For a given value of extinction coefficient β (hence optical thickness τ_L), a decrease in ω value implies decrease in scattering coefficient σ_S ($\omega = \sigma_s/\beta$). Under this situation, medium is highly absorbing-emitting. Most of the radiative energy in this situation is captured by medium resulting in an increase in wall heat flux.

Figures 4.5-4.7 represent the effect of anisotropy factor a_1 on variation of wall heat flux Ψ with enclosure optical thickness τ_L. For black enclosure ($\epsilon_w = 1$), results are presented for the two extreme limits of a_1, i.e. a_1=+1 and a_1=-1 and for isotropic scattering a_1=0. The two extreme limits represent 100% forward and backward scattering situations respectively. In Figs. 4.5-4.7, for three values of a_1, results are given for scattering albedo $\omega = 0.1$, 0.5 and 0.9 respectively. Results for all the cases are compared with results from the exact method [58].

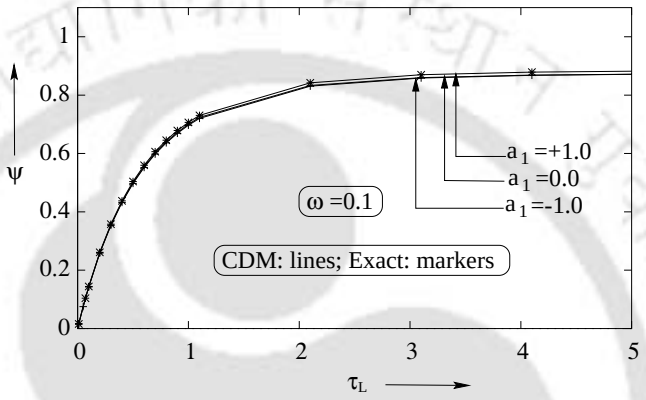

Figure 4.5: Effect of anisotropy factor a_1 on variation of wall heat flux Ψ with enclosure optical depth τ_L; ω=0.1.

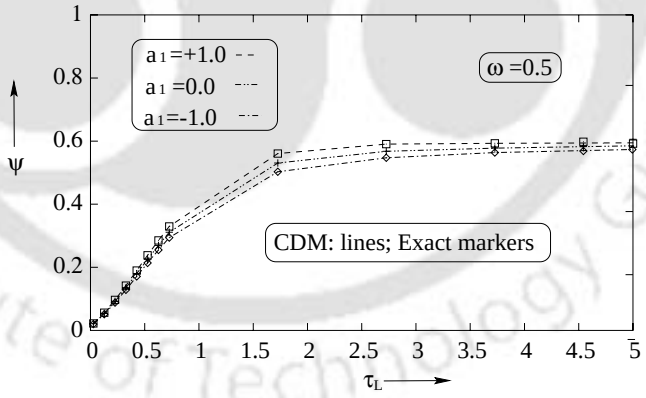

Figure 4.6: Effect of anisotropy factor a_1 on variation of wall heat flux Ψ with enclosure optical depth τ_L; ω=0.5.

In all the cases, 32 rays are considered in CDM. For isotropic scattering ($a_1 = 0$) and anisotropic scattering situations ($a_1 \neq 0$) considered herein, 50 and 150

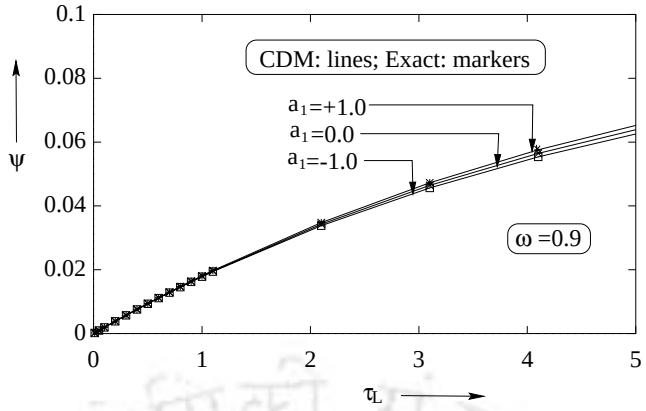

Figure 4.7: Effect of anisotropy factor a_1 on variation of wall heat flux Ψ with enclosure optical depth τ_L; ω=0.9.

control volumes have been found sufficient for the converged solution. From Figs. 4.5-4.7, it is observed that anisotropy factor a_1 is not having much effect on wall heat flux Ψ. As is clear from these figures, for all values of ω, at low optical thickness ($\tau_L \leq 1.0$), effect of a_1 can even be ignored.

To have some idea of the number of iterations required for getting the results presented in Figs. 4.5-4.7, in Table 4.2, for $\omega = 0.5$, results are presented for some test cases. From this table it is seen that for the two extreme limits of a_1, 22-24 iterations are required to get the converged solution, whereas 21-25 iterations are required for the isotropic scattering.

ω	a_1	τ_L	Control volume	Iterations
0.5	+1	0.1	150	24
		2.0		24
		5.0		24
0.5	0	0.1	50	21
		2.0		25
		5.0		24
0.5	-1	0.1	150	22
		2.0		24
		5.0		24

Table 4.2: Number of iterations required for getting results for some samples cases in Fig. 4.6.

For the geometry under consideration, effects of optical thickness τ_L, scattering albedo ω and the factor $a_1\omega$ on variations of non-dimensional heat flux Ψ in the medium have been shown in Figs. 4.8-4.12. These variations of Ψ in the medium have been given in the radial direction. This radial direction r has been normalized as r/R and has been written in all the figures as normalized optical depth τ/τ_L ($r/R = (\beta r)/(\beta R)$).

The effect of optical thickness τ_L on Ψ with normalized optical depth τ/τ_L has been shown in Figs. 4.8-4.10. In these figures, results are presented for three values of τ_L. In Fig. 4.8, results are presented for absorbing-emitting situation ($\omega = 0$), whereas the same are given for isotropic scattering with $\omega = 0.1$ and 0.5 in Figs. 4.9 and 4.10 respectively. Here CDM results with 32 rays have been compared with exact results [54, 58].

It is observed from Fig. 4.8 that throughout the enclosure, heat flux at τ_L=1.0 is more than that for τ_L=0.2. However, for τ_L=5.0, for $\tau/\tau_L < 0.85$, heat flux is less than that for τ_L=0.2. After $\tau/\tau_L > 0.85$, it is more. This trend is because of the fact that the geometry of the enclosure significantly influences the heat flux distribution in gas at higher values of τ_L. At lower values of τ_L, system behaves similar to 1-D Cartesian enclosure.

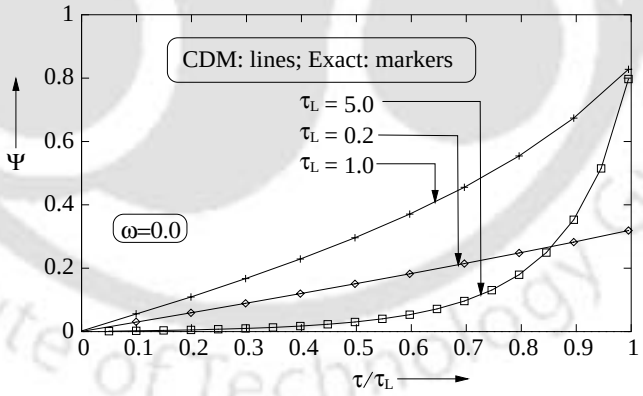

Figure 4.8: Effect of optical thickness τ_L on variation of heat flux Ψ in the medium with normalized optical depth τ/τ_L; ω=0.0.

Figures 4.9 and 4.10 present the effect of optical thickness τ_L on variations of Ψ with τ/τ_L. In Fig. 4.9, results are given for $\omega = 0.1$, whereas the same are

given for $\omega = 0.5$ in Fig. 4.10. For a given value of ω, trends similar to Fig. 4.8 are observed.

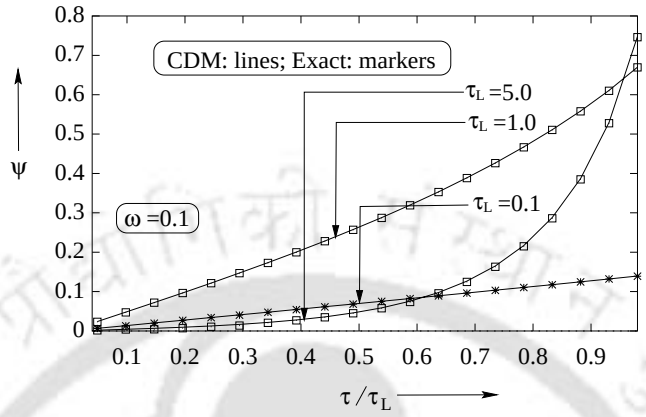

Figure 4.9: Effect of optical thickness τ_L on variation of heat flux Ψ in the medium with normalized optical depth τ/τ_L; ω=0.1.

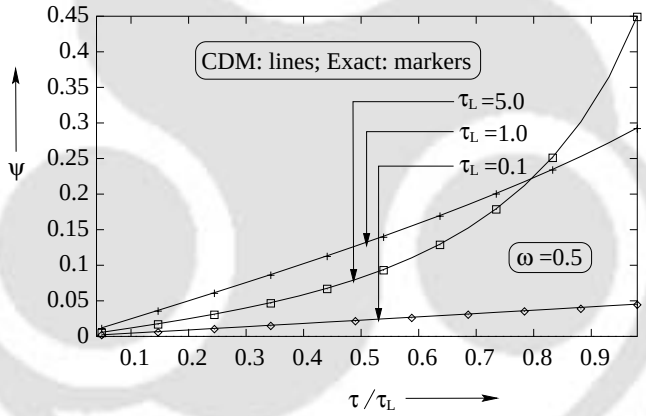

Figure 4.10: Effect of optical thickness τ_L on variation of heat flux Ψ in the medium with normalized optical depth τ/τ_L; ω=0.5.

Figure 4.11, presents results on the effect of scattering albedo ω on variations of heat flux Ψ in the medium with normalized optical depth τ/τ_L. These variations are considered for three different values of ω, i.e. 0.1, 0.5 and 0.9. For all the cases, results are given for τ_L=1.0. These CDM results are generated with 32 rays and 50-150 control volumes. Here the comparisons have been made with the results from the exact method [58]. From this figure, it is

observed that heat flux in gas decreases with increase in ω. Further, effect of wall geometry is less significant with higher values of ω.

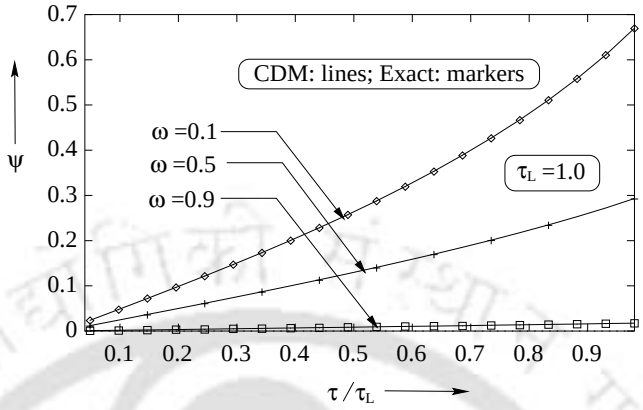

Figure 4.11: Effect of scattering albedo ω on variation of heat flux Ψ with normalized optical depth τ/τ_L; $\tau_L = 1.0$.

For given values of τ_L and ω, influence of anisotropy factor a_1 on the variation of non-dimensional heat flux Ψ in the medium with normalized optical depth τ/τ_L is presented in Fig. 4.12. Here CDM results with 32 rays and 150 control

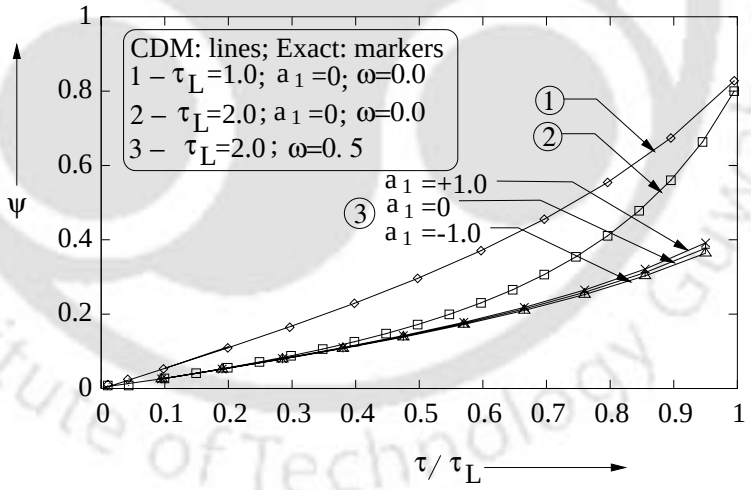

Figure 4.12: Effect of the factor $a_1\omega$ on variation of heat flux Ψ with normalized optical depth τ/τ_L.

volumes are compared with the results from the exact method provided by Azad and Modest [56]. Comparison of both is excellent. It is seen from this

figure that for given values of τ_L and ω, the anisotropy is not having much effect on heat flux.

For a given value of ω, to get the overall picture about the variations of non-dimensional heat flux Ψ in the medium with normalized optical depth τ/τ_L and enclosure optical thickness τ_L, some sample surface plots have been given in Fig. 4.13. Here results have been given for three different values of ω, i.e, 0.1, 0.5 and 0.9. Here enclosure optical thickness τ_L has been considered in the range [0.001,5].

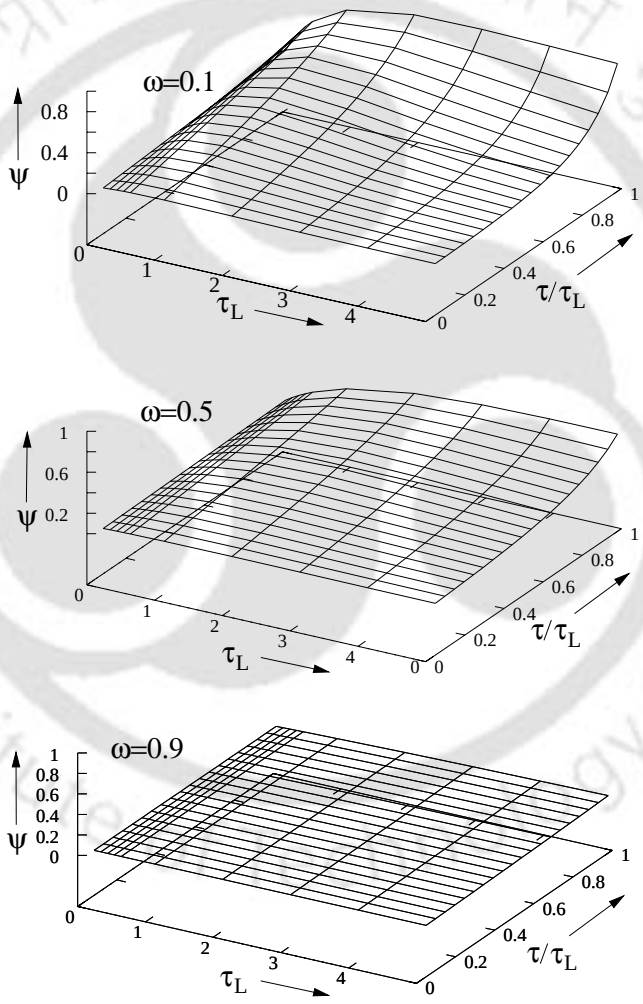

Figure 4.13: Surface plots for variations of heat flux Ψ in the medium with enclosure optical thickness τ_L and normalized optical depth τ_L.

These surface plots provide qualitative as well as quantitative picture about the variations of heat flux inside 1-D cylindrical enclosure. Due to the curvature of wall, at high enclosure optical thickness τ_L with low values of ω, the variation of Ψ is highly non-linear. This non-linearity decreases with increase in ω. With low optical thickness, as medium is less participating, most of the radiation directly impinges at the wall. As a result, heat flux distribution is linear with low optical thickness $\tau_L \leq 1.0$.

4.2.2 Infinite (1-D) Concentric Cylindrical Enclosure

In the following pages, applications of CDM to radiative transfer problems in infinite (1-D) gray concentric cylindrical enclosure (Fig. 4.14) have been described. The enclosure is infinite in Z direction, whereas it is finite in the radial direction r. Radii of inner and outer cylinders are r_1 and r_2 respectively. The gray and homogeneous participating medium enclosed between the two

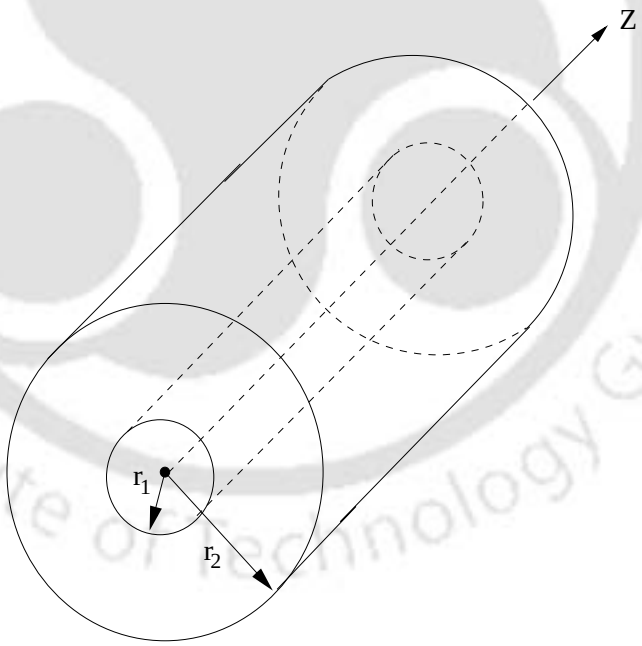

Figure 4.14: Concentric cylindrical enclosure under consideration.

cylinders is absorbing, emitting and isotropically scattering. The medium is

isothermal with temperature T_g and both the bounding walls are cold (zero temperature). Radiative properties for the bounding surfaces do not vary in the circumferential direction ϕ. Thus, as in the previous case, here too, the radiative information are required only in one dimension, i.e. the radial direction r. Further, for non-dimensionalization of heat flux, etc., description given in Section 4.2.1 holds true for the present case also.

In the following paragraphs, CDM results for different radius ratios r_1/r_2, optical thickness τ_L, scattering albedo ω, bounding wall emissivities ϵ_w are presented. As very limited literature are available on this problem, CDM results are compared with that of DTM [215] only for a sample case of absorbing-emitting medium.

In Fig. 4.15, variation of inner wall heat flux Ψ with enclosure optical thickness τ_L has been given for three different radius ratios r_1/r_2=0.1, 0.5 and 0.9. Here, enclosure walls are considered black (ϵ_w=1.0). In this figure, CDM results with 12 rays have been found matching very well with that of DTM results with 16 rays [215]. Comparison between the two is excellent.

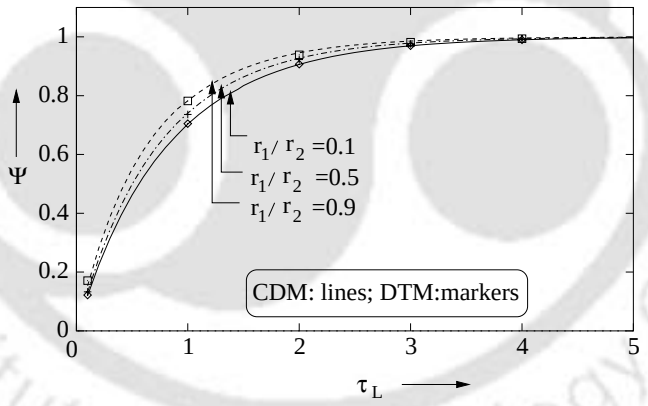

Figure 4.15: Effect of radius ratio r_1/r_2 on variation of wall heat flux Ψ with enclosure optical depth τ_L.

Effect of wall emissivity ϵ_w on wall heat flux Ψ has been shown in Fig. 4.16. Here, the inner wall is assumed black ($\epsilon_1 = 1$) and outer wall is gray ($\epsilon_2 \neq 1$). Results have been presented for three different values of outer wall emissivity ϵ_2 (=0.1, 0.5 and 0.9). These results are obtained with 12 rays and single

control volume. For a given value of ϵ_2, results are obtained for two radius ratios r_1/r_2 (=0.1 and 0.9). It is seen from this figure that with decrease in ϵ_2, Ψ on the inner cylinder decreases. The reason for the observed trend is the same as that for the similar case discussed in Fig. 4.3 for a single cylindrical enclosure.

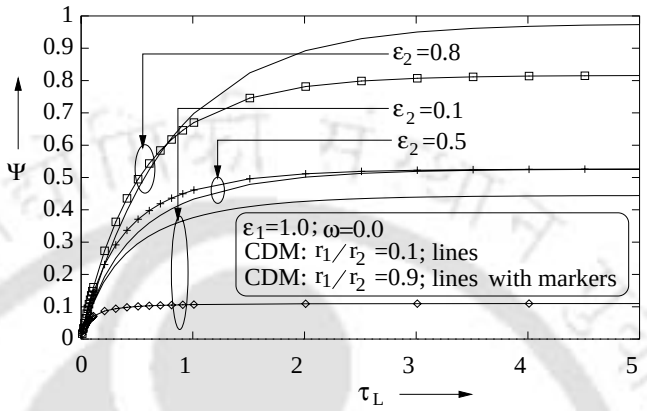

Figure 4.16: Effect of wall emissivity ϵ_w on variation of inner cylinder wall heat flux Ψ with enclosure optical depth τ_L.

For given values of ω and r_1/r_2, effect of τ_L on variations of gas heat flux Ψ with normalized optical thickness τ/τ_L has been given in Fig. 4.17. Here results are provided for $\omega = 0$ and r_1/r_2=0.5. These results are presented for τ_L=0.1, 1.0 and 5.0.

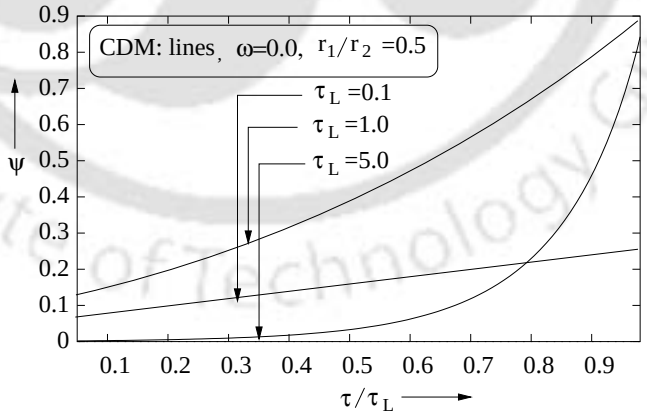

Figure 4.17: Effect of enclosure optical thickness τ_L on variation of heat flux Ψ in the medium with enclosure optical depth τ/τ_L; $\omega = 0$, $\frac{r_1}{r_2}$=0.5.

Effects of scattering albedo ω on variations of Ψ with τ/τ_L have been given in Figs. 4.18-4.20. Here, these effects are presented for given values of r_1/r_2 and τ_L. In Figs. 4.18 and 4.19 results have been presented for two values of ω (=0.1 and 0.5). For $\tau_L = 1$, these results have been presented r_1/r_2=0.9 in Fig. 4.18, whereas the same have been given for r_1/r_2=0.5 in Fig. 4.19. In Fig. 4.20, effects are shown for of ω =0.1, 0.5 and 0.9. Here $r_1/r_2 = 0.9$ and $\tau_L = 5$. For all the results presented in Fig. 4.18-4.20, 12 rays and 150 control volumes have been used.

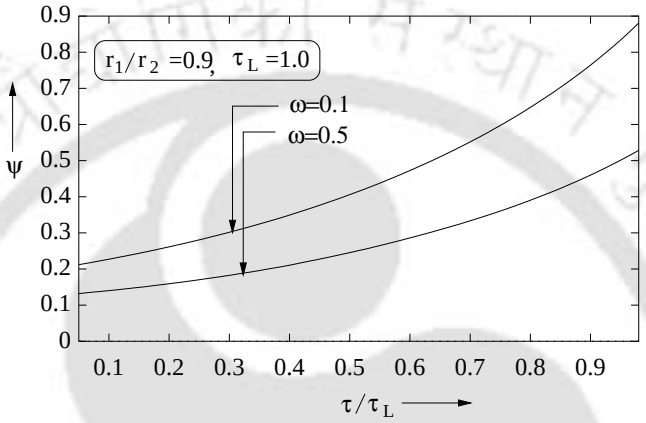

Figure 4.18: Effect of scattering albedo ω on variation of gas heat flux Ψ with normalized optical depth τ/τ_L; $\frac{r_1}{r_2} = 0.9$, τ_L=1.0.

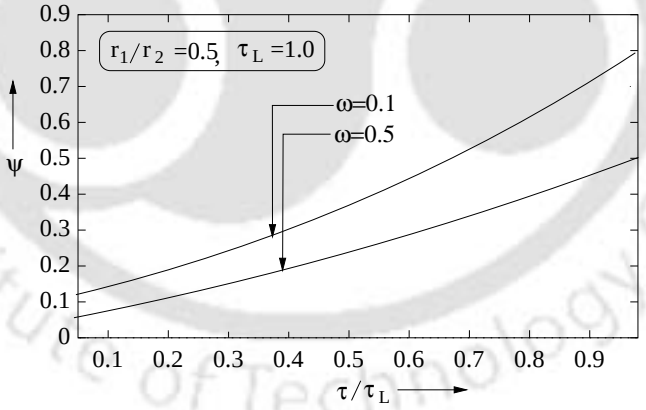

Figure 4.19: Effect of scattering albedo ω on variation of gas heat flux Ψ with normalized optical depth τ/τ_L; $\frac{r_1}{r_2}$=0.5, τ_L=1.0.

From Figs. 4.18 and 4.19, it is observed that for given values of τ_L and r_1/r_2, at any location τ/τ_L in the medium, with increase in ω, heat flux Ψ decreases.

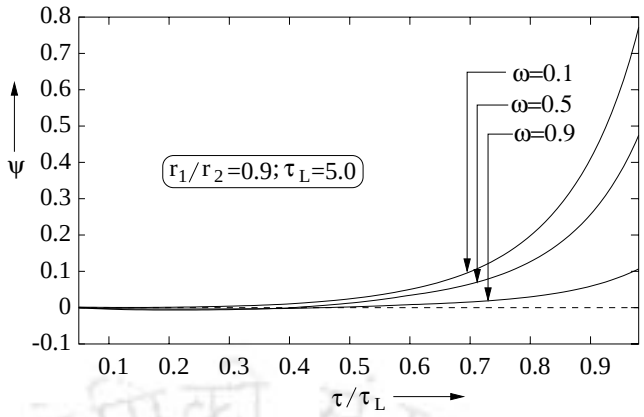

Figure 4.20: Effect of scattering albedo ω on variation of gas heat flux Ψ with normalized optical depth τ/τ_L; $\frac{r_1}{r_2}$=0.9, τ_L=5.0.

This decrease is more as one moves from inner cylinder to the outer cylinder. Further, by comparing Figs. 4.18 and 4.20, it is observed that for a given r_1/r_2, ω is having less effect at higher values of τ_L. From Figs. 4.18 and 4.19, it is observed that for given τ_L and ω, at any point in the enclosure, Ψ is higher for higher values of r_1/r_2.

For the 1-D concentric cylindrical enclosure under consideration, surface plots on variations of inner cylinder wall heat flux Ψ for a combination of two sets of parameters have been presented in Figs. 4.21 and 4.22. These surface plots are useful for better understanding of the influence of different parameters on variations of heat flux.

Variations of inner cylinder wall heat flux Ψ with radius ratio r_1/r_2 and enclosure optical thickness τ_L have been given in Fig. 4.21. These results are for different values of scattering albedo ω. From these surface plots, it is seen that for given values of r_1/r_2 and τ_L with increase in ω values, there is increase in Ψ. For any ω, for a given r_1/r_2, as τ_L increases, Ψ also increases.

In Fig. 4.22, Ψ variations are given with ω and τ_L. Here three different r_1/r_2 have been considered. It is seen from this figure that for a given r_1/r_2, at any ω, with increase in τ_L, Ψ also increases. However, this increase is less at higher values of ω. Further it is observed here that when $\omega \to 1$, Ψ approaches zero.

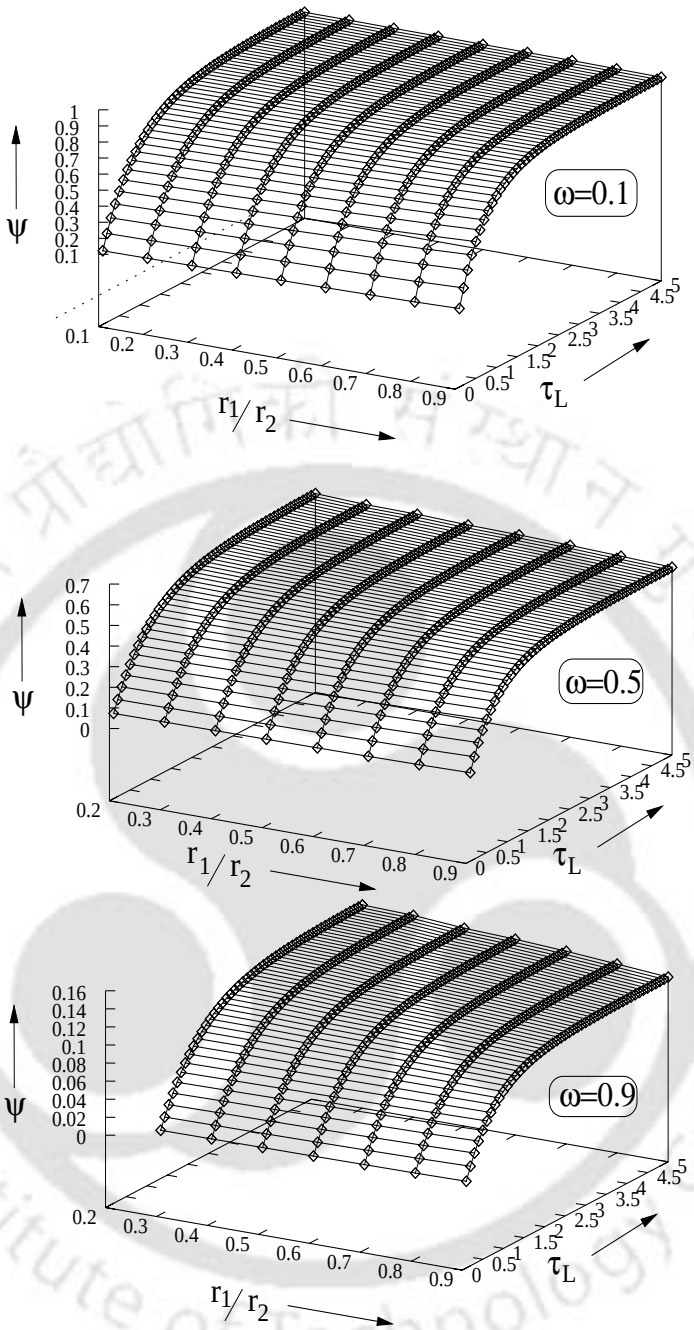

Figure 4.21: Variations of inner wall heat flux Ψ with radius ratio r_1/r_2 and enclosure optical thickness τ_L for different values of scattering albedo ω.

.

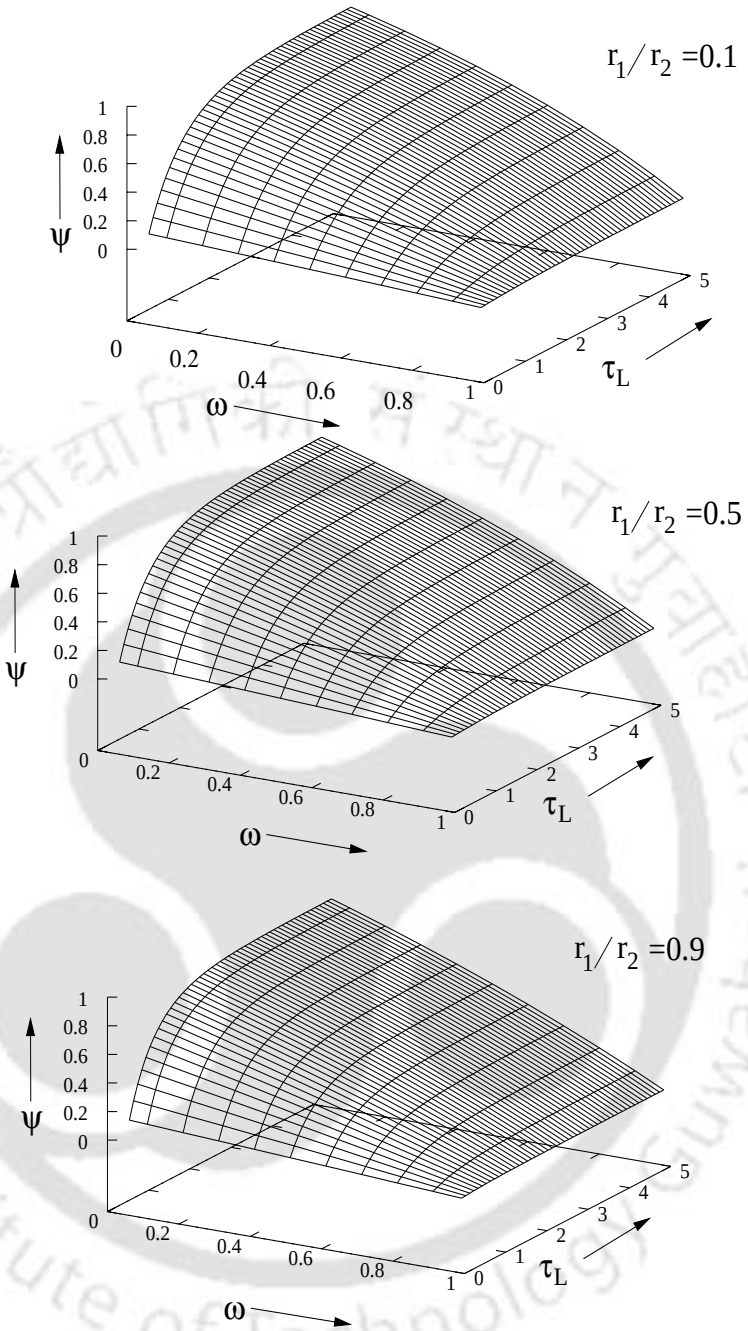

Figure 4.22: Variations of inner wall heat flux Ψ with scattering albedo ω and enclosure optical thickness τ_L for different values of radius ratio r_1/r_2.

4.2.3 Finite Cylindrical Enclosure

In this subsection, CDM has been applied to radiative transfer problems in finite (2-D) cylindrical enclosures. Both single (Fig. 4.1) as well as concentric cylindrical enclosures (Fig. 4.14) have been considered. The bounding walls are black and are at zero temperature. The enclosed gray and homogeneous medium is absorbing-emitting and is isothermal with temperature T_g.

For the finite cylindrical enclosure under consideration, both axial Z and radial r dimensions of the enclosure are finite. As in previous cases, here too, properties in the circumferential direction ϕ of the cylindrical enclosure do not vary. Hence, we are interested in finding radiative information only in the 2-D plane, i.e., the $R-Z$ plane.

Radiative transfer problems in finite cylindrical enclosures have been considered by many investigators. Dua and Cheng [54], Chui and Raithby [184], Menğuç and Viskanta [141], Moder et al. [186] and Murthy and Mathur [189] have reported results for wall heat flux in 2-D cylindrical enclosures.

Non-dimensionalization of different radiative quantities have been done as mentioned in Subsection 4.2.1.

For 2-D cylindrical enclosure, for radial variations of heat flux, enclosure optical thickness τ_L is defined as before. However, when heat flux variations are given along the side wall (curved wall along Z direction), the enclosure optical thickness along the side wall is $\tau_L = \frac{\beta L_Z}{2}$, where L_Z is the length of the cylinder. For the sake of uniformity, in case of 2-D cylindrical enclosure, extinction coefficient β, instead of the enclosure optical thickness τ_L, is taken as the variable to characterize the participating medium.

In Fig. 4.23, heat flux variations on the side wall (curved wall) are given for 2-D finite single cylindrical enclosure. These results are presented for three different extinction coefficients β=0.1, 1.0 and 5.0. In this figure, CDM results with 32 rays and (21$\times$ 1) control volumes are found in good agreement with FVM with 16×30 angular discretisations and 12×16 spatial discretizations [184,189] and

P_3 approximation [141].

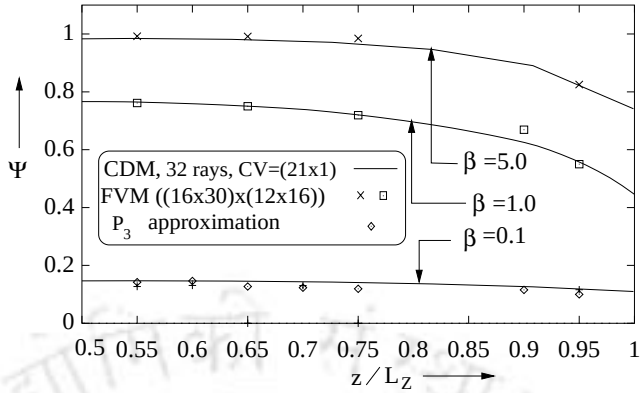

Figure 4.23: Variation of heat flux Ψ along the side wall of a finite cylindrical enclosure containing an absorbing-emitting medium.

It is should again be noted herein that for absorbing-emitting situations considered here, in CDM, with regard to the requirement of number of control volumes, discussions given in Subsecection 4.2.1 hold true. In this case, 21 control volumes in Z direction and only one control volume in the radial direction have been chosen to get heat flux information at 21 points on the side wall.

Heat flux variations on the side wall (curved wall) of 2-D concentric cylindrical enclosure are given in Figs. 4.24-4.26. In all these figures, results have been presented for β=0.1, 1.0 and 5.0. Here, because of the symmetry, Ψ variations have been given for only one half of the cylinder length.

In Fig. 4.24, variations of non-dimensional heat flux Ψ along the side wall of the outer cylinder have been presented for radius ratio r_1/r_2=0.5. It is seen from this figure that heat flux increases with increase in β. Here CDM results with 32 rays and (21 $\times$ 1) control volumes, have been compared with the exact results [54]. Both results compare very well.

It should be noted that wall heat flux Ψ for any optical thickness in case of finite concentric cylinder (Fig. 4.24) is lower than the wall heat flux of the 2-D finite cylinder (Fig. 4.23) for the same optical thickness. This is because, in 2-D concentric cylindrical enclosure radiation is effected by the presence of

cold and black inner cylindrical wall. However, at high extinction coefficient β, as the medium is highly participating, difference in wall heat flux between the cylindrical and concentric cylindrical enclosures is not much.

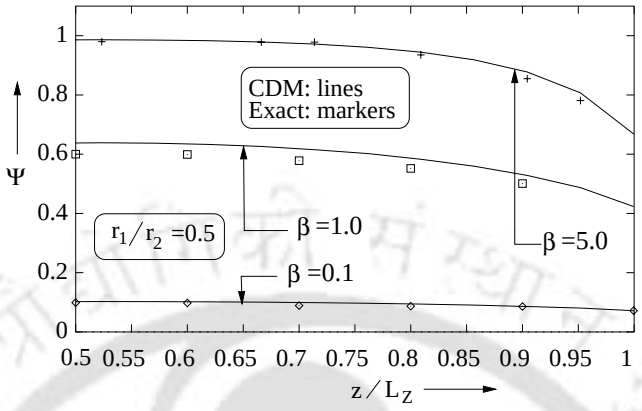

Figure 4.24: Variation of non-dimensional wall heat flux Ψ with normalized enclosure optical thickness z/L_Z for different radius ratios $\frac{r_1}{r_2}$.

In Figs. 4.25 and 4.26 effect of radius ratio r_1/r_2 on non-dimensional heat flux Ψ along the outer wall of the cylindrical enclosure has been shown. In both the figures, results have been presented for four different values of radius ratios, i.e., r_1/r_2=0, 0.1, 0.5 and 0.9. Extinction coefficient β=1.0 and 5.0 have been considered in Fig. 4.25 and 4.26 respectively.

It is observed from Figs. 4.24-4.26 that for a given r_1/r_2 and β, heat flux Ψ is maximum in the center of the side wall $z/L_Z = 0.5$ and is minimum at the extreme end $z/L_Z = 1.0$. This trend is because of the fact that at $z/L_Z = 0.5$, the surface receives maximum radiation whereas at $z/L_Z = 1.0$, because of the end wall, not much radiation is received. Walls being cold, contribution to Ψ at both the places from the enclosure wall is the same. It is entirely the gas radiation which contributes to the heat flux.

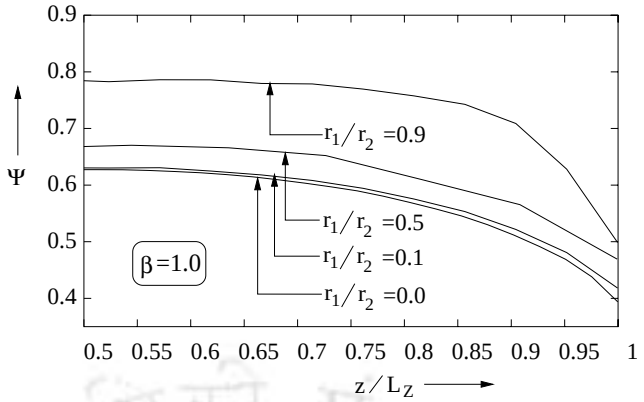

Figure 4.25: Variation of non-dimensional wall heat flux Ψ with normalized enclosure optical thickness z/L_Z for different radius ratios $\frac{r_1}{r_2}$.

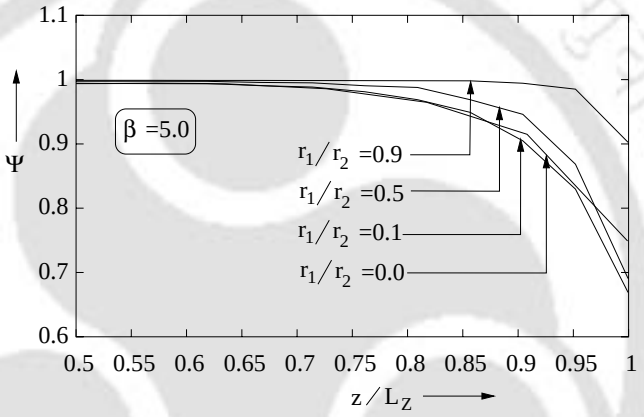

Figure 4.26: Variation of non-dimensional wall heat flux Ψ with normalized enclosure optical thickness z/L_Z for different radius ratios $\frac{r_1}{r_2}$.

4.2.4 Cylindrical Furnace

So far CDM has been successfully applied to various types of benchmark problems in 1-D and 2-D gray cylindrical enclosures with absorbing, emitting and/or scattering medium with constant medium temperature. In this section, a typical furnace problem is considered with variable medium temperature. The furnace under consideration is 6 m long and 2 m in diameter. The furnace walls are maintained at 500 K. The enclosed medium is absorbing-emitting. Medium temperature T_g varies only in the axial direction. This variation is shown in Fig. 4.25. Furnace walls are gray.

This problem has been reported by Chui and Raithby [184] and Kim and Baek [187]. Similar problems have also been dealt by Chui [255], Baek and Kim [256], Kim and Baek [187], Menğuç and Viskanta [141] and Jamaluddin and Smith [254].

In Fig. 4.27 variation of heat flux q (in kW/m^2) along the side wall of the cylindrical furnace has been given. As expected, the net heat flux q is positive as medium is at higher temperature than the enclosure walls. It is maximum at the region where temperature is the highest (2000 K). With decrease in temperature, its value also decreases. The asymmetry of the temperature profile is directly reflected in the distribution of net radiative heat flux q. Here CDM results have been obtained with 32 rays and (18 $\times$ 1) control volumes for extinction coefficient β=1.0. Results have been obtained for situations in which all the bounding walls are black as well as gray with emissivity ϵ_w=0.7. For black wall situation, CDM results have been compared with FVM [187] with (6 $\times$ 4) angular discretization and (8 $\times$ 8 $\times$ 18) spatial discretization. It is seen that CDM is able to correctly predict heat flux information in a practical furnace.

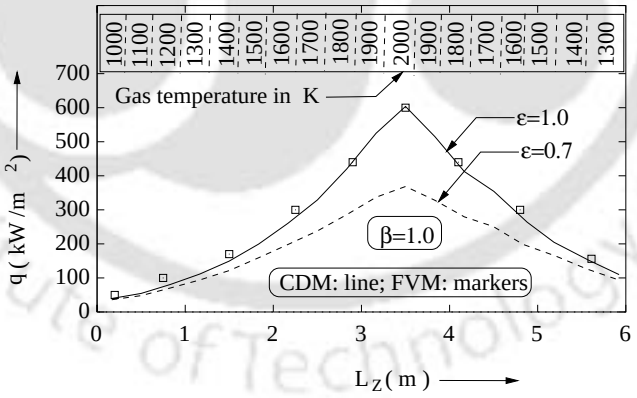

Figure 4.27: Variation of local radiative heat flux q (kW/m^2) along the side wall of the cylindrical furnace.

4.2.5 Finite Cylindrical Enclosure with Flux Boundary

In all the test problems considered in Chapter 3 and Chapter 4 (Section 4.1), CDM has been applied to radiative transfer problems in enclosures whose boundaries have been maintained at zero temperature. With the objective of proving the applicability of CDM to a more general situation, in this subsection, CDM is applied to a different class of problems. Here, we consider radiative transfer problem in a finite black cylindrical enclosure (Fig. 4.28) containing homogeneous absorbing but non-emitting medium. Medium is cold (at zero temperature) and all the bounding walls (including the bottom wall) are also at zero temperature. The top wall of the enclosure is subjected to a diffuse radiant flux Q_{in}. This problem has been dealt by Crosbie and Farrel [55] and Chui [255].

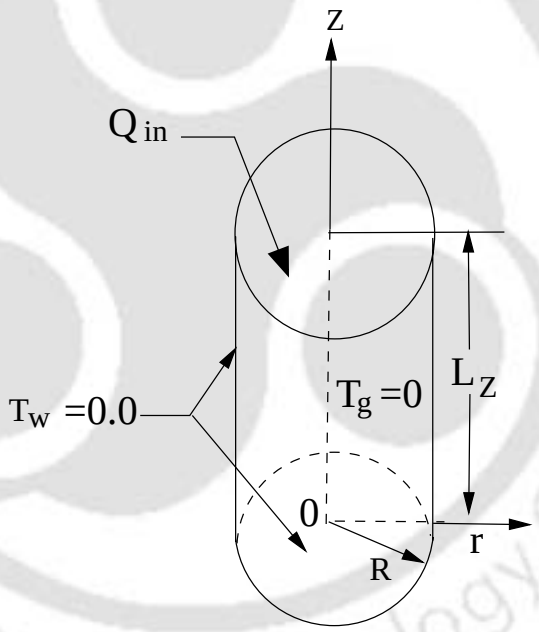

Figure 4.28: A finite cylindrical enclosure subjected to heat flux Q_{in} at one end.

Since top wall of the enclosure is subjected to a constant and uniform heat flux, following the procedures given in Chapter 2, Section 2.5.1, the effective boundary intensity of the top wall is found as $I_w = Q_{in}/2$. By knowing the

boundary intensity I_w, the solutions are found with the help of equations (Eqs. (3.1)-(3.4)) given in Chapter 3. In this problem, effective intensity has been non-dimensionalized with respect to top wall boundary intensity $I_w = Q_{in}/2$ whereas heat flux has been normalized with respect to Q_{in}.

For the problem under consideration, variations of heat flux Ψ with z/L_z along the side wall of the cylindrical enclosure have been given in Figs. 4.29a and b. Here these variations are given for three different aspect ratios, i.e., (AR=$\frac{\text{radius}}{\text{height}}$=0.4:1.0, 1.0:1.0 and 5.0:1.0). Results in Fig. 4.29a correspond to $\beta = 1$, whereas that in Fig. 4.29b correspond to β=5. These results have been

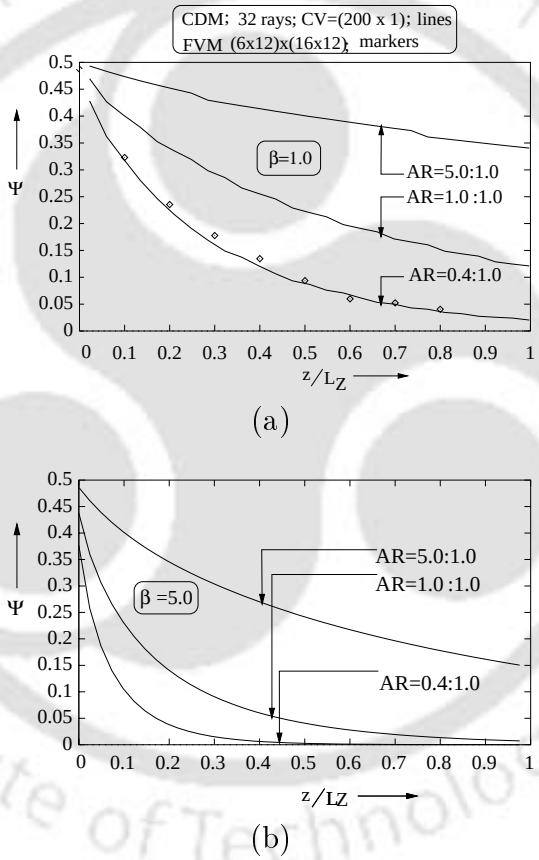

Figure 4.29: Variation of heat flux Ψ along the side wall (a) $\beta = 1$ and (b) $\beta = 5.0$.

obtained with 32 rays. For aspect ratio AR=0.4:1.0, CDM results have been compared with FVM [255] with (6 × 12) angular discretization and (16 × 12)

spatial discretization. Results from both the methods compare very well.

4.2.6 Economy

Apart from the study on the applicability of CDM to 1-D and 2-D cylindrical enclosures with different radiative parameters, boundary conditions, etc., it is important to know the computational effort required in this method. With this in mind, economy aspect of CDM has been discussed herein. For lack of computer codes from other methods, here comparison has been made with the exact method [58]. For comparison purpose, all the computations have been performed on HP-9000/J200 computer.

Comparison of CPU times (second) of CDM and exact method [58] has been given in Table 4.3. This comparison has been made for radiative transfer prob-

ω	τ_L	CPU time (second) on HP-9000/J200	
		CDM (32 rays)	Exact (32 Gaussian points)
0	0.1(1)	Time negligible	43.1
	1.0(1)	(computer	43.5
	2.0(1)	does not	43.6
	5.0(1)	show)	43.9
0.1	0.1(50)	0.1	72.5
	1.0(50)	0.1	73.0
	2.0(50)	0.1	73.3
	5.0(50)	0.1	73.9
0.5	0.1(100)	0.5	72.5
	1.0(100)	0.6	87.7
	2.0(100)	0.7	73.1
	5.0(100)	0.6	73.3
0.9	0.1(150)	3.3	72.5
	1.0(150)	4.6	72.5
	2.0(150)	4.8	87.2
	5.0(150)	4.5	87.6

Table 4.3: CPU time (second) required for the evaluation of wall heat flux Ψin case of absorbing-emitting-isotropically scattering isothermal gray medium confined in 1-D black cylindrical enclosure.

lem in infinite single cylindrical enclosure considered in Subsection 4.2.1. In this table, in the column for τ_L, numbers in bracket indicate the number of control volumes required to get the correct results in CDM. For this comparison, in CDM, 32 rays have been used. In the exact method, for all the cases, integrations have been performed using 32 Gaussian points. In case of CDM, for absorbing-emitting medium, time was so negligible that computer did not report. From this table, it is evident that CDM is economical than the exact method for all ranges of radiative parameters.

4.3 Radiative Equilibrium

In the following pages, applicability of CDM to radiative transfer problems in 1-D concentric cylindrical enclosures (Fig. 4.14) under radiative equilibrium situation has been studied. Gray and homogeneous medium inside the gray cylindrical enclosure is absorbing, emitting and anisotropically scattering. Anisotropy of the medium is approximated by linear anisotropic phase function (Eq. 2.33). Inner and outer cylinders are at temperatures T_1 and T_2 and emissivities ϵ_1 and ϵ_2 respectively. Temperature of the inner cylinder is more than the outer cylinder.

As discussed in earlier sections on 1-D concentric cylindrical enclosure, here also the Z dimension is infinite and radiative properties such as emissivity and the boundary condition do not vary along the circumference of the cylinder walls. Hence, radiative information are required only along the radial direction r.

It has been mentioned in Chapter 2 that radiative equilibrium situation prevails when medium temperature is very high. In this situation, compared to radiation, conduction and convection are negligible and thus the divergence of radiative heat flux (Eq. (2.41)) is zero. In radiative equilibrium situation, medium temperature is not known.

In the present case, for non-dimensionalization of effective intensity, heat flux,

etc., inner cylinder temperature T_1 has been taken as the reference temperature T_R, and definition of these non-dimensional quantities are same as that given in Sections 2.4-2.6 and Section 3.2. Here, T_g is replaced by T_1

With regard to the number of control volumes and iterations required for this class of problems, discussions given in Section 4.2.1 hold true.

In Figs. 4.30a-b, variation of inner wall heat flux Ψ with enclosure optical thickness τ_L is given for different radius ratios r_1/r_2. In both the figures, results are presented for black bounding walls and medium is absorbing-emitting ($\omega = 0$). In Fig. 4.30a, workability of CDM in low optical thickness range ($0.001 \leq \tau_L \leq 1.0$) has been demonstrated. Here, for radius ratios r_1/r_2=0.01, 0.05,

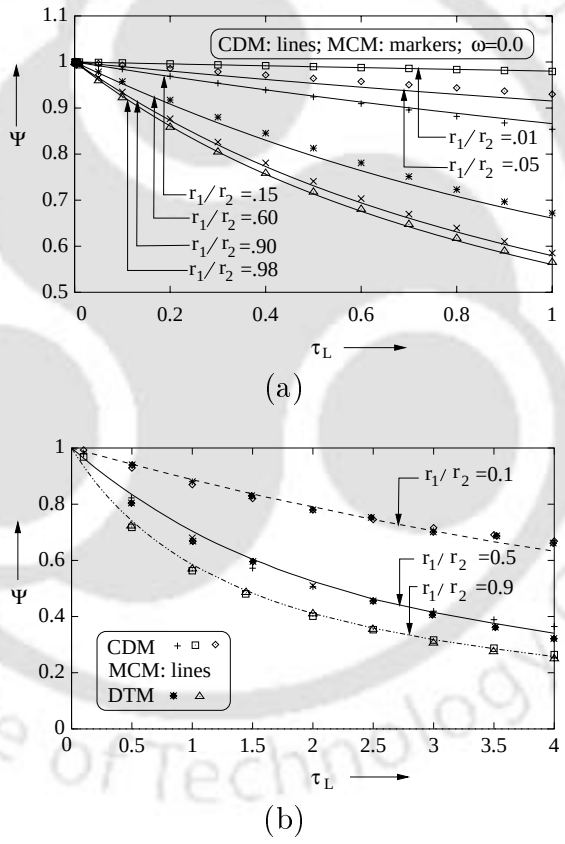

Figure 4.30: Variation of inner wall heat flux Ψ with enclosure optical thickness τ_L for different radius ratio $\frac{r_1}{r_2}$.

0.15, 0.65, 0.90 and 0.98, CDM results with 64 rays have been compared with

MCM[1]. In all the cases, CDM results compare well with MCM results. In Fig. 4.30b, effect of radius ratio r_1/r_2 on inner wall (hot) heat flux have been presented. Here CDM results with 64 rays are compared with DTM [215] with 128 rays and MCM [247]. For results presented in these figures, control volume requirements have been in the range of 400 to 800. With increase in r_1/r_2, the number of control volumes required is found to decrease.

In Figs. 4.31 and 4.32, for absorbing-emitting medium (ω=0), effects of wall emissivity ϵ_w on variations of outer wall heat flux Ψ with enclosure optical thickness τ_L are presented. In all these figures, results have been obtained with 64 rays in CDM. Further, here inner wall has been considered black (ϵ_1=1.0).

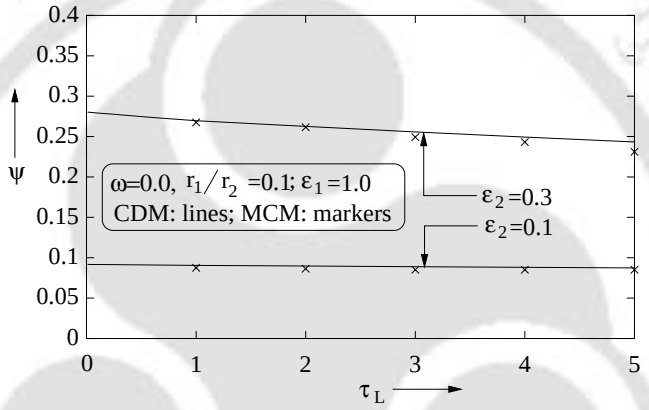

Figure 4.31: Variation of outer wall heat flux Ψ with enclosure optical depth τ_L for different wall emissivities, r_1/r_2=0.1.

In Fig. 4.31, Ψ variations with τ_L are presented for radius ratio r_1/r_2=0.1. Effect of two values of outer wall emissivities, i.e., ϵ_2=0.3 and 0.1 are considered here. From this figure, it is seen that with decrease in outer wall emissivity, wall heat flux decreases. This is because with decrease in wall emissivity, outer wall reflects more radiative energy. CDM results in this case have been compared with MCM [247]. Both results are in very good agreement.

With inner wall as black ($\epsilon_1 = 1$), effects of outer wall emissivity ϵ_2 on variations of outer wall heat flux Ψ for r_1/r_2=0.5 and 0.9 are given in Figs. 4.32a and 4.32b respectively. In both these figures, effects of three different values

[1]Based on [247], MCM data generated by the author

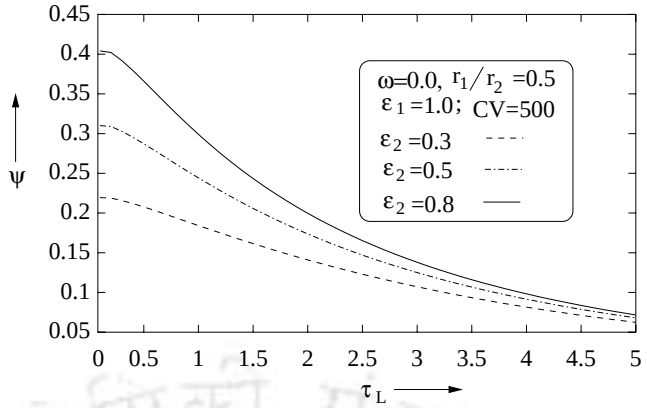

Figure 4.32: Variation of outer wall heat flux Ψ with enclosure optical depth τ_L for different wall emissivities, (a) r_1/r_2=0.5 and (b) r_1/r_2=0.9.

of outer wall emissivities, ϵ_2=0.3, 0.5 and 0.8, are considered. It is observed from these figures that at low optical thickness, ϵ_2 has more pronounced effect than at higher values of τ_L. It is further observed here that the effect of ϵ_2 is more at higher radius ratios.

Effects of anisotropy on variations of heat flux Ψ on inner wall with enclosure optical thickness τ_L are shown in Figs. 4.33a-b. These effects have been studied for 100% forward scattering $a_1\omega = +1$, isotropic scattering $a_1\omega = 0$ and 100% backward scattering $a_1\omega = -1$. In Fig. 4.33a, results are presented for the situation when $r_1/r_2 \to 0$, i.e., the concentric cylindrical enclosure approaches single cylindrical enclosure. On the other hand, in Fig. 4.33b, results are

presented for the other extreme $r_1/r_2 \rightarrow 1$, i.e., 1-D concentric cylindrical enclosure approaches 1-D Cartesian enclosure.

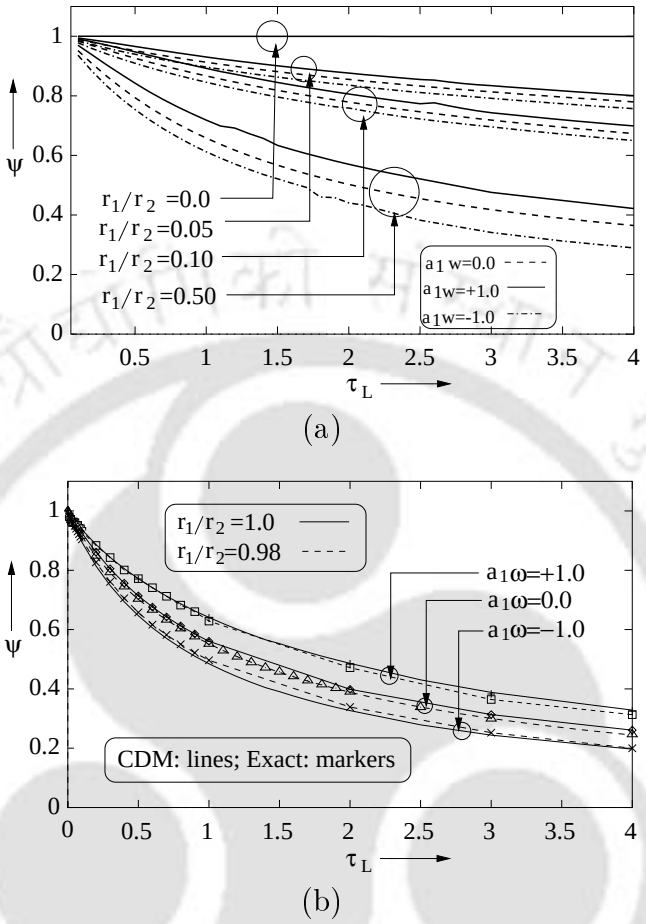

Figure 4.33: Effect of anisotropy on variation of wall heat flux Ψ with enclosure optical depth τ_L.

For results presented in Figs. 4.33a-b, CDM results have been obtained with 64 rays and control volumes required have been in the range of 400-800.

It is observed from Fig. 4.33a-b that for any τ_L, the effect of $a_1\omega$ on Ψ is more pronounced at higher r_1/r_2. Further, for a given r_1/r_2, effect of $a_1\omega$ is more at higher values of τ_L.

One interesting point to be noted from Fig. 4.33a is that for r_1/r_2=0, $a_1\omega$ has no effect on Ψ. This is because r_1/r_2=0 represent the situation for single

cylindrical enclosure. In this case, under radiative equilibrium situation, all radiations emitted from cylinder wall get redistributed on other locations on the same cylinder wall. Hence, anisotropy has no effect. For r_1/r_2=0, one other point which is noted from this figure is that Ψ remains independent of τ_L. This is because, the radiation emitted from the single cylindrical enclosure surface has to remain contained to itself.

In Fig. 4.33b, r_1/r_2=1 represents the case of a 1-D Cartesian enclosure and markers in this figure are results for this case. In this figure, CDM results for concentric cylindrical enclosure with $r_1/r_2 = 0.98$ are compared with the results from exact method [236] for 1-D Cartesian enclosure. It is seen from this figure that as $r_1/r_2 \to 1$, CDM results for concentric cylindrical enclosure approaches the results for 1-D Cartesian enclosure.

Table 4.4 presents number of iterations required for obtaining a converged solution for 1-D concentric cylindrical enclosure for different values of $\tau_L, a_1\omega$ and r_1/r_2. In all the cases, 64 rays have been used. From this table it is seen that with absorbing-emitting situation ($\omega = 0$), number of iterations (5-11) required for obtaining heat flux is small. But, in presence of scattering mechanism ($a_1\omega \neq 0$), iteration requirement (8-24) becomes high. Further, with low optical thickness, solution converges fast. This is because with low optical thickness, medium is more transparent and hence less participating. Under such situation, most of the radiation is captured by the enclosure boundary. Hence, iteration requirement signifies the degree of involvement of radiation with participating medium.

To have an idea on the accuracy in the evaluation of heat flux, % error of three methods, i.e, CDM, DTM [215] and exact method [53] are compared in Figs. 4.34-4.36. These comparisons have been done for CDM results presented in Fig. 4.30b for simple case of absorbing-emitting medium. Percentage error in all the cases have been found with MCM [247] results as the base.

In Figs. 4.34-4.36, percentage error in heat flux on the inner wall of the concentric cylindrical enclosure have been given for $r_1/r_2 = 0.1$, 0.5 and 0.9

τ_L	$a_1\omega$	r_1/r_2	Control volume	Iterations
		0.1	800	9
	-1.0	0.5	500	9
		0.9	400	8
		0.1	800	6
0.1	0	0.5	500	6
		0.9	400	5
		0.1	800	11
	+1.0	0.5	500	11
		0.9	400	9
	+1.0	0.1	800	24
		0.5	500	18
		0.9	400	14
		0.1	800	10
1.0	0	0.5	500	8
		0.9	400	7
		0.1	800	16
	-1.0	0.5	500	14
		0.9	400	10
		0.1	800	24
	+1.0	0.5	500	17
		0.9	400	13
		0.1	800	11
5.0	0	0.5	500	9
		0.9	400	7
		0.1	800	18
	-1.0	0.5	500	13
		0.9	400	14

Table 4.4: Number of iterations required for getting convergent solution for 1-D concentric cylinders in radiative equilibrium situation.

respectively. These variations are considered with τ_L in the range [0.05, 4]. From these figures it is observed that the % error in CDM is comparable to DTM. Moreover, error in CDM is lower than that reported by Loyalka [53] for radius ratios r_1/r_2=0.5 and 0.9. However, error in CDM and DTM are more than that of Loyalka's results for low radius ratio r_1/r_2=0.1. Both CDM and DTM being ray tracing methods, this deviation can be attributed to the

influence of the curvature of the wall.

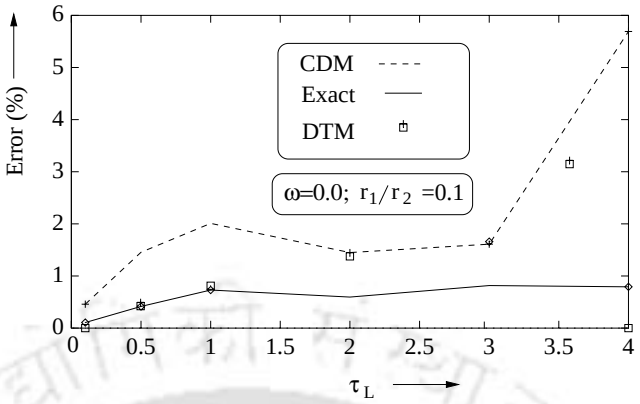

Figure 4.34: Variation of % error in wall heat flux Ψ with τ_L for r_1/r_2=0.1.

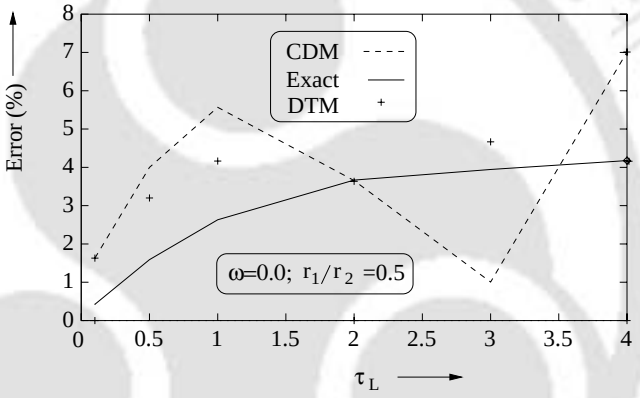

Figure 4.35: Variation of % error in wall heat flux Ψ with τ_L for r_1/r_2=0.5.

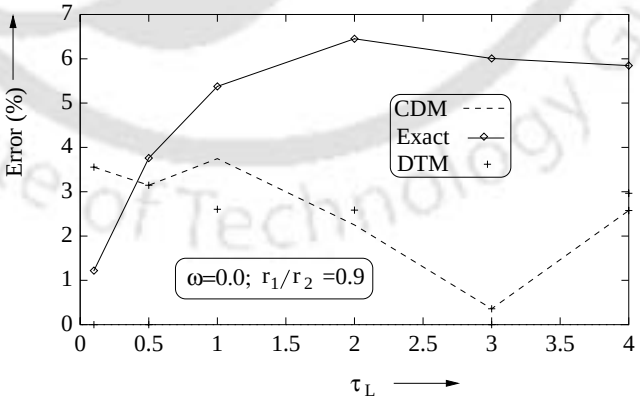

Figure 4.36: Variation of % error in wall heat flux Ψ with τ_L for r_1/r_2=0.9.

It has been discussed in Subsection 4.2.1 that under radiative equilibrium situation, correct prediction of heat flux Ψ demands large number of control volumes. This is even true for simple case of absorbing-emitting medium ($\omega = 0$). This is because under radiative equilibrium situation, source function (Eq. 2.31) is not constant.

In case of concentric cylindrical enclosures considered in the present study, computational grids are in the form of concentric rings. To calculate the source function over such grids, as we move from center towards the outer cylinder, between any two CVSCPs, for a given ray angle, optical path-leg changes. For a given ray angle, this path is maximum when CVSCPs are adjacent to the outer cylinder. This is true for the semi circle of the effective rays focusing towards the outer cylinder. These rays will have origin either from inner or outer cylinders.

From the above, it is clear that the requirement of control volume is attributed to the value of gradients of the source function. In the following paragraphs, its influence on number of control volumes has been discussed.

In Figs.4.37a-b, gradient of source function $dS^*/d(\tau/\tau_L)$ are plotted with non-dimensional enclosure optical depth τ/τ_L. Figures 4.37a and 4.37b present the variations of the gradient of source function S^* with normalized optical depth τ/τ_L for two different radius ratios r_1/r_2=0.1 and 0.9 respectively. In both these figures, calculations have been done with 64 rays. From Fig. 4.37a, it is seen that gradient in the source function is fluctuating in the range $0 \leq \tau/\tau_L \leq 0.28$. For $\tau/\tau_L > 0.28$, this gradient is stable and uniform and it is achieved with 400 control volumes. For low radius ratio, the fluctuation in the gradient of the source function can be minimized by considering sufficiently large number of control volumes. However, this will be at the cost of computational time. In the present study, for low r_1/r_2, 800 control volumes have been found sufficient.

From Fig. 4.37a and b, it is observed that with increase in radius ratio, the fluctuation in the gradient of the source function reduces and in this situation,

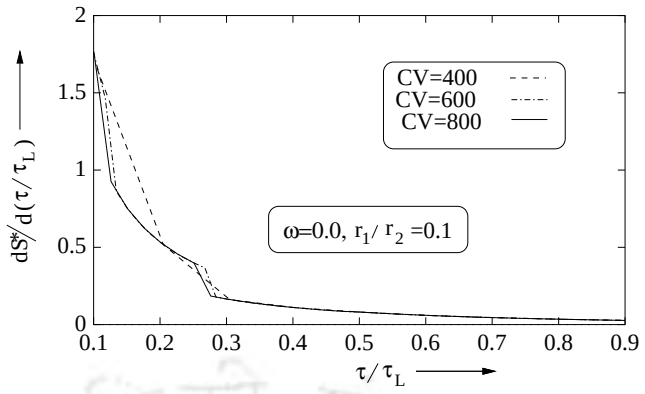

Figure 4.37: Variation of gradient of source function $dS^*/d(\tau/\tau_L)$ with optical thickness τ/τ_L.

comparatively less number of control volumes are required. In Fig. 4.37b, 400 control volumes have been found to be enough. In this section on radiative equilibrium, for getting the converged solution, in all our calculations we have used 800, 500 and 400 control volumes for radius ratios r_1/r_2=0.1, 0.5 and 0.9 respectively.

It has been mentioned before that in case of radiative equilibrium situation, temperature of the medium is an unknown. It varies from point to point. For the radiative transfer problems considered in this section, some sample results on emissive power are presented in the following paragraphs.

In this case, non-dimensional emissive power Φ has been obtained from

$$\Phi = \left(\frac{T_g}{T_1}\right)^4$$

where T_g is the medium temperature and T_1 is the reference temperature, which is the temperature of the inner cylinder. In case of radiative equilibrium situation, $\nabla \cdot q_R$ (Eq. (2.41)) is zero. With this, the relation between T_g and G' is found (Eq. (2.45)). Now, with G' known, T_g and hence Φ is calculated.

Variations of emissive power Φ with normalized optical depth τ/τ_L for 1-D concentric cylindrical enclosure under radiative equilibrium are given in Figs. 4.38-4.42. Effect of enclosure optical thickness τ_L on Φ has been given in Figs. 4.38-4.40. Effect of anisotropy has been shown in Figs. 4.41 and 4.42. These results are presented for different radius ratios $\frac{r_1}{r_2}$.

In Fig. 4.38, Φ variations are given for $\frac{r_1}{r_2} = 0.1$, whereas the same are given for $\frac{r_1}{r_2} = 0.5$ and 0.9 in Figs. 4.39 and 4.40.

In Fig. 4.38a and 4.38b, emissive power distribution Φ obtained from CDM with 64 rays and 800 control volumes have been compared with DTM [215] with 84 rays and MCM [247]. As optical thickness τ_L decreases, near the inner wall, Φ also decreases. Opposite is the trend at the outer cylinder. This is because with decrease in τ_L, the gas becomes more transparent, a gas element can 'see' the outer surface better, and its emissive power becomes closer to that of the outer wall, which is at the lower temperature. It is seen from these figures that for all the cases, CDM results are found in very good agreement with DTM and MCM.

In Fig. 4.39, for $r_1/r_2 = 0.5$, the effect τ_L on the variation of emissive power Φ has been presented. Here, effects of three different values of τ_L (=2.0, 3.0 and 5.0) have been shown.

It has been mentioned before that as $r_1/r_2 \to 1$, 1-D concentric cylindrical enclosure approaches 1-D planar medium. For this situation, Φ distribution for $r_1/r_2 \to 1$ will also approach Φ distribution for 1-D planar medium. This very fact has been demonstrated in Fig. 4.40. In this figure, CDM results

for Φ for $r_1/r_2 = 0.9$ have been compared with Φ distribution for 1-D planar medium [29]. It is seen that CDM results for $r_1/r_2 = 0.9$ are much closer to the exact results for 1-D planar medium.

Effect of anisotropy on Φ distribution in 1-D concentric cylindrical enclosure are presented in Figs. 4.41 and 4.42. Here two extreme cases, i.e, 100% forward scattering (a_1=+1) and 100% backward scattering (a_1=-1) are considered. For the sake of comparison, results are also presented for isotropic scattering

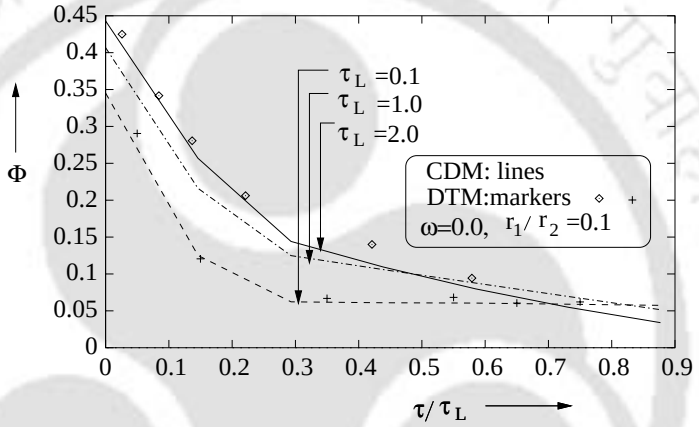

(a)

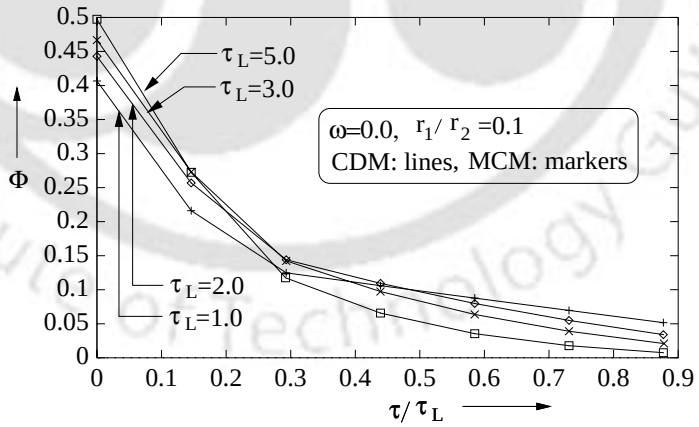

(b)

Figure 4.38: Effect of optical thickness τ_L on variation of emissive power Φ with normalized optical depth τ/τ_L.

(a_1=0).

In Figs. 4.41a -b, results are given for radius ratio r_1/r_2=0.5. with τ_L=1.0 and 4.0 respectively.

In Figs. 4.42a and 4.42b, we have considered enclosure thickness τ_L=0.1 with radius ratios r_1/r_2=0.1 and 0.9 respectively. From Figs. 4.41-4.42, it is seen

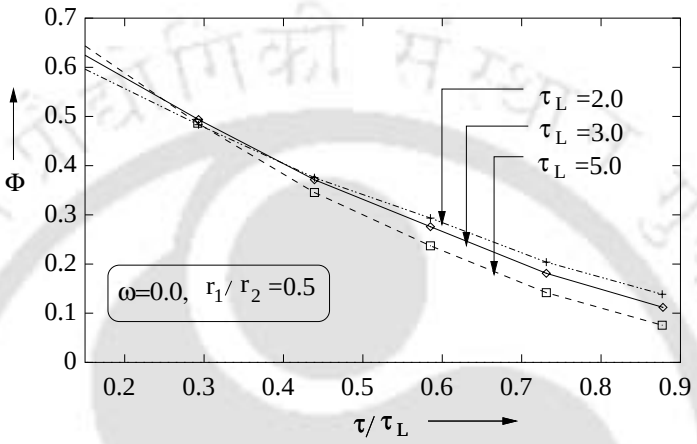

Figure 4.39: Variation of emissive power Φ with normalized optical depth τ/τ_L.

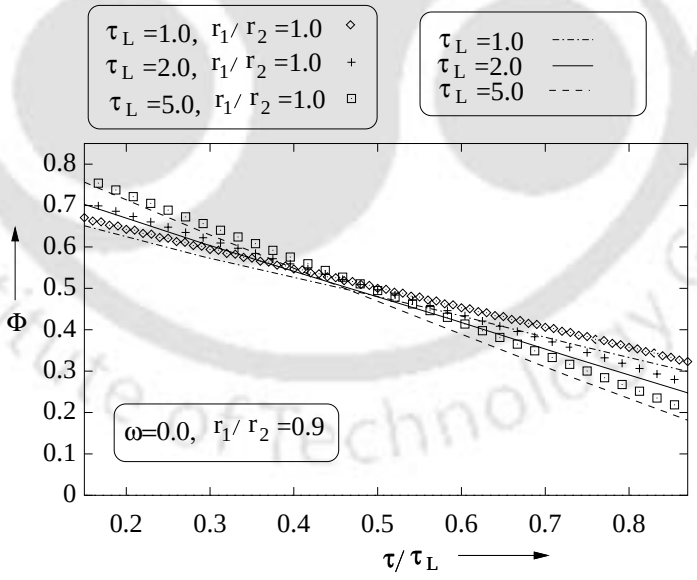

Figure 4.40: Effect of optical thickness τ_L on variation of emissive power Φ with normalized optical depth τ/τ_L.

that effect of anisotropy is less near the inner cylinder. It is further observed from results presented in Figs. 4.41 and 4.42 that at lower values of τ_L, $a_1\omega$ has negligible effect.

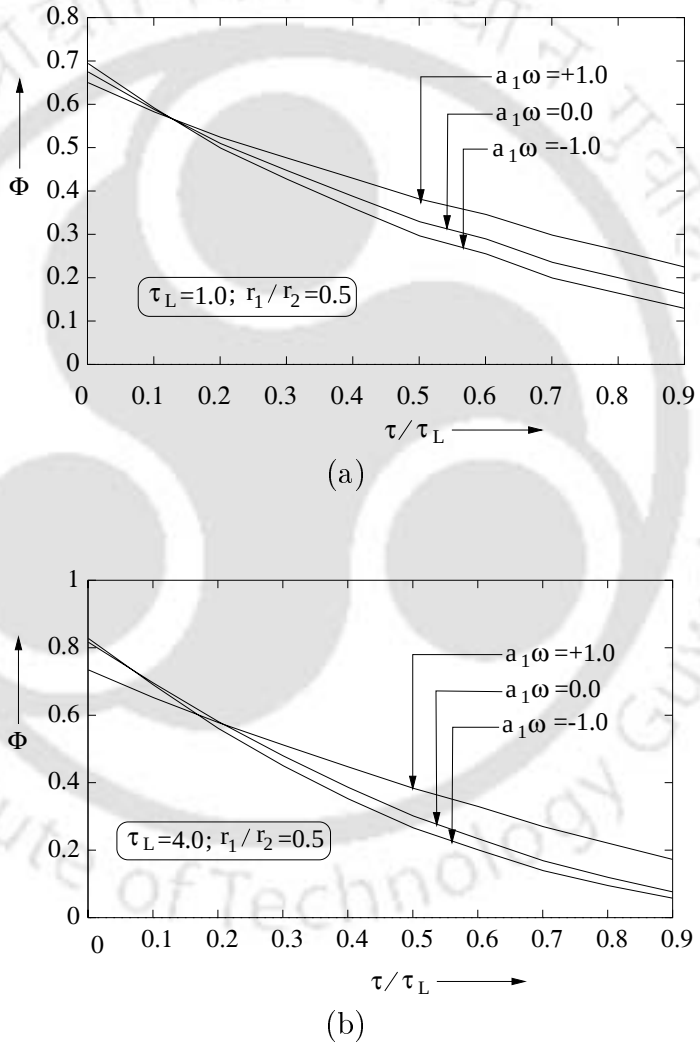

Figure 4.41: Variation of emissive power distribution Φ with normalized enclosure optical thickness τ/τ_L for different radius ratios $\frac{r_1}{r_2}$.

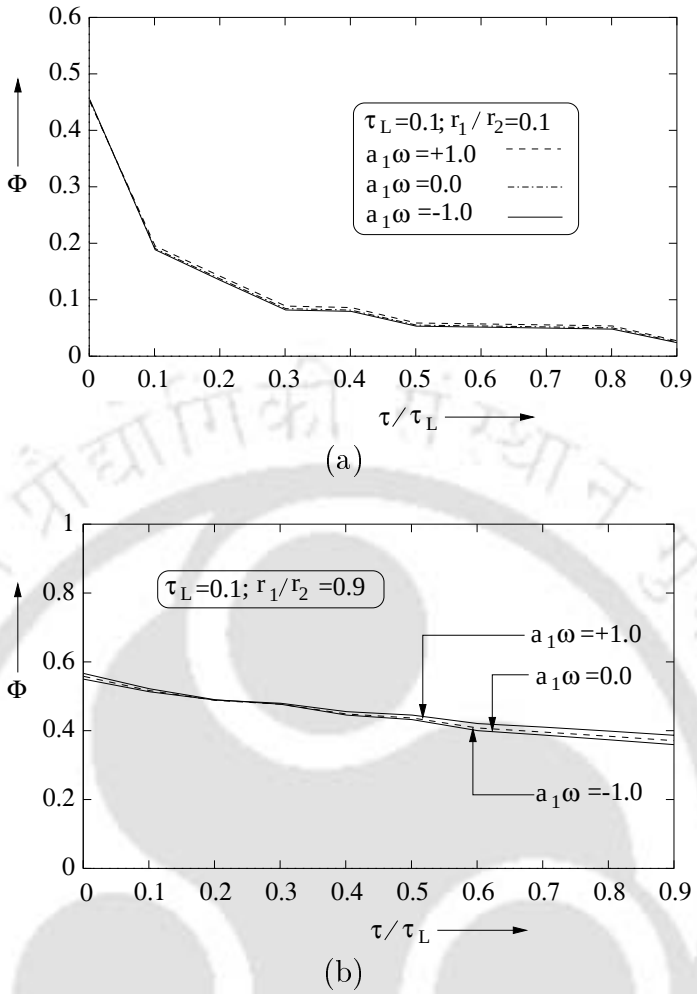

Figure 4.42: Variation of emissive power distribution Φ with normalized enclosure optical thickness τ/τ_L. $\frac{r_1}{r_2}$=0.1 and 0.9.

4.3.1 Economy

It has been mentioned before that in case of radiative equilibrium, even for the absorbing-emitting situation, source function appearing in Eq. (2.31) is not constant. It has to be recursively used over small optical path-leg, which means requirement of a large number of control volumes. It has been mentioned above that for correct prediction of CDM results, control volumes in the range of 400 to 800 were required. Further, as the source function is unknown, the solution procedure is an iterative one. To have an idea of CPU time required

$\frac{r_1}{r_2}$	τ_L	CPU time (seconds) on HP-9000/J200	
		CDM	MCM
0.1	0.1	0.5 (800)	6.1
	1.0	0.5 (800)	19.1
	2.0	0.5 (800)	39.7
	4.0	0.5 (800)	92.6
0.5	0.1	0.3 (500)	6.2
	1.0	0.3 (500)	19.6
	2.0	0.3 (500)	36.8
	4.0	0.3 (500)	71.8
0.9	0.1	0.2 (400)	6.5
	1.0	0.2 (400)	20.5
	2.0	0.2 (400)	36.3
	4.0	0.2 (400)	67.4

Table 4.5: CPU time (seconds) required for evaluation of wall heat flux Ψ in case of absorbing-emitting gray medium confined between concentric cylindrical enclosures. Numbers in the bracket in the CDM column indicate the number of control volumes required.

by CDM, for some sample test cases, a comparison is presented here in Table 4.5. For lack of codes from other methods such as DTM, FVM, DOM, etc., the comparison herein has been made with the MCM. MCM code written by the author is based on reference [247]. All computational runs have been taken on HP-9000/J200 computer. For generating MCM results, a total of 1,00,000 photons were emitted from the source wall.

From Table 4.5, it is seen that even with large number of control volumes, CDM takes very less time compared to MCM.

4.4 Summary

CDM has been validated by solving different types of radiative transfer problems in cylindrical enclosures with gray and homogeneous participating medium. Some sample benchmark problems have been solved in 1-D and 2-D single as

well as concentric gray cylindrical enclosures with absorbing, emitting and scattering medium. For the chosen geometry, problems have been solved for both radiative and non-radiative equilibrium conditions. Depending upon the geometry, OTCs have been suitably evaluated. For all the cases considered in this chapter, depending upon the availability of results in the literature, CDM results have been compared. In all the cases, CDM has been found to give correct prediction of radiative information.

In Chapters 3 and 4, with workability of CDM proved for different types of enclosures in which only radiative information were required, next step is to see how well this method works for a conjugate radiation, conduction and/or convection problems. This very aspect has been taken up in the next chapter.

Chapter 5

Validation Studies: Conjugate Problem

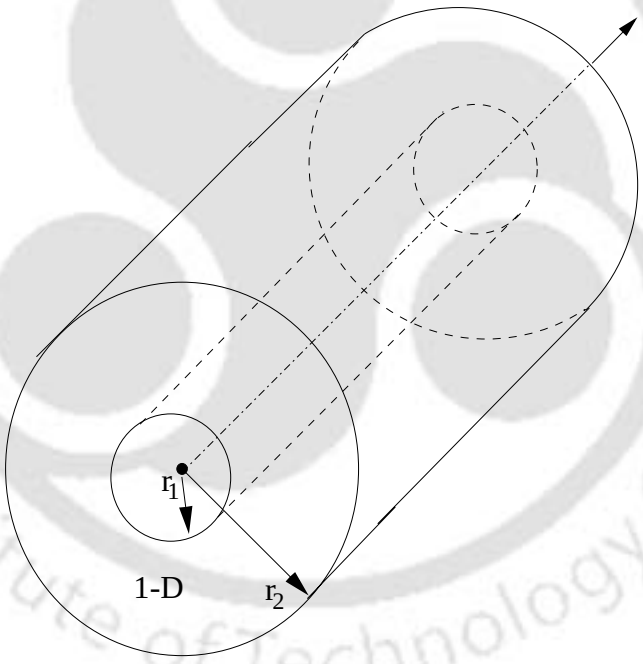

5.1 Introduction

Analysis of radiation combined with conduction and/or convection heat transfer in enclosures containing participating medium has got numerous engineering applications. Examples of such applications are in the analysis of heat transfer through high temperature energy conversion devices, semi-transparent materials, fibrous and foam insulations, porous materials, etc.

Because of the complex mechanism, analysis of problems involving radiation combined with conduction and/or convection in participating medium, is difficult. The equation for conservation of total energy (Eq. 1.1) is a highly non-linear integro-differential equation. For a general situation, its exact analytical solution is not possible. Hence, there has been the need for the development of numerical methods. Using various methods cited in the literature review presented in Chapter 1, Arpaci [257], Cess [258], Cheng and Özişik [259], Chawla and Chan [260], Chang et al. [261], Tan and Howell [262], Burns et al. [198], Borjini et al. [263], Krishnaprakash et al. [264], Hossain et al. [265], Baek et al. [266], Yamada [267], Yih [268], Yuner and Özişik [269],Yan and Li [270] and Yucel et al. [271] have reported results of some combined radiation-convection problems. Works on radiation combined with conduction and convection are not many. These have been reported in [133, 208, 209, 272–274].

Radiation combined with conduction has been the interest of many researchers. In high temperature applications, this situation occurs with stationary participating medium. Some details about the radiation-conduction problems with participating medium have been provided in [28–30]. Most of the works in this line are reported for 1-D and 2-D Cartesian enclosures [178, 199, 232, 275, 276]. Kamiuto et al. [145], Fernandes and Francis [201], Harris [277] and Kim and Smith [278] have solved combined radiation-conduction problems with regular cylindrical enclosures. Review of works on combined radiation-conduction problems in dispersed medium has been discussed by Reiss [279]. Sutton [280] has provided a convenient catalogue of major works pertaining to radiation-conduction problems. A summary of literature review made by the author on methods applied to combined radiation and conduction heat transfer problems

has been given in Table. 5.1.

Medium	Enclosure	Method	Investigator
isotropic scattering	1-D planar	FEM	Fernandes et al. [199]
do	Concentric cylindrical	FEM	Farnandes and Francis [201]
anisotropic scattering	2-D rectangular	S_N	Kim and Baek [178]
scattering	1-D planar	MCM	Abed and Sacadura [75]
anisotropic scattering	Annular	P_N	Harris [277]
absorbing emitting	2-D cylindrical	zone	Kim [278]
absorbing emitting scattering	2-D rectangular	DOM	Baek and Kim [281] Sakami et al. [177]
isotropic scattering	1-D planar	P_1/P_3	Ratzel and Howell [135]
isotropic scattering	2-D rectangular	P_N	Ratzell [136, 148]
anisotropic scattering	1-D planar	CDM	Talukdar and Mishra [249]
isotropic scattering	1-D planar	DIM	Shih and Chen [232]
absorbing emitting	1-D planar	iterative	Viskanta and Grosh [275]
scattering	1-D planar	iterative	Viskanta [248]
anisotropic scattering	1-D planar	SA	Yuan and Wong [250]
anisotropic scattering	1-D planar	DOM	Krishnaprakash et al. [282]
scattering	1-D planar	iterative	Lii and Özişik [283]
scattering	2-D rectangular	Galerkin	Ho and Özişik [284]
absorbing scattering	1-D planar	two-flux	Burgquam and Seban [285]

Table 5.1: Summary of literature survey for combined radiation-conduction heat transfer problems.

The literature survey has indicated that not all the methods which have been discussed in Chapter 1, are suitable for the combined radiation, conduction and/or convection heat transfer problems. The zone method and MCM are weak in solution of conjugate mode heat transfer problems as they are not compatible to different grids associated with radiation and conduction and/or convection. The FEM and P_N approximations are widely used by many researchers. But these methods are also having certain drawbacks.

In earlier chapters, applicability of CDM has been demonstrated for various types of problems in which only radiative information were required. In this chapter, applicability of CDM is demonstrated for radiation combined with conduction heat transfer. The study is made with 1-D concentric cylindrical enclosures containing absorbing, emitting and anisotropically scattering medium. Only steady state situation is considered. Effects of conduction-radiation parameter, optical thickness, scattering albedo, anisotropy factor, wall emissivity and radius ratio on temperature and heat flux are discussed. Depending upon the availability of results, CDM results are compared with those available in the literature.

5.2 Formulation

In Fig. 5.1, a gray concentric cylindrical enclosure is considered. The enclosure is infinite in Z direction, whereas it is finite in the radial direction r. Radiative properties as well as the conditions imposed on the bounding surfaces do not vary in the circumferential direction ϕ. Thus, similar to the cases discussed in Chapter 4, Subsections 4.2.1 and 4.2.2 on cylindrical enclosures, here too, the radiative information are required only in one dimension, i.e. the radial direction r. Radii of inner and outer cylinders are r_1 and r_2 respectively. The gray and homogeneous participating medium enclosed between the two cylinders is absorbing, emitting and anisotropically scattering. The inner wall of the enclosure is at uniform temperature T_1 and outer wall is at uniform temperature T_2. The inner wall is at higher temperature than the outer wall.

Enclosure walls are gray with wall emissivity ϵ_1 and ϵ_2 for the inner and outer walls respectively. Thermal conductivity of the medium is k and is assumed constant. Extinction coefficient β of the medium is also assumed constant.

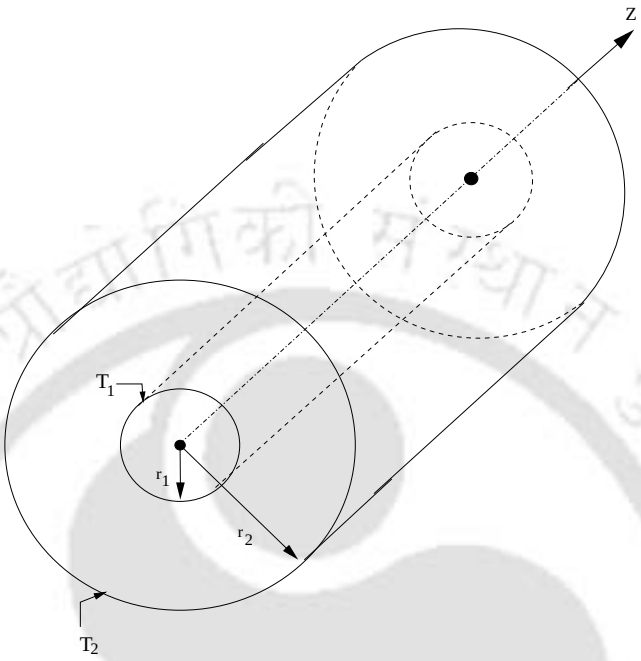

Figure 5.1: 1-D concentric cylindrical enclosure.

In absence of convection and heat generation, equation for conservation of total energy (Eq. 1.1) under steady state condition, in non-dimensional form is written as [144, 201]

$$\frac{d^2\theta}{d\tau^2} + \frac{1}{\tau}\frac{d\theta}{d\tau} = \frac{1}{4N}\frac{d\Psi_R}{d\tau} \tag{5.1}$$

where θ is the non-dimensional medium temperature and τ is the optical depth measured in the radial direction. Here for non-dimensionalization of temperature, inner wall temperature T_1 has been taken as reference. In Eq. (5.1), Ψ_R is the non-dimensional radiative heat flux and N is the conduction-radiation parameter (Stark number) defined as

$$N = \frac{k\beta}{4\sigma T_1^3} \tag{5.2}$$

In the study of combined radiation and conduction heat transfer problems, N is an important parameter. It tells us about the relative contributions of each mode of heat transfer. For $N \to 0$, the radiative component is very large. For N=0, the situation becomes entirely radiation dominant and is treated like problems under radiative equilibrium. On the other extreme, as $N \to \infty$, (∞ indicates a large finite value) radiation part is negligible. The problem is conduction dominated. In the range $0 < N < \infty$, both radiation and conduction modes of heat transfer will be present and relative contributions to the total heat flux can be estimated by knowing the value of this parameter.

For the problem under consideration, the energy equation (Eq. (5.1)) is subjected to the following boundary conditions.

$$\theta(0) = \left(\frac{T_1}{T_1}\right)_{r_1} = \theta_1 = 1 \tag{5.3}$$

$$\theta(\tau_L) = \left(\frac{T_2}{T_1}\right)_{r_2} = \theta_2 \tag{5.4}$$

Right hand side of Eq. (5.1) contains divergence of radiative heat flux $\frac{d\Psi_R}{d\tau}$, which from Eqs. (2.51) and (2.52) is given by

$$\frac{d\Psi_R}{d\tau} = \eta(1-\omega)\left[\pi\theta^4 - \frac{G'^*}{2}\right] \tag{5.5}$$

In Eq. (5.5), η is the OTC, ω is the scattering albedo and G'^* is the non-dimensional effective incident radiation. In CDM, G'^* is given by

$$G'^* = \frac{G'}{\frac{\sigma T_1^4}{2}} = \int_0^{2\pi} I^*(\alpha)d\alpha \tag{5.6}$$

where I^* is the non-dimensional effective intensity defined as

$$I^* = \frac{I}{\frac{\sigma T_1^4}{2}} \tag{5.7}$$

and α is the angle of the effective intensity measured from the control surface. In Eq. (5.6), effective intensity at any point n+1 in the direction α is given by

$$I^*_{n+1} = I^*_n \exp(-\tau\eta) + S^*_{av}\left[1 - \exp(-\tau\eta)\right] \tag{5.8}$$

This definition of I^* is based on the fact that the distance between points n and n+1 along the ray direction α is small enough and the source function given by the following equation can be assumed constant over the path-leg. This constant value of the source function is equal to its average value at points n and n+1.

$$S^* = (1-\omega)\theta^4 + \frac{\omega}{2\pi}\Big[G^{'*} + 2a_1 \sin\alpha \Psi_R(\tau)\Big] \tag{5.9}$$

It should be noted that the expression of the source function given by urface. In Eq. (5.6), effective intensity at any point n+1 in the direction α is given by

$$I^*_{n+1} = I^*_n \exp(-\tau\eta) + S^*_{av}\Big[1 - \exp(-\tau\eta)\Big] \tag{5.10}$$

This definition of I^* is based on the fact that the distance between points n and n+1 along the ray direction α is small enough and the source function given by the following equation can be assumed constant over the path-leg. This constant value of the source function is equal to its average value at points n and n+1.

$$S^* = (1-\omega)\theta^4 + \frac{\omega}{2\pi}\Big[G^{'*} + 2a_1 \sin\alpha \Psi_R(\tau)\Big] \tag{5.11}$$

It should be noted that the expression of the source function given by Eq. (5.9) in terms of incident radiation $G^{'*}$ and radiative

q. (5.9) in terms of incident radiation $G^{'*}$ and radiative heat flux $\Psi_R(\tau)$ results from approximating anisotropic phase function by linear phase function.

$$p(\alpha^{'} \rightarrow \alpha) = 1 + a_1 \sin\alpha \sin\alpha^{'} \tag{5.12}$$

In the above equation, a_1 is the anisotropy factor. In CDM, to find out non-dimensional net radiative heat flux Ψ_R appearing in Eq. (5.9), heat flux is first found due to effective intensities spanned over a semi-circle, $0 \leq \alpha \leq \pi$. Then radiative heat flux due to the effective intensities spanned over other half, i.e., $\pi \leq \alpha \leq 2\pi$ has to be found and vector sum of the two be taken. Heat flux due to the effective intensities spanned over $0 \leq \alpha \leq \pi$ is given by

$$\Psi_R = \frac{1}{2}\int_{\alpha=0}^{\pi} I^* \sin\alpha d\alpha \tag{5.13}$$

For evaluating $G^{'*}$ and Ψ_R, Eqs. (5.6) and (5.11) are numerically integrated as

$$G^{'*} = \int_0^{2\pi} I^*(\alpha) \sin\alpha d\alpha = \Sigma_{n=1}^{2M} I^*(\alpha_n) \Delta\alpha_n \tag{5.14}$$

$$\Psi_R = \frac{1}{2} \int_0^{\pi} I^*(\alpha) \sin\alpha d\alpha = \frac{1}{2} \Sigma_{n=1}^{M} c_n I^*(\alpha_n) \tag{5.15}$$

To solve the energy equation (Eq. (5.1)), the divergence of radiative heat flux given by Eq. (5.5) is substituted in Eq. (5.1). This yields the desired governing integro-differential equation to be solved in CDM.

$$\frac{d^2\theta}{d\tau^2} + \frac{1}{\tau}\frac{d\theta}{d\tau} = \frac{\eta(1-\omega)}{4N}\left[\pi\theta^4 - \frac{G^{'*}}{2}\right] \tag{5.16}$$

For the steady state problem under consideration, total heat flux q_T is the sum of the conductive q_c and the radiative q_R heat fluxes. Mathematically, this is written as

$$q_T = q_c + q_R = -k\frac{dT}{dr} + q_R \tag{5.17}$$

In non-dimensional form, above equation is expressed as

$$\Psi_T = -\frac{d\theta}{d\tau} + \frac{1}{4N}\,\Psi_R \tag{5.18}$$

Here non-dimensionalization has been done by dividing both sides of Eq. (5.15) with $(k\beta T_R)$. Here T_R is the reference temperature and for the particular configuration, $T_R = T_1$.

5.3 Solution Procedure

To solve Eq. (5.14), it is expressed in the finite difference form as

$$\frac{\theta_{j-1} - 2\theta_j + \theta_{j+1}}{\Delta\tau^2} + A\frac{\theta_{j+1} - \theta_j}{\Delta\tau^2} = \frac{\eta(1-\omega)}{4N}\left[\pi\theta_j^4 - \frac{G_j^{'}*}{2}\right] \tag{5.19}$$

where

$$A = \frac{1}{\frac{n\rho}{1-\rho} + (j-1)}$$

Here A is the factor arising due to the nature of the geometry. For 1-D Cartesian enclosure A=0. In the expression for A, $\rho = \frac{r_1}{r_2}$ is the radius ratio and n is the number of control volumes.

Depending upon the values of the conduction-radiation parameter N, solution of Eq. (5.17) proceeds in two ways. For $N \geq 0.01$, first a linear temperature profile is guessed for the right hand side of Eq. (5.17). With this guess value of θ, incident radiation $G^{'*}$ is calculated. For evaluation of $G^{'*}$, effective intensities I^* are found from Eq. (5.8). The calculation of intensity starts from the bounding wall. To find out intensity values next to the bounding wall where n+1 in Eq. (5.8) is 1, intensity values at the bounding wall are required. For a gray wall having emissivity ϵ_w and temperature T_w, boundary intensity in CDM is found from

$$I_0^* = \frac{\epsilon_w T_w^4}{T_1^4} + \frac{1-\epsilon_w}{2} \int_{\alpha=0}^{\pi} I^{*-}(\alpha) \sin\alpha d\alpha \tag{5.20}$$

In Eq. (5.18), I^{*-} are effective intensities incident at the point of interest on the concerned wall from which the boundary intensities are to be found. First term in the right hand side of Eq. (5.18) is the emitted component whereas the second term represents the reflected component of intensity.

With right hand side of Eq. (5.17) known, left hand side is solved for θ_j using Thomas algorithm. To get the convergence, under-relaxation is used for small values of N. For values of $N < 0.01$, again a linear profile is guessed as in the first case. However, in this case, left hand side of Eq. (5.17) and $G^{'*}$ are calculated simultaneously. Strong under-relaxation is used to get the convergence.

The combined mode problem considered herein, fall under non-radiative equilibrium situation. It has been discussed in earlier chapters that in non-radiative equilibrium situation, apart from radiation, conduction and/or convection are also present. For the evaluation of OTC η required in Eqs. (5.8) and (5.14), the OTC expressions given in Appendix B are used. The geometric factor required for appropriate values of OTC for this cylindrical enclosure is the same as that for the problems on 1-D concentric cylindrical enclosure considered in

Chapter 4.

5.4 Discussion of Results

In the validation studies of CDM on combined radiation and conduction heat transfer problem in 1-D concentric cylindrical enclosures, the range of various parameters considered are as given in Table 5.2.

Parameters	Range
Scattering albedo	$0 \leq \omega \leq 1.0$
Anisotropy factor	$-1.0 \leq a_1 \leq +1.0$
Radius ratio	$0 \leq r_1/r_2 \leq 1.0$
Enclosure optical thickness	$0.0001 \leq \tau_L \leq 5.0$
Conduction-radiation parameter	$0.001 \leq N \leq 10$

Table 5.2: Range of parameters considered in the validation studies on combined radiation-conduction heat transfer problem.

In the present chapter, effect of different parameters such as conduction-radiation parameter N, scattering albedo ω, anisotropy $a_1\omega$ and radius ratio r_1/r_2 on heat fluxes and temperature distribution in medium have been studied. These results have been presented in the following subsections.

5.4.1 Heat Flux Distribution

In this subsection, results on non-dimensional radiative heat flux Ψ_R, temperature gradient dT/dr and non-dimensional total heat flux Ψ_T at the inner (hot) wall of the 1-D concentric cylindrical enclosure have been presented. These results have been obtained for three different values of scattering albedo ω (=0, 0.5 and 1) and conduction-radiation parameter N (=0.05, 0.1 and 0.5). For r_1/r_2=0.5 and $\tau_L = 1$, these results have been obtained with 32 effective intensities/rays and two sets of control volumes. In one set, we have considered 19 control volumes, whereas in the other set, 300 control volumes have been considered. The reason for considering these two sets of control volumes

is that with 19 control volumes in CDM, author wanted to compare FEM results [201] provided with 19 elements. However, it has been found that with just 19 control volumes, results were not grid independent.

In Tables 5.3 and 5.4, CDM results for dT/dr, Ψ_R and Ψ_T at the inner (hot) cylindrical enclosure have been compared with FEM results provided by Fernandes and Francis [201]. Here, CDM results are found with 32 rays and 19 control volumes. In FEM, 19 elements have been used. For results presented in Table 5.3, both the bounding walls have been assumed black ($\epsilon_1 = \epsilon_2 = 1$), whereas in Table 5.4, results are provided for gray bounding walls ($\epsilon_1 = \epsilon_2 = 0.1$).

		dT/dr		Ψ_R		Ψ_T	
ω	N	CDM	FEM	CDM	FEM	CDM	FEM
0		-1.274	-1.263	0.773	0.718	1.643	1.660
0.5	0.5	-1.270	-1.249	0.765	0.785	1.618	1.653
1.0		-1.298	-1.297	0.702	0.721	1.621	1.649
0		-1.273	-1.261	0.748	0.750	3.094	3.144
0.5	0.1	-1.212	1.196	0.751	0.788	2.998	3.088
1.0		-1.298	-1.297	0.702	0.721	2.982	3.053
0		-1.366	-1.364	0.731	0.765	5.094	5.019
0.5	0.05	-1.218	-1.238	0.738	0.768	5.039	4.907
1.0		-1.298	-1.297	0.702	0.721	4.886	4.808

Table 5.3: Comparison between CDM and FEM results on temperature gradient dT/dr, radiative heat flux Ψ_R and total heat flux Ψ_T at the inner wall of 1-D concentric cylindrical enclosure for radius ratio $r_1/r_2 = 0.5$, wall emissivity $\epsilon_1 = \epsilon_2$=1.0 and $\tau_L = 1$.

From Table 5.3, it is seen that dT/dr in CDM compares well with FEM. The (absolute) percentage error is in the range 0.07-1.65 %. For Ψ_R and Ψ_T, the absolute errors are in the range 0.267-4.92% and 1.02-2.91% respectively. Similar variations in errors have also been observed in Table 5.4.

The reason for relatively higher percentage error in case of Ψ_R and Ψ_T in CDM is attributed to the less number of control volumes considered here. From Eq. (5.9), it is seen that source function is an unknown - it depends

		dT/dr		Ψ_R		Ψ_T	
ω	N	CDM	FEM	CDM	FEM	CDM	FEM
0		-1.372	-1.388	0.075	0.076	1.412	1.426
0.5	0.5	-1.332	-1.348	0.076	0.079	1.1.364	1.387
1.0		-1.296	-1.298	0.059	0.062	1.313	1.329
0		-1.702	-1.731	0.075	0.076	1.904	1.921
0.5	0.1	-1.514	-1.541	0.076	0.079	1.711	1.738
1.0		-1.297	-1.298	0.059	0.062	1.423	1.454
0		-2.099	-2.118	0.075	0.076	2.481	2.500
0.5	0.05	-1.352	-1.369	0.076	0.079	2.123	2.164
1.0		-1.297	-1.298	0.059	0.062	1.564	1.608

Table 5.4: Comparison between CDM and FEM results on temperature gradient dT/dr, radiative heat flux Ψ_R and total heat flux Ψ_T at the inner wall of concentric cylindrical enclosure for radius ratio $r_1/r_2 = 0.5$, wall emissivity $\epsilon_1 = \epsilon_2$=0.1 and τ_L=1.

on ω, a_1, θ and Ψ_R. With unknown values of θ and Ψ_R, the unknown source function between any two CVSCPs is calculated assuming small path-leg. In cylindrical medium, because of the nature of the geometry, these path-legs are not always small. Hence to obtain accurate information about the source function, large number of control volumes need to be considered. This very fact has already been mentioned in Chapter 4. Moreover, from Eq. (5.16), it is seen that non-dimensional total heat flux depends on the conduction-radiation parameter N. Hence, even though the temperature gradient dT/dr of CDM compares well with FEM, for small number of control volumes, radiative and hence the total heat flux require large number of control volumes for more accurate calculations. Therefore, in CDM, calculations have been carried out with large number of control volumes.

The grid independent CDM results on heat fluxes and temperature gradient have been presented in Table 5.5. With 32 rays, for r_1/r_2=0.5, for given values of ϵ_w, τ_L, ω and N, with a maximum of 300 control volumes, CDM results have been found grid independent. For results presented in this table, emissivity of both the walls are the same.

ϵ_w	ω	N	dT/dr	Ψ_R	Ψ_T
	0		-1.381	0.088	1.526
	0.5	0.5	-1.342	0.092	1.454
	1.0		-1.297	0.099	1.348
	0		-1.729	0.090	2.313
0.1	0.5	0.1	-1.538	0.093	2.021
	1.0		-1.297	0.099	1.545
	0		-2.116	0.091	3.137
	0.5	0.05	-1.367	0.093	2.650
	1.0		-1.297	0.099	1.793
	0		-1.329	0.442	1.622
	0.5	0.5	-1.297	0.453	1.583
	1.0		-1.296	0.479	1.538
	0		-1.491	0.444	2.881
0.5	0.5	0.1	-1.358	0.454	2.707
	1.0		-1.297	0.479	2.496
	0		-1.722	0.446	4.394
	0.5	0.05	-1.460	0.455	4.087
	1.0		-1.297	0.479	3.695
	0		-1.272	0.878	1.740
	0.5	0.5	-1.266	0.879	1.732
	1.0		-1.297	0.917	1.757
	0		-1.270	0.870	3.566
1.0	0.5	0.1	-1.209	0.875	3.496
	1.0		-1.297	0.917	3.592
	0		-1.364	0.865	5.894
	0.5	0.05	-1.214	0.872	5.739
	1.0		-1.297	0.917	5.886

Table 5.5: Temperature gradient dT/dr, radiative heat flux Ψ_R and total heat flux Ψ_T on the inner wall of concentric cylindrical enclosure for radius ratio $r_1/r_2 = 0.5$ and $\tau_L = 1$.

It is observed from Tables 5.3-5.5 that although, in grid independent situation, dT/dr matches more closely with that of FEM, heat flux results are quite different. This indicates that temperature information can be obtained with less number of control volumes. However, for the correct prediction of heat flux, large number of control volumes are required.

To have qualitative ideas about the effects of scattering albedo ω and temperature θ_2 of the outer wall, on Ψ_R, dT/dr and Ψ_T, surface plots are provided in Figures 5.2-5.4. These results are presented for $\tau_L = 1$, r_1/r_2=0.5 and N=0.03. These results have been obtained with 32 rays and 300 control volumes.

In Fig. 5.2, variations of radiative heat flux Ψ_R on the inner wall have been presented with ω and outer wall temperature θ_2. Here, these values have been considered in the range $(0 \leq \omega \leq 0.9)$ and $(0.1 \leq \theta_2 \leq 0.9)$. From this figure it is observed that for any θ_2, Ψ_R decreases with increase in ω. Further, for the chosen value of τ_L (=1.0) and N (=0.03) for a given ω, θ_2 is not having any influence over Ψ_R.

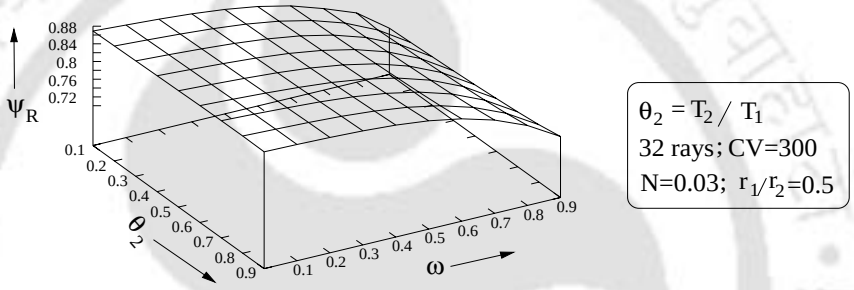

Figure 5.2: Variations of Ψ_R on the inner wall with scattering albedo ω and outer wall temperature θ_2.

In Figure 5.3, variations of temperature gradient dT/dr with ω and θ_2 have been presented. From this figure it is seen that for a given θ_2, with increase in ω, dT/dr increases. This increase is more near the walls. Further, for a given value of ω, it is seen that dT/dr decrease from higher to lower values and then again increases with change in θ_2 from 0.1 to 0.9. This change is less at lower values of ω.

Effects of ω and θ_2 on total heat flux Ψ_T on the inner wall have been presented in Fig. 5.4. The total heat flux is the summation of both the radiative as well as conductive modes of heat transfer. From this figure, it is seen that at any θ_2, Ψ_T decreases with ω. For given θ_2, Ψ_T is maximum at $\omega = 0$. Further, at higher values of ω, Ψ_T decreases with increase in θ_2.

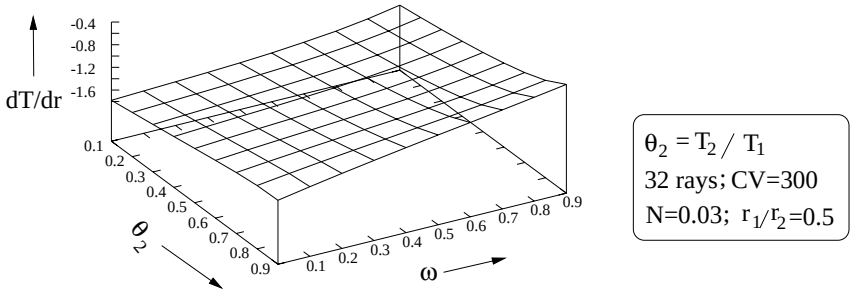

Figure 5.3: Variations of dT/dr on inner wall with scattering albedo ω and outer wall temperature θ_2.

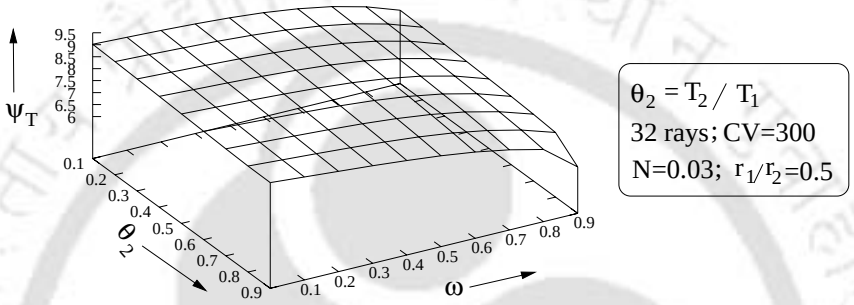

Figure 5.4: Variations of Ψ_T on the inner wall with scattering albedo ω and outer wall temperature θ_2.

5.4.2 Temperature Distribution

In this subsection, for the problem under consideration, effects of different parameters such as radius ratio r_1/r_2, scattering albedo ω, anisotropy $a_1\omega$, enclosure optical thickness τ_L and conduction-radiation parameter N on temperature distribution θ have been studied. For all the results presented in the following paragraphs, normalized medium temperature θ has been defined as $\left(\frac{T-T_2}{T_1-T_2}\right)$. Radial location is calculated from the surface of the inner cylinder towards the outer cylinder. This distance has been normalized as $\left(\frac{r-r_2}{r_1-r_2}\right)$.

Figures 5.5 and 5.6 present the variations of temperature θ with radial position $(\frac{r-r_2}{r_1-r_2})$ for absorbing-emitting medium. These results are presented for τ_L=1.0 and r_1/r_2=0.5. In Fig. 5.5 and 5.6, N values are given for 0.01 and 0.03 respectively. In both the figures, CDM results with 32 rays and 19 control

volumes have been compared with FEM [201] and successive approximation [286]. Comparison is excellent.

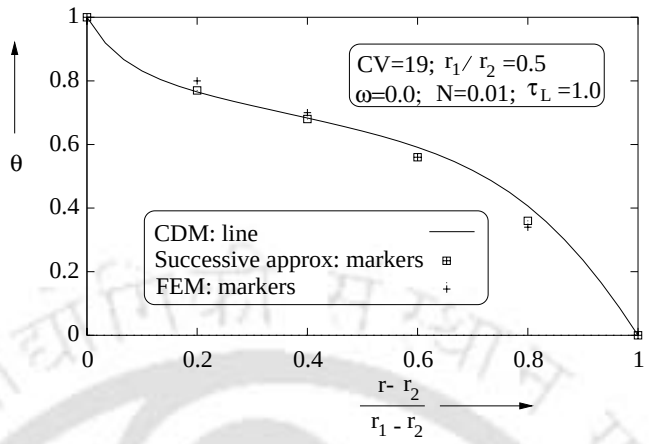

Figure 5.5: Variation of temperature θ with $(\frac{r-r_2}{r_1-r_2})$ for 1-D concentric cylindrical enclosure with an absorbing-emitting medium; N=0.01, τ_L=1.0.

From both the Figs. 5.5 and 5.6, it is observed that the gradient of θ is more stable for higher values of N. Further, for higher values of N, non-linearity in θ distribution is reduced.

Figures 5.7a-c present the effect of conduction-radiation parameter N on the variations of temperature θ with $(\frac{r-r_2}{r_1-r_2})$. All results are presented for τ_L=1 and r_1/r_2=0.5. For these results, 32 rays and 300 control volumes have been considered.

In Figs. 5.7a-c, θ variations are given for $\omega = 0.1, 0.5$ and 0.9 respectively. In all these figures, effect of six different values of N, i.e., 0.005, 0.01, 0.1, 1.0, 5.0 and 10.0 have been considered. Here lower values of N signify radiation dominated situation, whereas higher values of the same signify conduction dominated case. From these figures it is seen that in radiation dominated situation ($N = 0.005$ and 0.01), the gradient of θ changes a lot with $(\frac{r-r_2}{r_1-r_2})$. It is further observed that with increase in ω, this change decreases. For $\omega = 0.9$, near the outer cylinder, the effect of N is not seen much.

In Fig. 5.7b, CDM results for N=0.1 and 10 are compared with FEM [199]. Both methods compare very well.

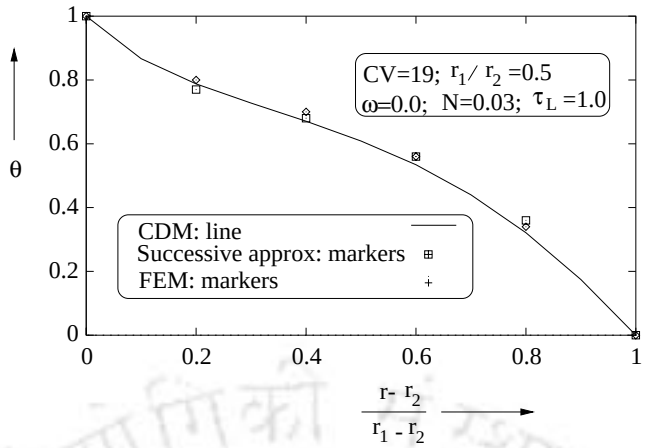

Figure 5.6: Variation of temperature θ with $(\frac{r-r_2}{r_1-r_2})$ for 1-D concentric cylindrical enclosure with an absorbing-emitting medium; N=0.03, τ_L=1.0.

Figure 5.8 presents the effect of anisotropy $a_1\omega$ on temperature profile for black bounding walls. Here, conduction-radiation parameter N=0.1 and scattering albedo ω=0.5 are considered. Three situations, i.e., forward scattering a_1=+1, isotropic scattering a_1=0 and backward scattering with a_1=-1 are considered. From Fig. 5.8, it is seen that for the chosen values of r_1/r_2, τ_L and N, anisotropy has not much effect on θ.

Figure 5.9 presents the effect of wall emissivity ϵ_w on variation of θ with $(\frac{T-T_2}{T_1-T_2})$. For r_1/r_2 = 0.5, for absorbing-emitting medium, this effect has been studied for different values of N. In this figure, results have been presented for wall emissivity $\epsilon_1 = \epsilon_2$=0.5 and 0.1. For $\epsilon_1 = \epsilon_2$=0.5, four different values of N=0.01, 0.03, 0.1 and 1.0 have been considered. With $\epsilon_1 = \epsilon_2$=0.1, results have been presented for N=0.03. These results have been compared with the method of successive approximation [286]. It is found that CDM results with 32 rays and 300 control volumes are in good agreement with the results from the method of successive approximation [286].

In Figs. 5.10a-d, effects of radius ratio r_1/r_2 on θ distribution have been shown. In these figures, three radius ratios, i.e., 0.1, 0.5 and 0.9 have been considered. In Figs. 5.10a-c, results are provided for τ_L=0.0001, whereas for results presented in Figs. 4.10d, τ_L=0.0001 and 0.5. Here for the chosen values

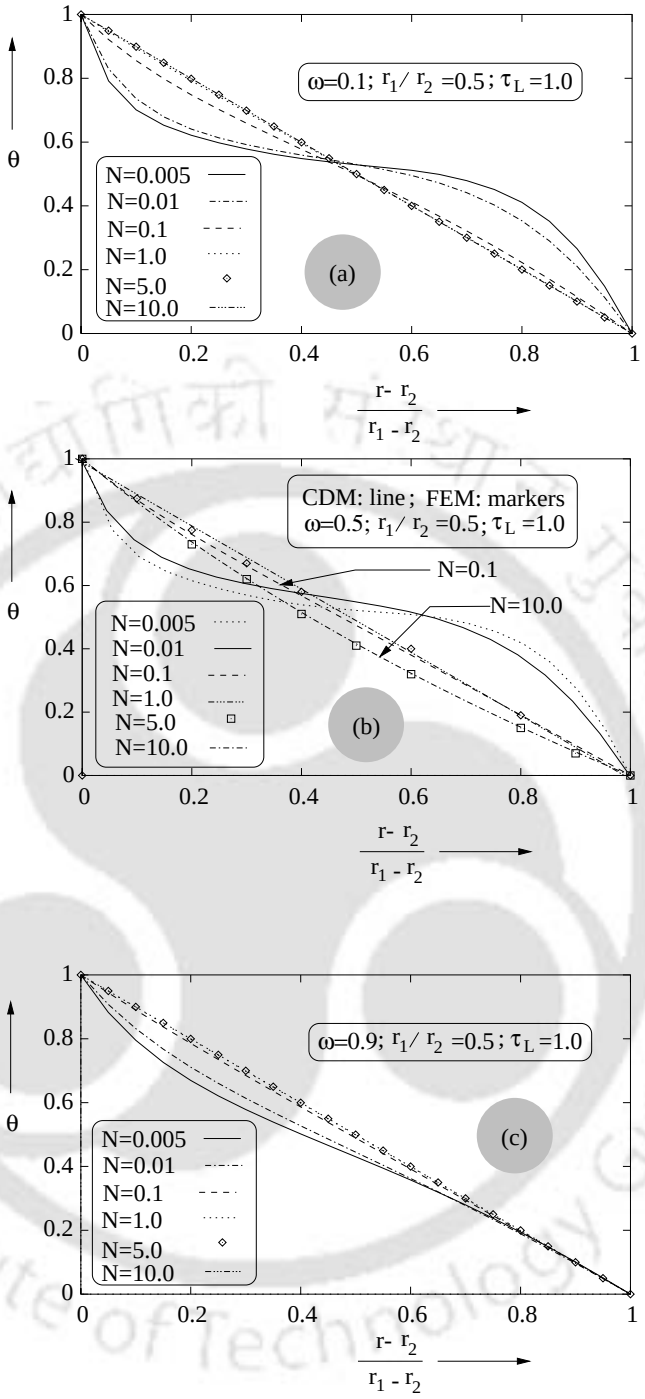

Figure 5.7: Effect of conduction-radiation parameter N on variations of temperature θ with $(\frac{r-r_2}{r_1-r_2})$.

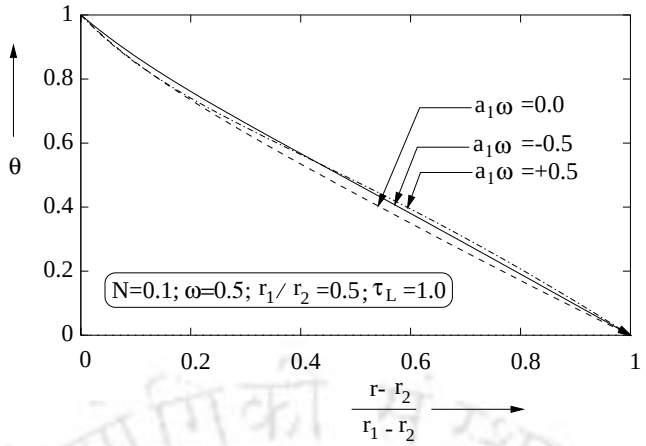

Figure 5.8: Effect of anisotropy factor a_1 on variation of θ with $(\frac{r-r_2}{r_1-r_2})$; ω=0.5, N=0.1 and τ_L=1.0.

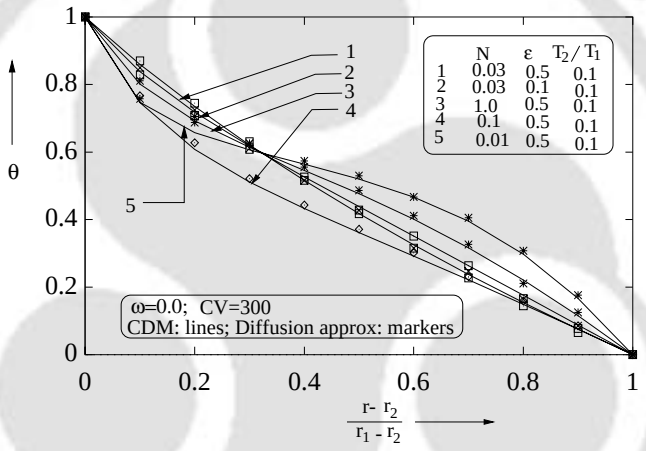

Figure 5.9: Effect of wall emissivity ϵ_w and conduction-radiation parameter N on temperature θ with $(\frac{r-r_2}{r_1-r_2})$.

of τ_L, effect of r_1/r_2 has been shown for three different values of N (0.003, 0.01 and 1.0). From these figures (Figs. 5.10a-c), it is seen that if the medium is optically thin, radius ratio has no effect on θ. However, with increase in optical thickness τ_L, some variation in θ is observed. This is evident from Fig. 5.10d.

In Figs. 5.11a and 5.11b, for $\omega = 0$ and $\tau_L = 1$, effect of radius ratios r_1/r_2 on θ variations with $(\frac{r-r_2}{r_1-r_2})$ have been shown. In both these figures, three different radius ratios r_1/r_2=0.1, 0.5 and 0.9 have been considered. In Fig.

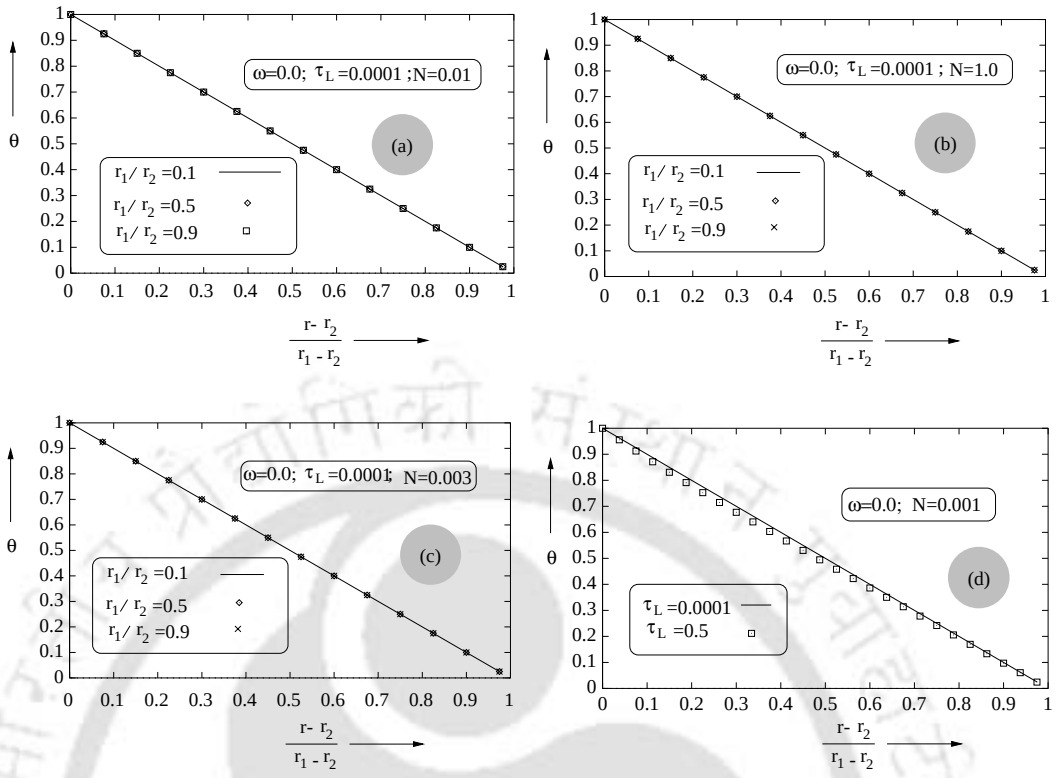

Figure 5.10: Effect of radius ratio r_1/r_2 on variation of temperature θ with $(\frac{r-r_2}{r_1-r_2})$. (a) N=0.01, τ_L = 0.0001, (b) N=0.1, τ_L = 0.0001, (c) N=0.003, τ_L = 0.0001 and (d) N=0.001, τ_L=0.0001 and 0.5.

5.11a, results are obtained for $N = 0.01$. In Fig. 5.11b, same are obtained for $N = 1.0$.

From these figures, it is seen that with low value of N, temperature θ in medium increases with increase in radius ratio r_1/r_2. However, with high value of N, effect of r_1/r_2 on θ becomes insignificant.

Some more results regarding the effects of r_1/r_2 on the variation of temperature θ with $(\frac{r-r_2}{r_1-r_2})$ have been presented in Figs. 5.12a and 5.12b. Here also, we have considered three different radius ratios, r_1/r_2=0.1, 0.5 and 0.9. In Both the figures, we have considered the conduction-radiation parameter N as 0.1. Results in Fig. 4.12a are for enclosure optical thickness τ_L=1.0, whereas in Fig. 4.12b, it is considered as 4.0.

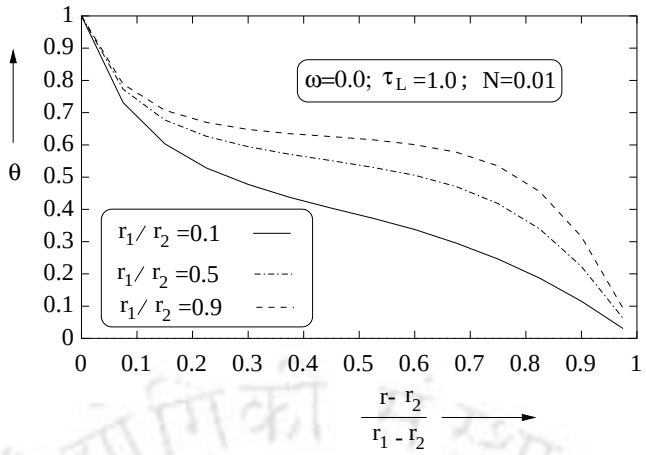

(a)

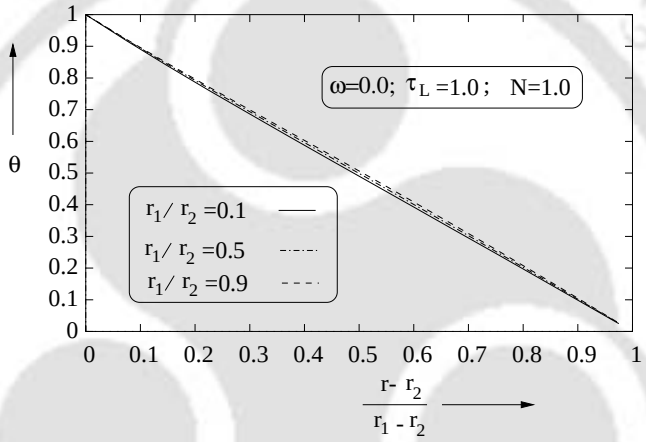

(b)

Figure 5.11: Effect of r_1/r_2 on variation of temperature θ with $(\frac{r-r_2}{r_1-r_2})$; (a) $\omega = 0, \tau_L = 1$ and $N = 0.01$, (b)$\omega = 0, \tau_L = 1$ and $N = 1$.

From both these figures, it is seen that with increase in enclosure optical thickness τ_L, effect of radius ratio on temperature distribution is significant.

For the problem considered in this chapter, it has been found that the number of iterations required for conduction dominated situations is very less compared to radiation dominated cases. For example, for τ_L=1, r_1/r_2=0.5 and $N \geq 1$, convergence was obtained in only 5-6 iterations, whereas for N=0.1, 0.01 and 0.003, approximately 280, 350 and 800 iterations were required respectively.

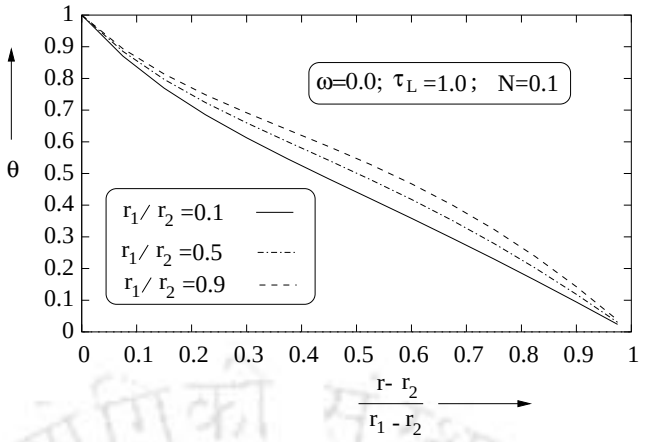

(a)

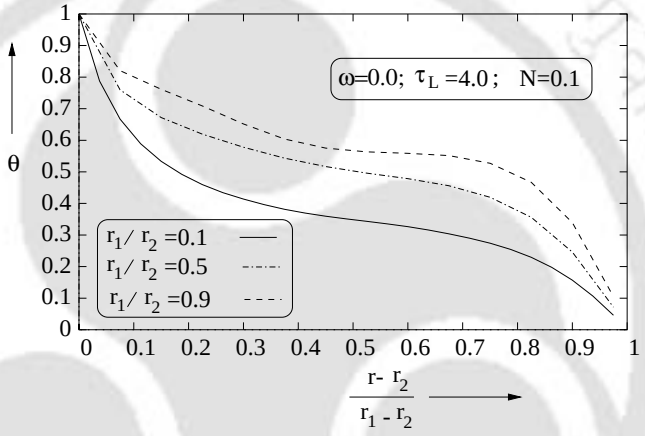

(b)

Figure 5.12: Variation of non-dimensional temperature ($\frac{T-T_2}{T_1-T_2}$) with non-dimensional radius ($\frac{r-r_2}{r_1-r_2}$).

For $N \leq 0.01$, under relaxation parameter of 0.02 has been used to get the convergence.

5.5 Summary

In this chapter, applicability of CDM has been shown for conjugate radiation and conduction heat transfer problems. The steady state study has been

performed for combined radiation and conduction heat transfer problem in 1-D gray concentric cylindrical enclosure containing absorbing, emitting and anisotropically scattering medium. For the gray and homogeneous medium, anisotropy has been approximated by linear anisotropic phase function. Effect of radius ratio r_1/r_2, scattering albedo ω, anisotropy a_1, enclosure optical thickness τ_L, wall emissivity ϵ_w and conduction-radiation parameter N on heat flux Ψ and temperature θ variations have been studied. For some sample cases, CDM results have been compared with those available in the literature. CDM has been found to give a very good comparison.

In Chapters 3-5, CDM has been applied to different types of problems in which participating medium has been considered gray and homogeneous. There are many situations in which gray and/or homogeneous assumption do not hold valid. How in CDM, non gray and/or inhomogeneous medium situation is handled, discussions have been provided in Chapter 6.

Chapter 6

Validation Studies: Inhomogeneous and Non Gray Medium

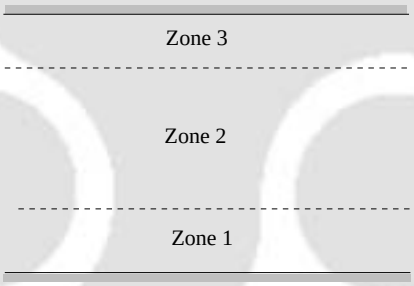

1-D Cartesian enclosure
with inhomogeneous medium

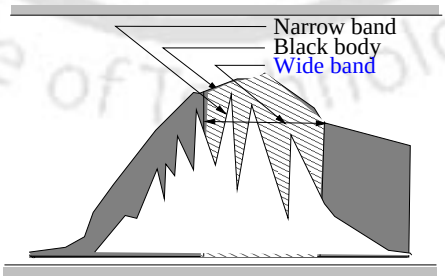

1-D Cartesian enclosure
with non gray medium

6.1 Introduction

In earlier Chapters, all validation studies have been performed with gray and homogeneous participating medium. Throughout the medium, thermo-physical properties have been assumed constant and independent of wavelength. In realistic situations, thermo-physical properties of the medium do vary from point to point, and they are also wavelength dependent. These situations are often encountered in coal combustions, exhaust emissions from internal combustion engines and gas turbines, multi-layer insulations, porous medium, etc. Solutions of RTE in such cases are difficult and results are quite different from that for gray and homogeneous medium. Radiative transfer problems with inhomogeneous and/or non-gray medium have been dealt in [214, 226–230, 287–295]

In this chapter, application of CDM is tested for gray inhomogeneous and non gray homogeneous participating medium. For both the situations, the validation studies have been performed on 1-D Cartesian enclosure. For gray inhomogeneous absorbing, emitting and anisotropically scattering medium, both radiative and non-radiative equilibrium cases have been considered. In case of non gray homogeneous absorbing-emitting medium, only radiative equilibrium situation has been considered. For some sample cases with inhomogeneous medium, CDM results have been compared with YIX [225] method and for all the cases, with self generated DTM results. In case of non gray medium, CDM results have been compared with [29].

6.2 Gray Inhomogeneous Medium

In the literature, most of the problems dealing with inhomogeneous medium consider multi-layered participating medium. In each layer, thermo-physical properties of the medium are assumed constant. Özişik and Shouman [296] and Stamnes and Conklin [297] have treated 1-D planar medium with layered properties. Sutton and Kamath [298] have considered 3-D Cartesian geometry

with layered properties. Zhang and Sutton [299] have solved radiative transfer problems in cylindrical medium with space dependent scattering albedo ω. The multi-layer medium has applications in many practical situations, such as inhomogeneous porous ceramic burners [300], porous solar collectors and reactors [301, 302], etc.

Inhomogeneous participating medium is characterized by variable thermo physical properties. In such medium, optical properties such as, extinction coefficient β, scattering albedo ω and anisotropy $a_1\omega$ vary in the spatial directions. In the present validation study, for 1-D Cartesian enclosure under consideration (Fig. 6.1), these properties vary in the Z direction.

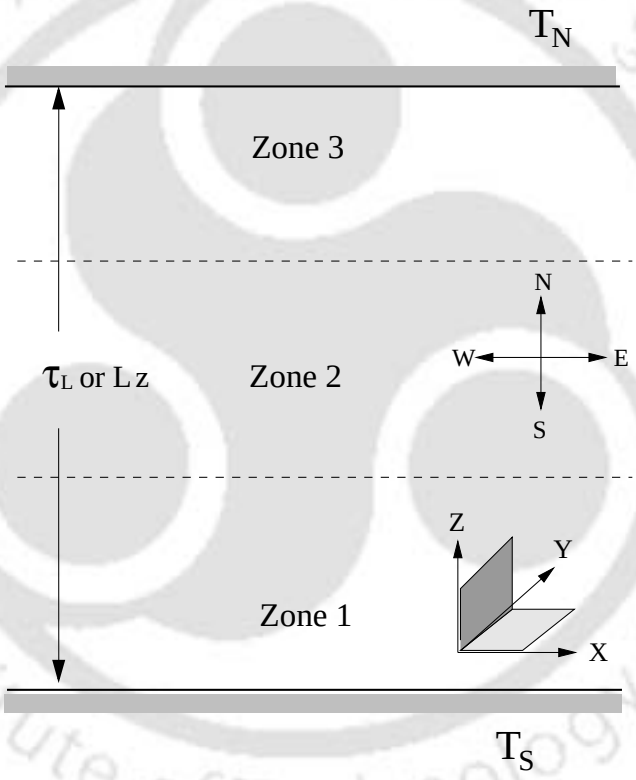

Figure 6.1: 1-D Cartesian enclosure with inhomogeneous medium.

For 1-D black Cartesian enclosure shown in Fig. 6.1, the south and the north walls are at temperatures T_S and T_N respectively. The enclosed medium is absorbing-emitting and anisotropically scattering. The radiative properties of the medium are spatially varying. Here, we have considered three different

layers for which radiative properties are different. In each layer, radiative properties are constant. For the sake of convenience, three layers are identified with three zones.

It has been mentioned in Chapter 2 that in CDM, OTCs are required for the solution of radiative transfer problems. OTCs given in Appendices A & B have been found for gray and homogeneous medium. From earlier works on CDM, how the OTCs found for gray and homogeneous medium will be applicable to gray and inhomogeneous medium, was not known. In this section, with reference to the problem cited above, this particular aspect of CDM has been dealt with.

In case of inhomogeneous medium, radiative properties in each control volume are considered homogeneous (constant) but are different in different control volumes. In CDM, corresponding to the properties such as optical dimensions of the control volume τ, scattering albedo ω and the factor $a_1\omega$, OTC η for each control volume is found from the expressions given in Appendices A & B. This way, unlike homogeneous medium, in case of inhomogeneous medium, OTCs will also be different from one control volume to the other. For determination of effective intensity at any point in a given direction in the enclosure, optical path-legs terminate at the boundaries of the control volumes.

Above points can better be explained with the help of a simple example considered herein. In Fig. 6.1, we first consider three-layer medium. In each zone (layer), radiative property, say extinction coefficient β is different. If the geometric depths of zones 1, 2 and 3 are Z_1, Z_2 and Z_3 (not shown in Fig. 6.1), the optical depths of the three zones in Z direction are βZ_1, βZ_2, and βZ_3. Now corresponding to these optical depths, depending upon whether our problem belongs to radiative or non-radiative equilibrium, OTCs for these zones are found from Appendices A & B. In case of homogeneous medium, OTCs for the three zones would be same. As far as the optical path-leg between points n and $n+1$ in Eq. (2.36) is concerned, depending upon the variations in the source function, it can be big or small. However, whatever be its length, in case of inhomogeneous medium, the points n and $n+1$ will never be in different

zones.

6.2.1 Non-radiative Equilibrium

In non-radiative equilibrium situation, in Fig. 6.1, we consider inhomogeneity caused due to scattering albedo ω. Here, extinction coefficient β in all three zones is the same. However, in each zone ω, and hence scattering coefficient σ_s ($\omega = \frac{\sigma_s}{\beta}$) has different values. The geometric depths of zones 1, 2 and 3 are $0 \leq z \leq 0.25$, $0.25 \leq z \leq 0.75$ and $0.75 \leq z \leq 1.0$ respectively.

In the following pages, effect of inhomogeneity caused by ω on variation of non-dimensional heat flux Ψ in the medium is discussed. For the 1-D Cartesian geometry (Fig. 6.1) considered here, both the bounding walls are at zero temperature and the medium is isothermal with temperature T_g. For all the results presented in this subsection, heat flux Ψ has been non-dimensionalized as

$$\Psi = \frac{q}{\sigma T_g^4}$$

With ω=0.1, 0.9 and 0.1 in zones 1, 2 and 3 respectively, variations of non-dimensional heat flux Ψ with normalized geometric depth z/L_z are shown in Fig. 6.2. These variations are shown for β=0.1, 1.0, 2.0 and 5.0. It is seen from this figure that inhomogeneity has significant effect on distribution of Ψ in the medium. Here, CDM results with 32 rays and 50 control volumes in each zone have been compared with DTM results with 100 rays and 50 control volumes. Results from both the methods compare well.

For Ψ variations given in Fig. 6.3, ω in zones 1, 2 and 3 are 0.9, 0.1 and 0.9 respectively. Geometric depth of each zone is the same as that for the case presented in Fig. 6.2. In this figure, results are presented for β=0.1 and 1.0. It is also seen from this figure that spatial variation of ω has significant bearing on distribution of Ψ in the medium. Here CDM results with 32 rays and 50 control volumes in each zone have been compared with DTM results with 160 rays with 50 control volumes. Comparison between the two is found to be excellent.

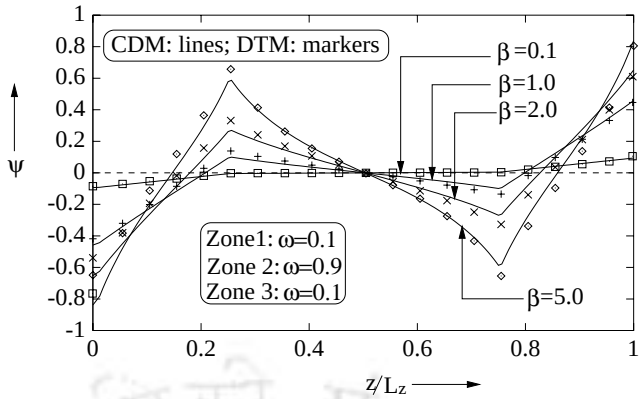

Figure 6.2: Effect of spatially varying scattering albedo ω on variations of heat flux Ψ with normalized geometric depth z/L_z.

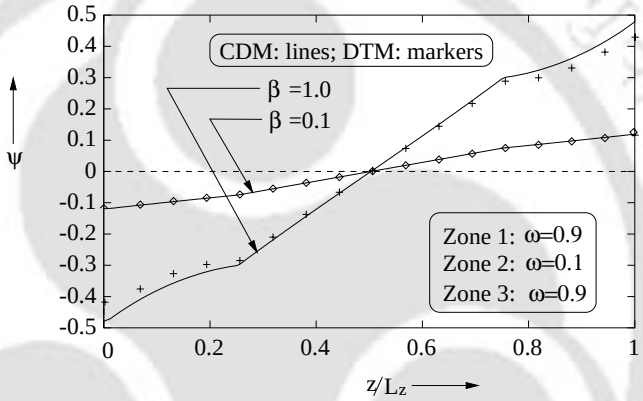

Figure 6.3: Effect of spatially varying scattering albedo ω on variations of heat flux Ψ with normalized geometric depth z/L_z.

Figures 6.4a and 6.4b present the effect of scattering albedo ω on the variations of gas heat flux Ψ with z/L_z . In Fig. 6.4a and 6.4b, results have been given for β=1.0 and 5.0 respectively. In both the figures, three different cases have been considered. For case (a), for zones 1, 2 and 3, ω=0.9, 0.1 and 0.9 have been considered respectively. Similarly, in case (b), ω=0.1, 0.9 and 0.1 have been considered for zones 1, 2 and 3 respectively. Further, a constant value of ω=0.1 for all the zones has been considered in case (c). For generating results, 32 rays in CDM has been considered in both the figures. In case (a), and (b), 50 control volumes in each zone have been considered whereas for case (c), 50 control volumes for the entire domain has been considered. For all the cases

considered in both the figures, CDM with 32 rays have been compared with 160 rays. Both the methods compare well.

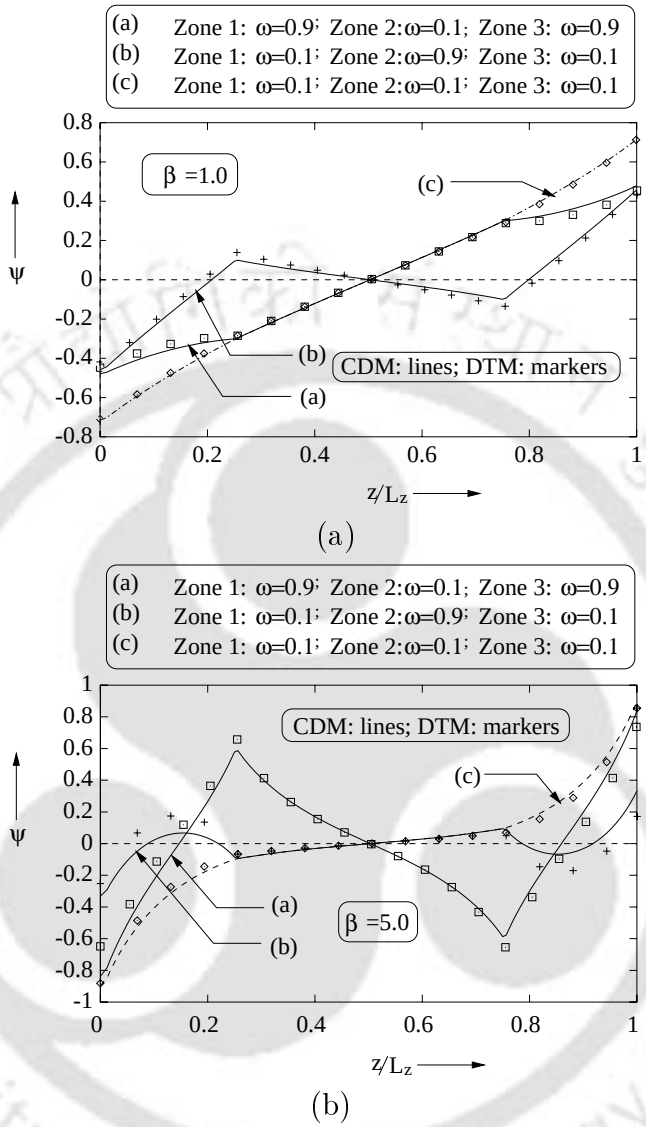

Figure 6.4: Effect of spatially varying scattering albedo ω on variations of wall heat flux Ψ with normalized geometric depth z/L_z; 1-D cylindrical enclosure under non-radiative equilibrium.

From both these figures it is seen that for β=1.0, heat flux variation in each zone is linear. With increase in β from 1.0 to 5.0, heat flux variation becomes non-linear in each zone. Further, from both these figures it is seen that results for layered variation in ω gives different results than that of constant ω.

6.2.2 Radiative Equilibrium

It has been discussed in earlier Chapters that radiative equilibrium situation is achieved at very high temperature. Under this situation, the divergence of radiative heat flux is zero. This indicates that radiative heat flux (in this case total heat flux) in the gas remains constant. In case of inhomogeneous medium, although inhomogeneity of the medium will have effect on total heat flux, for the reason just mentioned above, its zone-wise effect will not get reflected. Hence, this study is more relevant to emissive power distribution.

For the radiative equilibrium situation considered here, the medium temperature is an unknown. The south and north boundary walls are at temperature T_S and T_N respectively (Fig. 6.1). The south wall is at higher temperature than the north wall. The distance between south and the north bounding walls is unity. Here, non-dimensionalization of different radiative quantities have been done considering south wall temperature T_S as reference temperature. Emissive power Φ has been found in the same way as discussed in Chapter 4, Section 4.3, page 129.

For the geometry under consideration, effects of spatially varying anisotropy $a_1\omega$ and extinction coefficient β on emissive power Φ distribution have been discussed in the following paragraphs.

To study the effect of zone-wise varying extinction coefficient β, four cases are considered. In case 1, the entire medium is considered to be homogeneous with extinction coefficient β =20. As β for all three zones is the same, here geometric depths of the three zones are not required to be specified. In case 2, β in different zones are different. The geometric depths of zones 1, 2 and 3 are $0 \leq z \leq 0.4$, $0.4 \leq z \leq 0.6$ and $0.6 \leq z \leq 1.0$ respectively. Here in zones 1 and 2, $\beta = 1$, whereas in zone 2, $\beta = 20$. In case 3, the medium has been divided in two different zones with geometric depths $0 \leq z \leq 0.5$ and $0.5 \leq z \leq 1.0$. In case 4, linearly varying extinction coefficient has been considered. In this case β variation in the enclosure is given by

$$\beta = 20 \times (z/\mathrm{L}_z)$$

All the four cases mentioned above are summarized in Table 6.1. Tan and Howell [225] have solved problems for all these four cases using YIX method.

Case	Zone 1	Zone 2	Zone 3
1	20.0	20.0	20.0
2	1.0 (0-0.4)	20.0 (0.4-0.6)	1.0 (0.6-1.0)
3	1.0 (0-0.5)	20.0 (0.5-1.0)	–
4	$20 \times z/L_z$	$20 \times z/L_z$	$20 \times z/L_z$

Table 6.1: Values of extinction coefficient β in different zones for 1-D inhomogeneous absorbing-emitting medium; Numbers in bracket indicate geometric depth of the zone.

For all the four cases mentioned above, emissive power Φ distributions with normalized geometric depth z/L_Z are shown in Fig. 6.5. Here CDM results have been compared with YIX and P_1 approximation [225] and DTM. Both CDM and DTM results have been generated with 200 control volumes.

It is seen from this figure that comparison of CDM results with DTM and YIX methods is better in all the four cases. Small discrepancy with P_1 approximation is because of inability of P_1 approximation to provide accurate results at the low optical thickness range.

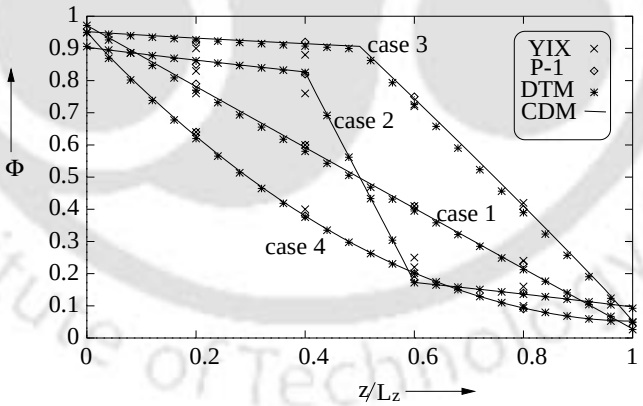

Figure 6.5: Effect of spatially varying extinction coefficient β on variations of emissive power Φ with normalized geometric depth z/L_z for 1-D Cartesian enclosure in radiative equilibrium situation.

Results obtained in Fig. 6.5 with CDM and DTM requires different number

of rays for grid independent solution. For example, fin case 1, 4 effective rays in CDM produced the same emissive power distribution as that with 100 rays with DTM. Ray requirement under both CDM and DTM for all the cases has been given in Table. 6.2. For all the cases, CPU time on HP9000/J200 has been found negligible to be reported here. But economy of CDM can easily be inferred as it requires less number of effective rays.

Case	CDM	DTM
1	4	100
2	12	64
3	32	80
4	8	100

Table 6.2: Ray required in CDM and DTM for the results presented in Fig. 6.5.

It should be mentioned here that OTCs expressions in Appendices A and B are given for optical thickness $\tau_L \leq 5$. In the problem just considered above, in some of the cases, optical depths ($\beta\times$ geometric depth) of some of the zones are more than 5. In such situations also, OTCs for τ_L =5 have been used. It has been shown in [236] that for optical depths more than 5, variation in OTC with τ_L is insignificant and hence for $\tau_L > 5$, OTCs for $\tau_L = 5$ can be used without any loss of accuracy.

In continuation of above discussion on variation of Φ for spatially varying radiative properties, some more results have been presented in Figs. 6.6 and 6.7. For all the cases considered in both the figures, the geometric depths of zones 1, 2 and 3 are $0 \leq z \leq 0.25$, $0.25 \leq z \leq 0.75$ and $0.75 \leq z \leq 1.0$ respectively.

In Fig. 6.6a, three different cases are considered. In case (a), in zones 1, 2 and 3, values of β are 1.0, 5.0 and 1.0 respectively. In case 2, β variation is considered as $\beta = z/L_z$. In case (c), a constant value of β (=5.0) throughout the enclosure has been taken. All the results in this figure are for an absorbing-emitting medium under radiative equilibrium situation. For all the

cases considered here, CDM results are compared with DTM. In both CDM and DTM, 70 control volumes have been considered in each zone. Here CDM results with 32 rays have been founding matching with 200 rays in DTM.

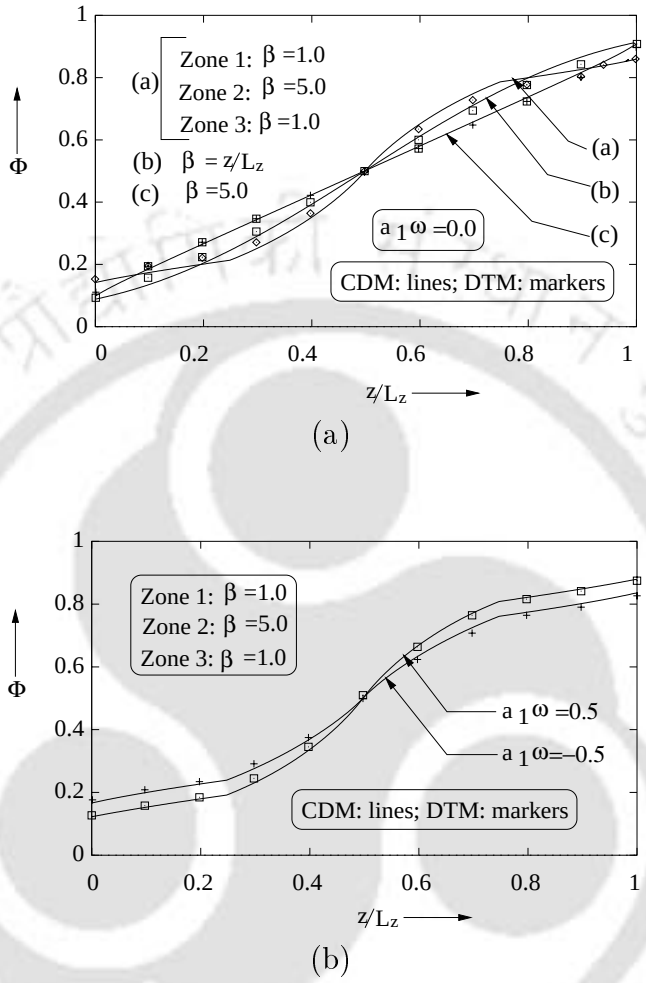

Figure 6.6: Effect of spatially varying extinction coefficient β on variations of emissive power Φ with normalized geometric depth z/L_z.

In Fig. 6.6b, for case (a) of Fig. 6.6a, Φ variations are given for two values of anisotropy $a_1\omega$, i.e., 100 % forward ($a_1 = +1.0$) and 100 % backward scattering ($a_1 = -1.0$). Here CDM results with 32 rays have been found in very good agreement with DTM results with 200 rays.

Effect of spatially varying factor $a_1\omega$ on the variations of Φ with z/L_Z have been shown in Figs. 6.7a and 6.7b. In both the figures, two cases have been

considered. In case (a), in zones 1, 2 and 3 the values of $a_1\omega$ are +1, -0.5 and +1.0 respectively. In case (b), these values are -1.0, +0.5 and -1.0 for zones 1, 2 and 3 respectively. In Fig. 6.7a, these variations are given for β=1.0 whereas in Fig. 6.7b, the same are given for β=5.0. For results presented in both the figures, in each zone 70 control volumes have been used. Here, CDM results with 32 rays have been found to compare very well with DTM results with 200 rays.

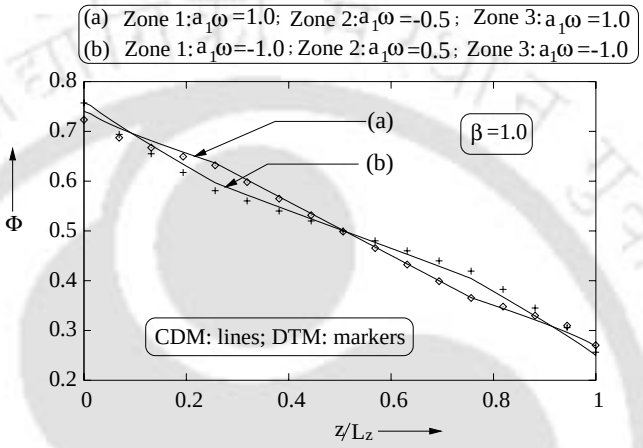

(a)

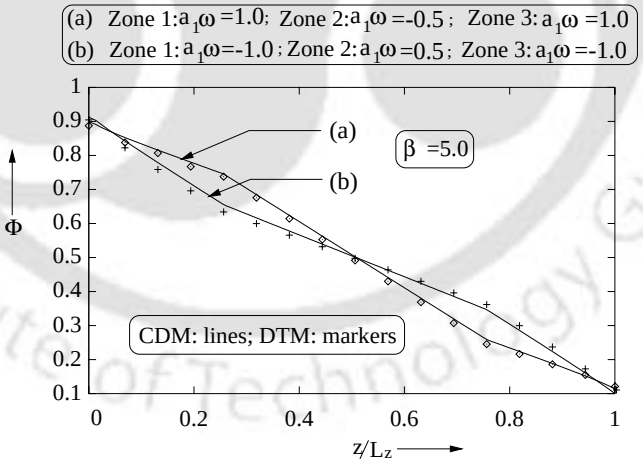

(b)

Figure 6.7: Effect of spatially varying anisotropy $a_1\omega$ on variations of emissive power Φ in enclosure with normalized geometric depth z/L_Z.

6.2.3 Economy

To have an idea of comparative computational effort involved in both CDM and DTM, for some test cases considered before, a comparison of CPU times of CDM and DTM is made here. This comparison is presented for sample cases in both non-radiative and radiative equilibrium situations.

In non-radiative equilibrium situation, for results presented in Fig. 6.4a, for all three cases, CPU times (seconds) of both CDM and DTM are compared in Table 6.3. All calculations have been performed on HP-9000/J200 computer. From this table, it is observed that CPU time for calculation of gas heat flux Ψ for CDM is always found to be much lower than that for DTM.

		CPU time (seconds) on HP-9000/J200 computer	
	β	CDM	DTM
case 1	0.1	0.2	1.8
	1.0	0.4	2.5
	5.0	0.5	3.3
case 2	0.1	0.1	0.8
	1.0	0.1	2.1
	5.0	0.1	3.3
case 3	0.1	0.1	0.1
	1.0	0.4	1.2
	5.0	0.3	2.2

Table 6.3: CPU time (seconds) required by CDM and DTM for the evaluation of gas heat flux Ψ for the anisotropy $a_1\omega$ in Fig. 6.4a.

In radiative equilibrium situation, for results presented for Φ distribution in Fig. 6.7a, for two cases each with three different zones, CPU times (seconds) of both CDM and DTM are compared in Table 6.4. From this table, it is seen that CPU times (seconds) for CDM is always less than DTM. Further, at high optical thickness CPU time is more than that for the optically thin situation.

β	case	CPU time (seconds) on HP-9000	
		CDM	DTM
0.1	case 1	0.4	1.5
	case 2	0.4	1.6
1.0	case 1	7.0	11.6
	case 2	7.5	13.5
5.0	case 1	22.5	45.9
	case 2	64.5	97.0

Table 6.4: CPU time (seconds) required by CDM and DTM for the evaluation of emissive power Φ for the cases presented in Fig. 6.7a.

6.3 Non Gray Homogeneous Medium

Apart from the influence of spatially varying parameters on radiative transfer discussed in earlier section, other important parameter influencing radiation is the wave length λ (wavenumber). In many situations, radiative properties vary over the spectrum of thermal radiation. Participating medium whose properties are wavelength dependent, is known as a non gray medium. For validation studies of CDM, here we consider homogeneous medium to be non gray.

In the literature, various approximations have been reported for spectral analysis of radiative transfer. There are four different models, which are widely used. These models have been reported in [29, 30, 303]. These models have been categorized according to the wavenumber scale.

The largest scale used is the entire spectrum of wavenumber as one interval. Here over entire interval, properties are assumed constant. This is known as the gray gas approximation [29]. Since gray gas approximation can lead to large errors, it is generally not used in heat transfer. The wide band model is used in the range of wavenumber from 100 to 1000 cm^{-1} [303–305]. Most of the thermal radiation takes place in this range. Hence, this model is widely used. Different types of wide band models are discussed by Edwards [303]. The next level of approximation is called narrow band model. In this, wavenumber is in

the range of 5-50 cm^{-1} [292,306]. Finally, there is the wavenumber scale in the range of 0.002-0.02 cm^{-1}. In this, line by line calculations are performed [290].

Review of various models presented in [29,152] shows that most of the models suffer from severe limitations in correctly predicting radiative information. For instance, the gray gas assumption covers a wide range of spectrum with constant radiative properties. This leads to a considerable error. Line by line calculation, though accurate, require very high computational time. Hence, these models have been modified by many researchers.

Analysis of radiative transfer in non gray participating medium has been reported by many researchers [71, 78, 79, 214, 227, 288–295, 307]. Howell and Perlmutter [71] are the first to take into account non gray radiation. Tiwari and Liu [78] used narrow band model with MCM for analysis of fully developed laminar flow between parallel plates. Modest [76], Taniguchi et al. [79] and Edwards [110] applied different non gray models with MCM to analyze radiative transfer problems. Spherical harmonics method (P_N) is also used to treat non gray medium [93,308]. Kim [152] used S_N method for non gray problems in radiative transfer. Hsu and Tan [227] used YIX method for combined radiative-conductive mode problems in L-shaped enclosures. Pierrot et al. [309] made comparisons between four approximate models. They reported that the weighted-sum-of-gray-gases model [29] is less time consuming than the other methods.

The weighted-sum-of-gray-gases approach has been introduced by Hottel and Sarofim [105]. They used it with zone method for simple absorbing-emitting medium. Modest [29,307] has demonstrated its ease in applicability for solving RTE. He demonstrated that this approach can be used with the exact, P_N approximations, DOM, etc. In this approach the non gray gas is replaced by a number of gray gases, for which the heat transfer rates are calculated independently.

Application of CDM to radiative transfer problems with non gray participating medium has been discussed in this section. In this method, some ideas of

weighted-sum-of-gray-gases has been considered.

In CDM, equations developed in Chapter 2 for gray and homogeneous medium, hold valid for spectrally dependent properties also. However, for radiative equilibrium situation, Eq. (2.41) is non-zero for spectrally dependent properties. Under the circumstances, the divergence of radiative heat flux is calculated considering total heat flux. The heat flux for a semi circle of rays have been obtained by summing up all the effective intensities within the semi circle. Further, for a ray direction, net effective intensity is obtained by summing up all the spectrally dependent intensities at a location.

$$I(\alpha, s) = \Sigma_k^N I_k(\alpha, s) \tag{6.1}$$

where, k is the number of bands considered.

To demonstrate its applicability, in this subsection, CDM has been applied to a 1-D planar medium. The lower wall is at temperature T_1 and is at higher temperature (=2200 K) than the upper wall which is at a temperature T_2=1000 K. The enclosure walls are assumed black.

For ease in calculations, medium temperature is assumed to be known. A linear temperature profile has been considered with temperature of 2200 K and 1000 K at both the ends. Further, the participating medium is considered to be containing a mixture of gases (CO_2-H_2O). These mixtures are generally encountered in exhaust emissions of automobile engines, gas turbines, coal fired boilers, etc. These mixture of gases emit different spectral bands. The enclose medium is considered absorbing-emitting.

Under radiative equilibrium situation, non-dimensionalization of radiative quantities, such as, heat flux and effective intensities etc. has been done by considering the lower wall temperature T_1 (=2200 K) as the reference temperature T_R.

For the mixture of gases (CO_2-H_2O), three different spectrally dependent absorption coefficients has been considered. At a location along a ray direction, corresponding to the spectral absorption coefficient, for a known temperature

profile, RTE has been evaluated. For, all the three absorption coefficients, three spectrally dependent effective intensities have been calculated along the ray direction. Sum of all these intensities at the location will give the net intensity along the ray direction (Eq. (6.1)).

In this study, different band parameters and values of spectrally dependent absorption coefficients have been taken from [29, 309]. The band absorption coefficient has been taken for the mixture of gases from [29, 310]. The effective absorption coefficient is taken as the weighted average of all the band absorption coefficients. These weights are taken from [309].

By knowing both the band as well as effective absorption coefficient, the absorption coefficient factor or extinction coefficient factor is calculated. Replacing this factor in expressions in Appendix A, OTCs are found.

Workability of CDM with this concept has been demonstrated with some sample results.

In Fig. 6.9, variations of heat flux with optical thickness τ_L at gas band center for a mixture of gases (CO_2-H_2O) have been presented. For the three bands considered (κ=0.01275, 0.12662 and 1.1813 $cm^{-1}.atm^{-1}$), a line overlap β=0.01 parameter of these bands has been considered. CDM results have been obtained with a linear temperature profile varying from 2200 K to 1000 K. Here, results have been presented with 32 rays and 20 control volumes in CDM. These results have been compared with MCM and picket fence model [29]. From this figure, it is seen that CDM with 32 rays compare very well with the picket fence model.

In Fig. 6.10, effect of number of bands on total heat flux Ψ with optical thickness τ_L have been shown. Here, results are presented with three, two and single bands. Results are obtained in CDM with 32 rays and 20 control volumes. From this figure it is observed that with decrease in number of bands, heat flux decreases. Hence in reality, for spectral analysis, large number of bands have to be considered for obtaining correct radiative information.

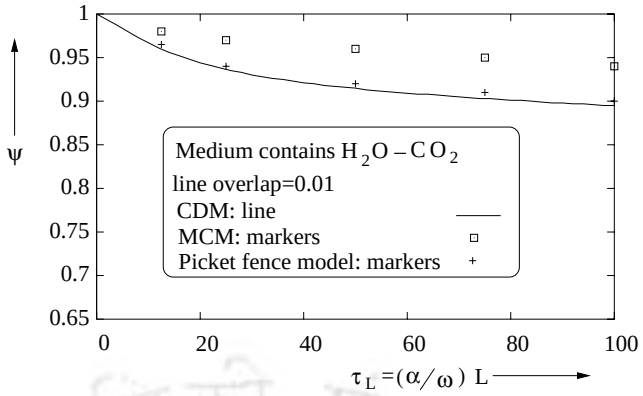

Figure 6.8: Variations of heat flux Ψ across a mixture of gases bounded by parallel, black walls.

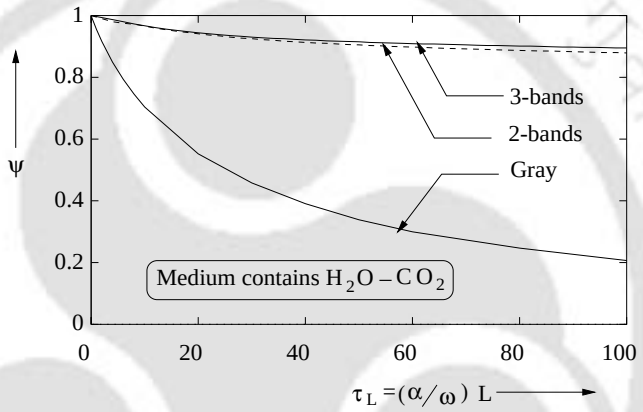

Figure 6.9: Variations of heat flux Ψ across a mixture of gases bounded by parallel, black walls.

6.4 Summary

In this Chapter, applicability of CDM has been shown for gray and inhomogeneous absorbing, emitting and anisotropically scattering medium. For both non-radiative and radiative equilibrium situations considered for 1-D planar medium, inhomogeneity caused due to spatially varying properties like extinction coefficient, scattering albedo and anisotropy has been discussed. For a sample test situation, CDM results have been compared with results from YIX method. For all the situations, CDM results have also been compared with self generated DTM results. CDM has been found to give very good

comparisons. Further, CDM has also been found economical than DTM. For a sample case, applicability of CDM has also been proved for non gray and homogeneous medium.

Chapter 7

A New Angular Discretization Scheme

7.1 Introduction

In all the test cases presented so far, in validation studies with CDM, for angular integrations, discretization scheme given in Chapter 2, Eqs. 2.46-2.48, has consistently been used. In this scheme, entire planar angle α is divided into a finite number of differential planar angles $\Delta\alpha$, each of same angular width. In each differential planar angle $\Delta\alpha$, effective intensity is assumed isotropic. This angular discretization scheme has been used in all earlier works on CDM, and the same has been followed so far in the present work. Although, even with this angular discretization scheme, CDM has been found economical, it was thought that if angular integrations are performed as per Gaussian quadrature, CDM might become more economical. Gaussian quadrature scheme is followed for angular integrations in DOM.

With above objective in mind, in this chapter, some improvements in CDM in terms of computational time and accuracy are aimed at. With the new

scheme, for a chosen accuracy level, computational time will be less, or in other words, for the same computational time, results with new scheme will be more accurate.

In the following sections, study on the impact of the proposed scheme on computational time/accuracy is made. Although proposed discretization scheme is applicable to all types of enclosures, for the sake of simplicity, here it is tested over radiative transfer problems in 1-D Cartesian enclosure with gray and homogeneous absorbing, emitting and anisotropically scattering medium. Both radiative and non-radiative equilibrium situations are considered. For the sake of comparison, here results obtained from CDM with new discretization scheme will be designated as that from the modified collapsed dimension method (MCDM) and that from scheme used in earlier chapters, as before, results from CDM.

7.2 The Scheme

As discussed in Chapter 2, in CDM, at any CVSCP m in a given direction M, heat flux due to a semi circle of effective intensities is given by

$$q_{M,m} = \int_{\alpha=0}^{\pi} I(\alpha) \sin\alpha \, d\alpha \tag{7.1}$$

Further at any CVSCP m, effective incident radiation $G^{'}$ is given by

$$G^{'}_{m} = \int_{\alpha=0}^{\pi} I(\alpha) d\alpha \tag{7.2}$$

In Chapter 2, Eqs. (2.46) -(2.48) (equations presented below), numerical integration scheme for both these equations have been given. Equations (2.46) (here Eq. 7.3) and Eq. (2.48), here Eq. (7.5)) are the non-dimensional forms of Eqs. (7.1) and (7.2).

$$\Psi_{M,m} = \frac{1}{2}\Big[\int_{\alpha=0}^{\pi} I^{*}(\alpha) \, \sin\alpha \, d\alpha\Big] = \frac{1}{2}\Big[\Sigma_{n=1}^{N} c_n I^{*}(\alpha_n)\Big]_{M,m} \tag{7.3}$$

where in general

$$c_n = \Big|\cos(\alpha_n + \frac{\Delta\alpha_n}{2}) - \cos(\alpha_n - \frac{\Delta\alpha_n}{2})\Big| \tag{7.4}$$

Here, $||$ indicates the absolute value, and the term $\Delta\alpha_n$ is the angle over which the n th effective ray, $I^*(\alpha_n)$ is acting. The non-dimensional effective incident radiation, $G^{'*}$, at any CVSCP m is found from Eq. (2.5) as

$$G^{'*} = \left[\int_{\alpha=0}^{2\pi} I^*(\alpha)d\alpha\right]_m = \left[\Sigma_{n=1}^{2N} I^*(\alpha_n)\Delta\alpha_n\right]_m \tag{7.5}$$

where in the above equation, N is the number of effective rays over angle π. In the above scheme, as shown in Fig. 7.2a, angular thickness $\Delta\alpha$ of each discrete plane (shown as DP in the figure), is the same. In this figure, for a semi-circle of effective intensities at any CVSCP, five token discrete planes have been shown. In each discrete plane, effective intensity contained in it, is isotropic.

With angular thickness of all the discrete planes the same, and effective intensity being isotropic in each discrete plane (of angular width $\Delta\alpha$), angular integration in Eqs. (7.1) and (7.2) is a simple summation.

In the modified scheme, angular integrations in Eqs. (7.3) and (7.5) are performed using Gaussian quadrature. In this, for a chosen number of effective intensities (in other words, discrete planes), angular thickness of discrete planes are not the same. The angular span over which, each effective intensity is isotropic, is determined from the number of quadrature points considered. This point has been made clear from Fig. 7.2b. Here, as in Fig. 7.2a, angular span of five effective intensities have been shown. The angular spans $\Delta\alpha$ over which effective intensities work, are not same for all.

In the light of the above, in MCDM, heat flux $q_{M,m}$ and the incident radiation G_m at the CVSCP m given by Eqs. (7.1) and (7.22) respectively are calculated from the following:

$$q_{M,m} = \frac{\pi}{2}\Sigma w(\mu)I(\mu)\ \sin\alpha \tag{7.6}$$

$$G_m^{'} = \frac{1}{2}\Sigma w(\mu)I(\mu) \tag{7.7}$$

where $\mu = \cos\alpha$ and $w(\mu)$ is the weight factor.

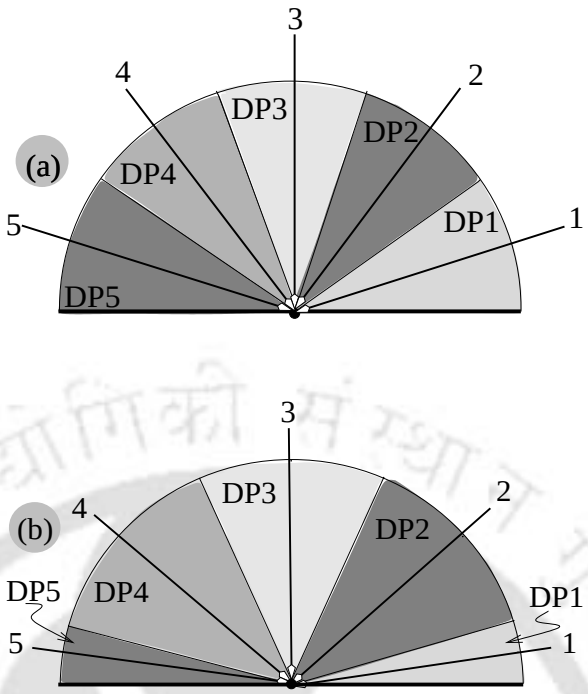

Figure 7.1: Distribution of effective intensities and angular thickness of the discrete planes (a) CDM and (b) MCDM.

7.3 Validation Studies

Shown in Fig. 7.2 is a general 1-D gray Cartesian enclosure under consideration. The participating medium is absorbing, emitting and anisotropically scattering. South and north walls of the enclosure are at temperatures T_S and T_N respectively. Emissivities of south and north walls are ϵ_s and ϵ_n respectively. Enclosure optical thickness corresponding to finite distance L_Z is τ_L.

For problem considered under non-radiative equilibrium, the absorbing, emitting and isotropically scattering gray and homogeneous medium is isothermal at temperature T_g, and black bounding walls are cold (at zero temperature). In this situation, variations of wall heat flux Ψ with enclosure optical thickness τ_L are studied. For chosen number of rays, both CDM and MCDM results are compared with exact results provided in [236]. Here, for

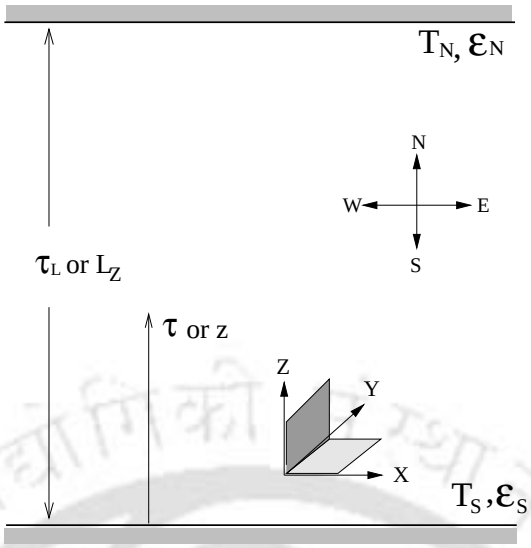

Figure 7.2: 1-D Cartesian enclosure under consideration.

non-dimensionalization of heat flux, medium temperature T_g has been chosen as reference temperature T_R.

Under radiative equilibrium situation, south wall is at a finite temperature T_s, whereas north wall is at zero temperature. Gray and homogeneous medium is absorbing, emitting and anisotropically scattering. In this case, variations of wall heat flux Ψ with τ_L, and variations of emissive power Φ with τ/τ_L from MCDM and CDM are compared with the exact results from [236]. Here, south wall temperature T_S has been taken as the reference temperature for non-dimensionalization of heat flux and emissive power.

In MCDM, Gaussian quadrature points and corresponding weight data have been taken from [311].

7.3.1 Non-radiative Equilibrium

Variations of non-dimensional wall heat flux Ψ with enclosure optical thickness τ_L have been given in Figs. 7.3 and 7.4. For non-radiative equilibrium situation, these results have been given for absorbing, emitting and isotropically scattering medium.

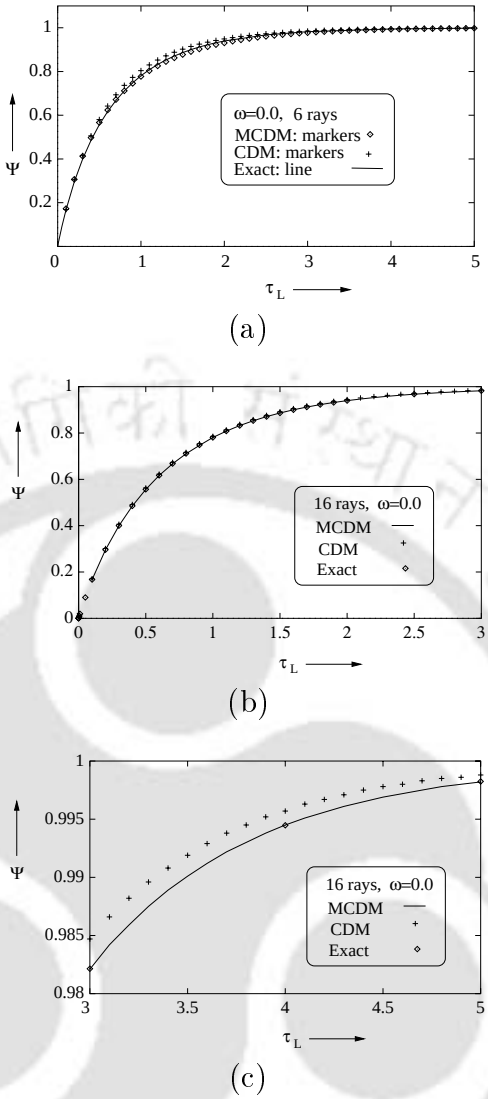

Figure 7.3: Comparison MCDM and CDM results for variation of wall heat flux Ψ with enclosure optical thickness τ_L for absorbing and emitting medium under non-radiative equilibrium condition; (a) 6 rays, (b) 16 rays and (c) 16 rays.

In Figs. 7.3a-c, for absorbing-emitting medium ($\omega = 0$), MCDM and CDM results have been compared with the exact results [236]. For both CDM and MCDM, 6 and 16 number of rays have been considered. Results with 6 number of rays from MCDM compare better with the exact results. Further, from Fig. 7.3c it is observed that at higher optical thickness, in both CDM and MCDM,

more number of rays are required for the accurate prediction of Ψ.

For the results presented in Figs. 7.3a-c, deviations of MCDM results from exact results have been found in the range of 0.002%-0.545%. Corresponding deviation in case of CDM have been calculated to be 0.056 % -1.780 %. For both CDM and MCDM, 16 rays have been used. Thus it is seen that for the same number of rays, MCDM is more accurate than CDM. In other words, for the same level of accuracy, CDM requires more number of rays.

Effects of scattering albedo on non-dimensional wall heat flux Ψ are presented in Figs. 7.4a-c . Result presented in Fig. 7.4a is for scattering albedo, ω=0.5 and that of Figs. 7.4b and c, for ω= 0.9. In both CDM and MCDM, for results presented in Fig. 7.4a, 6 rays and 100 control volumes have been used, whereas 16 rays and 350 control volumes have been used for results presented in Figs. 7.4b and c. Here also it is observed that comparison of MCDM results with exact results is much better than that of CDM.

For the problem under consideration, to have quantitative idea about the percentage deviation of wall heat flux results of MCDM and CDM, some results are presented in Tables 7.1-7.4. Here, % deviation of MCDM and CDM results have been found with respect to the exact results [236]. In all the Tables 7.1-7.4, results have been presented for enclosure optical thickness τ_L=0.1, 0.5, 1.0, 2.0, 3.0 and 5.0.

Table 7.1 presents percentage deviation of Ψ for an absorbing-emitting medium ($\omega = 0$) under non-radiative equilibrium situation. Here, for the justification given in Chapter 3 for isothermal absorbing-emitting medium under non-radiative equilibrium, Ψ values at wall have been found by considering only one control volume. Here, comparison has been made for 10 rays in both MCDM and CDM. From this table it is observed that for equal number of rays, percentage deviation MCDM results is much lower than that for CDM.

For scattering albedo ω=0.1, 0.5 and 0.9, results on % deviation in wall heat flux Ψ have been presented in Tables 7.2-7.4 respectively.

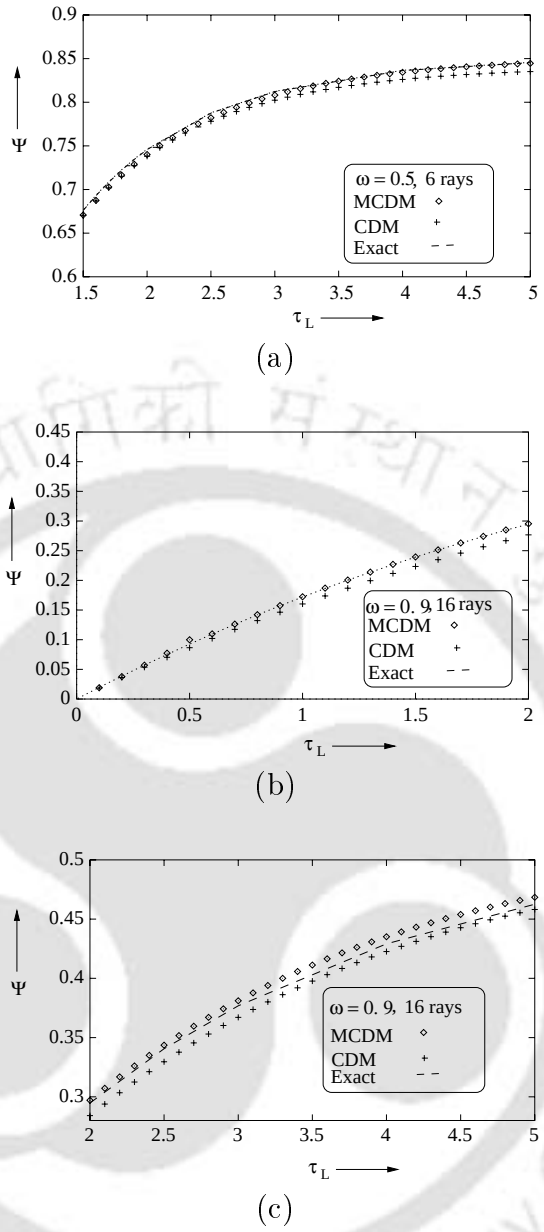

Figure 7.4: Comparison MCDM and CDM results for variation of wall heat flux Ψ with with enclosure optical thickness τ_L for absorbing, emitting and isotropically scattering media; (a) ω=0.5, (b) ω=0.9 and (c) ω=0.9.

In Table 7.2, results have been presented for ω=0.1. Here, % deviation in MCDM and CDM results have been found for 10 rays and 200 control volumes. It is seen from this table that percentage deviation of Ψ in MCDM is in the

τ_L	Exact	MCDM	% deviation	CDM	% deviation
0.1	0.1674	0.1691	1.0155	0.1711	2.2103
0.5	0.5568	0.5550	0.3233	0.5698	2.3348
1.0	0.7806	0.7790	0.2050	0.7896	1.1530
2.0	0.9397	0.9403	0.0639	0.9446	0.5214
3.0	0.9821	0.9823	0.0204	0.9848	0.2749
5.0	0.9982	0.9982	0	0.9988	0.0601

Table 7.1: Percentage % deviation (absolute) in wall heat flux Ψ for MCDM and CDM with respect to exact solution; ω=0.

range 0.0401 %-0.9791 %, whereas the same in CDM is in the range of 0-1.8504 %.

In Table 7.3, percentage deviation of Ψ is given for ω=0.5. Here, 16 rays and 350 control volumes have been considered. In Table 7.4, results have been provided for ω=0.9. These results have been generated with 16 rays 500 control volumes.

τ_L	Exact	MCDM	% deviation	CDM	% deviation
0.1	0.1532	0.1547	0.9791	0.1557	1.6319
0.5	0.5242	0.5245	0.0572	0.5339	1.8504
1.0	0.7473	0.7467	0.0803	0.7534	0.8163
2.0	0.9122	0.9132	0.1096	0.9153	0.3398
3.0	0.9579	0.9584	0.0522	0.9594	0.1566
5.0	0.9759	0.9763	0.0410	0.9759	0

Table 7.2: % deviation (absolute) in wall heat flux Ψ for MCDM and CDM with respect to exact solution; ω=0.1.

It is observed from results presented above that in non-radiative equilibrium situation, for all the cases, for given number of rays, MCDM is more accurate than CDM, or vise versa for a given level of accuracy, MCDM is computationally economical than CDM.

τ_L	Exact	MCDM	% error	CDM	% error
0.1	0.0911	0.0904	0.7684	0.0909	0.2195
0.5	0.3572	0.3547	0.6999	0.3534	1.0638
1.0	0.5585	0.5592	0.1253	0.5520	1.1638
2.0	0.7461	0.7479	0.2413	0.7416	0.6031
3.0	0.8126	0.8139	0.1600	0.8096	0.3692
5.0	0.8457	0.8463	0.0709	0.8439	0.2128

Table 7.3: % deviation (absolute) in wall heat flux Ψ for MCDM and CDM with respect to exact solution; ω=0.5.

τ_L	Exact	MCDM	% deviation	CDM	% deviation
0.1	0.0196	0.0190	3.0612	0.0192	2.0408
0.5	0.0925	0.0925	0	0.0890	3.7838
1.0	0.1720	0.1726	0.3488	0.1644	4.4186
2.0	0.2948	0.2967	0.6445	0.2838	3.7313
3.0	0.3768	0.3805	0.9820	0.3664	2.7601
5.0	0.4626	0.4671	0.9728	0.4569	1.2322

Table 7.4: % deviation (absolute) in wall heat flux Ψ for MCDM and CDM with respect to exact solution; ω=0.9.

7.3.2 Radiative Equilibrium

For the geometry considered in Fig. 7.2, for the problem under radiative equilibrium, comparisons of wall heat Ψ results of MCDM and CDM with that of exact results [236] have been made in Tables 7.5-7.7. These comparisons have been made for absorbing, emitting and anisotropically scattering medium. In all three tables, comparisons have been made for τ_L=0.1, 0.5, 1, 2, 3 and 5.

For results presented in Table 7.5, anisotropy $a_1\omega$=+1, whereas for both the Tables 7.6 and 7.7, $a_1\omega$=-1. For linear anisotropic phase function considered in this work, these two values represent 100% forward and 100% backward scattering situations respectively. For results presented in Table 7.5 and 7.6, comparisons have been made with 6 rays and 50 control volumes, whereas in Table 7.7, for comparison, in both MCDM and CDM, 16 rays and 50 control volumes have been used. It is seen from these tables that for all the cases, for

equal numbers of rays and control volumes, accuracy in MCDM is more than that of CDM.

τ_L	Exact	MCDM	% deviation	CDM	% deviation
0.1	0.9371	0.9342	0.3095	0.9360	0.1174
0.5	0.7716	0.7632	1.0886	0.7622	1.2182
1.0	0.6409	0.6401	0.1248	0.6330	1.2326
2.0	0.4860	0.4831	0.5967	0.4823	0.7613
3.0	0.3883	0.3898	0.3863	0.3956	1.8800
5.0	0.2796	0.2804	0.2861	0.2957	5.7582

Table 7.5: Comparison of % deviation (absolute) in wall heat flux Ψ for MCDM and CDM with respect to exact solution; $a_1\omega$=+1.0, 6 rays and 50 control volumes.

τ_L	Exact	MCDM	% deviation	CDM	% deviation
0.1	0.8952	0.8907	0.5027	0.8958	0.0670
0.5	0.6467	0.6392	1.1597	0.6438	0.4484
1.0	0.4849	0.4852	0.0619	0.4833	0.3300
2.0	0.3267	0.3308	1.2550	0.3275	0.2449
3.0	0.2441	0.2524	3.4002	0.2498	2.3351
5.0	0.1623	0.1704	4.9908	0.1723	6.1643

Table 7.6: Comparison of % deviation (absolute) in wall heat flux Ψ for MCDM and CDM with respect to exact solution; $a_1\omega$=-1.0, 6 rays and 50 control volumes.

τ_L	Exact	MCDM	% deviation	CDM	% deviation
0.1	0.8952	0.8939	0.1452	0.8949	0.0335
0.5	0.6467	0.6451	0.2474	0.6487	0.3093
1.0	0.4849	0.4873	0.4949	0.4907	0.5800
2.0	0.3267	0.3294	0.8264	0.3345	2.3875
3.0	0.2441	0.2502	2.4990	0.2556	4.7112
5.0	0.1623	0.1680	3.5120	0.1766	8.8108

Table 7.7: Comparison of % deviation (absolute) in wall heat flux Ψ for MCDM and CDM with respect to exact solution; $a_1\omega$=-1.0, 16 rays and 50 control volumes.

Figures 7.5 and 7.6 give the variations of non-dimensional emissive power Φ with enclosure optical depth τ/τ_L for various enclosure optical thicknesses. In

Fig. 7.5, Φ variations are given for τ_L=0.1, 0.5 and 1.0, whereas the same have been given for τ_L=1.0, 2.0 and 5.0 in Fig. 7.6. In Figs. 7.5 and 7.6, for 48 control volumes, CDM and MCDM results have been obtained with 10 and 32 rays respectively. In both the figures, for all τ_L, comparisons have been made with exact results. It is seen that for correct prediction of emissive power, CDM requires 32 rays, whereas MCDM requires just 10 rays.

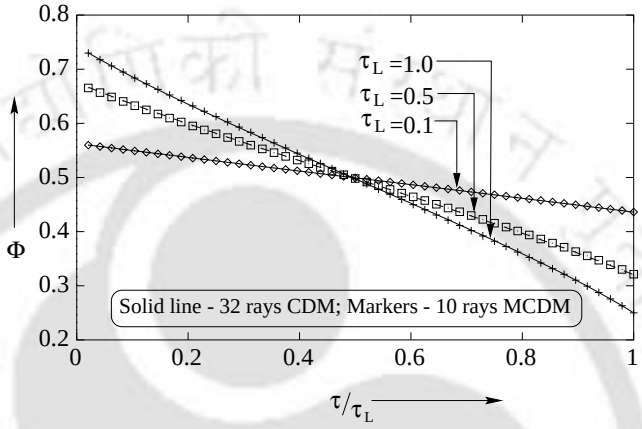

Figure 7.5: Variation of emissive power Φ with normalized optical depth τ/τ_l in 1-D Cartesian enclosure; Absorbing, emitting medium under radiative equilibrium.

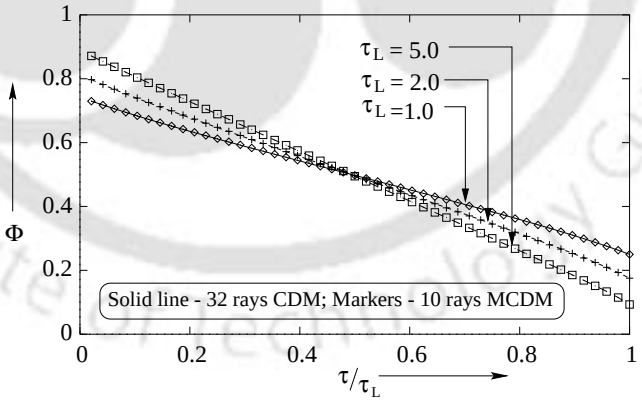

Figure 7.6: Variation of emissive power Φ with normalized optical depth τ/τ_l in 1-D Cartesian enclosure; Absorbing, emitting medium under radiative equilibrium.

7.3.3 Economy

To get the feel of computational effort involved in MCDM and CDM, for some sample cases, a comparison of CPU time required in both the methods have been provided in Table 7.8. Here for radiative equilibrium situation, for τ_L = 0.1, 1, 2 and 5, three cases, i.e, $a_1\omega$=+1.0, $a_1\omega$=0 and $a_1\omega$=-1.0 have been considered. These three cases respectively represent 100% forward scattering, isotropic scattering and 100% backward scattering. For forward and backward scattering cases, CPU times of CDM and MCDM have been compared with 16 rays and 150 control volumes. For the same number of rays and control volumes, number of iterations and hence CPU time in both methods are different. For isotropic scattering condition, same number rays have been considered. However, in this case, with converged solution, 48 control volumes have been found sufficient. It is observed this table that MCDM is economical than CDM.

Anisotropy factor $a_1\omega$	rays	CV	τ_L	CPU time (seconds) on HP-9000	
				MCDM	CDM
$a_1\omega$=+1.0	16	150	0.1	0.2	0.5
			1.0	0.7	1.4
			2.0	1.3	2.5
			5.0	4.5	8.1
$a_1\omega$=0	16	48	0.1	0.1	0.3
			1.0	0.4	0.9
			2.0	0.7	1.5
			5.0	2.8	4.1
$a_1\omega$=-1.0	16	150	0.1	0.2	0.4
			1.0	0.5	1.3
			2.0	0.9	2.3
			5.0	2.5	7.7

Table 7.8: CPU time (seconds) required for evaluation of wall heat flux Ψ in case of absorbing, emitting and anisotropically scattering gray homogeneous medium confined between 1-D planar enclosure under radiative equilibrium situation.

7.4 Summary

In this Chapter, with the objective of making CDM computationally more efficient, a new angular Discretization scheme has been adopted. This has been done by utilizing the concept of Gaussian quadrature. The new scheme has been tested for radiative transfer problems in 1-D black Cartesian enclosure with absorbing, emitting, anisotropically scattering gray and homogeneous medium. Sample cases in both radiative and non-radiative equilibrium situations have been considered. The validation studies have shown that with new scheme, CDM is more economical.

Chapter 8

Summary and Suggestions for Future Work

8.1 Summary

Development of an efficient method for the solution of radiative transfer problem with participating medium has always been a challenging task. The 3-D nature of radiation associated with a large number of variables in participating medium, poses enormous complexity in the solution of equation for the conservation of total energy. Extensive literature review reveal that most of the existing radiation methods suffer from limitations as described in Chapter 1. These limitations are particularly experienced in applications with irregular, multi-dimensional geometries, anisotropic scattering, and spatially and spectrally varying radiative properties along with huge computational time.

Collapsed dimension method, considered in the present work, is designed to provide a wider range of applicability than the competing methods. Its formulations, presented in Chapter 2, are based on collapsing 3-D radiative information to a 2-D solution plane. As in CDM, radiative information are contained only in the solution plane, governing equations are entirely different from other numerical methods.

Part of the developments on CDM have been reported by Blank [235], Mishra

[236] and Mishra and Prasad [239] for prediction of radiative transfer in 1-D and 2-D Cartesian enclosures with absorbing, emitting and anisotropically scattering medium. In these studies, most of the efforts were directed to calculate the transformation parameter OTC for the gray and homogeneous medium. OTC is the backbone of CDM. For the lack of OTC data under different situations, the method could not be applied to other type of enclosures and even to 1-D Cartesian and 2-D rectangular enclosures with variable radiative properties. Further, for gray and homogeneous medium, its applicability for conjugate mode problems had not been dealt with.

In the present work, foundation of CDM has been strengthened by extending the applicability of OTCs found in [236] to a very general situation. It has been shown that OTCs given for radiative and non-radiative equilibrium situations in [236] for gray and homogeneous medium can very well be applied to different geometries and medium conditions.

Major contributions of the present work are summarized in the following lines:

With introduction given in Chapter 1, research in thermal radiation has been justified, and complexities involved in the analysis of thermal radiation with participating medium have been highlighted. Complexities in the analysis of thermal radiation have necessitated the development of numerical methods for the solution of radiative transfer problems. To understand the method and its strong and weak points, an extensive literature review has been provided in Chapter 1. With this literature review, need for a more versatile method has been felt. Citing some of the strong points of CDM, further research in CDM has been justified.

The physics of the CDM has been explained in Chapter 2. All pertinent equations used in CDM have been described. The limitations of OTCs in earlier works on CDM and the procedure for its generalization to all types of enclosures and media have been explained. Solution procedure in CDM has been given with reference to a 2-D diffuse gray Cartesian enclosure containing gray homogeneous absorbing, emitting and anisotropically scattering medium.

To prove that CDM can be applied to more general situations, different class of

benchmark problems have been taken up. In Chapter 3, benchmark problems on radiative transfer problems in various types of 2-D Cartesian enclosures, such as rectangular, L-shaped and quadrilateral enclosures have been solved. In this chapter, applicability of CDM has been shown for a 3-D Cartesian enclosure. Depending upon the availability of results, CDM results have been compared with those available in the literature. In all types of 2-D and 3-D Cartesian enclosures considered, CDM has been found to give correct prediction of radiative information. Applicability of CDM for benchmark problems on cylindrical enclosures has been shown in the next chapter. Here for absorbing, emitting and/or scattering situations, CDM has been tested for radiative transfer problems in 1-D and 2-D single as well as concentric cylindrical enclosures. Problems with temperature as well as flux boundary conditions have been taken up. Applicability of CDM for a typical furnace problem has also been shown. For all the test problems considered for cylindrical geometries, CDM has been found to give correct prediction of radiative information.

For a conjugate radiation, conduction and/or convection problems, compatibility of radiation module of a method with that of conduction and/or convection modules is an important aspect. With successful application of CDM for combined radiation and conduction heat transfer in 1-D concentric cylindrical enclosure with absorbing, emitting and anisotropically scattering medium, given in Chapter 5, it has been shown that CDM can easily be applied for conjugate mode heat transfer problems.

In many practical situations, gray and homogeneous assumption for a participating medium causes deviation from the correct radiative information. Versatility of a method is also tested by its capability to work for non gray and inhomogeneous medium. This point applies more to CDM as it treats radiation in 2-D plane and has been working with OTCs found for gray and homogeneous medium. By taking test problems in Chapter 6, it has been proved that CDM works well for gray and inhomogeneous medium, and homogeneous and non gray medium.

From different types of test problems considered in the present work, it has been shown that CDM is economical than exact method, DTM and MCM. To make CDM computationally more efficient, a new discretization scheme has

been introduced in Chapter 7. With this new scheme, it has been shown that with CDM, computational time can further be reduced.

In the present work, in most of the cases, CDM results presented are validated with those available in the literature. However, some new results have also been generated for which results are not available in the literature. For example, Fig. 4.13, Figs. 4.17-4.22, Figs. 4.25-4.26, Figs. 4.32-4.33, Figs. 4.37, Figs. 4.41-4.42, Figs. 5.7-5.8, Figs. 5.10-5.12 and Fig. 6.9 are some of the new results incorporated in the present work. Justification for these results are provided in the thesis.

8.2 Suggestions for Future Research

A few suggestions for the next round of development on CDM are listed below:

1. In dealing with the anisotropically scattering medium, we have considered linear anisotropically scattering phase function only. OTCs for other form of phase functions are needed for extending CDM to tackle different phase functions.

2. Further investigation is needed for application of CDM for collimated radiation and specularly reflecting boundary conditions.

3. CDM can be extended to practical problems associated with combustion, solidification of semi-transparent metals, porous medium, etc.

4. In different methods, as found in literature, ray and false scattering effects are prevalent. In CDM, so far, such effects have not been reported. Hence, this method has to be tested for ray effects/false scattering effects.

5. Improvements suggested for CDM in Chapter 7 were tested and validated for 1-D planar medium only. This improved scheme in angular discretization has to be tested for multi-dimensional enclosures.

6. A comparative study of CDM with FVM, DTM and DOM are needed to establish its relative merits in terms of accuracy and computational efforts.

7. More study is needed for 3-D enclosure with absorbing, emitting and scattering medium.

References

[1] S. Manickavasagam and M. P. Menğuç. Effective optical properties of pulverized coal particles determined from FT-IR spectrometer experiments. *Energy & Fuels*, 7:860–869, 1993.

[2] C. L. Tien. Thermal radiation in packed and fluidized beds. *Trans. ASME Journal of Heat Transfer*, 110:1230–1242, November 1988.

[3] A. K. Kolar. Heat transfer in circulating fluidised bed boilers: Perspective and issues. In *Proceedings of the fourth ISHMT-ASME Heat and Mass Transfer Conference and Fifteenth National Heat and Mass Transfer Conference, Pune, India*, pages 105–116. Tata McGraw-Hill Publishing Company Limited, New Delhi, 2000.

[4] G. Y. Han and Y. J. Cho. Radiative heat transfer in a circulating bed coal combustor. *Powder Technology*, 102:266–273, 1999.

[5] W. Luan, C. J. Lim, C. M. H. Brereton, B. D. Bowan, and J. R. Grace. Measurement of radiative heat transfer in a circulating fluidized bed combustor. *Fluidized Bed Combustion, ASME*, 2:879–883, 1997.

[6] G. Flamant, B. Variot, M. R. Golritz, and J. D. Lu. Radiative heat transfer in a pilot scale circulating fluidized bed boiler. In *HM*, volume 10, pages 1–6, 1996.

[7] W. Bauer and R. Steinhardt. Measurement of radiative properties of refractories and steel. *Eurotherm Seminat n, Portugal*, 17, 1990.

[8] D. A. Gould. *Hierarchical p Version Finite Elements for Radiation Heat Transfer*. PhD thesis, University of Virginia, 1999.

[9] K. Badari Narayana. Spacecraft thermal control system. In *Proceedings of the fourth ISHMT-ASME Heat and Mass Transfer Conference and Fifteenth National Heat and Mass Transfer Conference, Pune, India*, pages 57–63. Tata McGraw-Hill Publishing Company Limited, New Delhi, 2000.

[10] T. W. Tong and C. L. Tien. Radiative transfer in fibrous insulations-Part 1: Analytical study. *Journal of Heat Transfer*, 105(1):70–75, 1983.

[11] L. Glicksman, M. Schuetz, and M. Sinofsky. Radiation heat transfer in foam insulation. *International Journal of Heat and Mass Transfer*, 30(1):187–197, 1987.

[12] R. Mathes, J. Blumenberg, and K. Keller. Radiative heat transfer in insulations with random fibre orientation. *International Journal of Heat and Mass Transfer*, 33(4):767–770, 1990.

[13] L. K. Matthews, R. Viskanta, and F. P. Incropera. Combined conduction and radiation heat transfer in porous materials heated by intense solar radiation. *Solar Energy Engineering*, 107:29–34, 1985.

[14] N. D. Eryou and L. R. Glicksman. An experimental and analytical study of radiative and conductive heat transfer in molten glass. *Journal of Heat Transfer*, 94:224–230, 1972.

[15] U. E. Condon. Radiative transport in hot glass. *Journal of Quant. Spectros. Radiat. Transfer*, 8(1):369–385, 1968.

[16] E. R. Streed, G. R. Cunnington, and C. A. Zierman. Performace of multi layer insulation system for 300-800 K temperature range. In *Proceedings Astro Aero*, volume 18, pages 735–772, 1965.

[17] R. P. Careen and G. R. Cunnington. Heat transfer in multi layer insulations. In *Chemical Engineering Symposium Ser*, volume 64, pages 67–81, 1967.

[18] S. Maruyama and T. Aihara. Radiation heat transfer of a Czochralski crystal growth furnace with arbitrary specular and diffuse surfaces. *International Journal of Heat and Mass Transfer*, 37(12):1723–1731, 1994.

[19] K. Kuo. *Principles of Combustion. Chap. 7.* Wiley, New York, 1986.

[20] P. F. Sens. Strategies for future R & D in combustion processes. *Combustion Science and Technology*, 93:1–8, 1993.

[21] S. Maruyama and M. Higano. Radiative heat transfer of torus plasma in large helical device by generalized numerical method REM^2. *Energy Conversion and Management*, 38:1187–1195, 1997.

[22] J. S. Lee, K. H. Lee and M Choi. Parametric analysis of radiative-convective heat transfer around a circular cylinder in a cross flow using the finite volume radiation solution method. *Numerical Heat Transfer, Part A*, 29:181–196, 1996.

[23] T. Li. *Optical Fiber Communications, Volume 1 - Fiber Fabrication.* Academic Press, San Diego, Calif., 1985.

[24] F. Incropera and D. P. De Witt. *Fundamentals of Heat and Mass Transfer.* John Wiley and Sons, New York, 3rd edition edition, 1990.

[25] S. Chandrasekhar. *Radiative Transfer.* Dover Publication, New York, 1960.

[26] R. D. Cess and E. M. Sparrow. *Radiative Heat Transfer.* Broks/Cole Publishing Company, 1966.

[27] M. N. Özişik. *Radiative Transfer and Interactions with Conduction and Convection.* John Wiley & Sons, New York, 1973.

[28] R. Siegel and J. R. Howell. *Radiative Heat Transfer.* Hemisphere, Washington DC, 3rd edition, 1996.

[29] M F. Modest. *Radiative Heat Transfer.* McGraw-Hill, Inc, 1993.

[30] M. Q. Brewster. *Thermal Radiative Transfer and Properties*. John Wiley & Sons, New York, 1992.

[31] J. H. Jeans. The equations of radiative transfer of energy. *Monthly Notices Royal Astronomical Society*, 78:28–36, 1917.

[32] B. Davison. *Neutron Transport Theory*. Clarendon, Oxford, 1958.

[33] C. E. Lee. The discrete S_{n} approximation to transport theory. Technical Report Technical Information Series Report LA2595, Lawrence Livermore Laboratory, 1962.

[34] K. D. Lathrop. Use of discrete ordinate methods for solution of photon transport problems. *Nuclear Science and Engineering*, 24:381–388, 1966.

[35] J. R. Howell. Recent advances and opportunities in engineering radiation heat transfer. In *Proceedings of the fourth ISHMT-ASME Heat and Mass Transfer Conference and Fifteenth National Heat and Mass Transfer Conference, Pune, India*, pages 13–22. Tata McGraw-Hill Publishing Company Limited, New Delhi, January 2000.

[36] M. Q. Brewster and C. L. Tien. Radiative transfer in packed fluidized beds: Dependent versus independent scattering. *Journal of Heat Transfer*, 104:573–579, 1982.

[37] S. C. Lee and C. L. Tien. Effect of soot shape on soot radiation. *Journal of Quant. Spectros. Radiat. Transfer*, 29(3):259–265, 1983.

[38] T. Kunitomo and T. Sato. Experimental and theoretical study on the infrared emission of soot particles in luminous flames. In *Fourth International Heat Transfer Conference*. Paris-Versailles, September 1970.

[39] N. Ramesh and S. P. Venkateshan. Effect of surface radiation and partitioned resistance on natural convection heat transfer in a partitioned enclosure; an experimental study. *Trans. ASME Journal of Heat Transfer*, 121:616–622, 1999.

[40] V. R. Rao and S. P. Venkateshan. Experimental study of free convection and radiation in horizontal fin arrays. *International Journal of Heat and Mass Transfer*, 39(4):779–789, 1996.

[41] J. R. Howell. Radiative transfer in multi-dimensional enclosures with participating media. *ASME, 83-HT-32*, 1983.

[42] K. T. Yang. Numerical modeling of natural convection-radiation interactions in enclosures. In *Proceedings of the 8th International Heat Transfer Conference*, volume 1, pages 131–140. San Francisco, CA, August 18-23 1986.

[43] R. Viskanta and M. P. Menğuç. Radiation heat transfer in combustion systems. *Prog. Energy Combust. Sci.*, 13:97–160, 1987.

[44] S. C. Mishra and M. Prasad. Radiative heat transfer in participating media- a review. *Sadhana*, 23(2):213–232, 1998.

[45] V. Kourgnaoff. *Basic Methods in Transfer Problems*. Oxford University Press, London, 1952.

[46] E. E. Lewis and Jr W. F. Miller. *Computational Methods of Neutron Transport*. Wiley, New York, 1984.

[47] Max. A. Heaslet and Robert F. Warming. Radiative transport and wall temperature slip in an absorbing planar medium. *International Journal of Heat and Mass Transfer*, 8:979–994, 1965.

[48] A. Dayan and C. L. Tien. Heat transfer in a gray planar medium with linear anisotropic scattering. *Trans. ASME Journal of Heat Transfer*, 97:391–396, August 1975.

[49] A. Dayan and C. L. Tien. Radiative transfer with anisotropic scattering in an isothermal slab. *Journal of Quant. Spectros. Radiat. Transfer*, 16:113–125, 1976.

[50] W. H. Sutton and M. N. Özişik. An iterative solution for anisotropic radiative transfer in a slab. *Trans. ASME Journal of Heat Transfer*, 101:695–698, November 1979.

[51] Max. A. Heaslet and Robert F. Warming. Theoretical predictions of radiative heat transfer in homogeneous cylindrical medium. *Journal of Quant. Spectros. Radiat. Transfer*, 6:751–774, 1966.

[52] A. S. Kesten. Radiant heat flux distribution in a cylindrically symmetric nonisothermal gas with temperature-dependent absorption coefficient. *Journal of Quant. Spectros. Radiat. Transfer*, 8(1):419–434, 1968.

[53] S. K. Loyalka. Radiative heat transfer between parallel plates and concentric cylinders. *International Journal of Heat and Mass Transfer*, 12:1513–1517, 1969.

[54] S. Shyam Dua and Ping Cheng. Multi-dimensional radiative transfer in non-isothermal cylindrical media with non-isothermal bounding walls. *International Journal of Heat and Mass Transfer*, 18:245–259, 1975.

[55] A. L. Crosbie and J. B. Farrell. Exact formulation of multiple scattering in a three-dimensional cylindrical geometry. *Journal of Quant. Spectros. Radiat. Transfer*, 31(5):397–416, 1984.

[56] F. H. Azad and M. F. Modest. Evaluation of the radiative heat flux in absorbing, emitting and linear-anisotropic scattering cylindrical media. *Trans. ASME Journal of Heat Transfer*, 103:350–356, May 1981.

[57] A. L. Crosbie and R. L. Dougherty. Two-dimensional radiative transfer in a cylindrical geometry with anisotropic scattering. *Journal of Quant. Spectros. Radiat. Transfer*, 25:551–569, 1980.

[58] P. Mahanta and Subhash C. Mishra. Solution of radiative heat transfer problems in long-cylindrical enclosures with participating media. In *Proceedings of the fourth ISHMT-ASME Heat Transfer Conference and fifteenth National Heat and Mass Transfer Conference, Pune, India*, pages 665–672, January 2000.

[59] G. E. Hunt. The transport equation of radiative transfer in a three-dimensional space with anisotropic scattering. *Journal of the Institute of Mathematics and its Applications*, 3(2):181–192, 1967.

[60] P. Cheng. Thermal control and radiation. In *Progress in Astonautics and Aeronautics, C. L. Tien ed*, pages 269–308. MIT Press, Cambridge, 1973.

[61] A. L. Crosbie and J. W. Koewing. Two-dimensional radiative transfer in a finite scattering planar medium. *Journal of Quant. Spectros. Radiat. Transfer*, 21:573–595, 1979.

[62] A. L. Crosbie and R. L. Dougherty. Two-dimensional linearly anisotropic scattering in a finite-thick cylindrical medium exposed to a laser beam. *Journal of Quant. Spectros. Radiat. Transfer*, 33(5):487–520, 1985.

[63] A. L. Crosbie and R. G. Schrenker. Exact expressions for a radiative transfer in a three-dimensional rectangular geometry. *Journal of Quant. Spectros. Radiat. Transfer*, 28(6):507–526, 1982.

[64] A. L. Crosbie and R. G. Schrenker. Multiple scattering in a two-dimensional rectangular medium exposed to collimated radiation. *Journal of Quant. Spectros. Radiat. Transfer*, 33(2):101–125, 1983.

[65] A. L. Crosbie and G. W. Davidson. Dirac-delta function approximations to the scattering phase function. *Journal of Quant. Spectros. Radiat. Transfer*, 33:391–409, 1985.

[66] R. J. Davies. *Journal of Atmospheric Science*, 35:1712, 1978.

[67] T. Aruga and D. F. Heath. *Journal of Atmospheric Science*, 31:1885, 1974.

[68] J. R. Howell. The Monte Carlo method in radiative heat transfer. *Journal of Heat Transfer*, 120:547–560, 1997.

[69] N. Metropolis and S. Ulam. The Monte Carlo Method. *Journal Am. Statistical Assoc.*, 44(247):335–341, 1949.

[70] J. R. Howell and M. Perlmutter. Monte Carlo solution of thermal transfer through radiant media between gray walls. *Trans. ASME Journal of Heat Transfer*, 86:116–122, February 1964.

[71] J. R. Howell and M. Perlmutter. Monte Carlo solution of radiant heat transfer in a nongray, nonisothermal gas with temperature-dependent properties. *American Institute of Chemical Engineers*, 10(4):562–567, 1964.

[72] Masayoshi Kobiyama, Hiroshi Taniguchi, and Takeshi Saito. The numerical analysis of heat transfer combined with radiation and convection (1st report, the effect of two-dimensional radiative transfer between isothermal parallel plates. *Bulletin of Japan Society of Mechanical Engineers*, 22(167):707–714, May 1979.

[73] R. P. Gupta, T. F. Wall, and J. S. Truelove. Radiative scatter by fly ash in pulverized-coal-fired furnaces: Application of the Monte Carlo method to anisotropic scattering. *International Journal of Heat and Mass Transfer*, 26(11):1649–1660, 1983.

[74] M. Mishkin and G. J. Kowalski. Application of Monte Carlo techniques to the steady-state radiative and conductive heat transfer problem through a participating media. *ASME Paper 83-WA/HT-27*, 1983.

[75] A. Al. Abed and J. F. Sacadura. A Monte Carlo-finite difference method for coupled radiation-conduction heat transfer in semitransparent media. *Trans. ASME Journal of Heat Transfer*, 105:931–933, November 1983.

[76] M. F. Modest. The Monte Carlo method applied to gases with spectral line structure. *Numerical Heat Transfer, Part B*, 22:273–284, 1992.

[77] Jeff T. Farmer and John R. Howell. Monte Carlo solution of radiative heat transfer in a three-dimensional enclosure with an anisotropically scattering ,spectrally dependent, inhomogeneous medium. *Trans. ASME Journal of Heat Transfer*, 203(1):301–309, August 1992.

[78] S. N. Tiwari and J. Liu. Investigation of radiative interaction in laminar flows of nongray gases using Monte Carlo simulation. In *Proceedings of the National Heat Transfer Conference, San Diego, CA, USA*, pages 187–195. ASME, 1992.

[79] H. Taniguchi, K. Kudo, M. Otaka, M. Sumarsono, and M. Obata. Development of a Monte Carlo Method for numerical analysis on radiative energy transfer through non-gray-gas layer. *International Journal for Numerical Methods in Engineering*, 35:883–891, 1992.

[80] J. Liu and S. N. Tiwari. Radiative interactions in chemically reacting compressible nozzle flows using Monte Carlo simulation. In *6th AIAA/ASME Joint Thermophysics and Heat Transfer Conference*, pages 1–13. Colorado Springs CO, 1994.

[81] Jeff T. Farmer and J. R. Howell. Hybrid Monte Carlo/diffusion method for enhanced solution of radiative transfer in optically thick non-gray media. *Radiative Transfer: Current Research, Y. Bayazitoglu et al., eds, ASME, New York*, pages 203–212, 1994.

[82] J. F. Farmer. *Improved Algorithms for Predicting Monte Carlo Analysis of Radiative Heat Transfer in Complex Participating Medium.* PhD thesis, University of Texas at Austin, Austin, TX, 1995.

[83] Subhash C. Mishra and David A. Blank. High to low optical thickness Monte Carlo solutions of the radiative heat transfer problems in 2-D rectangular enclosures with absorbing-emitting-isotropic scattering. In *Proceedings of the International Conference on Advances in Mechanical Engineering*, pages 1657–1668. I.I.Sc. Bangalore, India, December 1995.

[84] Subhash C. Mishra and Manohar Prasad. Monte Carlo prediction of radiative heat transfer in absorbing-emitting-scattering isothermal media in one- and two-dimensional Cartesian enclosures. In *Proceedings of the third ISHMT-ASME Heat Transfer Conference and 14 th National Heat and Mass Transfer Conference, Kanpur, India*, pages 513–516, December 1997.

[85] J. F. Farmer and J. R. Howell. Monte Carlo strategies for radiative transfer in participating media. *Advances in Heat Transfer*, 31:1–97, 1998.

[86] P. Mahanta and Subhash C. Mishra. Generalized Monte Carlo formulations for radiative heat transfer problems in cartesian enclosures with absorbing, emitting and scattering media. In *Proceedings of the fourth ISHMT-ASME Heat Transfer Conference and fifteenth National Heat and Mass Transfer Conference, Pune, India*, pages 659–664, January 2000.

[87] J. R. Howell. *Applications of Monte Carlo to Heat Transfer Problems*, volume 5. Academic Press, New York, 1968.

[88] A. Haji-Sheikh. *Monte Carlo Methods, Handbook of Numerical Heat Transfer*. Wiley Interscience, New York, 1988.

[89] J. R. Howell. Thermal radiation in participating media: The past, the present, and some possible future. *Trans. ASME Journal of Heat Transfer*, 110:1220–1229, November 1988.

[90] W. J. Yang, H. Taniguchi, and K. Kudo. *Radiative Heat Transfer by the Monte Carlo Method*, volume 27. Advances in Heat Transfer, Academic Press, San Diego, 1995.

[91] W. W. Yuen and E. E. Takara. Development of a generalized zonal method for analysis of radiative transfer in absorbing and anisotropically scattering media. *Numerical Heat Transfer, Part B*, 25:75–96, 1994.

[92] H. Taniguchi and A. Mochida. Radiative heat transfer in the mixture of gas and particle with anisotropic scattering effect. In *Proc Pacific Rim Conf and Environmental Control of Combustion processes*, pages 13–31, 1994.

[93] M. F. Modest and K. K. Sikka. The application of the stepwise-gray P_1 approximation to molecular gas-particulate mixtures. *Fundamental of Radiation Heat Transfer*, HTD-160, ASME:97–103, July 1991.

[94] Jeff T. Farmer and John R. Howell. Monte Carlo prediction of radiative heat transfer in inhomogeneous, anisotropic, nongray media. *Journal of Thermophysics and Heat Transfer*, 8(1):133–139, Jan.-March 1994.

[95] Masayoshi Kobiyama. A study on the reduction of computing time of the Monte Carlo method applied to the radiative transfer. *Bulletin of Japan Society of Mechanical Engineers*, 29(255):3000–3006, September 1986.

[96] N. Samsundar, E. M. Sparrow, and R. P. Heinisch. Monte Carlo radiation solutions -effects of energy partitioning and number of rays. *International Journal of Heat and Mass Transfer*, 16:690–694, 1973.

[97] Y. R. Sivathanu and J. P. Gore. A discrete probability function method for the equation of radiative transfer. *Journal of Quant. Spectros. Radiat. Transfer*, 49(3):269–280, 1993.

[98] Y. R. Sivathanu and J. P. Gore. A discrete probability function method for radiation in enclosures and comparison with the Monte Carlo method. In Y. Bayazitoglu et al., editor, *Radiative Heat Transfer: Current Research*, pages 213–218, 1994.

[99] Y. R. Sivathanu and J. P. Gore. Radiative heat transfer inside a cylindrical enclosure with nonparticipating media using a deterministic statistical method. In P. D. Jones, editor, *Proceedings of ASME Heat Transfer Division*, volume 1, pages 145–152, 1996.

[100] H. Taniguchi, K. Kudo, M . Ohtaha A. Kuroda, A. Machida, T. Komatsu, S. Kosaka, and M. Fujisaki. Monte Carlo simulation of non-gray radiation heat transfer on highly parallel computer AP1000. In *Proceedings of 3rd International Symposium on Heat Transfer*. Beijing, October 1992.

[101] W. L. Dunn. Inverse Monte Carlo solutions for radiative transfer in inhomogeneous media. *Journal of Quant. Spectros. Radiat. Transfer*, 29(1):19–26, 1983.

[102] S. Subramaniam and M. P. Menğuç. Solution of inverse radiation problem for inhomogeneous and anisotropically scattering media using a Monte Carlo technique. *International Journal of Heat and Mass Transfer*, 34(1):253–266, 1991.

[103] Donald V. Walters and Richard O. Buckius. Rigorious development for radiation heat transfer in nonhomogeneous absorbing, emitting and scattering media. *International Journal of Heat and Mass Transfer*, 35(12):3323–3333, 1992.

[104] H. C. Hottel and H. S. Cohen. Radiant heat exchange in a gas filled enclosure: Allowance for nonuniformity of gas temperature. *A.I.Ch.E. Journal*, 4:3–14, 1958.

[105] H. C. Hottel and A. F. Sarofim. *Radiative Heat Transfer*. McGraw-Hill, New York, 1967.

[106] James J. Noble. The zone method: Explicit matrix relations for total exchange areas. *International Journal of Heat and Mass Transfer*, 18:261–269, 1975.

[107] F. R. Steward and K. N. Tennankore. Towards a finite difference solution coupled with the zone method for radiative transfer for a cylindrical combustion chamber. *J. Inst. Energy LIII*, page 107, 1979.

[108] A. J. Sistino. Mean beam length and zone method (without and with scattering) for a cylindrical enclosure. *ASME Paper No. 82-HT-3*, 1982.

[109] M. E. Larsen and J. R. Howell. The exchange factor method: An alternative basis for zonal analysis of radiating enclosures. *Journal of Heat Transfer*, 107:936–942, 1985.

[110] D. K. Edwards. Hybrid Monte- Carlo matrix inversion formulation of radiation heat transfer with volume scattering. In *ASME National Heat Transfer conference, Denver, Colorado*, volume 45, pages 273–278. ASME HTD, 1985.

[111] M. H. N. Naraghi and B. T. F. Chung. A unified matrix formulation for the zone method: A stochastic approach. *International Journal of Heat and Mass Transfer*, 28(1):245–251, 1985.

[112] M. H. N. Naraghi and B. T. F. Chung. A stochastic approach for radiative exchange in enclosures with drectional-bidirectional properties. *Trans. ASME Journal of Heat Transfer*, 108:264–270, 1986.

[113] T. F. Smith, K. H. Byun, and M. J. Ford. Heat transfer. volume 2, pages 803–808. Hemisphere, Washington, D. C., 1986.

[114] F. C. Lockwood and N. G. Shah. An improved flux model for calculation of radiation heat transfer in combustion chambers. In *ASME Paper 76-HT-55*, 1976.

[115] H. Khalil, J. K. Shultis, and T. W. Lester. Comparison of three numerical methods for evaluation of radiant energy transfer in scattering and heat generating media. *Numerical Heat Transfer*, 5:235–252, 1982.

[116] A. Schuster. Radiation through a foggy atmosphere. *Astrophysical Journal*, 21:1–22, 1905.

[117] K. Schwarzschild. Equilibrium of Sun's atmosphere. *Astrophysical Journal*, 21:1–22, 1905.

[118] W. Richer and R. Quack. A mathematical model of a low-volatile pulverized flame. In *Proceedingd 8th Int. Heat Transfer in Flames*, volume 2, pages 95–109. N. H. Afgan and J. M. Beer, eds, Washington D. C.: Scriptia Book Co., 1974.

[119] T. M. Lowes, H. Bartelds, M. P. Heamp, S. Michelfelder, and B. E. Pai. Prediction of radiant heat flux distribution. pages 179–190. Scriptia Book Co., Washington D. C., 1974.

[120] S. A. Verma. Radiative heat transfer in pulverized-coal flame. In *Pulverized Coal Combustion and Gasification, Plenum Press, New York*, volume 2, pages 95–109. L. D. Smoot and D. T. Pratt, eds, 1974.

[121] R. G. Siddal and N. Selçuk. Evaluation of a new six-flux model for radiative transfer in rectangular enclosures. *Trans. I. Ch. E.*, 7:163–169, 1979.

[122] S. V. Patankar and D. B. Spalding. A computer model for three-dimensional flow in furnace. In *14 th Symp (Int.) on Combustion*, pages 605–614. The Combustion Institute, 1972.

[123] Christian Sasse, Ronald Koenigsdorff, and Stefan Frank. Evaluation of an improved hybrid six-flux/zone model for radiative transfer in rectangular enclosures. *International Journal of Heat and Mass Transfer*, 38(18):3423–3431, 1995.

[124] M. N. Abramzon and F. N. Lisin. Methods for solving the radiant-transfer equations in cylindrical geometry. *High Tempt.*, 22:95–100, 1984.

[125] N. Selçuk. Evaluation of multidimensional flux models for radiative transfer in combustion chambers-a review. Technical Report 28, AGARD CP-353, 1983.

[126] N. Selçuk. Evaluation of multi-dimensional flux models for radiative transfer in combustors. *Heat and Technology, Calore e tecnologia*, 13(2):73–89, 1995.

[127] C. M. Spuckler and R. Siegel. Two-flux and diffusion methods for radiative transfer in composite layers. *Trans. ASME Journal of Heat Transfer*, 118:218–223, 1996.

[128] A. G. Demarco and F. C. Lockwood. A new flux model for the calculation of radiation in furnaces. *La Rivista du Combustibili*, (5):184, 1975.

[129] F. C. Lockwood and N. G. Shah. Evaluation of an efficient radiation flux model for furnace prediction procedures. In *Proc. 6th Int. Heat Transfer Conf, Paper-EC-6, Torento*, page 33, 1978.

[130] V. Kourganoff. *Basic Methods in Transfer Problems.* Oxford University Press, Oxford, 1952.

[131] J. Higenyi and Y. Bayazitoglu. Differential approximation of radiative heat transfer in a gray medium. *Trans. ASME Journal of Heat Transfer*, 102:719–723, 1980.

[132] J. Higenyi and Y. Bayazitoglu. Radiative transfer of energy in a cylindrical enclosure with heat generation. *AIAA*, 18:723–726, 1980.

[133] R. K. Ahluwalia and K. H. Im. Combined conduction, convection, gas radiation and particle radiation in MHD diffusers. *International Journal of Heat and Mass Transfer*, 24(8):1421–1430, 1981.

[134] Szu-Cheng S. Ou and Liou Kuo-Nan. Generalization of the spherical harmonics method to radiative transfer in multi-dimensional space. *Journal of Quant. Spectros. Radiat. Transfer*, 28(4):271–288, 1982.

[135] A. C. Ratzel III and J. R. Howell. Two-dimensional energy transfer in radiatively participating media with conduction by P_N method. *In Seventh International Heat Transfer Conference, Munichi, Washington, D. C.,Hemisphere*, 2:535–540, 1982a.

[136] A. C. Ratzel III and J. R. Howell. Two-dimensional radiation in absorbing-emitting -scattering media using the P_N approximation. *ASME Paper No. 82-HT-19*, 1982b.

[137] R. M. Cotta, M. Benassi, and C. E. Siewart. The P_N method for radiative transfer problems with reflecting boundary conditions. *Journal of Quant. Spectros. Radiat. Transfer*, 30(6):547–553, 1983.

[138] A. H. Karp and S. Petrack. On the spherical harmonics and discrete ordinates methods for azimuth-dependent intensity calculations. *Journal of Quant. Spectros. Radiat. Transfer*, 30(4):351–356, 1983.

[139] W. H. Wells and J. J. Sidorowich. Computational techniques for radiative transfer by spherical harmonics. *Journal of Quant. Spectros. Radiat. Transfer*, 33:347–363, 1985.

[140] M. P. Menğuç and R. Viskanta. Radiative transfer in three-dimensional rectangular enclosures containing inhomogeneous, anisotropically scattering media. *Journal of Quant. Spectros. Radiat. Transfer*, 33(6):533–549, 1985.

[141] M. P. Menğuç and R. Viskanta. Radiative transfer in axisymmetric, finite cylindrical enclosures. *Trans. ASME Journal of Heat Transfer*, 108:271–276, May 1986.

[142] M. P. Menğuç and R. K. Iyer. Modelling of radiative transfer using multiple spherical harmonics approximations. *Journal of Quant. Spectros. Radiat. Transfer*, 39(6):445–461, 1988.

[143] Tae-kuk Kim and Haeok Lee. Effect of anisotropic scattering on radiative heat transfer in two-dimensional rectangular enclosures. *International Journal of Heat and Mass Transfer*, 31(8):1711–1721, 1988.

[144] J. A. Hariss. Solution of the conduction/radiation problem with linear-anisotropic scattering in an annular medium by the spherical harmonics method. *Trans. ASME Journal of Heat Transfer*, 111:194–197, February 1989.

[145] K. Kamiuto, S. Saito, and K. Ito. Numerical model for combined conductive and radiative heat transfer in annular packed beds. *Numerical Heat Transfer, Part A*, 23:433–443, 1993.

[146] L. C. Hartung and H. A. Hassan. Radiation transport around axisymmetric blunt body vehicles using a modified differential approximation. *Journal of Thermophysics and Heat Transfer*, 7(2):220–227, 1993.

[147] Fengshan Liu, G. S. Garbett, and J. Swithernbank. Effect of anisotropic scattering on radiative heat transfer using the P_1-approximation. *International Journal of Heat and Mass Transfer*, 35(10):2491–2499, 1992.

[148] A. C. Ratzel III and J. R. Howell. Heat transfer by conduction and radiation in one dimensional planar medium using differential approximation. *Trans. ASME Journal of Heat Transfer*, 104:388–391, 1982.

[149] B. G. Carlson and K. D. Lathrop. Transport theory - the method of discrete ordinates. In Greenspan et al., editor, *Computing Methods in Reactor Physics*, pages 269–308. MIT Press, Cambridge, 1973.

[150] D. J. Hyde and J. S. Truelove. The discrete ordinate approximation for radiative heat transfer. Technical Report AERE-R 8502, 1977.

[151] W. A. Fiveland. Discrete-ordinate solutions of the radiative transport equation for rectangular enclosures. *Trans. ASME Journal of Heat Transfer*, 106:699–706, November 1984.

[152] Tae-Kuk Kim. *Radiation and Combined Mode Heat Transfer Analysis in Absorbing, Emitting, and Mie-Anisotropic Scattering Media Using S-N Discrete Ordinate Method*. PhD thesis, University of Minnesota, 1990.

[153] W. A. Fiveland. Discrete ordinate methods for radiative heat transfer in isotropically and anisotropically scattering media. *Trans. ASME Journal of Heat Transfer*, 109:809–812, August 1987.

[154] W. A. Fiveland. Three-dimensional radiative heat transfer solutions by the discrete ordinate method. *Journal of Thermophysics and Heat Transfer*, 2(4):309–316, October 1988.

[155] W. A. Fiveland. The selection of discrete ordinate quadrature sets for anisotropic scattering. In *Fundamentals of Radiation Heat Transfer, ASME HTD*, volume 160, pages 89–96, 1991.

[156] W. A. Fiveland and J. P. Jessee. Comparison of discrete ordinate formulations for radiative heat transfer in multidimensional geometries. *Journal of Thermophysics and Heat Transfer*, 9(1):47–54, 1995.

[157] A. S. Jamaluddin and P. J. Smith. Predicting radiative transfer in rectangular enclosures using the discrete-ordinate method. *Combustion Science and Technology*, 59:321–340, 1988.

[158] A. S. Jamaluddin and W. A. Fiveland. Radiative transfer in multidimensional enclosures with specularly reflecting walls. *Journal of Thermophysics and Heat Transfer*, 6(1):190–192, 1991.

[159] J. S. Truelove. Discrete-ordinate solutions of the radiative transport equation. *Trans. ASME Journal of Heat Transfer*, 109(4):1048–1051, November 1987.

[160] J. S. Truelove. Three-dimensional radiation in absorbing-emitting-scattering media using the discrete-ordinate approximation. *Journal of Quant. Spectros. Radiat. Transfer*, 39(1):27–31, 1988.

[161] R. Vaillon, M. Lallemand, and D. Lemonnier. Radiative heat transfer in orthogonal curvilinear coordinates using the discrete ordinate method. *Journal of Quant. Spectros. Radiat. Transfer*, 55(1):7–17, 1996.

[162] R. Vaillon, M. Lallemand, and D. Lemonnier. Radiative equilibrium in axisymmetric semi-transparent gray shells using the discrete ordinate method. In *Proceedings of the First International Symposium on Radiative Heat Transfer, Kusadasi, Turkey*, August 1995.

[163] A. S. Jamaluddin and P. J. Smith. Discrete-ordinates solution of radiative transfer equation in nonaxisymmetric cylindrical enclosures. *Journal of Thermophysics and Heat Transfer*, 6(2):242–245, 1992.

[164] A. S. Jamaluddin and P. J. Smith. Discrete ordinate solution of radiative heat transfer equation in non-axisymmetric cylindrical enclosures. In *28th National Heat Transfer Conference, HTD-96 ASME*, pages 227–232, 1988.

[165] S. Jendoubi and T-K. Kim. Discrete ordinates solutions for radiatively participating media in a cylindrical enclosure. *Journal of Thermophysics and Heat Transfer*, 7(2):213–219, 1993.

[166] Chih-Yang Wu and Bo-Ting Liou. Discrete-ordinate solutions for radiative transfer in a cylindrical enclosure with fresnel boundaries. *International Journal of Heat and Mass Transfer*, 40:2467–2475, 1997.

[167] Y. Wang and Y. Bayazitoglu. Wavelets and discrete ordinates method in solving one-dimensional nongray radiation problem. *International Journal of Heat and Mass Transfer*, 42:385–393, 1999.

[168] W. A. Fiveland and A. S. Jamaluddin. Three-dimensional spectral radiative heat transfer solutions by the discrete-ordinates method. *Journal of Thermophysics and Heat Transfer*, 5(3):335–339, 1991.

[169] K. D. Lathrop. Ray effects in discrete ordinate equations. *Nuclear Science and Engineering*, 32:357–369, 1968.

[170] J. Pessoa-filho and S. T. Thynell. An approximate solution to radiative transfer in two-dimensional rectangular enclosure. *Trans. ASME Journal of Heat Transfer*, 119:738–745, 1997.

[171] J. C. Chai, H. S. Lee, and S. V. Patankar. Treatment of irregular geometries using a cartesian coordinates finite-volume radiation heat transfer procedure. *Numerical Heat Transfer, Part B*, 26:225–235, 1994.

[172] S. Pasini and L. Castiliano. Numerical experiments on the application of the diamond scheme to sets of discrete directions obtained from a random number generator. In *ASME-HTD*, volume 274, pages 99–104, 1994.

[173] S. T. Thynell and M. N. Özişik. Radiation transfer due to a point source in an isotropically scattering,inhomogeneous solid sphere. *Journal of Quant. Spectros. Radiat. Transfer*, 35(5):349–356, 1986.

[174] S. T. Thynell and M. N. Özişik. Radiation transfer in absorbing, emitting, isotropically scattering, homogeneous cylindrical media. *Journal of Quant. Spectros. Radiat. Transfer*, 38(6):413–426, 1987.

[175] F. Liu, H. A. Becker, and A. Pollard. Spatial diffencing schemes of the discrete-ordinates method. *Numerical Heat Transfer, Part B*, 30:23–43, 1996.

[176] Kyeong-Beom Cheong and Tae-Ho Song. Examination of solution methods for the second-order discrete ordinate formulation. *Numerical Heat Transfer, Part B*, 27:155–173, 1995.

[177] M. Sakami, A. Charete, and V. Le Dez. Application of the discrete ordinate methods to combined conductive and radiative heat transfer in two-dimensional complex geometry. *Journal of Quant. Spectros. Radiat. Transfer*, 56:517–533, 1996.

[178] T. Y. Kim and S. W. Baek. Analysis of combined conductive and radiative heat transfer in a two-dimensional rectangular enclosure using the discrete ordinate method. *International Journal of Heat and Mass Transfer*, 34(9):2265–2273, 1991.

[179] T. K. Lim and H. S. Lee. Scaled isotropic results for two-dimensional anisotropic scattering media. *Journal of Thermophysics and Heat Transfer*, 112:721–727, 1990.

[180] J. Goncalves and P. J. Coelho. Parallelization of the discrete ordinates method. *Numerical Heat Transfer, Part B*, 32:151–173, 1997.

[181] G. D. Raithby and E. H. Chui. A finite volume method for predicting a radiant heat transfer in enclosures with participating media. *Trans. ASME Journal of Heat Transfer*, 112:415–423, May 1990.

[182] G. D. Raithby and G. E. Schneider. In *Handbook of Numerical Heat Transfer*, pages 241–291. John Wiley and Son Inc, 1988.

[183] E. H. Chui, D. Raithby, and P. M. J. Hughes. Prediction of radiative heat transfer in cylindrical enclosures using the finite volume method. *Journal of Thermophysics and Heat Transfer*, 6(4):605–611, 1992.

[184] E. H. Chui and G. D. Raithby. Computation of radiant heat transfer on a nonorthogonal mesh using the finite volume method. *Numerical Heat Transfer, Part B*, 23:269–288, 1993.

[185] M. Y. Kim and S. W. Baek. Prediction of radiative heat transfer in a three-dimensional gas turbine combustor with the finite volume Method. *Trans. Korean Soc. Mech. Eng. (B)*, 20(8):2681–2692, 1996.

[186] J. P. Moder, C. Chai, Parthasarathy, S. Lee, and S. V. Patankar. Nonaxisymmetric radiative transfer in cylindrical enclosures. *Numerical Heat Transfer, Part B*, 30:437–452, 1996.

[187] M. Y. Kim and S. W. Baek. Analysis of radiative transfer in cylindrical enclosures using finite volume method. *Journal of Thermophysics and Heat Transfer*, 11(2):246–252, 1997.

[188] S. W. Baek, Y. Kim, and J. S. Kim. Nonorthogonal finite-volume solutions of radiative heat transfer in a three-dimensional enclosure. *Numerical Heat Transfer, Part B*, 34:419–437, 1998.

[189] J. Y. Murthy and S. R. Mathur. Radiative heat transfer in axisymmetric geometries using an unstructured finite-volume method. *Numerical Heat Transfer, Part B*, 33:397–416, 1998.

[190] J. Y. Murthy and S. R. Mathur. Finite volume method for radiative heat transfer using unstructured Meshes. *Journal of Thermophysics and Heat Transfer*, 12(3):313–321, 1998.

[191] S. R. Mathur and J. Y. Murthy. Radiative heat transfer in periodic geometries using a finite volume scheme. *Journal of Heat Transfer*, 121:357–364, 1999.

[192] S. R. Mathur and J. Y. Murthy. Radiative heat transfer in periodic geometries using a finite volume scheme. *Journal of Heat Transfer*, 121:357–364, 1999.

[193] G. D. Raithby. Discussion of the finite volume method for radiation and its application using 3-D unstructured meshes. *Numerical Heat Transfer, Part B*, 35:389–405, 1999.

[194] T. M. Shih. *Numerical Heat Transfer*. Series in Computational Methods in Mechanics and Thermal Sciences. Hemisphere Publishing Corporation, New York, 1984.

[195] R. H. Gallagher. *Finite Element Analysis, Fundamentals*. Prentice-Hall, Englewood Cliffs, N. J., 1975.

[196] K. H. Huebner. *The Finite Element Method For Engineers*. Wiley, New York, 1975.

[197] J. N. Reddy and V. D. Murty. Finite element solution of integral equations arising in radiative heat transfer and laminar boundary layer theory. *Numerical Heat Transfer*, 1:389–401, 1978.

[198] S. P. Burns, J. R. Howell, and D. E. Klein. Application of the finite element method to the solution of combined natural convection -radiation in a horizontal cylindrical annulus. In *Numerical Methods in Thermal Problems, R. W. Lewis and P. Durbetaki, eds*, volume lX, pages 327–338. Pineridge Press, Swansea, U. K., 1995.

[199] R. Fernandes, J. Francis, and J. N. Reddy. A finite element approach to combined conductive and radiation heat transfer in a planar medium. In *Heat Transfer and Thermal Control*, pages 93–109. AIAA, 1981.

[200] S. T. Wu, R. E. Furguson, and L. L. Altgilbers. Application of finite element techniques to the interaction of conduction and radiation in participating media. In *Heat Transfer and Thermal Control, Progress in Aeronautics and Astronautics*, volume 78, pages 61–92, New York, 1981.

[201] R. Fernandes and J. Francis. Combined conductive and radiative heat transfer in an absorbing, emitting, and scattering cylindrical medium. *Trans. ASME Journal of Heat Transfer*, 104:594–601, November 1982.

[202] M. M. Razzaque, D. E. Klein, and J. R. Howell. Finite element solution of radiative heat tansfer in a two-dimensional rectangular enclosure with gray participating media. *Journal of Heat Transfer*, 105(4):933–935, 1983.

[203] W. J. Minkowyez and A. Haji-Seikh. The Sparrow-Galerkin solution of radiation exchange and transition to finite element. *International Journal of Heat and Mass Transfer*, 42:1353–1362, 1999.

[204] W. Ritz. Über eine neue methode zur lösung gewisser variationsprobeme der mathematischen physik. *J. Reine Angew. Math*, 135:1–61, 1908.

[205] Z. Tan. Radiative heat transfer in multidimensional emitting, absorbing, and anisotropic scattering media: Mathematical formulation and numerical method. *Journal of Heat Transfer*, 111:141–147, 1989.

[206] M. M. Razzaque, J. R. Howell, and D. E. Klein. Coupled radiative and conductive heat transfer in a two- dimensional enclosure with gray

participating media using finite elements. *Trans. ASME Journal of Heat Transfer*, 106(3):613–619, 1984.

[207] C. N. Sokman and M. M. Razzaque. Finite element analysis of conduction radiation heat transfer in an enclosure with heat flux boundary conditions. In *Radiation, Phase Change Heat Transfer, and Thermal Systems*, volume 81, pages 17–23. ASME HTD, 1987.

[208] L. R. Utreja and T. J. Chung. Combined convection-conduction-radiation boundary layer flows using optimal control penalty finite element. *Journal of Heat Transfer*, 111(2):433–437, 1989.

[209] T. J. Chung and J. Y. Kim. Two-dimensional, combined-mode heat transfer by conduction , convection, and radiation in emitting, absorbing, and scattering media- solution by finite elements. *Trans. ASME Journal of Heat Transfer*, 106:448–452, 1984.

[210] S. Maruyama and T. Aihara. Radiative heat transfer of arbitrary 3-D participating media and surfaces with non-participating media by a generalized numerical method REM^2. In *Radiative Transfer-1, First International Symp. on Radiative Heat Transfer, Kusadasi, Turkey*, pages 153–167. Ed. M. P. Menğuç, Begell House, New York, 1996.

[211] S. Maruyama and T. Aihara. Radiation heat transfer of arbitrary three-dimensional absorbing, emitting and scattering media and specular and diffuse surfaces. *Journal of Heat Transfer*, 119:129–136, 1997.

[212] Shigenao Maruyama and Toshio Aihara. Radiative heat transfer of a Czochralski crystal growth furnace with arbitrary specular and diffuse surfaces. *International Journal of Heat and Mass Transfer*, 37(12):1723–1731, 1994.

[213] H. Hayasaka, K. Kudo, H. Taniguchi, Nakamachi, Omori, and T. Katayama. Radiative heat transfer analysis by the radiative heat ray method. *Trans. ASME Journal of Heat Transfer*, 52:1734–1740, 1986.

[214] S. Maruyama and Z. Guo. Radiative heat transfer in arbitrary configurations with nongray absorbing, emitting, and anisotropic scattering media. *Trans. ASME Journal of Heat Transfer*, 121:722–726, 1999.

[215] N. G. Shah. *New Method of Computation of Radiation Heat Transfer in Combustion Chambers.* PhD thesis, Imperial College, University of London, England, 1979.

[216] F.C. Lockwood and N. G. Shah. A new radiation solution method for incorporation in general combustion prediction procedures. In *Proceedings of the Eighteenth International Symposium on Combustion*, pages 1405–1414. The Combustion Institute, Pittsburg, PA, 1981.

[217] M. Fairweather, W. P. Jones, and R. P. Lindstedt. Predictions of radiative transfer from a turbulent reacting jet in a cross-wind. *Combustion and Flame*, 89:45–63, 1992.

[218] J. Y. Murthy and D. Choudhury. Computation of participating radiation in complex geometries. In *28th National Heat Transfer Conference, San Diego, CA, USA*, pages 153–160. ASME, Heat Transfer Div, 1992.

[219] P. S. Cumber. Application of adaptive quadrature to fire radiating modeling. *Trans. ASME Journal of Heat Transfer*, 121:203–205, 1999.

[220] P. S. Cumber, M. Fairweather, and H. S. Ledin. Application of wide band radiation models to non-homogeneous combustion systems. *International Journal of Heat and Mass Transfer*, 41(11):1573–1584, 1998.

[221] P. J. Novo, P. J. Coelho, and M. G. Carvalho. Parallezation of the discrete transfer method. *Numerical Heat Transfer, Part B*, 35:137–161, 1999.

[222] P. J. Coelho and M. G. Carvalho. A conservative formulation of the discrete transfer method. *Trans. ASME Journal of Heat Transfer*, 119:118–128, 1997.

[223] P. J. Coelho, J. M. Goncalves, M. G. Carvalho, and D. N. Trivic. Modelling of radiative heat transfer in enclosures with obstacles. *International Journal of Heat and Mass Transfer*, 41(4-5):745–756, 1998.

[224] P. S. Cumber. Improvements to the discrete transfer method of calculating radiative heat transfer. *International Journal of Heat and Mass Transfer*, 38(12):2251–2258, 1995.

[225] Z. Tan and J. R. Howell. New numerical method for radiation heat transfer in nonhomogeneous participating media. *Journal of Thermophysics and Heat Transfer*, 4(4):419–424, 1990.

[226] Pei-feng Hsu, Z. Tan, and J. R. Howell. Radiative transfer by the YIX method in nonhomogeneous scattering, and nongray media. *Journal of Thermophysics and Heat Transfer*, 7(3):487–495, July-Sept. 1993.

[227] Pei-feng Hsu and Z. Tan. Radiative and combined-mode heat transfer within L-shaped nonhomogeneous and nongray participating media. *Numerical Heat Transfer, Part A*, 31:819–835, 1997.

[228] J. C. Henson and W. M. G. Malalasekara. Comparison of the discrete transfer and Monte Carlo methods for radiative heat transfer in three-dimensional nonhomogeneous scattering media. *Numerical Heat Transfer, Part A*, 32:19–36, 1997.

[229] Pei-feng Hsu and J. T. Farmer. Benchmark solutions of radiative heat transfer within nonhomogeneous participating media using the Monte Carlo method. *Journal of Heat Transfer*, 119:185–188, 1997.

[230] P. F. Hsu, Z. M. Tan, S. H. Wu, and C. Y. Wu. Radiative heat transfer in finite cylindrical homogeneous and nonhomogeneous scattering media exposed to collimated radiation. *Numerical Heat Transfer, Part A*, 35:655–679, 1999.

[231] H. Taniguchi, Yang, W. J., Kudo, K., H. Hayasaka, M. Oguma, M. Kusama, I. Nakamachi, and N. Okigani. Heat transfer - 1986. vol-

ume 2, pages 757–762. Hemisphere Publishing Cor., Washington, D. C., 1986.

[232] T. M. Shih and Y. N. Chen. A discretized-intensity method proposed for two-dimensional systems enclosing radiative and conductive media. *Numerical Heat Transfer*, 6:117–134, 1983.

[233] T. M. Shih and A. L. Ren. Combined convective and radiative recirculating flows in enclosures. *Numerical Heat Transfer*, 8:149–167, 1985.

[234] T. M. Shih and A. L. Ren. Combined convective and radiative recirculating flows in enclosures. *Natural Convection in Enclosures -HTD*, 26:49–57, 1983.

[235] David A. Blank. The Cartesian collapsed-dimension method for use in numerical 2-D radiative calculations in absorbing-emitting media. *International Journal for Numerical Methods in Engineering*, 37:3023–3036, 1994.

[236] Subhash C. Mishra. *A Novel Computational Approach for the Solution of Radiative Heat Transfer Problems in Participating Media*. PhD thesis, IIT Kanpur, India, 1997.

[237] David A. Blank and Subhash C. Mishra. Use of the 2-D collapsed dimension method in absorbing-emitting media with isotropic scattering. In *Proceedings of the First International Symposium on Radiative Heat Transfer, Kusadasi, Turkey*, pages 138–151, August 1995.

[238] David A. Blank and Subhash C. Mishra. Use of the 2-D collapsed dimension method in gray enclosures with absorbing-emitting-isotropic scattering media in radiative equilibrium. *Numerical Heat Transfer: Part B*, 30(4):469–481, 1996.

[239] Subhash C. Mishra and Manohar Prasad. Radiative heat transfer in absorbing-emitting-scattering gray media inside 1-D cartesian enclosure using collapsed dimension method. *International Journal of Heat and Mass Transfer*, 1998 (under review).

[240] David A. Blank and Subhash C. Mishra. 2-D collapsed dimension method for absorbing-emitting media with linear anisotropic scattering. In *Proceedings of the 1996 National Heat Transfer Conference, Houstan, Texas*, August 1996.

[241] R. W. Preisendorfer. *Radiative Tansfer Theory On Discrete Spaces*. Pergamon Press, New York, 1965.

[242] E. G. Harris and A. Simon. Physics fluid. 3, 1960.

[243] D. H. Sampson. *Radiative Contributions to Energy and Momentum Transport in a Gas*. Interscience Publishers, New York, 1965.

[244] W. G. Vincenti and Jr C. H. Kruger. *Introduction to Physical Gas Dynamics*. Wiley, New York, 1965.

[245] Richard N. Thomas. *Some Aspects of Nonequilibrium Thermodynamics in the Presence of a Radiation Field*. University of Colorado Press, Boulder, 1965.

[246] C. L. Tien and B. L. Drolen. Thermal radiation in particulate media with dependent and independent scattering. In *Annual Review of Numerical Fluid Mechanics and Heat Transfer*, volume 1, pages 1–32. Hemisphere, New York, 1987.

[247] M. Perlmutter and J. R. Howell. Radiant heat transfer through a gray gas between concentric cylinders using Monte Carlo. *Trans. ASME Journal of Heat Transfer*, pages 169–179, May 1964.

[248] R. Viskanta. Heat transfer by conduction and radiation in absorbing and Scattering Materials. *Trans. ASME Journal of Heat Transfer*, pages 143–150, February 1965.

[249] P. Talukdar and Subhash C. Mishra. Analysis of conduction-radiation problem in absorbing-emitting media using collapsed dimension method: Paper no. NHTC 2000-12129. In *34th National Heat Transfer Conference Pittsburgh, PA, USA*, August 2000.

[250] W. W. Yuen and L. W. Wong. Heat transfer by conduction and radiation in a one-dimensional absorbing, emitting and anisotropically-scattering medium. *Trans. ASME Journal of Heat Transfer*, 102:303–307, May 1980.

[251] W. M. G. Malalasekara and E. H. James. Calculation of radiative heat transfer in three-dimensional complex geometries. In *Proceedings 30th National Heat Transfer Conference, Portland, OR, ASME-HTD*, volume 315, pages 53–61, 1995.

[252] J. Chai, G. Parthasarathy, and H. Lee. A finite volume radiation heat transfer procedure for irregular geometries. In *AIAA Paper 94-2095*, June 1993.

[253] M. F. Modest and D. S. Stevens. Two-dimensional radiative equilibrium of a gray medium between concentric cylinders. *Journal of Quant. Spectros. Radiat. Transfer*, 19:353–365, 1978.

[254] A. S. Jamaluddin and P. J. Smith. Predicting radiative transfer in axisymmetric cylindrical enclosures using the discrete-ordinate method. *Combustion Science and Technology*, 62:173–186, 1988.

[255] E. H. Chui. *Modelling of Radiative Heat Transfer in Participating media by the Finite Volume Method.* PhD thesis, University of Waterloo, Onterio, Canada, 1990.

[256] S. W. Baek and M. Y. Kim. Modification of the discrete-ordinate method in an axisymmetric cylindrical geometry. *Numerical Heat Transfer, Part B*, 31:313–326, 1997.

[257] V. S. Arpaci. Effects of thermal radiation on the laminar free convection from a heated vertical plate. *International Journal of Heat and Mass Transfer*, 11:871–881, 1968.

[258] R. D. Cess. The interaction of thermal radiation with free convection heat transfer. *International Journal of Heat and Mass Transfer*, 9:1269–1277, 1966.

[259] E. H. Cheng and M. N. Özişik. Radiation with free convection in an absorbing, emitting and scattering medium. *International Journal of Heat and Mass Transfer*, 15:1243–1252, 1972.

[260] T. C. Chawla and S. H. Chan. Combined radiation convection in thermally developing Poiseuille flow with scattering. *Trans. ASME Journal of Heat Transfer*, 102:297–307, 1980.

[261] L. C. Chang, K. T. Yang, and J. R. Lloyd. Radiation-natural convection interactions in two-dimensional complex enclosures. *Trans. ASME Journal of Heat Transfer*, 105:89–95, 1983.

[262] Z. Tan and J. R. Howell. Combined radiation and natural convection in a two-dimensional participating square medium. *International Journal of Heat and Mass Transfer*, 32(3):785–793, 1991.

[263] M. N. Borjini, C. Mbow, and M. Daguenet. Numerical analysis of the effect of radiation on laminar steady natural convection in a two-dimensional participating medium between two horizontal confocal elliptical cylinders. *Numerical Heat Transfer, Part A*, 35:467–494, 1999.

[264] C. K. Krishnaprakas, K. Badari Narayana, and P. Dutta. Interaction of radiation with natural convection. *Journal of Thermophysics and Heat Transfer*, 13(3):387–390, 1999.

[265] M. A. Hossain, M. A. Alim, and D. A. S. Rees. Effect of radiation on free convection from a porous vertical plate. *International Journal of Heat and Mass Transfer*, 42:181–191, 1999.

[266] S. W. Baek, M. J. Yu, and T. Y. Kim. Thermally developing Poiseuille flow affected by radiation. *Numerical Heat Transfer, Part A*, 35:681–694, 1999.

[267] Y. Yamada. Combined radiation and free convection heat transfer in a vertical channel with arbitrary wall emissivities. *International Journal of Heat and Mass Transfer*, 31(2):429–440, 1988.

[268] K. A. Yih. Effect of radiation on natural convection about a truncated cone. *International Journal of Heat and Mass Transfer*, 42:4299–4305, 1999.

[269] Y. Yuner and M. N. Özişik. Simultaneous radiation and forced convection in themally developing turbulent flow through a parallel plate channel. *Trans. ASME Journal of Heat Transfer*, 108:985–988, 1986.

[270] W. M. Yan and H. Y. Li. Radiation effects on laminar mixed convection in an inclined square duct. *Trans. ASME Journal of Heat Transfer*, 121:194–200, 1999.

[271] A. Yucel, S. Acharya, and M. L. Williams. Natural convection and radiation in a square enclosure. *Numerical Heat Transfer, Part A*, 15:261–278, 1989.

[272] S. Desoto. Coupled radiation, conduction and convection in entrance region flow. *International Journal of Heat and Mass Transfer*, 11:39–53, 1968.

[273] D. M. Kim and R. Viskanta. Effect of wall conduction and radiation on natural convection in a rectangular cavity. *Numerical Heat Transfer*, 7:449–470, 1984.

[274] David A. Blank. Conjugate conduction-convection heat transfer for the valve flow-field region of four stroke piston engines. *Numerical Heat Transfer, Part A*, 18:283–308, 1990.

[275] R. Viskanta and R. J. Grosh. Heat transfer by simultanous conduction and radiation in an absorbing medium. *Trans. ASME Journal of Heat Transfer*, 84:63–72, 1962.

[276] W. W. Yuen and E. E. Takara. Analysis of combined conductive-radiative heat transfer in a two-dimensional rectangular enclosure with gray medium. *Trans. ASME Journal of Heat Transfer*, 110(2):468–474, 1988.

[277] J. A. Harris. Solution of the conduction/radiation problem with linear-anisotropic scattering in an annular medium by the spherical harmonics method. *Trans. ASME Journal of Heat Transfer*, 111:194–203, 1988.

[278] T. K. Kim and T. F. Smith. Radiative and conductive transfer for a real gas in a cylindrical enclosure with gray walls. *International Journal of Heat and Mass Transfer*, 28(12):2269–2277, 1985.

[279] H. Reiss. *Radiative Transfer in Nontransparent Dispersed Media.* Springler-Verlag, Berlin, 1988.

[280] W. H. Sutton. A short time solution for coupled conduction and radiation in a participating slab geometry. In *ASME Paper No. 84-HT-34*, 1984.

[281] S. W. Baek and T. Y. Kim. The conductive and radiative heat transfer in rectangular enclosure using the discrete ordinate method, 1990.

[282] C. K. Krishnaprakash, K. Badarinarayana, and P. Dutta. Coupled conduction and radiation heat transfer in a gray anisotropically scattering planar medium with reflecting boundaries. In *Proceedings of the fourth ISHMT-ASME Heat and Mass Transfer Conference and Fifteenth National Heat and Mass Transfer Conference, Pune, India*, pages 647–652. Tata McGraw-Hill Publishing Company Limited, New Delhi, January 2000.

[283] C. C. Lii and M. N. Özişik. Transient radiation and conduction in an absorbing, emitting, scattering slab with reflective boundaries. *International Journal of Heat and Mass Transfer*, 15:1175–1179, 1972.

[284] C. H. Ho and M. N. Özişik. Combined conduction and radiation in a two-dimensional rectangular enclosure. *Numerical Heat Transfer*, 13:229–239, 1988.

[285] J. B. Bergquam and R. A. Seban. Heat transfer by conduction and radiation in absorbing and scattering materials. *Trans. ASME Journal of Heat Transfer*, pages 236–238, May 1971.

[286] Y. Chang and R. S. Smith. Steady and transient heat transfer by radiation and conduction in a medium bounded by two coaxial cylindrical surfaces. *International Journal of Heat and Mass Transfer*, 13:69–80, 1970.

[287] G. L. Stephens. Radiative transfer in spatially heterogeneous, two-dimensional, anisotropic scattering media. *Journal of Quant. Spectros. Radiat. Transfer*, 36:51–67, 1986.

[288] G. Parthasarathy, J. C. Chai, and S. V. Patankar. A simple approach to non-gray gas modelling. *Numerical Heat Transfer, Part B*, 29:113–123, 1996.

[289] J. A. Menart, H. S. Lee, and Tae Kuk Kim. Discrete ordinates solutions of nongray radiative transfer with diffusely reflecting walls. *Trans. ASME Journal of Heat Transfer*, 115:184–193, February 1993.

[290] G. N. Schenker and B. Keller. Line-by-line calculations of the absorption of infrared radiation by water vapor in a box-shaped enclosure filled with humid air. *International Journal of Heat and Mass Transfer*, 38(17):3127–3134, 1995.

[291] A. B. De Miranda and J. F. Sakadura. An alternative formulation of the $S-N$ discrete ordinates for predicting radiative transfer in nongray gases. *Trans. ASME Journal of Heat Transfer*, 118:650–653, August 1996.

[292] Z. Yan and G. Holmstedt. Fast, narrow-band computer model for radiation calculations. *Numerical Heat Transfer, Part B*, 31:61–71, 1997.

[293] S. Tabanfar and M. F. Modest. Radiative heat transfer in a cylindrical mixture of non-gray particulates and molecular gases. *Journal of Quant. Spectros. Radiat. Transfer*, 30(6):555–570, 1983.

[294] S. T. Thynell. Effect of linear-anisotropic scattering on spectral emission from cylindrical plume. *Journal of Thermophysics and Heat Transfer*, 6(2):224–231, 1992.

[295] S. S. Manohar, A. K. Kulkarni, and S. T. Thynell. In-depth absorption of externally incident radiation in nongray media. *Trans. ASME Journal of Heat Transfer*, 117:146–151, March 1995.

[296] M. N. Özişik and S. M. Shouman. Radiative transfer in an isotropically scattering two-region slab with reflecting boundaries. *Journal of Quant. Spectros. Radiat. Transfer*, 26:1–9, 1981.

[297] K. Stamnes and P. Conklin. A new multi-layer discrete ordinate approach to radiative transfer in vertically inhomogeneous atmospheres. *Journal of Quant. Spectros. Radiat. Transfer*, 31(3):273–282, 1984.

[298] W. H. Sutton and R. Kamath. Participating radiative heat transfer in a three dimensional rectangular medium with layered properties. *In Proceedings of the 1986 joint AIAA/ASME Thermophysics and Heat Transfer Conference, Boston, M. A., ASME Paper No. 86-HT-25*, 1986.

[299] J. M. Zhang and W. H. Sutton. Multidimensional radiative tansfer in absorbing, emitting, and linearly anisotropic scattering cylindrical medium with space-dependent properties. *Journal of Quant. Spectros. Radiat. Transfer*, 52(6):791–808, 1994.

[300] P.-F. Hsu, W. D. Evans, and J. R. Howell. Experimental and numerical study of premixed combustion within nonhomogeneous prous ceramics. *Combustion Science and Technology*, 90:149–172, 1993.

[301] G. Flamant, T. Menigault, and D. Schwander. Combined heat transfer in a semitransparent multilayer packed bed. *Journal of Heat Transfer*, 110:463–467, 1988.

[302] D. A. Kaminski. Coupled convection and radiation in a two-layer, porous, volumetric solar collector. In *Proceedings ASME Winter Annual Meeting, ASME-HTD*, volume 151, pages 47–53, 1990.

[303] D. K. Edwards. Molecular gas band radiation. *Advances in Heat Transfer, Academic Press, New York*, 12:115–193, 1976.

[304] R. D. Cess, P. Mighdoll, and S. N. Tiwari. Infrared radiative heat transfer in nongray gases. *International Journal of Heat and Mass Transfer*, 10:1521–1532, 1967.

[305] R. O. Buckius. The effect of molecular gas absorption on radiative heat transfer with scattering. *Journal of Heat Transfer*, 104:580–586, 1982.

[306] A. Soufiani and J. Taine. Experimental and theoretical studies of combined radiative and convective transfer in CO_2 and H_2O laminar flows. *International Journal of Heat and Mass Transfer*, 32(3):477–486, 1989.

[307] M. F. Modest. Radiative heat transfer in a plane-layer mixture of nongray particulates and molecular gases. 26(6):523–533, 1981.

[308] W. W. Yuen and D. J. Rasky. Application of the P_1 approximation of radiative heat transfer in a non-gray medium. *Journal of Heat Transfer*, 103:182–183, 1981.

[309] L. Pierrot, A. Soufiani, and J. Taine. Accuracy of various gas ir radiative property models applied to radiative transfer in planar medium. In *First International Symposium on Radiative Heat Transfer, Kusadasi, Turkey*, August 1995.

[310] A. Soufiani and J. Taine. Application of statistical narrow-band model to coupled radiation and convection at high temperature. *International Journal of Heat and Mass Transfer*, 30(3):437–447, 1987.

[311] M. Abramowitz and I. A. Stegun. *Handbook of Mathematical Functions*. Dover Publications, Inc, New York, ninth edition edition, 1972.

Appendix A

OTC Results for 1-D Cartesian Enclosure under Radiative Equilibrium situation

Regressed equations of OTC [236]

Expression of the optical thickness coefficient, η, for the case of absorbing, emitting, and isotropically scattering media ($a_1\omega = 0.0$) at radiative equilibrium, $0.0001 \leq \tau_L \leq 5.0$.

$$\eta = \begin{cases} 1.27276 - 1.22505\,\tau_L + 23.6226\,\tau_L^2 - 136.935\,\tau_L^3 \\ - 22.2416\,\tau_L^4 \\ \qquad\qquad \text{for } 0.0001 \leq \tau_L \leq 0.1 \\ 1.25684 - 0.108915\,\tau_L + 0.075431\,\tau_L^2 - 0.028079\,\tau_L^3 \\ + 0.005164\,\tau_L^4 - 0.000363\,\tau_L^5 \\ \qquad\qquad \text{for } 0.1 < \tau_L \leq 5.0 \end{cases} \tag{A1.1}$$

Expression of the optical thickness coefficient, η, for absorbing, emitting and, forward scattering ($0.0 \leq (a_1\omega) \leq +1$) media at radiative equilibrium, $0.0001 \leq \tau_L \leq 5.0$.

$$\eta = \begin{cases} 1.27388 - 2.22853\,\tau_L + 0.192067\,(a_1\omega) - 0.00337\,\tau_L^2 \\ + 0.107663\,(a_1\omega)^2 - 0.421894\,\tau_L(a_1\omega) - 0.000004\,\tau_L^3 \\ - 0.019215\,(a_1\omega)^3 - 0.000633\,\tau_L^2(a_1\omega) + 0.098177\,\tau_L(a_1\omega)^2 \\ + 0.052034\,(a_1\omega)^4 \\ \qquad\qquad \text{for } 0.0001 \leq \tau_L \leq 0.001 \end{cases} \tag{A1.2}$$

Equation (A1.2) continued on next page

Equation (A1.2) continued from previous page

$$\eta = \begin{cases} 1.27122 - 0.858938\,\tau_L + 0.186669\,(a_1\omega) + 9.91455\,\tau_L^2 \\ + 0.121449\,(a_1\omega)^2 + 0.287198\,\tau_L(a_1\omega) + 0.645137\,\tau_L^3 \\ - 0.039495\,(a_1\omega)^3 + 0.916318\,\tau_L^2(a_1\omega) - 0.349831\,\tau_L(a_1\omega)^2 \\ + 0.034\,\tau_L^4 + 0.061678\,(a_1\omega)^4 + 0.059332\,\tau_L^3(a_1\omega) \\ - 1.60615\,\tau_L^2(a_1\omega)^2 + 0.751796\,\tau_L(a_1\omega)^3 \\ \qquad\qquad \text{for } 0.001 < \tau_L \le 0.05 \\ \\ 0.914212 + 0.349684\,e^{\tau_L} + 0.236812\,e^{(a_1\omega)} - 0.095366\,e^{2\tau_L} \\ - 0.120884\,e^{2(a_1\omega)} + 0.034325\,e^{(\tau_L+a_1\omega)} - 0.255125\,e^{3\tau_L} \\ + 0.001043\,e^{3(a_1\omega)} - 0.0066423\,e^{(2\tau_L+a_1\omega)}\,0.161457\,e^{(\tau_L+2(a_1\omega))} \\ + 0.127448\,e^{4\tau_L} - 0.000276\,e^{4(a_1\omega)} + 0.033147\,e^{(3\tau_L+a_1\omega)} \\ - 0.714446\,e^{2(\tau_L+(a_1\omega))} + 0.0073869\,e^{(\tau_L+3(a_1\omega))} \\ \qquad\qquad \text{for } 0.05 < \tau_L \le 0.3 \\ \\ 0.637025 + 0.428143\,e^{\tau_L} + 0.222816\,e^{(a_1\omega)} + 0.082986\,e^{2\tau_L} \\ - 0.0546623\,e^{2(a_1\omega)} + 0.0747083\,e^{(\tau_L+a_1\omega)} - 0.236335\,e^{3\tau_L} \\ + 0.009714\,e^{3(a_1\omega)} - 0.074199\,e^{(2\tau_L+a_1\omega)} + 0.0.032067\,e^{(\tau_L+2(a_1\omega))} \\ - 0.066945\,e^{4\tau_L} - 0.00006\,e^{4(a_1\omega)} + 0.019123\,e^{(3\tau_L+a_1\omega)} \\ - 0.008603\,e^{2(\tau_L+(a_1\omega))} - 0.004242\,e^{(\tau_L+3(a_1\omega))} \\ \qquad\qquad \text{for } 0.3 < \tau_L \le 0.6 \\ \\ 0.8229324 + 0.346256\,e^{\tau_L} + 0.232337\,e^{(a_1\omega)} - 0.234194\,e^{2\tau_L} \\ - 0.018415\,e^{2(a_1\omega)} - 0.007966\,e^{(\tau_L+a_1\omega)} + 0.066665\,e^{3\tau_L} \\ + 0.008110\,e^{3(a_1\omega)} + 0.001464\,e^{(2\tau_L+a_1\omega)} - 0.001593\,e^{(\tau_L+2(a_1\omega))} \\ - 0.006939\,e^{4\tau_L} \\ \qquad\qquad \text{for } 0.6 \le \tau_L \le 1.1 \\ \\ 0.4211904 + 0.47735\,e^{\tau_L} + 0.227627\,e^{(a_1\omega)} - 0.131372\,e^{2\tau_L} \\ - 0.016862\,e^{2(a_1\omega)} - 0.00692\,e^{(\tau_L+a_1\omega)} + 0.011927\,e^{3\tau_L} \\ + 0.007450\,e^{3(a_1\omega)} + 0.000887\,e^{(2\tau_L+a_1\omega)} - 0.000869\,e^{(\tau_L+2(a_1\omega))} \\ \qquad\qquad \text{for } 1.1 < \tau_L \le 1.4 \end{cases} \qquad (A1.2)$$

Equation (A1.2) continued on next page

Equation (A1.2) continued from previous page

$$\eta = \begin{cases} 1.1226 + 0.226783\,\tau_L + 0.208173\,(a_1\omega) - 0.235362\,\tau_L^2 \\ + 0.172638\,(a_1\omega)^2 - 0.024636\,\tau_L(a_1\omega) + 0.100116\,\tau_L^3 \\ - 0.064356\,(a_1\omega)^3 + 0.007054\,\tau_L^2(a_1\omega) - 0.016186\,\tau_L(a_1\omega)^2 \\ - 0.015509\,\tau_L^4 + 0.115300\,(a_1\omega)^4 - 0.000869\,\tau_L^3(a_1\omega) \\ + 0.006016\,\tau_L^2(a_1\omega)^2 - 0.010091\,\tau_L(a_1\omega)^3 \\ \qquad\qquad \text{for } 1.4 < \tau_L \le 1.9 \\ \\ 0.000006 + 0.000043\,e^{\tau_L} + 0.003820\,e^{(a_1\omega)} + 0.000322\,e^{2\tau_L} \\ - 0.020365\,e^{2(a_1\omega)} + 0.028226\,e^{(\tau_L + a_1\omega)} + 0.002403\,e^{3\tau_L} \\ + 0.007403\,e^{3(a_1\omega)} \\ \qquad\qquad \text{for } 1.9 < \tau_L \le 2.0 \\ \\ 0.028369 + 0.571812\,\tau_L + 0.094233\,(a_1\omega) + 0.101823\,\tau_L^2 \\ - 0.077326\,(a_1\omega)^2 + 0.123788\,\tau_L(a_1\omega) + 0.131043\,\tau_L^3 \\ + 0.174435\,(a_1\omega)^3 - 0.025907\,\tau_L^2(a_1\omega) + 0.0133349\,\tau_L(a_1\omega)^2 \\ - 0.042919\,\tau_L^4 \\ \qquad\qquad \text{for } 2.0 < \tau_L \le 3.0 \\ \\ 0.00206328 + 0.006882\,\tau_L + 0.003875\,(a_1\omega) + 0.020265\,\tau_L^2 \\ + 0.013869\,(a_1\omega)^2 + 0.011363\,\tau_L(a_1\omega) + 0.0441790\,\tau_L^3 \\ + 0.029304\,(a_1\omega)^3 + 0.024815\,\tau_L^2(a_1\omega) + 0.030658\,\tau_L(a_1\omega)^2 \\ - 0.007814\,\tau_L^4 + 0.089411\,(a_1\omega)^4 - 0.004000\,\tau_L^3(a_1\omega) \\ - 0.001477\,\tau_L^2(a_1\omega)^2 - 0.013172\,\tau_L(a_1\omega)^3 \\ \qquad\qquad \text{for } 3.0 < \tau_L \le 5.0 \end{cases} \tag{A1.2}$$

Expression of the optical thickness coefficient, η, for absorbing, emitting, and backward scattering ($-1.0 \le (a_1\omega) \le 0.0$) media at radiative equilibrium, $0.0001 \le \tau_L \le 5.0$.

$$\eta = \begin{cases} 0.8956717 + 0.549960\,e^{\tau_L} + 0.617736\,e^{(a_1\omega)} + 0.203833\,e^{2\tau_L} \\ + 0.165633\,e^{2(a_1\omega)} + 0.124876\,e^{(\tau_L + a_1\omega)} - 0.143041\,e^{3\tau_L} \\ + 0.046864\,e^{3(a_1\omega)} - 0.368914\,e^{(2\tau_L + a_1\omega)} - 0.337473\,e^{(\tau_L + 2(a_1\omega))} \\ - 0.490442\,e^{4\tau_L} + 0.009614\,e^{4(a_1\omega)} \\ \qquad\qquad \text{for } 0.0001 < \tau_L \le 0.001 \end{cases} \tag{A1.3}$$

Equation (A1.3) continued on next page

Equation (A1.3) continued from previous page

$$
\eta = \begin{cases}
1.27039 - 0.8223\,\tau_L + 0.1968052\,(a_1\omega) + 9.5065\,\tau_L^2 \\
+ 0.0789672\,(a_1\omega)^2 + 0.0123934\,\tau_L(a_1\omega) + 0.6176416\,\tau_L^3 \\
+ 0.0275371\,(a_1\omega)^3 + 1.50584\,\tau_L^2(a_1\omega) + 0.0631003\,\tau_L(a_1\omega)^2 \\
+ 0.0325394\,\tau_L^4 + 0.0054380\,(a_1\omega)^4 \\
\qquad\qquad \text{for } 0.001 < \tau_L \leq 0.05 \\
\\
1.72279 - 1.7256\,e^{\tau_L} + 0.4188386\,e^{(a_1\omega)} + 1.49491\,e^{2\tau_L} \\
- 0.390911\,e^{2(a_1\omega)} + 0.084323\,e^{(\tau_L+a_1\omega)} - 0.582313\,e^{3\tau_L} \\
+ 0.226899\,e^{3(a_1\omega)} - 0.11012\,e^{(2\tau_L+a_1\omega)} + 0.098081\,e^{(\tau_L+2(a_1\omega))} \\
+ 0.08526\,e^{4\tau_L} - 0.061339\,e^{4(a_1\omega)} + 0.031135\,e^{(3\tau_L+a_1\omega)} \\
- 0.024207\,e^{2(\tau_L+(a_1\omega))} - 0.007705\,e^{(\tau_L+3(a_1\omega))} \\
\qquad\qquad \text{for } 0.05 < \tau_L \leq 0.6
\end{cases} \qquad (A1.3)
$$

$$
\eta = \begin{cases}
.25354 - 0.102345\,\tau_L + 0.216011\,(a_1\omega) + 0.074936\,\tau_L^2 \\
+ 0.098738\,(a_1\omega)^2 - 0.020235\,\tau_L(a_1\omega) - 0.031101\,\tau_L^3 \\
+ 0.037217\,(a_1\omega)^3 + 0.005483\,\tau_L^2(a_1\omega) - 0.005653\,\tau_L(a_1\omega)^2 \\
+ 0.005532\,\tau_L^4 + 0.007617\,(a_1\omega)^4 - 0.000768\,\tau_L^3(a_1\omega) \\
+ 0.000338\,\tau_L^2(a_1\omega)^2 - 0.001312\,\tau_L(a_1\omega)^3 \\
\qquad\qquad \text{for } 0.6 < \tau_L \leq 1.4 \\
\\
1.0951 + 0.245402\,\tau_L + 0.124994\,(a_1\omega) - 0.211869\,\tau_L^2 \\
+ 0.095429\,(a_1\omega)^2 + 0.140345\,\tau_L(a_1\omega) + 0.074985\,\tau_L^3 \\
+ 0.035418\,(a_1\omega)^3 - 0.087716\,\tau_L^2(a_1\omega) - 0.002751\,\tau_L(a_1\omega)^2 \\
- 0.009470\,\tau_L^4 + 0.007192\,(a_1\omega)^4 + 0.017470\,\tau_L^3(a_1\omega) \\
+ 0.000060\,\tau_L^2(a_1\omega)^2 - 0.000561\,\tau_L(a_1\omega)^3 \\
\qquad\qquad \text{for } 1.4 < \tau_L \leq 1.9 \\
\\
0.396660 + 0.442016\,\tau_L + 0.131939\,(a_1\omega) + 0.267895\,\tau_L^2 \\
+ 0.092459\,(a_1\omega)^2 + 0.089914\,\tau_L(a_1\omega) - 0.218468\,\tau_L^3 \\
+ 0.030919\,(a_1\omega)^3 - 0.041290\,\tau_L^2(a_1\omega) - 0.002676\,\tau_L(a_1\omega)^2 \\
+ 0.036379\,\tau_L^4 + 0.006011\,(a_1\omega)^4 + 0.005908\,\tau_L^3(a_1\omega) \\
+ 0.0003727\,\tau_L^2(a_1\omega)^2 + 0.000902\,\tau_L(a_1\omega)^3 \\
\qquad\qquad \text{for } 1.9 < \tau_L \leq 3.0 \\
\\
0.022837 + 0.067017\,\tau_L + 0.191682\,(a_1\omega) + 0.146402\,\tau_L^2 \\
+ 0.075457\,(a_1\omega)^2 - 0.001260\,\tau_L(a_1\omega) - 0.022708\,\tau_L^3 \\
+ 0.016858\,(a_1\omega)^3 \\
\qquad\qquad \text{for } 3.0 < \tau_L \leq 5.0
\end{cases} \qquad (A1.3)
$$

Appendix B

OTC Results for 1-D Cartesian Enclosure under Non-radiative Equilibrium Situation

Regressed equations of OTC [236]

Expression of the optical thickness coefficient, η, for the case of absorbing, emitting, isotropically scattering ($\omega \neq 0.0$, $a_1\omega = 0.0$) media at non-radiative equilibrium, $0.0001 \leq \tau_L \leq 5.0$.

$$\eta = \begin{cases} 7.2638 - 5.33231\, e^{\tau_L} - 0.24256\, e^{\omega} - 6.15798\, e^{2\tau_L} \\ + 0.00118\, e^{2\omega} + 0.23927\, e^{(\tau_L+\omega)} + 5.50250\, e^{3\tau_L} \\ \qquad\qquad \text{for } 0.0001 \leq \tau_L < 0.05 \\ \\ 1.26384 - 0.25003\,\tau_L + 0.05515\,\omega + 0.65438\,\tau_L^2 \\ - 0.128667\,\omega^2 + 0.122951\,\tau_L\,\omega - 1.14301\,\tau_L^3 \\ + 0.12475\,\omega^3 - 0.10899\,\tau_L^2\,\omega + 0.03722\,\tau_L\,\omega^2 \\ + 0.78499\,\tau_L^4 + 0.037331\,\omega^4 \\ \qquad\qquad \text{for } 0.05 \leq \tau_L < 0.6 \end{cases} \qquad (B1.1)$$

Equation (B1.1) continued on next page

Equation (B1.1) continued from previous page

$$\eta = \begin{cases} 0.99729 + 0.39907\, e^{\tau_L} - 0.01500\, e^{\omega} - 0.30004\, e^{2\tau_L} \\ + 0.01286\, e^{2\omega} + 0.04399\, e^{(\tau_L+\omega)} + 0.08583\, e^{3\tau_L} \\ - 0.00450\, e^{3\omega} - 0.00466\, e^{(2\tau_L+\omega)} - 0.00299\, e^{(\tau_L+2\omega)} \\ - 0.00869\, e^{4\tau_L} + 0.00037\, e^{4\omega} \\ \qquad\qquad \text{for } 0.6 \le \tau_L < 1.2 \\ \\ 1.17601 - 0.04592\, e^{\tau_L} + 0.08810\, e^{\omega} + 0.00464\, e^{2\tau_L} \\ - 0.02700\, e^{2\omega} + 0.01813\, e^{(\tau_L+\omega)} - 0.00020\, e^{3\tau_L} \\ + 0.00394\, e^{3\omega} - 0.00063\, e^{(2\tau_L+\omega)} - 0.00252\, e^{(\tau_L+2\omega)} \\ \qquad\qquad \text{for } 1.2 \le \tau_L < 1.7 \\ \\ 1.20500 - 0.01958\,\tau_L + 0.03500\,\omega - 0.00692\,\tau_L^2 \\ + 0.05273\,\omega^2 + 0.04568\,\tau_L\,\omega + 0.00247\,\tau_L^3 \\ - 0.06107\,\omega^3 - 0.00322\,\tau_L^2\,\omega - 0.00971\,\tau_L\,\omega^2 \\ - 0.00021\,\tau_L^4 + 0.02524\,\omega^4 \\ \qquad\qquad \text{for } 1.7 \le \tau_L \le 5.0 \end{cases} \qquad (B1.1)$$

Expression of the optical thickness coefficient, η, for absorbing-emitting media (without scattering, $\omega = 0.0$) at non-radiative equilibrium, $0.0001 \le \tau_L \le 5.0$.

$$\eta = \begin{cases} 1.27338 - 1.34631\,\tau_L + 26.78364\,\tau_L^2 - 159.953\,\tau_L^3 \\ \qquad\qquad \text{for } 0.0001 \le \tau_L < 0.1 \\ \\ 1.26002 - 0.145619\,\tau_L + 0.125726\,\tau_L^2 - 0.067566\,\tau_L^3 \\ + 0.006472\,\tau_L^4 - 0.006152\,\tau_L^5 \\ \qquad\qquad \text{for } 0.1 \le \tau_L \le 1.0 \\ \\ 1.2376 - 0.068275\,\tau_L + 0.018395\,\tau_L^2 - 0.002886\,\tau_L^3 \\ + 0.000185\,\tau_L^4 \\ \qquad\qquad \text{for } 1.0 < \tau_L \le 5.0 \end{cases} \qquad (B1.2)$$

Expression of the optical thickness coefficient, η, for absorbing, emitting and, forward scattering ($a_1\omega = 0.5$, $\omega = 0.5$ and $a_1 = +1.0$) media at non-radiative equilibrium, $0.0001 \leq \tau_L \leq 5.0$.

$$\eta = \begin{cases} 1.27355 - 2.22853\,\tau_L + 0.192067\,(a_1\omega) - 0.00537\,\tau_L^2 \\ + 0.107663\,(a_1\omega)^2 - 0.451894\,\tau_L(a_1\omega) - 0.000004\,\tau_L^3 \\ - 0.018215\,(a_1\omega)^3 - 0.000735\,\tau_L^2(a_1\omega) + 0.098177\,\tau_L(a_1\omega)^2 \\ \qquad\qquad \text{for } 0.0001 \leq \tau_L \leq 1.0 \\ \\ 1.27127 - 0.857938\,\tau_L + 0.186669\,(a_1\omega) + 9.81455\,\tau_L^2 \\ + 0.121449\,(a_1\omega)^2 + 0.297198\,\tau_L(a_1\omega) + 0.675137\,\tau_L^3 \\ - 0.049495\,(a_1\omega)^3 + 0.986318\,\tau_L^2(a_1\omega) - 0.349831\,\tau_L(a_1\omega)^2 \\ + 0.04401\,\tau_L^4 + 0.061678\,(a_1\omega)^4 + 0.059332\,\tau_L^3(a_1\omega) \\ - 1.60615\,\tau_L^2(a_1\omega)^2 + 0.751796\,\tau_L(a_1\omega)^3 \\ \qquad\qquad \text{for } 0.1.0 < \tau_L \leq 5.0 \end{cases} \tag{$B1.3$}$$

Expression of the optical thickness coefficient, η, for absorbing, emitting and, backward scattering ($a_1\omega = -0.5$, $\omega = 0.5$ and $a_1 = -1.0$) media at non-radiative equilibrium, $0.0001 \leq \tau_L \leq 5.0$.

$$\eta = \begin{cases} 0.7857617 + 0.569860\,e^{\tau_L} + 0.637736\,e^{(a_1\omega)} + 0.203843\,e^{2\tau_L} \\ + 0.165533\,e^{2(a_1\omega)} + 0.123876\,e^{(\tau_L + a_1\omega)} - 0.142041\,e^{3\tau_L} \\ + 0.046964\,e^{3(a_1\omega)} - 0.378914\,e^{(2\tau_L + a_1\omega)} - 0.357473\,e^{(\tau_L + 2(a_1\omega))} \\ - 0.460442\,e^{4\tau_L} + 0.019614\,e^{4(a_1\omega)} \\ \qquad\qquad \text{for } 0.0001 < \tau_L \leq 1.0 \\ \\ 1.27539 - 0.9223\,\tau_L + 0.1568052\,(a_1\omega) + 9.8065\,\tau_L^2 \\ + 0.17896722\,(a_1\omega)^2 + 0.0123934\,\tau_L(a_1\omega) + 0.6176416\,\tau_L^3 \\ + 0.0275371\,(a_1\omega)^3 + 1.50584\,\tau_L^2(a_1\omega) + 0.0631003\,\tau_L(a_1\omega)^2 \\ + 0.0325394\,\tau_L^4 \\ \qquad\qquad \text{for } 1.0 < \tau_L \leq 5.0 \end{cases} \tag{$B1.4$}$$

भारतीय प्रौद्योगिकी संस्थान गुवाहाटी
Indian Institute of Technology Guwahati

Acknowledgements

I am grateful to Dr. Subhash C. Mishra, Associate Professor, Department of Mechanical Engineering, Indian Institute of Technology, Guwahati for permitting me to use Figs. 2.1-2.8.

भारतीय प्रौद्योगिकी संस्थान गुवाहाटी
Indian Institute of Technology Guwahati